FIBRE OPTIC PARAMETRIC AMPLIFIERS FOR TRANSIENT LIMITED OPTICAL FIBRE SYSTEMS

CHANDRA BHANU GAUR

Doctor of Philosophy

Aston University

April 2021

©Chandra B Gaur, 2021

Chandra B Gaur asserts his moral right to be identified as the author of this thesis

This copy of the thesis has been supplied on condition that anyone who consults it is understood to recognize that its copyright belongs to its author and that no quotation from the thesis and no information derived from it may be published without appropriate permission or acknowledgment.

Aston University

Fibre Optic Parametric Amplifiers for Transient limited Optical Fibre Systems

Chandra Bhanu Gaur

Doctor of Philosophy

2021

Summary

The thesis explores fibre optical parametric amplifiers (FOPAs) to implement and develop the FOPA ability to provide transient free burst mode signal amplification, presenting potential applications in reach extended access networks and time-varying optical transmission systems. This document experimentally demonstrates FOPA as a potential drop-in amplifier candidate for transient limited optical systems by experimentally investigating and comparing transient effects in conventional fibre amplifiers. For example, future reach extended optical access networks. Additionally, this work provides evidence for transient free burst traffic amplification enabled by FOPA. A number of experimental techniques were implemented to demonstrate an ultra- fast response, high burst signal gain, and the ability to simultaneously amplify bi- directionally transmitted signals in a dual telecom band. Novel polarisation-insensitive FOPA employed in a 50 km reach extended access network link to achieve clean burst mode signal amplification. PI-FOPA targeted varied burst durations and burst traffic density amplification to evaluate performance compared to a commercial erbium-doped fibre amplifier (EDFA) and a discrete Raman amplifier. FOPA enhances link receiver sensitivity by >3 dB compared to EDFA and Raman amplifier for a varied burst duration amplification from 70 μs to 5 μs. For high burst traffic density amplification from 5% to 97%, FOPA allows burst traffic amplification up to 97% traffic, while EDFA and discrete Raman amplifier traffic density amplification was limited to 15% and 30%. We first presented a bi-directional non- burst and burst signal amplification by implementing a novel dual-band FOPA setup. FOPA achieved polarisation insensitive net gain of >16 dB for >50 nm apart signals in C and L bands. FOPA's ability to provide a wide broadband gain of ~10THz is utilized to amplify a non-burst and bursty signal in a dual-band transmission with a single in-line PI-FOPA amplifier simultaneously.

Keywords: Optical fibre parametric amplifier, optically amplified access networks, burst mode, discrete Raman amplifier, erbium-doped fibre amplifier, reach extended access networks

ACKNOWLEDGMENT

I would like to take this opportunity to acknowledge and thank several people who have helped me throughout this journey and during this thesis. Firstly, I would like to thank my supervisor, Prof. Nick J Doran, for pursuing my Ph.D. at Aston University. I am very grateful to him for the highly competent guidance, remarkable patience, and great financial support, which indeed made a change.

I would like to express my deep gratitude to my associate supervisor Dr. Filipe Ferreira and Dr. Vladimir Gordienko, for everything I learned from them and enormous assistance in the lab and with all the help in writing.

I would also like to thank Dr. Vitor Ribeiro and Dr. Aron Szabo for helping me in simulations and general technical discussions.

I would also like to thank Dr. Ian Phillips for lending me L-band EDFA and other useful equipment I enjoyed within my experimental work.

I would also like to thank Prof. Andrew Ellis for recommending me to the prestigious Rank Prize Symposium to present my work.

I also would like to thank Dr. Asif Iqbal and Dr. Lukasz Krzczanowicz for helping me out with providing equipment for discrete Raman fibre amplifiers. For general discussion and help around in the lab from Dr. Abdallah Al. Ali, Mahmood Abu-Romah, and Dr. MAZ Al-Khateeb for getting me to understand the VPI modelling tool.

Finally, special love to my parents, wife Chandni, and daughter Evaniya for standing with me throughout and motivating me.

TABLE OF CONTENTS

LIST OF ABBREVIATIONS

ADC	Analog-to-Digital Convertor
AOM	Acousto-Optic Modulator
ASE	Amplified Spontaneous Emission
AUT	Amplifier Under Test
AWG	Arbitrary Waveform Generator
B2B	Back-to-back
BER	Bit error ratio
BM	Burst mode
DRA	Discrete Raman amplifier
DRFA	Discrete Raman fibre amplifier
DCF	Dispersion compensating fibre
DSF	Dispersion shifted fibre
DS	Downstream signal
EDF	Erbium-doped fibre
EDFA	Erbium-doped fibre amplifier
FOPA	Fibre optical parametric amplifier
FWM	Four-wave mixing
GV	Gain variation
GVD	Group velocity dispersion
HNLF	Highly nonlinear fibre
NF	Noise figure
NLF	Non-Linear Fibre
NLSE	Nonlinear Schrodinger equation
NRZ	Non return to zero
OLT	Optical line terminal
OOK	On-Off Keying
ONU	Optical networking unit
OSA	Optical spectrum analyser
OSNR	Optical signal-to-noise ratio
US	Upstream signal
PBS	Polarisation beam splitter
PC	Polarisation controller
PDG	Polarisation dependent gain

PI	Polarisation Insensitive
PM	Phase modulator
PMD	Polarisation mode dispersion
PON	Passive optical networks
RE	Reach Extended
RF	Radio frequency
RIN	Relative intensity noise
SBS	Stimulated Brillouin scattering
SOA	Semiconductor optical amplifier
SPM	Self-phase modulation
SRS	Stimulated Raman scattering
SSMF	Standard single mode fibre
TL	Tuneable laser
VOA	Variable optical attenuator
WDM	Wavelength division multiplexer
XPM	Cross-phase modulation
YDFA	Ytterbium-doped fibre amplifier
ZDW	Zero dispersion wavelength

LIST OF FIGURES

LIST OF TABLES

Chapter 1 INTRODUCTION

1.1 Introduction

Today, the internet has become part and parcel of our ordinary daily thing in the lives of billions of people around the globe. From writing an email to streaming YouTube or a long video call on ZOOM, the internet has revolutionized our daily communication life. As the world is stranded from the COVID-19 pandemic, robust internet connectivity delivered by optical fibres has not only supported people around the globe but saved our daily bread via enabling working remotely throughout the world in this challenging time. Traditional optical networks were modernized by deploying coherent optical transmission equipment, wavelength division multiplexing, and advanced optical amplification techniques. Now capable of transmitting terabits of optical data in core networks (reaching 12 terabits by 2021) and 5.3 billion internet users by 2023 [1] as predicted by the *Cisco VNI* report. With the increase in connectivity to the end-users, it has become more critical to resolve the "*Capacity Crunch*" within the access networks to access the massive volume of data [2], [3]. With the evolution of data-based applications, for example, wireless networking, HD-TV, and triple-play services, tremendous growth in data traffic, especially in access networks connecting the last mile, is predicted [4] and shown in Figure 1.1.

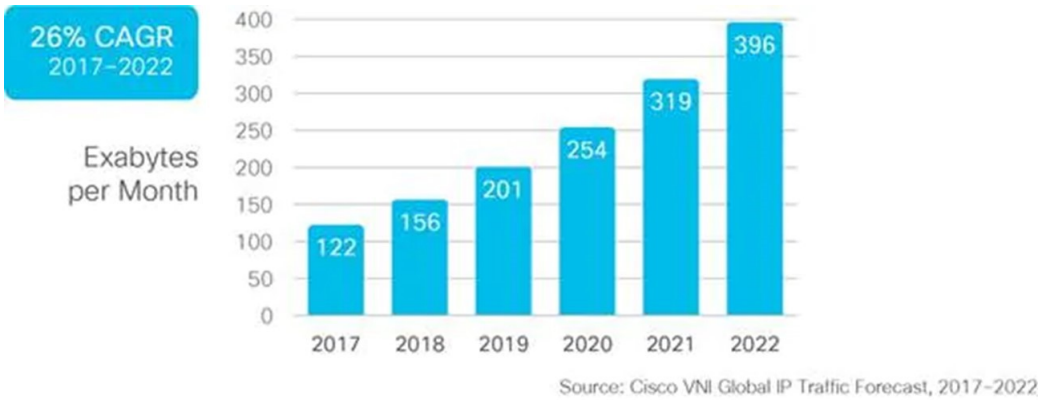

Figure 1.1 Cisco VNI forecast 396 exabytes per month of IP traffic by 2022[1]

Although optical fibre is not expensive, deploying fibre underground is the most expensive part and is subject to legal clearance, especially in access networks. Therefore, it becomes essential to extend the standard physical reach of access networks to tens of kilometers for consolidation of multiple exchanges to a single node section and enhance the number of customers [5]. Optical to electric to optical (OEO) conversion techniques are promising but not scalable for future access networks, including ultra-dense time and wavelength division

multiplexing (TWDM) transmission. Current research on coherent access networks is of significant interest, although subject to costly coherent receivers and limitations for detecting burst mode signals [6]. On the other hand, optical amplifiers are well-matured technology. Since the inception of erbium-doped fibre amplifiers (EDFAs) in the 1980s, they have revolutionized them as a pillar for fibre optical communications by enabling WDM amplification. Currently, internet access enabled by all-optical networks is equipped with optical amplifiers [7]. It place optical amplification as a potential solution for reach extension and increasing link power budget to connect more customers [8] in access networks or passive optical networks (PON). Recently ITU-T recommendation for gigabit-capable reach extended passive optical networks suggests employing optical amplification schemes in access networks. Where passive nature of access networks is still preserved by performing optical amplification with no grooming of data signal over the optical transmission link [9] employing bit rates including symmetrical 10Gbps and higher [10], [11]. Optical amplifiers within access networks envisaged enhancing overall link performance by:

i. Extended physical reach

ii. Increase signal gain

iii. Fewer local exchanges (replaced by amplifiers)

iv. Enhance splitter to customer ratio

State-of-the-art optical amplifiers proposed for standard access network reach extensions, including semiconductor optical amplifiers (SOA), erbium-doped fibre amplifiers (EDFA), and Raman fibre amplifiers [12]. Reach extension up to 100 km is demonstrated by hybrid Raman and SOA amplification [13]. Another demonstration with hybrid EDFA and SOA presents downstream non-burst signal amplification by EDFA, and the burst signal was amplified by SOA for 100 km reach extended access link [14]. However, suggested optical amplification techniques show limitations like slow response time for burst amplification, patterning effects, small signal gain, low output signal powers, and restrictions on operating in arbitrary wavelengths required for access networks. Recently with the development of fibre optic parametric amplifiers (FOPA), a window for potentially employing FOPA in access networks has become a high probability. FOPA supports all required specifications to be employed as a drop-in optical amplifier in an access network with features like large gain [15], gain on arbitrary wavelength [16], and high output signal power [17]. FOPA also demonstrates ultra- fast response time suitable for burst mode signal amplification [18]. The FOPA is presented as a leading candidate within this thesis to show

transient free burst signal amplification for an optically amplified reach extended access network link.

1.2 Background

Optical access networks have become the most cost-effective way to maximize the optical fibre infrastructure sharing and information capacity among as large a population as possible in the last few decades. Indeed last-mile connectivity to connect multiple users was approached through passive optical networks (PON) in various connectivity configurations, for example, Fibre to the Premises (FTTP) and Fibre to the Home (FTTH). A point-to-multipoint tree-like optical network architecture using passive optical splitters enables a single trunk feeder to connect to multiple drops using an optical distribution network (ODN) [19] for the standard physical reach of 20 km. However, recently, the demand for more bandwidth to feed various data-hungry applications like HD streaming, 4K TV, online gaming, and E-education has increased required large bandwidth and data transmission. Therefore, building passive optical networks by deploying more fibres and constructing more local exchange sites have significantly increased. Hence, sizeable passive infrastructure development increased operational and capital expenditure for different telecom operators.

The more logical way is to utilize existing network infrastructure to capture a large population over large areas with increased network sharing and feed them with more capacity, bandwidth, and quality of service. Therefore, a scalable in the future approach known as reach extended PON (access networks) is a more convincing route. Through extended reach, architecture, the traditional physical reach and splitting capacity of a conventional local access network link can be significantly enhanced by inline optical amplification [14]. Reach extended access network architecture effectively can integrate metro and access networks into a single all-optical system. They enable most local exchange sites to be bypassed, resulting in the consolidation of metro and access layers, substantially reducing the operational and capital expenditure required to build multiple exchange sites. Furthermore, deploying optical amplifiers as drop-in regenerators extend the physical reach and splitting ratio while increasing capacity through employing matured protocols in a hybrid transmission of time-division multiplexing (TDM) and wavelength division multiplexing (WDM) [20].

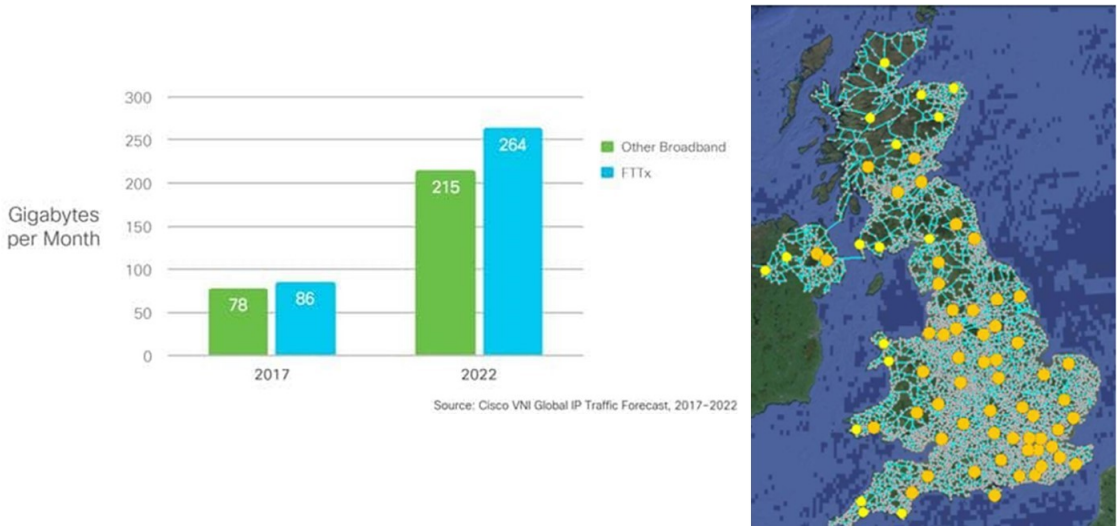

Figure 1.2 Cisco VNI report for fibre-connected fixed broadband household traffic to grow by 264 Gigabits per month[21] and a picture metro-core consolidation nodes for LR-PON in the UK[22]

1.3 Motivation

In the past, research projects such as "DISCUS" [5] and "Sardana" [23] have successfully demonstrated the advantages of increasing the physical reach, split, and capacity of access networks through in-line optical amplification and hybrid signal multiplexing schemes. However, optically amplified reach extended access networks employing conventional state-of-the-art amplifiers as SOAs, EDFA, and Raman amplifiers, as discussed in [24]. All struggles to provide a robust solution for modern reach extended access networks. Conventional optical amplification technology suffers limitations to amplify upstream bursty traffic transmitted through TDMA protocol as observed with EDFA and Raman amplifiers. Although SOAs employed in access networks as optical amplifiers as pre- amplifiers, shown limitations due to inter-symbol interference and high output signal powers limiting them for high-capacity access networks. Similarly, EDFA and Raman amplifiers suffer from transient effects for burst signal amplification. Interestingly, all required specifications for an optical amplifier to be employed as drop-in amplification technology for reach extended access networks could be potentially satisfied by using a fibre-optic parametric amplifier (FOPA).

In this work, we study and successfully demonstrate experimentally the potential feasibility of employing FOPA as a reach extended high gain burst-mode drop-in amplifier. We employ a novel polarisation-insensitive FOPA (PI-FOPA) in an optically amplified 50 km reach extended access link transmitting non-burst and bursts-mode of 10 Gbps on-off keying traffic. We compare PI- FOPA with employing a commercial EDFA and a tested discrete Raman amplifier (DRA) with

the PI-FOPA for a range of burst durations and traffic densities. We compare receiver sensitivity for all tested amplifiers and observe PI-FOPA performance by calculating the bit error ratio.

Further, a novel experimental setup was developed to investigate dual-band amplification by PI-FOPA in a bi-directional reach extended access network. The PI-FOPA was employed to amplify C and L band signals in a non-burst and burst mode for the first time. Dual-band FOPA achieved >15 dB net gain for bi-directional signals propagating in counter- propagation. Subsequently, we investigate the results of signal amplification by calculating bit error rates and overall link power budget improvement.

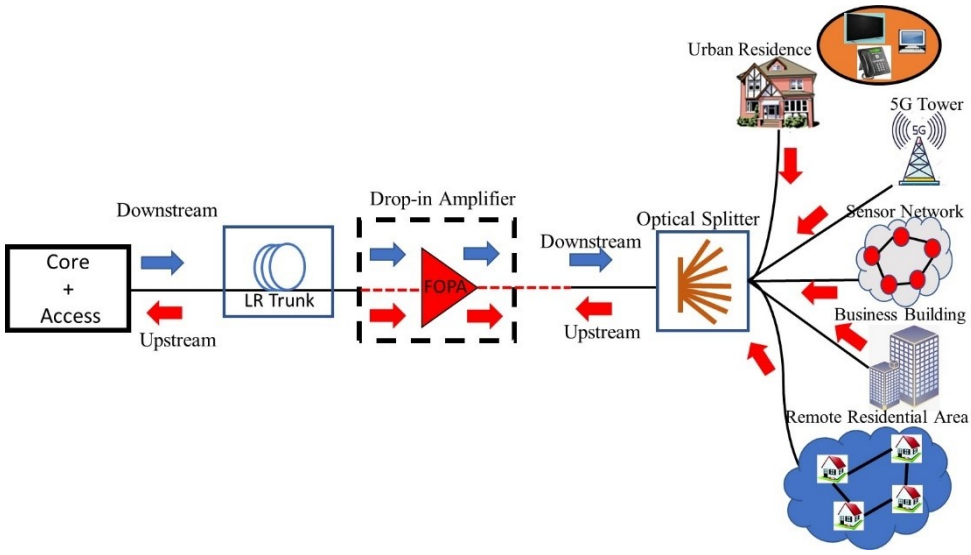

Figure 1.3 Schematic representation of FOPA amplified reach extended access network link presenting single bi-directional amplifier for future access networks

1.4 Thesis Outline

This thesis consists of seven chapters. Here I provide a broad outline of the organization of this thesis. A chapter-wise summary is presented below.

Chapter 1

This chapter is primarily motivated towards presenting a broad overview of the scope and goals of this thesis. In the first part of chapter one, the introduction discusses the evolution of access networks while listing the requirements of future optical networks. Later, the background of optical access networks with the employment of optical amplification was discussed. Finally, motivation leads to the use of FOPA to sequentially utilize its features to modernize optical access network links.

Chapter 2

Chapter 2 primarily discuss fundamental optical transmission sub-systems, including the basic design of the transmitter, optic transmission line, and an optical receiver. Further, this chapter discusses underlying fibre optics transmission impairments such as attenuation, dispersion effects, and different nonlinear effects like stimulated Brillouin scattering (SBS) and stimulated Raman scattering (SRS) and together with others are discussed in their contribution in limiting signal performance. Finally, typical signal performance characteristics are discussed to measure signal quality and the impact of linear and nonlinear impairments like bit error rates and Q-factor. In addition, a common impairment in optical amplifiers known as noise figure is discussed briefly.

Chapter 3

Chapter 3 reviews optical amplifiers in reach extended access networks. Standard optical access network link discussed to understand the optical transmission system within this architecture. Reach extended optical access network architecture discussed optical amplifier placement and its advantages over standard access network links. Different optical amplifiers discussed with their working principle highlighting the significant properties required for optical amplification in access networks. Discussion on the principle of operation and transient effects of semiconductor optical amplifier, Erbium-doped fibre amplifier (EDFA), and Raman fibre amplifier discussed. Finally, fibre optical parametric amplifier theory is explained, including response time, propagation equations, and signal gain in FOPA. In the end, polarisation, insensitive FOPA employed in this work for burst signal amplification is described with theory, and a different configuration of PI-FOPAs is explained.

Chapter 4

Chapter 4 the experimental setup of a reach extended access network with transmitting burst and non-burst mode signals. Configuration employs three in-line optical amplifiers: a commercial EDFA, a discrete Raman amplifier, and a polarisation-insensitive FOPA to amplify transmitted signals. Three tested amplifiers amplified a non-burst and various durations of bursty signals. Non-burst and burst signals amplified by 20 dB with parametric and erbium-doped fibre amplifiers. Further including Raman fibre amplifier gain fixed at 13 dB, including Raman amplifier. I compared the performance of PI-FOPA with conventional EDFA and Raman amplifier by calculating bit error rate and receiver sensitivity at different burst durations. Results of this experimental work are published in [25]–[27].

Chapter 5

Chapter 5 further extends experimental work demonstrated in chapter 4, and for the first time, amplification of high capacity burst traffic density from 5% to 97% by PI-FOPA is presented. This

chapter employed an extended experimental setup to amplify high capacity burst at 13 dB gain. Performance at each traffic density was compared between FOPA with EDFA, discrete Raman amplifier by calculating bit error rates against received burst power. Further, receiver sensitivity against varied duty cycles from 5% to 97% was measured at a BER level of 10^{-3} for all tested AUTs. FOPA performance comparison with commercial EDFA and a tested discrete Raman amplifier demonstrated by BER measurements. The part of the results for this experimental work is also published in [28].

Chapter 6

In chapter 6, a novel bi-directional dual-band FOPA setup was arranged for the first time. The arrangement was employed to amplify C+L band signals. A single amplifier, bi-directional non-burst, and a burst signal amplified by >15 dB net gain. Signals in the C+L band with >50 nm apart wavelengths were transmitted downstream and upstream and amplified simultaneously. Bi-directional signals amplified, with net polarisation-independent gain obtained was ∼17 dB for downstream and 16 dB for upstream signals. Further, performance analysis of amplified signals was measured by calculating BER. Later BER against splitter attenuation was measured to demonstrate the overall link power budget. The result of this work is published in [29] and under preparation for a journal article.

Chapter 7

Finally, chapter 7 will provide an overall conclusion of the work presented in this thesis and is summarized. Future work suggested expanding the development of fibre optic parametric amplifiers to get employed in access networks potentially.

1.5 Publication Summary

Papers in italics are not yet published but submitted or under preparation

Journal Articles:

1. **C.B Gaur**, F. Ferreira, V. Gordienko, V Ribeiro, A. Szabo, and N. J. Doran, “Experimental comparison of fibre-optic parametric, Raman and erbium amplifiers for burst traffic for extended reach PONs,” *Opt. Express*, vol. 28, no. 13, pp. 19362-19373, Jun. 2020.
2. **C.B Gaur**, V. Gordienko, F. Ferreira, V. Ribeiro, and N. J. Doran, "Fibre-optic parametric amplifier for high capacity burst-mode access networks," Opt. Express 29, 21190-21198 (2021)

3. V. Gordienko, A. Szabo, M. F. C. Stephens, V. Vassiliev, **C. B. Gaur** and N. J. Doran, "Limits of Broadband Fibre Optic Parametric Devices due to Stimulated Brillouin Scattering," Optical Fibre Technology (Accepted for publication).
4. V. Gordienko, F. M. Ferreira, **C. B. Gaur** and N. J. Doran, "Looped Polarisation-Insensitive Fibre Optical Parametric Amplifiers for Broadband High Gain Applications," in *Journal of Lightwave Technology*, vol. 39, no. 19, pp. 6045-6053, Oct.1, 2021.
5. ***C.B Gaur**, V. Gordienko, and N.J. Doran, "C and L dual-band fibre Optic Parametric Amplifier for bi-directional reach extended access networks", Journal of Lightwave Technology (Special Edition, Submitted)*

Conference Proceedings:

1. V. Ribeiro, V. Gordienko, **C. B. Gaur**, N.J. Doran, "The Impact of Zero-Dispersion Wavelength Fluctuations in> 110 nm Fibre Optical Raman+ Parametric Amplification," in 44th European Conf. on Optical Commun. (ECOC), Rome, Italy, 2018, paper.
2. **C. B. Gaur,** F. Ferreira, V. Gordienko, V. Ribeiro, N. J. Doran, "Demonstration of improved performance provided by FOPA for extended PON in burst-mode operation," in *45th European Conf. on Optical Commun. (ECOC)*, Dublin, Ireland, 2019, paper.
3. **C. B. Gaur,** F. Ferreira, V Gordienko, A. Iqbal, W. Forysiak and N. J. Doran, "Comparison of Erbium, Raman and Parametric Optical Fibre Amplifiers for Burst Traffic in Extended PON", in Optical Fibre Commun. Conf. and Exhibition (OFC), Los Angeles, CA, 2020, paper
4. V. Gordienko, F. Ferreira, C. Laperle, M. O. Sullivan, **C.B. Gaur**, K. Roberts and N. J. Doran, "Noise Figure Evaluation of Polarisation-insensitive Single-pump Fibre Optical Parametric Amplifiers," in *Optical Fibre Commun. Conf. and Exhibition (OFC)*, Los Angeles, CA, 2020, paper Th4A.1.
5. À D Szabó, V Ribeiro, V Gordienko, F Ferreira, **C B Gaur**, N J Doran, "Verification of signal-to-crosstalk measurements for WDM fibre optical parametric amplifiers," in Conference on Lasers and Electro-Optics, OSA Technical Digest (Optical Society of America, 2020), paper JTu2E.1.
6. **C. B. Gaur**, V. Gordienko, F. Bessin and N. J. Doran, "Dual-Band Amplification of downstream L-band and upstream C-band signals by FOPA in extended reach PON," 2020 *European Conference on Optical Communications (ECOC)*, Brussels, Belgium, 2020, pp. 1-4,
7. V Gordienko, **C B. Gaur**, F Bessin, I D. Phillips, N J. Doran," A robust polarisation-insensitive C & L band FOPA with >17dB gain for both WDM and bursty traffic", *Optical Fibre Commun. Conf. and Exhibition (OFC ,2021 (Accepted))*

8. A´D. Szabo, V Ribeiro, **C B. Gaur**, A A.I Ali, A Mussot, T Quiquempois, G Bouwmans and N J Doran, “Dual-Polarisation C+L-Band Wavelength Conversion in a Twin-Core Highly Nonlinear Fibre”, Optical Fibre Commun. Conf. and Exhibition (OFC ,2021 (Accepted))
9. **C.B. Gaur**,” Parametric Amplification of C&L band Bi-directional signals in optical access networks”, *Rank Prize Funds Symposium on Fibre and Free Space Optical Communications,* Oct. 2020. Poster Presentation
10. **C.B Gaur**, V. Gordeinko, A.A.I. Ali, P. Hazarika, A. Ellis and N.J Doran, "Polarisation-insensitive fibre optic parametric amplifier with gain bandwidth of 35 nm in L-band", Tu2A.4 14th Sept. 11:45 -12:00 Room A, ECOC 2021, Bordeaux (France)

Chapter 2 STATE OF THE ART

TABLE OF CONTENTS

Optical fibre communication networks typically consist of multiple optical sub-system devices integrated to provide a robust high-speed digital communication technology. Optical fibre, in general, has become a holy grail of different optical networks, including undersea, terrestrial, and local networks replacing traditional copper cables. Besides, modern non-linear devices developed using optical fibres which are capable of potentially revolutionizing modern communications.

A general optical communication system block diagram is shown in Figure 2.1. An electrical signal containing the sequence of information is modulated into an optical signal at the desired permittable wavelength within the transmitter section. The modulated optical carrier wave launched into an optical fibre acting as a transmission medium. An optical amplifier block regenerates attenuated optical signals through the propagation of transmission fibre. Inside a receiver, section consists of an optical filter, a photodetector converting the optical signal to electrical using an electrical preamplifier. An optical signal is then converted again into an electrical signal for further signal processing and performance analysis.

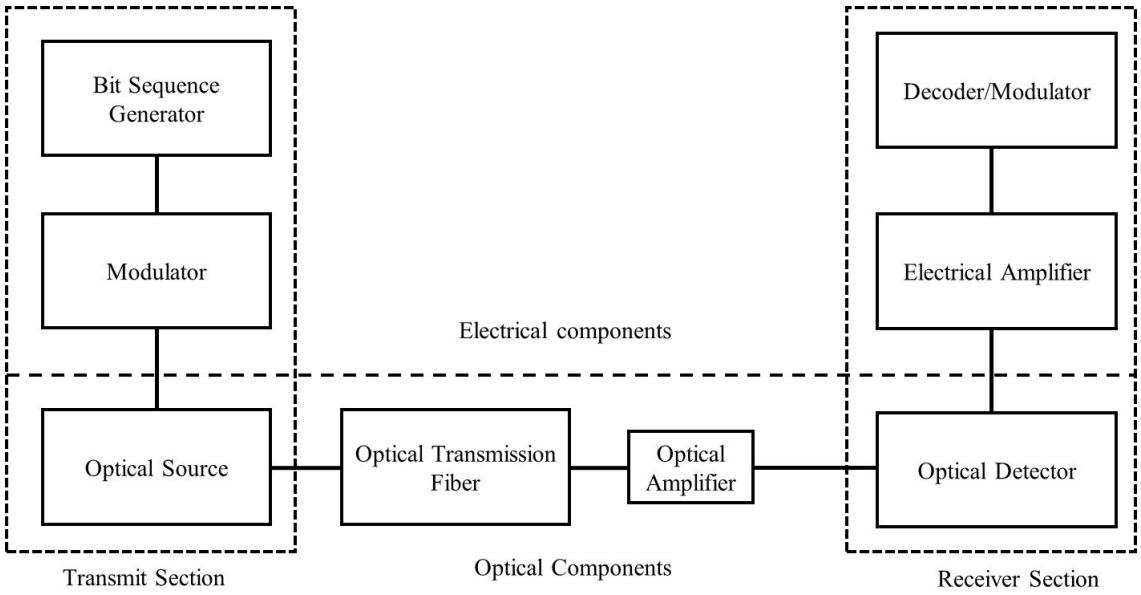

Figure 2.1 Schematic of an optical communication system with the block of electrical and optical components

Therefore, this chapter discusses the relevant optical fibre subsystem of fibre optic transmission medium, as shown in Figure 2.1. The main optical sub- system parts employed in an optical network link are optical signal transmitters, including Mach-Zehnder modulator (MZM), optical transmission fibre, and an optical signal detector within the receiver section. Additionally, acousto optic modulators specific to this work were also explained briefly. Optical wave propagation in silica-based fibres is shown, and corresponding equations are discussed. General properties of optical fibre transmission are described, including fibre loss, dispersion,

birefringence, and nonlinearity. Later, signal performance analysis methods were discussed as bit error ratio (BER), Q factor, and Noise figure (NF) specific for optical amplifier performance.

2.1 Transmitter

Transmission of encoded information over an optical fibre communication system requires modulating a coherent optical light generated at a wavelength of choice. In an intensity modulation scheme, the stream of bits sequence is encoded on the amplitude of the optical carrier wave according to the employed modulation format.

If we consider an electrical envelope of an emitted laser signal with an amplitude A_s, phase φ_s and angular frequency ω the electrical field E_s as expressed in 2.1:

$$E_s(t) = A_s \sin(\omega t + \varphi_s) \qquad 2.1$$

Therefore, information modulated on the amplitude or phase of the electrical carrier wave is shown in equation 2.1. Amplitude modulation (AM), or amplitude shift keying (ASK), is also commonly known as an intensity modulation (IM). In an intensity-modulated signal, the signal's amplitude is encoded to modulate bits stream over an optical carrier. Figure 2.2 presents the schematic of the non-return to zero (NRZ) coding technique. In NRZ format, optical energy level always remains high for bit sequence of 1 and always remains low for bit sequence of 0. The non-return to zero (NRZ) format is bandwidth efficient in comparison to the return to zero (RZ) modulation format as the on-off transition of bits occurs fewer times than RZ pulse in NRZ [30].

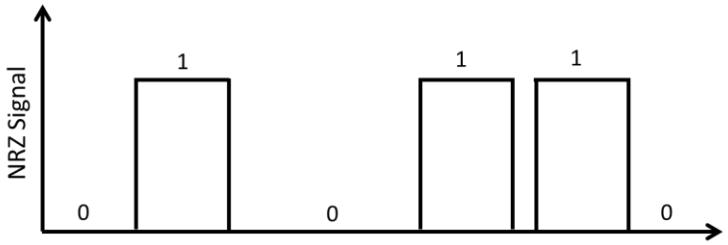

Figure 2.2 Bit sequence of 010110 Non-retuning to zero (NRZ) coding format

2.1.1 Mach Zehnder Modulator

A Mach-Zehnder modulator (MZM) or electro-optic modulator (EOM) is generally employed to modulate the information data stream onto the optical carrier frequency. The principle of MZM is based on the coherent interference of incident light in waveguides such as titanium diffused $LiNbO_3$ used as a nonlinear material. The effective index of a waveguide material N_{eff} can be modified by applying an external voltage through a coated electrode. The optical channel can be modulated in phase and amplitude [31]. This effect is known as an electro-optic effect which is a working principle of MZM.

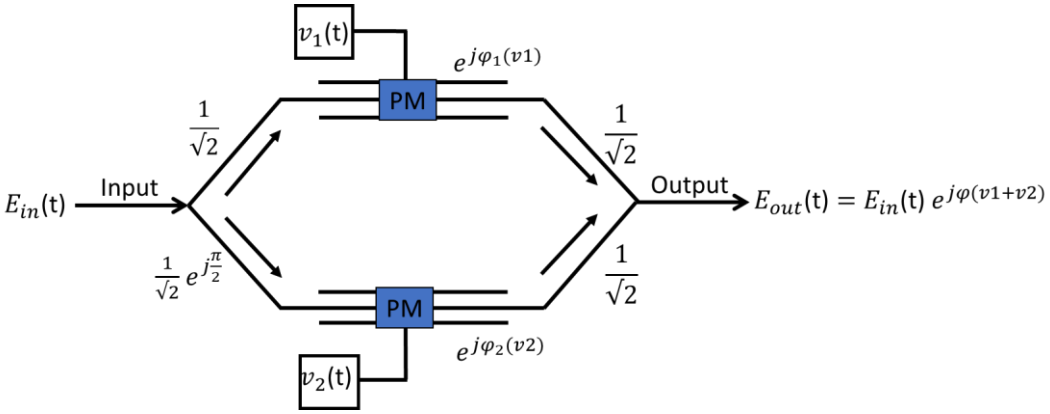

Figure 2.3 A basic schematic of a Mach Zehnder Modulator

Figure 2.3 shows a simple operational schematic of a dual-drive MZM fabricated using $LiNbO_3$ as an electro-optic material. The $LiNbO_3$ refractive index is modified by applying external voltage using two voltage sources shown in Figure 2.3 as v_1& v_2. The input optical field is split into two different paths using an input 3 dB directional coupler before going through a phase shift. As shown in the case of dual-drive MZM employed in this work. A phase shift of $\frac{\pi}{2}$ is applied using the phase modulator shown at upper and lower arm, respectively, to match the phase between optical and electrical signals constructively [30]. As discussed, at the output of MZM, the two fields combine in a constructive interference pattern depending on the modulated phases. The output power depends on the relative phase between the fields, determining the maximum and minimum transmission when the phase difference is 0 and π respectively. The transfer function of an MZM is given by equation 2.2

$$E_{out}(t) = P(v1, v2)E_{in}(t) \tag{2.2}$$

$$P(v1, v2) = \frac{1}{2}\left\{e^{j\varphi_1(v_1)} + e^{j\varphi_2(v_2)}\right\} = e^{j[\varphi_1(v_1)+\varphi_2(v_2)]/2}\cos\left\{\frac{\varphi_1(v_1) - \varphi_2(v_2)}{2}\right\} \tag{2.3}$$

$P(v1, v2)$ represents the ideal transfer function which is essentially determined by the phase difference of the optical field of two respective paths. The voltage modulates optical phases of both arms of the MZM are given by $\varphi_1(t)$ and $\varphi_2(t)$. A linear function of the drive voltages in the phase modulators. The required voltages to have π phase shifts in the arms are specified as $V_{\pi 1}$ and $V_{\pi 2}$. The phase of the respective optical field with applied drive voltage can be defined as equation 2.4

$$\varphi_1(t) = \frac{\pi}{V_{\pi 1}}v_1, \varphi_2(t) = \frac{\pi}{V_{\pi 2}}v_2 \tag{2.4}$$

For achieving pure amplitude modulation, the voltage applied in each arm is described as $v_1 = -v_2 = \frac{v}{2}$. The pure amplitude modulation achieved, and the power transfer function can express as equation 2.5:

$$P\ (v1, v2) = \cos\left(\frac{v\pi}{2V_\pi}\right) \tag{2.5}$$

The phase term removed in a pure amplitude modulation scenario allows for the chirp-free condition in a push-pull operation when equal. Still, an opposite voltage is applied in the arms with alternative phase shifts. The power transfer function can be obtained from the optical field transfer function, and equation 2.5 can be written as equation 2.6:

$$P_p\ (v1, v2) = \frac{1}{2} + \frac{1}{2}\cos\left(\frac{v\pi}{V_\pi}\right) \tag{2.6}$$

P_p represent the power transfer function in push-pull operation. The modulation in intensity can be achieved by operating the MZM at the quadrature point, with a DC bias voltage of $\frac{-V_\pi}{2}$ and modulation with an input voltage swing of $V_\pi$peak to peak as shown in Figure 2.4(a) at the maximum power transfer point. Moreover, when the MZM operated at the minimum transmission point with a DC bias point at - V_π and a peak to peak input voltage swing of $2V_\pi$, a phase shift π occurred at the crossing point of minimum transmission as shown in Figure 2.4 (b) [32].

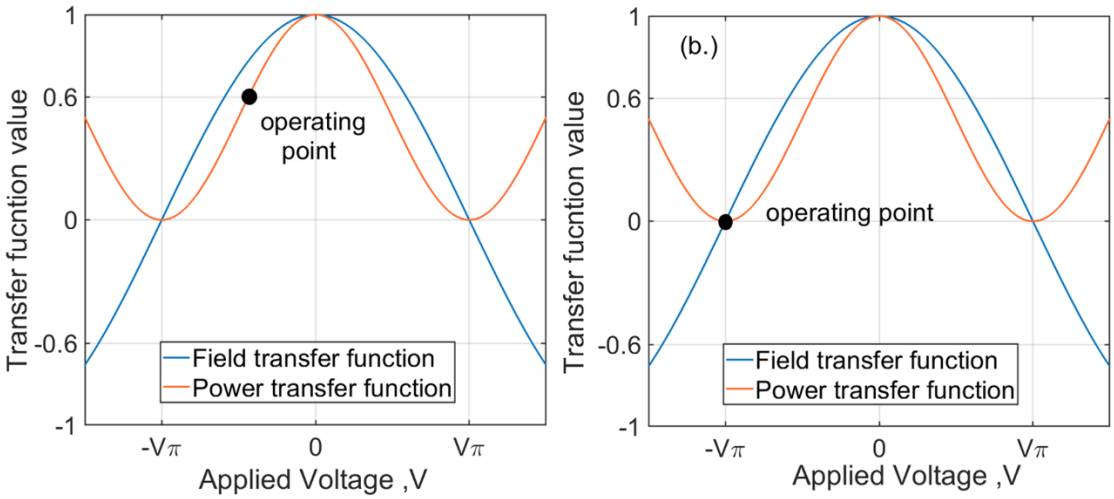

Figure 2.4 Operation of an ideal MZM in the (a) quadrature point and (b) minimum transmission point

Figure 2.4 (a) and (b) show the optical field plots and power transfer functions with two different operation regimes of an ideal MZM: in pure amplitude modulation such as in on-off keying operation and at the minimum transmission point with a minimum phase alternation of π. MZMs can use for intensity and phase modulations.

2.1.2 Acousto Optic Modulator

Acousto optics is a method of intermixing sound and light. The refractive index of an incident light wave modified by an acoustic wave is generated by applying external voltage [33]. An acousto optic modulator (AOM) is a device based on photo-elastic effects to control the power of a laser beam with an electrical driver. An AOM can be used as an intensity modulator for modulating optical laser beams. AOMs similar to the electro-optic modulators (EOM) can control an incident light beam's power, frequency, or spatial direction with an incident light beam electrical drive signal. Although, unlike EOMs, acoustic modulators allow higher input powers to generate high peak power pulses. One of the applications of an AOM is to create a fast-ultrashort wave (nanosecond scale), which can be less than <10 ns rise time with high peak powers. There are multiple applications like acousto-optic frequency shifters or deflectors, AOMs are also employed in high power laser material processing.

Figure 2.5 shows a schematic of the AOM or Bragg deflection modulator. The surface acoustic wave is generated within the transparent waveguide material through which the light beam propagates. The photo-elastic effect is a strain produced by generated acoustic waves, which modifies the material's refractive index to modulate the incident light beam [33]. The principle is known as the photo-elastic effect. The waveguide material is generally a $LiNbO_3$ substrate fabricated onto the thin film surface. As shown in Figure 2.5, the incident light at wavelength λ gets diffracted, dependent on the frequency of the sound wave. The frequency and direction of the scattered beam are dependent on the frequency of acoustic waves, also is given as equation 2.7.

$$\sin\theta_B = \frac{\lambda}{2\Lambda} \qquad 2.7$$

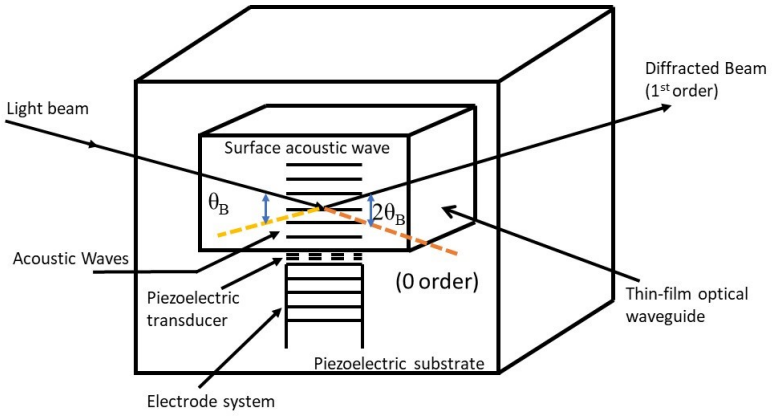

Figure 2.5 Operational view of acousto-optical waveguide modulator. Bragg deflection of a light beam due to surface acoustic waves

θ_B is the angle between the light beam and the acoustic beam wavelengths, λ is the wavelength of the light in the thin-film waveguide, and Λ is the acoustic wavelength. The light will be deflected by $2\theta_B$ from its original path, as shown in Figure 2.5. Similarly, an AOM can be used for creating bursts of modulated optical signals with desired frequency. AOM found its applications in generating fast optical bursts [34]. In this work, AOM is employed for generating bursts with various durations and periods for experimental analysis.

2.2 Optical Detectors

Optical receivers are an essential part of an optical communication system as it determines the performance of the received signal. Therefore, optical detectors should comply with a few critical parameters such as high sensitivity and large quantum efficiency to convert photons to electrical current. Additionally, low noise introduction to the signal and sizeable analog bandwidth determines the speed at which incident varied optical power can be detected, known as Δf. Semiconductor photodiodes provide state-of-the-art signal detections in optical communications. Widely fabricated germanium (Ge) based semiconductor photodetectors between wavelength range of 0.8 μm–1.6 μm is primarily employed in direct detection optical networks. One of the disadvantages of Ge-based photodetectors (PD) is the addition of large dark currents due to their narrow bandgaps. Therefore, further developing more comprehensive bandgap semiconductor alloys with heterojunction semiconductor structures was fabricated, such as InGaAs and GaAs structures.

PIN photodetectors are generally employed in optical networks, as they provide detection over a wide wavelength range with operation on longer wavelengths due to the broad depletion region available. PIN states for p-n type semiconductor structure with small n-type doping material as shown in Figure 2.6 (a), demonstrating parallel light injecting PIN photodetector. Figure 2.6 (b) is mushroom waveguide type Ge-based PD used to overcome quantum efficiency and bandwidth limitation. The indium phosphide (InP) structure provides operation at a 1.55 μm wavelength. Electron charge trapping is avoided by additional layers of p^+InGaAsP and n^+InGaAsP [33]. The generic block diagram of an optical detector, as shown in Figure 2.6(c), consists of a photodiode (PIN or APD), an electrical pre-amplifier to amplify the detected signal, automatic gain control, and a decision circuit connected to a clock recovery circuit to suppress jitter in an optical signal. Bits identified as '1' demodulated as high amplitude and '0' bit demodulated as low amplitude [30].

The responsivity of the optical detector given as $I_P = RP_{in}$ .That is, incident photons with energy hv exceed the bandgap energy and generate an electron-hole pair equivalent to the

number of photons received. Generated photocurrent I_P, due to the flow to electron-hole pair is directly proportional to the input optical power P_{in}.

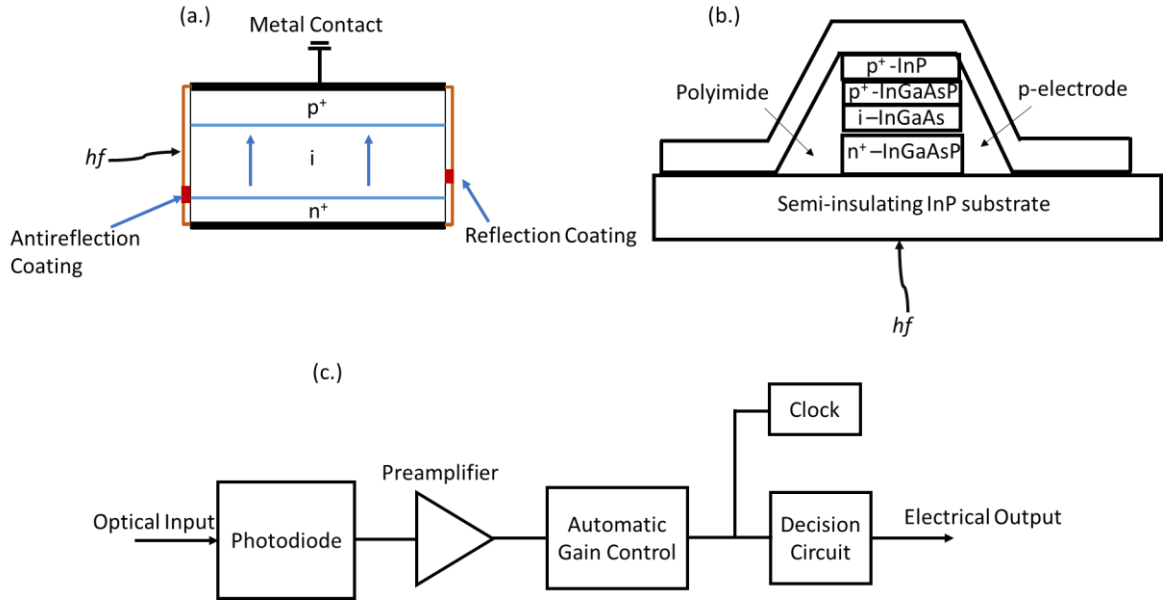

Figure 2.6 Structure of (a) a side-illuminated PIN photodetector, (b) mushroom waveguide photodiode, and (c) block diagram of an optical detector [33]

Quantum efficiency η is related to responsivity R of the photodetector given as

$$\eta = \frac{I_p/q}{P_{in}/hv} = \frac{hv}{q}R \tag{2.8}$$

Where q is the electric charge constant, responsivity R can be written as Equation 2.9; at a longer wavelength, responsivity increase as relation below. Although not possible for all cases where photon energy becomes smaller and more photons present for the same optical power.

$$R = \frac{\eta\lambda}{1.24} \tag{2.9}$$

The above-absorption coefficient α is absolute power equivalent to the difference between incident and reflected optical power and quantum efficiency η provided by equations 2.10 and 2.11. W is the width of the semiconductor slab employed as photodetector material.

$$P_{abs} = P_{in} - P_{tr} = [1 - e^{-\alpha W}]P_{in} \tag{2.10}$$

$$\eta = \frac{P_{abs}}{P_{in}} = 1 - e^{-\alpha W} \tag{2.11}$$

Other important parameters of the optical detector are response time and bandwidth. The rise time of an optical detector determines the time required to process incident optical power to electrical power. It is dependent on incident optical power to provide time over which the current

build-up from minimum to maximum. The rise time *Tr,* where photocurrent builds from 10% to 90% of incident photocurrent value: $T_r = 2.2\ (\tau_{tr} + \tau_{RC})$, where τ_{tr} is the transit time and τ_{RC} is the time constant for the equivalent resistor-capacitor (RC) circuit [35]. Depending on the response, the time bandwidth of the photodetector can be limited. Equation 2.12 shows the bandwidth of a photodetector given as Δf, related to the transit time $\tau_{tr}$and time constant τ_{RC}.

$$\Delta f = \frac{1}{[2\pi(\tau_{tr} + \tau_{RC})]} \qquad 2.12$$

Noise generated within optical signal detectors from dark current and electronic components can be detrimental. For reliable PD, dark currents should be negligible (I_d<10nA) [36]. A PIN-type photodetector consists of an additional intrinsic layer in between the PN junction structure [37]. Through this depletion region, width W is dependent upon the required quantum efficiency η and response time. For example, direct bandgap semiconductors as InGaAs depletion region width W is around 3-5 μm. The response time for PIN photodetector of InGaAs is τ_{tr}~ 10 ps, with supported detector bandwidth of Δf~ 10GHz.

ITU-T specification suggests using burst mode receivers for detecting upstream burst mode or on-off keying modulated signals transmitted from different user to back to central office receiver in generic point to multipoint architecture [10]. Advanced burst mode receivers are required to detect random upstream bursty traffic while improving access networks' power budget and capacity [38], [39]. Generally, DC-coupled direct-detection photodetectors are employed in detecting burst mode signals. However, advanced burst mode receivers with fast settling time <100 ns are still within research. The accurate threshold detection and compatibility to coherent signal detection is also important requirement. Burst mode receivers detect dynamic burst durations and can adjust with varied traffic conditions. They require a long preamble time to train the receiver while degrading overall transmission and quality of service [40], an essential parameter in access networks.

2.3 Transmission Impairments in optical fibres

Propagation of light through total internal reflection is known from the 19th century. Since the inception of uncladded glass fibre, multiple chains of events from 1920 to the late 1970s resulted in achieving low loss (<0.5 dB/km) of optical fibres at optical telecom wavelengths [30]. The introduction of low-loss fibres revolutionized optical communication. Different types of silica-based optical fibres were fabricated, such as standard single-mode fibre (SSMF), multi-mode fibres (MMF), and multicore fibres (MCF). SSMF is widely deployed in almost all-optical communication links covering long-haul, metro, and access. Ultralow loss optical fibres span

telecom frequency bands from ~0.8-1.6 micron telecom wavelengths [33]. Design of single-mode fibre with a step-index refractive profile with core n_{co} and cladding n_{cl} in circular symmetry shown in Figure 2.7 where $n_{co} > .n_{cl}$. As a standard fabrication process, the optical fibre core is doped with GeO_2 and P_2O_5 type dopants to increase core refractive index while fluorine is used to dope the outer layer to lower refractive index of cladding[41]. The core size is generally ten times smaller than the cladding diameter of 125 μm in most conventional optical fibres.

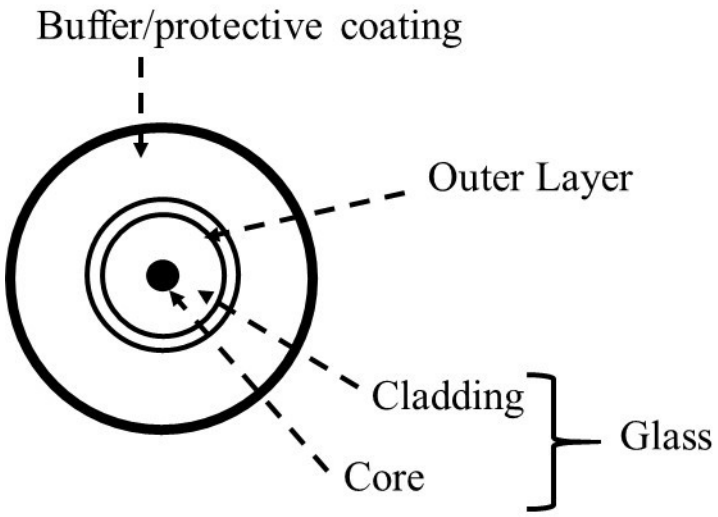

Figure 2.7 Cross-sectional view of an optical fibre cable showing various sections

The normalized frequency *V* is defined as Equation 2.13, where *V* <2.405 describes single-mode (one transverse mode) transmission for SSMF [30].

$$V = \frac{2\pi}{\lambda} a \sqrt{n_{co}^2 - n_{cl}^2} \qquad 2.13$$

The core radius is defined as a, the difference of core is n_{co} and cladding refractive index is n_{cl} given by $(n_{co} - n_{cl})^2$ and wavelength is given by λ defining normalized frequency. The core diameter of SSMF is $a = 8.4\ to\ 9.5\ \mu m$, and the cladding diameter is $125\ \mu m$ [42]. The frequency or wavelength, at *V*=2.405, is called a cut-off frequency or cut-off wavelength of standard optical fibre. Single-mode fibres are designed as such V=2…2.4 within a wavelength range of operation (the lower boundary of *V* is defined by bend loss as discussed in section 2.3.1). The other types of optical fibres employed in this work were dispersion-shifted fibre (DSF) having a smaller core area than SSMF [43], where the core diameter for SSMF is 9.4 μm , DSF core size is 8.4 μm and a highly non-linear fibre (HNLF) with a much smaller core radius of 3.4 μm [44], in comparison with SSMF and DSF core. A smaller effective core area in optical fibres is responsible for stimulating nonlinearity with strong beam confinement.

2.3.1 Fibre Attenuation

One of the essential impairments in optical fibres for signal propagation is the power loss between input and output signal given by Equation 2.14. The simplified definition of fibre attenuation is a decrease of transmitted optical power along fibre length [33]

$$P_{OUT} = P_{in} exp^{(-\alpha L)} \tag{2.14}$$

Input signal power P_{in} propagated through fibre length L with transmitted output power P_{out}. Where, α_{lin} is known as the attenuation coefficient of fibre. The attenuation coefficient $\alpha_{dB}$is in dB expressed as Equation 2.15

$$\alpha_{dB} = -\frac{10}{L} log\left(\frac{P_{out}}{P_{in}}\right) \approx 4.34\alpha_{lin} \tag{2.15}$$

Attenuation in optical fibre stems due to intrinsic (absorption at ultraviolet and infrared region plus Rayleigh Scattering) and extrinsic (Material Impurities: OH, ions, and bend loss) [45]. Power loss in optical fibre is dependent on the signal wavelength. The low loss window of standard SMF is from 0.8 μm to 1.7 μm, the range with ~0.15-0.3 dB/Km power degradation as shown in Figure 2.8. there is a water peak in E-band wavelengths due to water ions (OH) observed around 1.4 μm. With the development of dry and zero water peak optical fibres, this limitation was almost zero. Rayleigh scattering in optical fibres occurred due to microscopic density fluctuations of silica atoms, causing random refractive index variations along the fibre length and always smaller in scale than the incident optical beam wavelength [46]. The loss in power due to Rayleigh scattering varies as λ^{-4} of the wavelength and hence sets the lower limit for fibre low loss window to 0.8 μm wavelength as shown in 2.16.

$$\alpha_R = \frac{C}{\lambda^4} \tag{2.16}$$

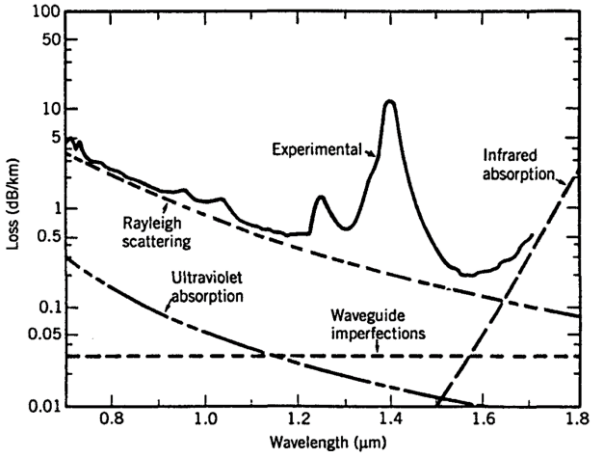

Figure 2.8 Attenuation vs. wavelength loss spectrum of a single-mode fibrefibre spanning from 800 nm to 1800 nm [35]

Where $C_R$is Rayleigh scattering coefficient varying with of 0.7-0.9 (dB/km)-μm^4 and Rayleigh scattering dominated loss is quantified between 0.12-0.16 dB/km and is denoted by α_R . Figure 2.8 shows the loss vs. wavelength plot for SSMF, suggesting low loss telecom windows at 1.3 μm to 1.7 μm. Special fibres like highly non-linear ones (HNLFs) with a high concentration of dopants have an attenuation of up to 1 dB/km. Further, that ultraviolet and infrared absorption are severe in silica-based fibres and come within intrinsic material losses. UV and IR absorption are related to electronic and vibrational resonances associated with specific molecules within silica fibres, contributing ~0.03 dB/km attenuation loss in silica-based fibre in the wavelength range from 1.3 μm to 1.6 μm.

Overall, fibre attenuation strongly depends on wavelength. The low-loss transmission window is defined by Rayleigh scattering infrared intrinsic absorption and water absorption. Modern SSMFs have two transparency windows around the water peak with a loss of ~0.3 dB/km around 1310 nm and ~0.2 dB.km around 1550 nm. It is located in the second and third telecom windows of O-band and C-band.

2.3.2 Chromatic Dispersion

Another one of the most practical limitations in optical fibres is chromatic dispersion. It stems due to the frequency dependence of the refractive index $n(\omega)$ of optical fibre [47]. Due to the impact of chromatic dispersion, spectral components of a traveling optical pulse propagate at different speeds given by $\frac{c}{n_g(\omega)}$,where c is speed of light and $n_g(\omega)$ is dependence of frequency ω on refractive index n_g. It causes spreading or broadening of a propagating pulse also known as group velocity dispersion (GVD). GVD broadens signal pulse which limits propagation of the optical envelope for long transmission length in SSMF [47]. The group velocity of different spectral components expressed as equation 2.17

$$v_g = \left(\frac{d\beta}{d\omega}\right)^{-1} \tag{2.17}$$

Where $\beta(\omega)$ is the frequency-dependent propagation constant and can expand as a Taylor series expansion shown as 2.18 [30].

$$E(z,\omega) = E(0,\omega)e^{(-i\omega t)}e^{\left(\left[-\frac{\alpha}{2}+i\beta(\omega)\right]z\right)}$$

$$\beta(\omega) = \beta^{(0)} + \beta^{(1)}(\omega-\omega_0) + \frac{1}{2}\beta^{(2)}(\omega-\omega_0)^2 + \frac{1}{6}\beta^{(3)}(\omega-\omega_0)^3 + \cdots \tag{2.18}$$

Where, $E(z,\omega)$ is the optical field measured at fibre length z and propagating at radial frequency $\omega, \beta(\omega)$ is the propagation constant of optical spectral tone $\omega, \beta(1/km)$ is a constant phase shift $\beta(ps/km)$ is the group time delay,$\beta^2(ps^2/km)$ is broadening, which relates to the optical chromatic dispersion $D_c(ps/km\ /nm)$ coefficient as:

$$\beta^{(2)} = -\frac{\lambda^2}{2\pi c} D_c \qquad 2.19$$

and $\beta^3 (ps^3/km)$ is known as third-order propagation constant, also related to dispersion slope.$S\ (ps/km/\ nm^2)$

$$S = \frac{4\pi c}{\lambda^3}\beta^2 + \left(\frac{2\pi c}{\lambda^2}\right)^2 \beta^3 \qquad 2.20$$

The standard value of chromatic dispersion in SSMF ranges around $16 ps/km/nm$. SSMF has a dispersion slope of $0.08 ps/km/nm^2$. And can significantly increase over large bandwidth (higher than 10 nm) with a longer propagation distance. The higher-order ($\beta^{(3)}$:3rd, $\beta^{(4)}$:4th order) dispersion generally has insignificant effects in C+L optical bands and is often ignored, although over large bandwidths become dominant [48]. The inverse of group velocity is $\beta^{(1)}$ as shown in equation 2.17 , whereas $\beta^{(2)}\ and\ \beta^{(3)}$ are known as second and third order dispersion parameters and dominated pulse broadening in optical fibres.

The spectral broadening of an optical pulse in a dispersive media with a pulse width of $\Delta\omega$ expressed as equation 2.21

$$\Delta T = \frac{dT}{d\omega}\Delta\omega = \frac{d}{d\omega}\left(\frac{L}{v_g}\right)\Delta\omega = L\frac{d^2\beta}{d\omega^2}\Delta\omega = L\beta_2\Delta\omega \qquad 2.21$$

The temporal spread generally expressed in wavelength ($\Delta\lambda$)

$$\Delta T = \frac{d}{d\lambda}\left(\frac{L}{v_g}\right)\Delta\lambda = LD\Delta\lambda \qquad 2.22$$

Where D is the dispersion parameter defined in ps/(km-nm) unit, L is the length of optical fibre, and $\Delta\lambda$ is the bandwidth of the source channel. Equation 2.23, also known as the walk-off factor, shows the spreading of different wavelength components due to dispersion in optical fibres. Zero dispersion in optical fibres is related to $\beta^{(2)} \approx 0$ when no pulse broadening is present. This is also known as zero-dispersion wavelength or zero dispersion frequency. ZDW plays a critical role in maintaining phase synchronism important for four-wave mixing (FWM). For nonlinear FWM devices such as FOPA, ZDW is an essential parameter for fibres employed as the parametric gain medium. Silica-based single-mode fibres (SMF) have a ZDW around 1300 nm. They are available within 1300- 2000 nm by controlling fibre core radius via optical fibre fabrication with a smaller fibre core radius [49]. The ZDW can be shifted to a longer wavelength, for example, to C-band for HNLFs through decreasing core radius and increasing refractive index difference $(n_{co} - n_{cl})$ and via suitable doping of silica [50].

2.3.3 Fibre Birefringence and Polarisation Mode Dispersion

A linearly polarised electric field can have a different orientation of propagation in x $(\overrightarrow{E_x})$and y $(\overrightarrow{E_y})$ direction. Single-mode fibre, therefore, supports two modes of orthogonal polarisations. In an ideal isotropic fibre, the polarisation maintains the same propagation constant $\beta_{x,y}$. Single mode fibres suffer from birefringence, which stems from non-symmetrical core circularity. Additionally, birefringence also arises from externally induced stress originating from fibre bending and physical movements [51]. Both polarisation modes β_x and β_y propagates with different phase velocity within the SMF. Modal birefringence is expressed as B_F which exhibit difference in phase velocity and expressed as equation 2.23 as a difference of two polarisation states to the frequency.

$$B_F = \frac{\beta_x - \beta_y}{\omega} \tag{2.23}$$

An incident optical pulse will retain its polarisation through fibre propagation when traveling via one principal axis. On the other hand, incident pulse polarized at an angle with the principle axes passes through various polarisation states. Such wave faces a superimposition of orthogonal modes with different phase velocities leading to phase retardation between them. The phase change is given as $\Phi(z) = (\beta_x - \beta_y) \times z$. The length $L_B = {}^{\lambda}/_{B}$ is called the beat length covering all possible phases of polarisation state, i.e., $\Phi(L_B) = 2\pi$. After one beat length, the SOP becomes symmetrical for the input optical pulse.

2.3.4 Light propagation in optical fibres

As discussed in previous sections, as light or modulated light propagates through optical fibre it undergoes various impairments in the linear regime. With lower power, linear impairments dominate over non-linear impairments. Fibre attenuation (loss), chromatic dispersion, and polarisation mode dispersion are present are linear impairments. Kerr-induced nonlinear impairments come into play with the high signal power propagation within fibres. Generalized light wave propagation in single-mode optical fibre shown as Equation 2.24 [52]

$$\frac{\partial A}{\partial z} = -\frac{\alpha}{2}A - \frac{j}{2}\beta_2 \frac{\partial^2 A}{\partial T^2} + j\gamma|A|^2 A \tag{2.24}$$

The equation is known as nonlinear Schrodinger equation (NLSE), where A defined as the varying amplitude of propagating light envelope T is time measured in a frame of reference moving with a pulse, group velocity v_g . Fibre distance and attenuation coefficient are defined by z and α , the nonlinear coefficient written as γ. Right-hand side terms of eq. 2.24 described as fibre attenuation, dispersion, and nonlinearity of the propagating optical pulse.

2.4 Kerr nonlinearities in optical fibres

Nonlinearity in optical fibres significantly impacts optical transmission performance for future high-capacity optical networks using higher launch powers and high cardinality signals [53]. Nonlinear response in fibre arises due to higher-order terms of electric susceptibility $\chi^{(2)}$, $\chi^{(3)}$ etc. Terms combined as a nonlinear power vector $\vec{P}_{NL} = \varepsilon_0(\chi^{(2)}\vec{E}\vec{E} + \chi^{(3)}\vec{E}\vec{E}\vec{E} + \cdots)$. $\chi^{(2)}$ Susceptibility is nonzero in materials with inversion symmetry. SiO_2, which is the bulk material of silica-based fibres, has $\chi^{(3)}$ susceptibility. SiO_2 is a symmetric molecule, and $\chi^{(2)}$ susceptibility is zero for symmetric molecule materials. Therefore, second-order susceptibility in optical fibre does not have any effects. Hence, nonlinear contribution in optical fibres originates from the third-order electric susceptibility $\chi^{(3)}$, known as third-order nonlinearity [52].

The Kerr effect in optical fibre stems from refractive index modification in the presence of a substantial incident light wave [52], expressed as equation 2.25.

$$n = n_0 + n_2|E|^2 \tag{2.25}$$

Where n_0 is the weak field refractive index, $|E|^2$ is optical intensity inside the optical fibre and n_2 is the nonlinear refractive index coefficient which related to $\chi^{(3)}$ is given as equation 2.26.

$$n_2 = \frac{3}{8n_0}Re(\chi^{(3)}) \tag{2.26}$$

Four waves combined in third-order nonlinearity. This intermixing generates nonlinear effects like self-phase modulation (SPM), cross-phase modulation (XPM), and four-wave mixing (FWM). When *E* as optical intensity consists of multiple frequency components, and two them for example $\omega_1$and ω_2, cause together with modulation of refractive index at frequencies $\pm\omega_1 \pm \omega_2$ or modulates its phase in the case of SPM. SPM induces spectral broadening of optical pulses due to nonlinear phase shift (NPS) and XPM occurring between two different waves and induces nonlinear coupling and originated nonlinear crosstalk to the coupling between adjacent waves.

2.4.1 Nonlinear Scattering Effect

In section 2.4, nonlinear elastic effects as SPM and XPM, having no energy exchange between the optical field and the medium. In this section, inelastic nonlinear effects in which the optical field transfers a part of its energy to the medium are explained. Stimulated Raman scattering (SRS) and stimulated Brillouin scattering (SBS) are two main inelastic nonlinear effects and can have a crucial impact on optical fibre propagation containing a high-intensity optical field. Both SRS and SBS principally occur in Raman and Parametric amplification process [52]. The main difference

between SBS and SRS is that stimulated Raman scattering stimulated via transfer of energy between higher energy photon to lower energy photon occurs between different silica molecules, and optical phonons participate within this energy transfer process. Whereas, in the stimulated Brioullin scattering process, energy transfer between photons occurs with the participation of acoustic phonons to facilitate inelastic energy transfer. Raman scattering demonstrates a significant frequency shift leading up to around 30 THz [30].

In contrast, Brioullin scattering has a smaller frequency shift within the GHz range. Also, SBS is a unidirectional process and occurs as reflected energy, while the SRS process is a bi-directional process. The Stokes waves generated in non-linear processes travel bi-directionally for the SRS effect. At the same time, SBS Stokes waves travel unidirectionally at higher frequencies to the pump [52].

2.4.1.1 Stimulated Brioullin Scattering (SBS)

SBS generates a narrow band gain (located at approximately -10 GHz away from the pump [52]); this can be utilized for narrowband filtering (Brillouin amplification) [54], [55]. SBS is also considered a limitation factor, especially in parametric amplification [54], as it limits the maximum pump power injected into the parametric gain fibre by reflecting the maximum pump energy. The Stokes intensity of reflected backscattered light propagates exponentially with the below relation as shown in eq. 2.27 [52]

$$\frac{I_s(0)}{I_s(L_{eff})} = exp\left(\frac{g_B L_{eff} P_0}{A_{eff} - \alpha L}\right) \quad 2.27$$

Where effective length is $L_{eff} = \frac{1}{\alpha}[1 - exp(-\alpha L)]$, and $P_0 = I_p(0)A_{eff}$ and A_{eff} known as an effective core area of optical fibre. It limits the maximum power injected as P_{th} is threshold power that injected into the fibre within the SBS interaction linewidth Δv_B(this interaction range is typically from 20 to 100 MHz) as shown in equation 2.28

$$P_{th} = \frac{21kA_{eff}}{g_B L_{eff}}(1 + \frac{\Delta v_p}{\Delta v_B}) \quad 2.28$$

A_{eff} is the effective core area of the fibre, $L_{eff}$is the effective length of the fibre and Δv_p is the pump linewidth and k is the coefficient between 1 and 2 depending on polarisation or birefringence. Figure 2.9 shows reflected power due to SBS effect conducted in simulating software VPI transmission maker demonstrating optical fibre output power and reflected SBS power as a function of the input power from a CW laser propagated through 50km of SSMF, where the effective core area of fibre was $A_{eff} = 80e^{-12}m^2$, SBS gain coefficient $g_B = 4.6 \times 10^{-11}\, m/W$, CW laser linewidth $\Delta v_p = 1Hz$ and value of absorption $\alpha = 0.2\ dB/km$. For lower CW laser power (<-10 dBm), the reflected light is dominated by Rayleigh scattering, which is a constant

portion of the forward power. For an increased power range from -5 dBm to 5 dBm, the backscattered light becomes dominated by SBS, which manifests as growth in the reflected intensity as a function of the input CW power. For very high laser power >5 dBm, the output power within the fibre saturates and reflects all the excessive input power. Overall, SBS limits scaling of non-linear phase shift $\Phi = \gamma$ (PL) and subsequently the achieving maximum FOPA gain in silica fibres.

Several approaches were used to mitigate SBS or specifically to disrupt acoustic stokes wave propagation along fibre length via amending the shift in Brillouin frequency v_B longitudinally. This shift is introduced by a longitudinal variation of temperature [56], strain [57], core radius [58], or varying dopant concentration [59]. However, mentioned techniques are not sufficient for suppressing SBS and increasing the threshold required for high pump power in large broadband FOPAs. One of the successful techniques is known as pump dithering, by which pump linewidth v_p is broadened by phase modulating the pump [15]. Multiple phase modulating tones are used to increase SBS threshold increasing it by ~20 dB. The related disadvantage of boarding pump linewidth is adding noise and creating signal fluctuations degrading signal quality [60].

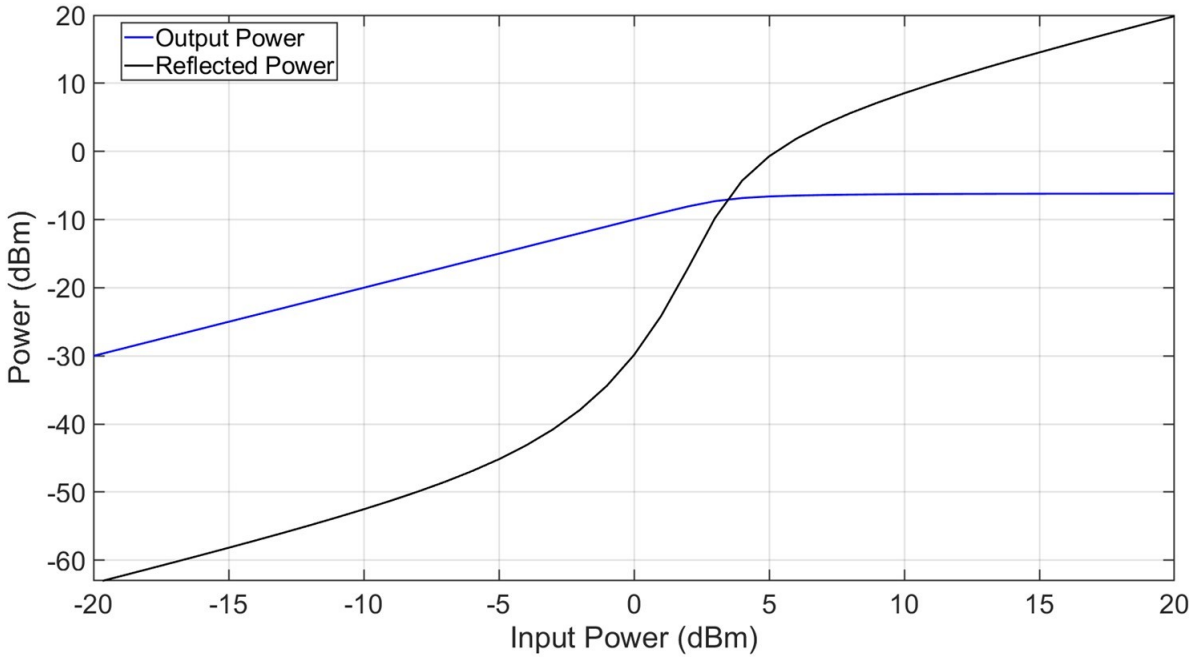

Figure 2.9 Simulated Brioullin scattering (SBS) effect in 50 km SSMF simulated by VPI Transmission Maker

2.4.1.2 Stimulated Raman Scattering (SRS)

The phenomenon of stimulated Raman scattering (SRS) is attractive to amplify modulated signals via Raman amplifiers. Due to SRS, the Raman gain peak is spectrally located at approximately 13 THz from a Raman pump [60]. Inherently, the SRS effect is swift and has a fast response time in silica fibres [61].

Figure 2.10 shows simulated Raman Gain spectrum conducted by simulation software VPI Transmission maker in 100 km SSMF with backward Raman pump at 1455 nm. Raman gain coefficient (g_r) was 0.37 $W^{-1}km^{-1}$ and the probe signal peak was at 1600 nm. Raman gain is not flat inherently due Raman gain coefficient of the fibre, the power, and the spectral width of the Raman pump [62]. Raman gain is not flat inherently and has a small gain peak at 13 THz from the pump. However, the Raman gain spectrum is broadband and potentially can span up to 30 THz. Achieving flat Raman gain generally involves a gain flattening filter (GFF) similar to EDFAs or requires multiple Raman pumps at a different wavelength for increasing gain spectrum flatness [63] [64].

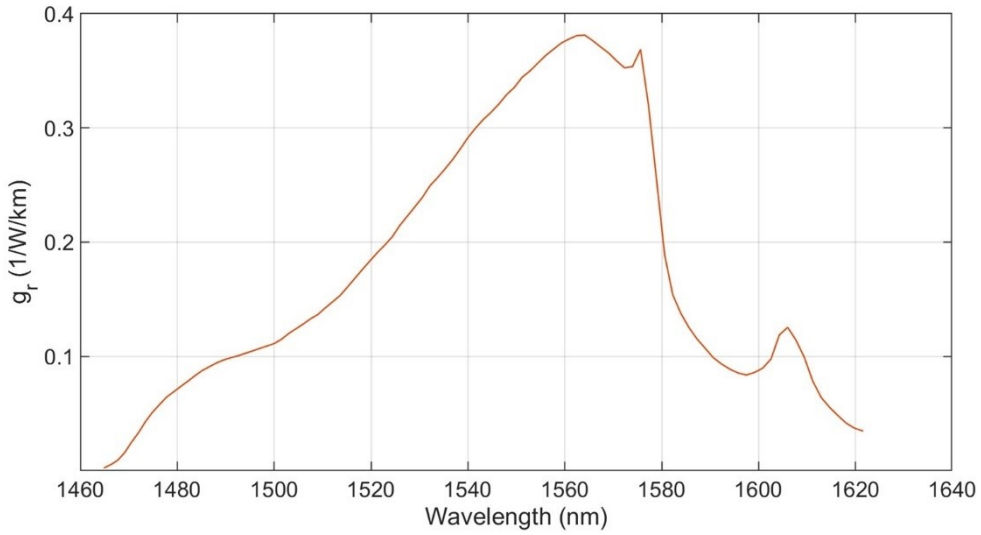

Figure 2.10 Raman gain coefficient in 100 km SSMF with backward Raman pump at 1455 nm simulated by VPI-Transmission-Maker

The complex Raman susceptibility introduce the effect of SRS on optical fibre in the frequency domain $\tilde{\chi}_R^{(3)}(\Delta f)$ acting as Fourier transform of the delayed Raman response, which is normalized as $\tilde{\chi}_R^{(3)}(\Delta f) = 1$. Figure 2.10 shows imaginary Raman susceptibility $\tilde{\chi}_R^{(3)}$ in silica fibre, the real part is detailed in [65] and not simulated in this work. The imaginary part of Raman susceptibility $Im\left(\tilde{\chi}_R^{(3)}(\Delta f)\right)$ is responsible for power transfer between frequency components (Raman gain).

In wideband FOPAs, SRS effects triggered by high power pumps intermix with parametric and Raman gain [65]. High pump powers for parametric amplification invokes Raman gain within parametric gain fibres observed at a longer wavelength and adds up with a parametric gain. For significant signal gain, Raman and parametric phase-matched gain ($\exp(2\gamma P_z)/4$) differ in the scaling of the gain coefficient by $f_R Im\left(\tilde{\chi}_R^{(3)}\right)$ and have a fixed shift by 6 dB. The Raman fractional strength f_R can be as high as ~0.3 and typically is ~ 0.18 [66]. Phase matched parametric gain peak compared with Raman gain peak is 2-3 times higher for frequency detuning of >5THz and

peaks at ~13 THz away from the pump. For broadband FOPAs with >10 THz bandwidth real part of Raman susceptibility $Re\left(\tilde{\chi}_R^{(3)}\right) = 1$ can also affect FOPA gain spectrum.

2.5 Performance Characterisation Parameters

Performance analysis of optically transmitted and the detected signal is generally done by various methodologies. In this section, a brief overview of signal performance methods employed in this work is discussed. The most common and accurate performance analysis method is the Bit Error ratio (BER) or bit error rate measurement calculated as a ratio of the detected number of errors of the received bits over the total number of bits transmitted. Bit by bit error detection is performed via bit error testers generally inbuilt in optical receivers. Advanced high cardinality and special modulation formats require offline digital signal processing (DSP) techniques to calculate the BER performance of the signals. For example, in this work, BER for optically amplified and detected burst mode signals calculated via offline signal processing developed for bursty signals enabled with threshold detection and compensation techniques. Analytically BER calculation is performed using the equation below as a function of the Q factor $\left(Q_{eff}\right)$ [35]

$$\text{BER} = \frac{1}{2}\text{erfc}\left(\frac{Q_{eff}}{\sqrt{2}}\right) \tag{2.29}$$

$$Q_{eff}(dB) = 20\log_{10}\left[\sqrt{2} \times erfcinv(2 \times BER)\right] \tag{2.30}$$

The Q factor is defined as the mean value ratio to the standard deviation, which is equivalent to the signal-to-noise ratio (SNR). Q-factor can also be represented as Gaussian distribution beyond a given decision threshold and expressed in terms of the complementary error function:

$$Q = \frac{(\mu_1 - \mu_0)}{(\sigma_1 - \sigma_0)} = \sqrt{SNR} \tag{2.31}$$

$$Q(x) = \frac{1}{2}erfc\left(\frac{x}{\sqrt{2}}\right) \tag{2.32}$$

Where $\mu_{1,0}$and $\sigma_{1,0}$ of the Q factors are the mean value and standard deviation of marks and spaces, respectively.

2.5.1 Noise Figure

Another system performance method specifically related to optical amplifiers is known as noise figure (NF). Noise Figure (NF) is identified as the ratio between input signal to the output signal for an optically amplified system, it determines the addition of noise within the amplified signal and is given as equation 2.33:

$$NF = \frac{SNR_{in}}{SNR_{out}} \quad 2.33$$

Further, the noise figure is measured in the optical and electrical domains. The pre-amplified and amplified signals are detected by a photodetector and converted into an electrical signal, or pre-amplified and amplified signals are measured via an optical signal analyser in the optical domain. Both scenarios impacted SNR before and after amplification with random noise measure noise addition on the signal.

SNR_{in} and SNR_{out} are identified as below [30] equation 2.34 and2.35:

$$SNR_{in} = \frac{P_{in}}{2hv} \quad 2.34$$

$$SNR_{out} = \frac{G^2 {P_{in}}^2}{[S_e(f,v) + \eta^{-1} S_{shot}]} \quad 2.35$$

where P_{in} is input signal power, h is universal Planck's constant, v frequency of the signal, and η is quantum efficiency determining the number of photons. Output signal to noise SNR_{out} have additional parameters, including S_{shot} shot noise from photodetector and G is signal gain where $S_e(f,v)$ is the spectral density dependent on optical frequency v and baseband frequency f .Using 2.34, 2.35 and substituting in equation 2.33, generalized noise factor can be written as below equation

$$NF_{tot} = \frac{S_e(f,v) + S_{shot}}{2hvG^2 P_{in}} \quad 2.36$$

For optical noise figure addition of shot noise induced from PD is neglected identified as below

$$NF_{opt} = \frac{2\rho_{ase}}{Ghv} \quad 2.37$$

where ρ_{ase} is known as ASE spectral density. For electrical domain detected signal to noise, figure measurement was performed using equation 2.36. The minimum noise figure level of 3 dB in optical amplifiers is generally referred to as quantum-limited noise level. Quantum limited noise level is defined by the minimum noise addition in the signal from inherent sources like thermal noise, spontaneous emission of excited atoms in optical amplifiers, and intensity noises. It generally arises from electrical amplifiers employed in transmitters and detectors, dark current, and shot noise. For example, in EDFAs, NF is equal to 3 dB when the net gain provided by the EDFA is large ($G \gg 1$) ,and reached below <3 dB as the EDFA gain approaches the no gain state ($G \to 0$) [7]. Phase-sensitive amplifiers can potentially demonstrate noise figure levels below quantum-limited 3 dB values and reach up to 0 dB NF [67]. Phase-sensitive FOPA with ultralow noise figures was recently shown experimentally [68].

Chapter 3 OPTICAL AMPLIFICATION IN EXTENDED REACH ACCESS NETWORKS

TABLE OF CONTENTS

All-optical communication network architectures, including long-haul (undersea and terrestrial), metro (core), and access networks, require optical amplification after a certain length of transmission to overcome the loss in signal power [69]. Transmitted signals suffer from power loss due to attenuation in optical fibres dependent on wavelength and are proportional to the length of transmission fibre, as discussed in Chapter 2 section 2.3.1. For example, signal transmission at 1550 nm over 100 km will attenuate the signal power by 20 dB with ~0.2 dB/km of attenuation factor in current low loss SSMF. Optical amplifiers, irrespective of the type, provide several advantages over previous electric signal regeneration. These include energy-efficient, transparency towards WDM, bit rate, modulation formats, and protocols including low noise figures, colourlessness, and further.

The recent advancement in state-of-the-art single-mode fibres with significant nonlinearity coefficient, modern doping of rare earth materials like ytterbium and bismuth, and accurate dispersion management with around near-zero dispersion slope in the conventional transmission windows (i.e., C, L band) have significantly improved the advanced amplifier designs [70]–[72]. Advanced optical amplification technology has enabled the transmission of >terabit optical data over large bandwidths in hundreds of kilometers to trans-oceanic distances [73].

Progress in optical access networks has enabled low-cost optical data transmission to connect multiple users. Access network architectures, for example, passive optical networks (PON) topology, have advanced recently from 2.5 Gbps PON to XGS-PON (10G PON)[74], transmitting 10 Gbps optical data symmetrically. Future access networks are envisaged to optically transmit ~100 G, including the potential of ultra-dense TWDM-PON [75]. Currently, the reach of generic PON architecture is limited to 20 km, mainly due to power budget availability and signal broadening due to chromatic dispersion [8]. Although the introduction of extended reach, access network architecture increased the distance of connectivity from traditional 20 km to 100 km [13] and more. ITU-T G.984.6 reach extension PON recommends two possible ways for GPON reach extension approaches: optical-electrical-optical conversion (OEO) and optical amplification(OA) as an in-line extender [76]. Coherent access networks are another technology enabling a high capacity reach extended access network. However, its practicality is dependent on the equipment (receiver) cost and handling burst mode signals through coherent receivers [77]. Optical to electrical to optical (O-E-O) conversion provides a reasonable low-cost solution for access networks for reach extension, although it is not scalable due to its compatibility with WDM signals [78] and bandwidth restrictions to support wideband access network transmission wavelengths.

Overall, the optical amplifiers provide multiple features to regenerate high-capacity optical data within the optical system architecture and with reach extension in PON. Optical networks differ in architecture, power budget, modulation formats, and transmission types. For example, access networks have bi-directional topology to support downstream and upstream data with a different kind of multiplexing technology obtained and prepared to transmit at distinct wavelengths (non- burst and burst traffic in C and O-bands) [79]. Therefore, it becomes a necessity to have a suitable optical amplifier employed for reach extension. Some critical features of optical amplifiers are:

- high gain
- small gain variations
- transparent towards signal modulation
- broad spectral bandwidth
- low coupling loss
- high conversion efficiency (electrical to optical)

Optical amplifiers are diversified into many different categories depending on the applications and technologies. This work focuses on employing optical fibre amplifiers in RE- PON (access network) comparing doped (i.e. erbium) fibre amplifier, discrete Raman amplifier, and Semiconductor Optical Amplifier already demonstrated as in- line amplification in access networks. The primary candidate of this work is Fibre Optic Parametric Amplifier (FOPA), discussed in detail. A brief overview of reach extended PON is discussed in section 3.1 with access network architecture and features required for an optical amplifier as an in-line amplifier. Discussion on various optical amplifiers is presented from section 3.2 to section 3.5, including SOA, EDFAs, Raman amplifiers, and FOPA focusing on design, working principle, and transient behaviour observed in EDFA and Raman amplifiers. The fibre optic parametric amplifier (FOPA) is described in detail, concentrating on its ultrafast response time and development on polarisation-independent FOPA in section 3.6.

3.1 Reach Extended Access Networks

In this section, I will explain generic access network architecture for point to multipoint distribution. Further, discussion on reach extended optical access links with in-line optical amplification is also described in section 3.1. In the later part of this section, different existing optical amplification technologies are discussed already demonstrated for extended reach access networks. Optical amplifier response towards burst mode signal amplification is discussed in this section analytically.

Optical amplification could provide two primary credentials in a reach extended access network:

- Enhanced link power budget (splitter power budget)
- Reach extension

Figure 3.1. shows typical bi-directional access network architecture with a 20 km feeder link reach [80]. Optical Line Terminal (OLT) connected to a metro ring acting as a downstream non-burst signal transmitter with a burst upstream receiver connected via optical fibre trunk. Optical power splitter distributes signal power via drop fibre cables from splitter output to different services, such as households, business towers, data centres, radio networks, etc. The downstream signal is broadcasted in a Time-division multiplex (TDM) protocol to all customers connected over the access link. The upstream traffic from the different customers is transmitted in burst mode employing time-division multiple access (TDMA) protocol in varying durations and periods. ITU-T standards define transmitting and received powers for downstream (DS) and upstream (US) traffic in standard 20 km PON link [79]. Power levels of upstream and downstream signals include fibre attenuation, splitter insertion loss (17 dB@1:32 splitter), and other passive link losses. Downstream (DS) signal is transmitted from wavelength 1480- 1500 nm, while upstream signal (US) in burst mode transmitted in O-band from wavelength 1260-1360 nm [81].

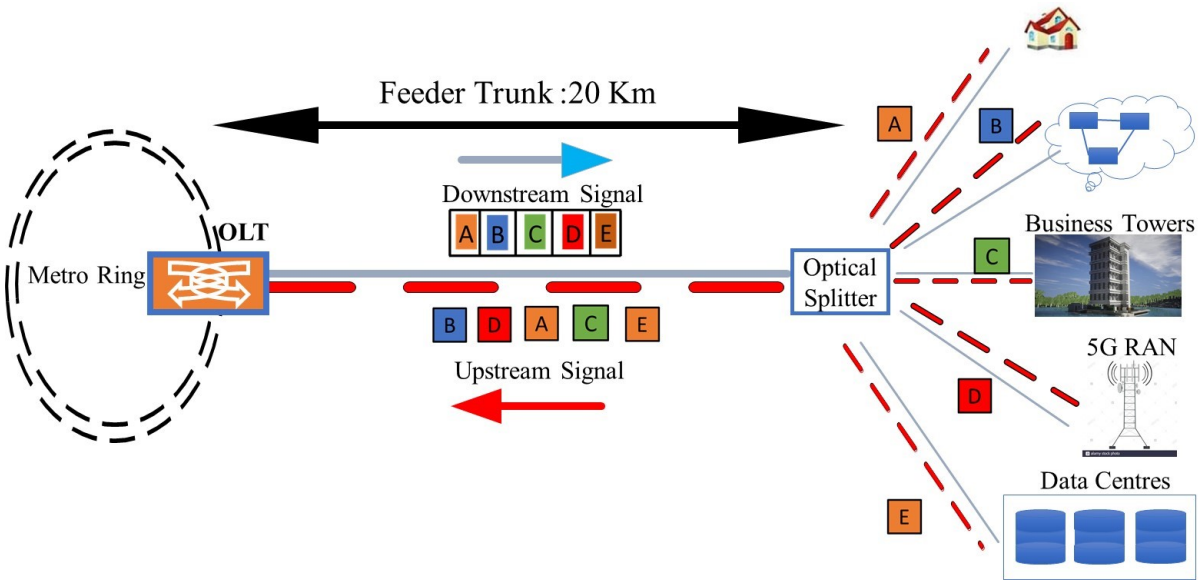

Figure 3.1 Standard 20 km GPON point to multipoint architecture showing downstream broadcast packets and upstream TDMA data packets from different users

Figure 3.2 shows a schematic of long reach (LR) access network architecture employed with an optical amplifier for bi-directional signal amplification demonstrated in [5]. Local exchanges consolidating metro and access are bypassed and replace multiple exchange nodes by an optical

amplifier explained in [5]. Therefore, employing an optical amplifier increases the reach of access links beyond 20 km by ~100 km via improving the overall link power budget of bi-directional signals [13]. This architecture converges metro and access via reducing local exchange with optical amplifiers minimizing operational cost [5]. With optical amplification reach, extended access networks can regenerate signal power without changing the properties of the signal like modulation format, bit rate, and bandwidth of the signal post-amplification, or it can be said that no signal grooming occurs within this process. Recent progress within various published work demonstrate employing state-of-the-art fibre amplifiers, including SOA in extended reach PONs [82]–[84]. Conventional optical amplifiers suffer from issues like slow response time for burst signal amplification, low signal gain, and low output signal power [12]. SOA's are demonstrated as pre-amplifiers at customer transmitters to amplify the upstream signal at O-band wavelength [85]. Erbium-doped amplifiers are used as in-line or booster amplifiers to reach extended PON in [12]. ITU-T G.984.6 recent recommended progress shows a Raman amplifier for downstream PON signal [76].

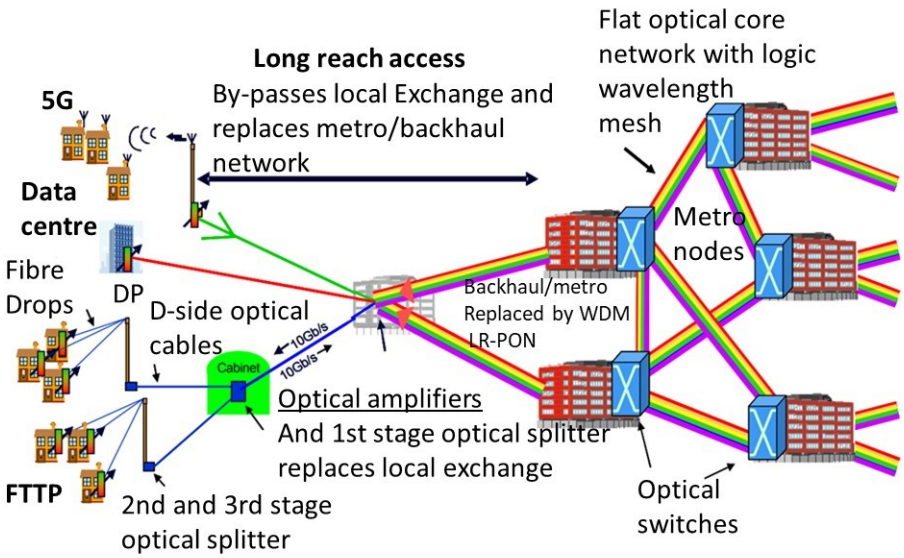

Figure 3.2 Optically amplified reach extended access network architecture showing the consolidation of Metro +Access optical network layer [5]

Overall, in a reach extended access network, in-line optical amplifiers should comply with some important features to accommodate network requirements:

- support bursty traffic amplification
- gain on arbitrary wavelengths
- high output signal power
- high gain
- wide dynamic range

- transparent to TWMD protocol

3.2 Semiconductor Optical Amplifiers

Semiconductor optical amplifiers (SOA's) are the first practical optical amplification technology outside the silica-based (optical fibres) optical amplification technology. The principle of operation of SOAs is similar to semiconductor laser structure [86], and hence they are also known as semiconductor laser amplifiers (SLA). The SOA semiconductor waveguide acts as a gain medium, working without any optical feedback to avoid lasing, where the amplified signal always travels in a forward direction. The schematic in Figure 3.3 presents a basic SOA structure, an active region that provides excited electrons via electrical driving current across the SOA. The SOA resembles a Fabry- Perot cavity structure but with suppressed reflections from the end facets to provide single-pass amplification of the signal. Anti-reflection coated mirrors generally suppress the reflection with reflectivity <0.1%, and SOA acts as a traveling wave or a single-pass amplifier.

Signal amplification in SOA occurs with the recombination of electrons and holes at the p-n structure of the semiconductor waveguide [86], acting as the gain medium. Like another optical amplifier, an external optical pump laser source is not used to excite electrons in SOA's. Instead, it is done electronically via applying external current. SOA's are packaged in a "butterfly" arrangement and are very compact. Significant characteristics of SOAs are small size and direct electrical pumping. Commercially available off-the-shelf SOA's have an average gain of <15 dB within 3 dB bandwidth with a peak gain up to ~20 dB but have low output powers at ~14 dBm [87]. An exciting feature of SOA is that amplification is available on multiple wavelengths ranging from 1200-1650 nm, covering almost all bands of telecom window (although each specific semiconductor device has a limited bandwidth up to ~80 nm) [88].

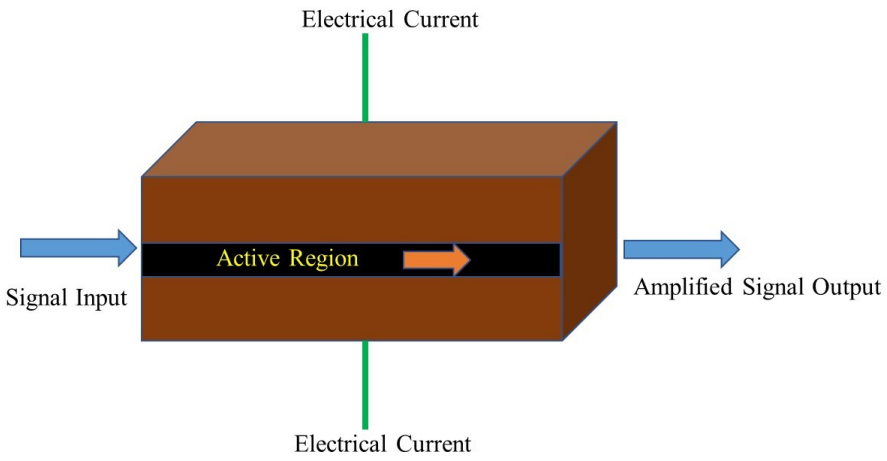

Figure 3.3 Schematic of standard semiconductor optical amplifier (SOA)

SOA's response time is fast, almost equivalent to a bit length in the picosecond range [89], and therefore it is suitable for amplifying burst signal transmitted as upstream traffic. Another major limitation of SOAs is known as the patterning effect [89] or inter-symbol interference. The patterning effect arises in SOA due to long carrier recovery lifetimes of electrons acting as a gain medium. When amplifying high bit-rate signals with high input signal powers in SOAs, the electrons get quickly drained by a large signal gain by the leading bits within the signal. High-speed burst signal (e.g., 10 Gbps) suffers from these patterning effects when amplified by SOA due to the slow recovery process of semiconductor structures within SOA [90]. Therefore, SOA's in reach extended access links transmitting high-speed signals are not suitable for amplification. Also, semiconductor amplifiers are limited for high output power signals and have a limited linear regime of signal gain operation [91].

SOAs suffer from channel crosstalk when amplifying WDM signals [92]. Fast response time of SOAs related to the very short lifetime of injected carriers in the order 100 ps trigger inter- channel crosstalk due to cross gain modulation in WDM channels amplification [93], [94]. Hence operating SOA in saturation is recommended to avoid crosstalk. Another drawback of SOA is the high noise figure. Stimulated noise generation associated with the stimulated emission process increases the noise figure of SOA's. In addition to ASE residual back reflections at the cavity, facets degrade the noise figure increasing insertion loss to the input signal. Noise figure for typical SOA is 3 dB greater than that of erbium-doped fibre amplifiers varying between 8- 10 dB. Figure 3.4 shows the ASE spectrum measured from a commercial SOA at input and output ports.

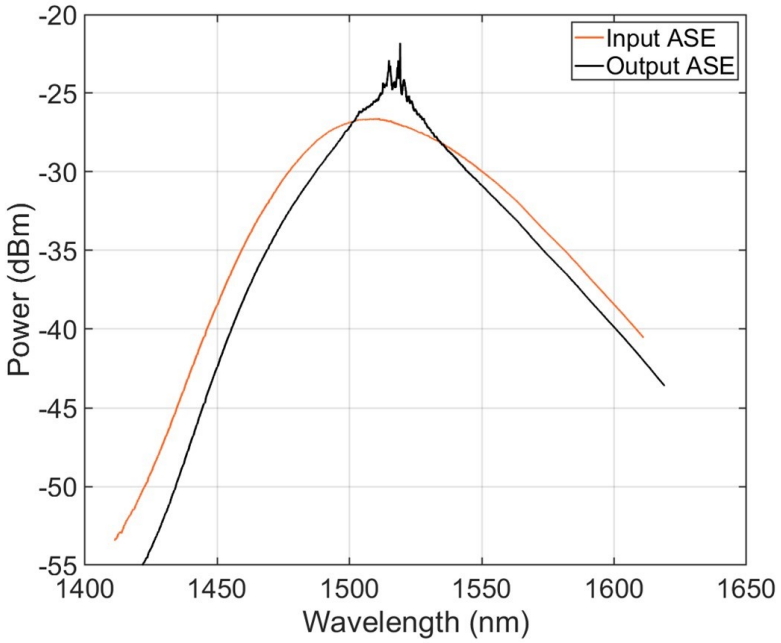

Figure 3.4 Commercial SOA ASE spectrum measured at input and output of the SOA

The SOA demonstrates essential features like a large signal amplification window, fast response time, and compact size. There are though significant drawbacks for modern optical communication include the patterning effect for high-speed signals, crosstalk, polarisation sensitivity, and high coupling loss. However, these drawbacks have been reduced by using different approaches, but still not on par with modern fibre amplifier technologies in WDM communication. The other application employed by SOA is wavelength conversion, optical switching, and optical detection. Research is still on for SOA with recent demonstrations as wideband high gain SOA operating in the SCL band [95].

3.3 Erbium-Doped Fibre Amplifiers

One of the most mature and widely deployed optical amplification technologies is erbium-doped fibre amplifiers (EDFA) in current optical communication sub-systems. A silica core optical fibre doped with erbium ions (Er^{3+}) acts as the gain medium. The emission spectrum of Er^{3+} spans in C-band within the low loss telecom window of modern optical communication networks.

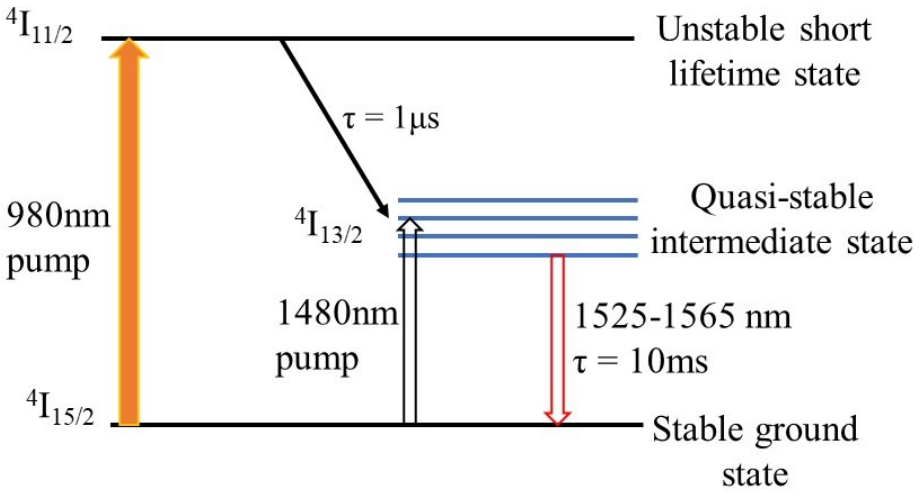

Figure 3.5 Schematic of energy level transition of Er^{3+}in EDF at pump wavelengths of 980 nm and 1480 nm

EDFA working principle is a three-level system, with an underlying principle of stimulated emission process occurring inside erbium-doped fibre gain medium [33]. The pumping scheme in EDFA is usually emitted around a chosen wavelength of 980 nm or 1480 nm. The energy translation process between the ground and excited states is shown in Figure 3.5 for Er^{3+}ions in EDF. When EDF is pumped at a lower wavelength of 980 nm, the transfer of ground energy state electrons to an excited state occurs to an unstable energy state. Excited electrons at higher energy levels are unstable and rapidly decay with around 1 μs decay time to a lower mid-level energy state. The transition from a short lifetime state to an intermediate state creates a quasi- stable

energy level with a lower energy level. Pump at 1480 nm wavelength directly excites Er^{3+} and transfer to a steady ground energy level state with a more significant decay time of 10 ms releasing photons. This longer decay lifetime significantly converts the high ground state population to the quasi-stable state, allowing stimulated amplification. Stimulated amplification occurs via a transfer of Er^{3+}back to ground level, emitting photons in the C-band window (1525- 1565 nm). The incident signal between 1525-1565 nm will face amplification via absorbing this emitted photon. A 980 nm pump is employed to excite Er^{3+} ions far away from signal wavelengths in C-band. Pump location far away from the signals provides low noise figure by decreasing pump to signal noise transfer. Low noise figure EDFAs nearing quantum level NF level of ~3 dB are designed using 980 nm pumps [96]. Although this scheme is not efficient in providing significant EDFA signal gain but valuable for low noise EDFA, 1480 nm pumps provide significant EDFA gain related to large population inversion of Er^{3+} ions.

3.3.1 Basic EDFA configurations

Since the first EDFAs in the late 80s [97], designs of erbium amplifiers improved over the period. Current EDFA amplification is available for operation in C and L bands covering around 95 nm of telecom bandwidth [98]. Discussing the basic configuration of EDFA consisting of a suitable wavelength of the pump (980 nm and 1480 nm) is shown in Figure 3.6. The gain medium is EDF with a typical length of 10~30m, a WDM coupler used to combine pump and signal source. The pump wavelength is related to noise performance and gain. For significant signal gain, pumps at both 980 nm and 1480 nm are employed in EDFAs.

EDFA pumping scheme is essential and can implement in three different methods such as a co-propagating pump (forward), counter-propagating pump (backward), and bi-directional (co+counter propagation) concerning the signal direction of propagation. Figure 3.6 shows a forward pumping scheme, for example, with a 980 nm pump scheme. Isolators are placed to protect both signal and pump sources from creating damage. The first isolator at input protects the signal source from pump back-reflections. Similarly, the isolator placed after EDF prevents pump wavelengths from propagating with the signal at the output.

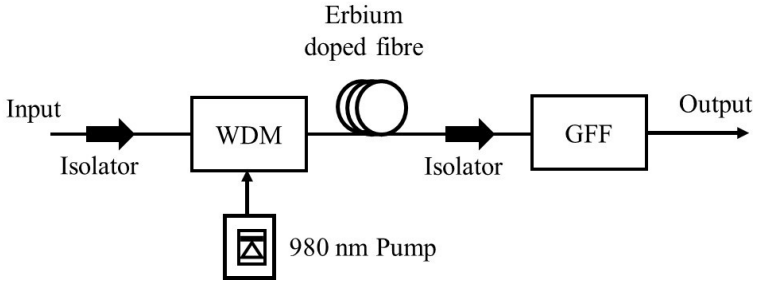

Figure 3.6 Schematic diagram of EDFA configuration with a single-stage gain medium in forwarding pumped with a 980 nm wavelength

As inherent EDFA gain spectrum is not flat and a gain flattening filter (GFF) is employed for getting a flat EDFA gain spectrum as shown in schematic Figure 3.6. Using a GFF is quite helpful for amplification of WDM channels to avoid gain variation between multiple channels. As discussed above, two pump wavelengths are employed as a pump source in EDFA. 980 nm was providing low noise penalty addition and configured in the forward pumping scheme [99]. On the other hand, a longer wavelength pump at 1480 nm has improved pump efficiency [99]. Simultaneous pumping configurations with 980 nm and 1480 nm pumps were employed for EDFA at different inversion levels. A 980 nm pump, with a low inversion level, allows the best noise figure, whereas pumping at 1480 nm provides the best pump efficiency with more gain is achieved. Gain flatness across the gain bandwidth optimized via cascading multi-stage EDFAs with two or more than two pumps [100], [101].

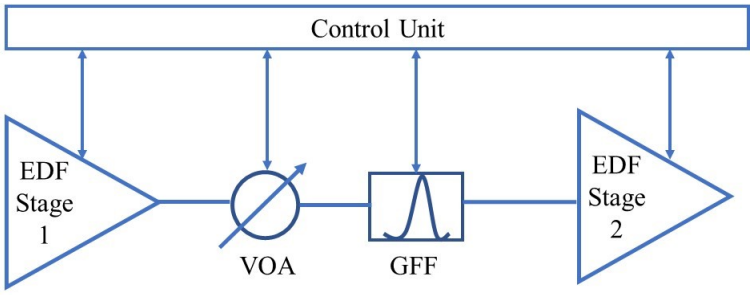

Figure 3.7 Diagrammatic representation of variable gain EDFA for WDM application

Figure 3.7 presents a dual-stage variable gain EDFA, including a pre-amplifier stage-1, main amplifier stage-2, mid-stage VOA, and gain flattening filter. The Control unit monitors the pre-amplifier output power from the EDF stage-1 and, following VOA, sets attenuation to control the total gain of the pre-amplifier. A flattening filter is employed to optimize and minimize the gain variation between the WDM channels amplifier via the previous stage. Final amplification is provided via EDF stage 2 to optimize the WDM comb. The advanced control unit provides automatic pump power adjustments, also known as automatic gain control, to protect sudden power surges or transient effects[102]. Efficient noise figure performance over different gain values is controlled via the careful design of EDF length and pump powers [103].

State-of-the-art EDFA typically provides 20-30 dB signal gain with an EDF length of ~10m. Available input pump powers determine output signal powers, and typical EDFA saturated output power varies between 17-20 dBm. Specific EDFA gain bandwidth is 35 nm (~4THz) around 1550 nm range from 1528~1565 nm. EDFA amplification is present in the L-band of the telecom spectrum from 1570~1603 nm with total EDFA bandwidth of ~33 nm. The extended bandwidth of EDFAs in the C and L-band makes them more attractive for wideband amplification. Although, around a 5 nm gap between C and L band gain bandwidth creates an issue of extended gain

bandwidth EDFAs. This trench between the C+L band establishes a requirement of 5- 8 nm non-erbium amplification between two rounds [104].

Two significant fundamental limitations with EDFA are amplified spontaneous emission (ASE) and transient effects related to stimulated emission. ASE noise accumulates over EDFA and degrades the signal-to-noise ratio (SNR), degrading the amplifier performance. EDFA placement in optical links is carefully designed to avoid ASE accumulation and avoid saturating the amplifiers. Another inherent fundamental degrading effect arises from the electronic transfer process in EDFAs. Transient in EDFA is discussed in detail in section 3.3.2.

3.3.2 Transient effect in EDFA's

Erbium-doped fibre amplifier had become an amplifier of choice to amplify the signal in various optical communication networks. EDFA presents attractive features like low insertion loss, polarisation insensitivity, and excellent operational performance in the C+L band of the telecom band [105]. However, EDFA suffers from an inherent limitation of slow response time observed for time-varying signal amplification [106]. Gain dynamics of EDFA were studied extensively [107] and established that quiet response time in doped erbium fibre can last over milliseconds to a microsecond time scale [108]. Population inversion of Er^{3+} ions leads to a transient effect in erbium-doped amplifiers. Incident pumps excite Er^{3+} ions, elevating from a low energy level state to an unstable short lifetime energy level for a short period. From a non-radiative excited state, electrons decay to an intermediate metastable state with a non-radiative decay time of around 1 μs. All excited electrons at quasi-stable intermediate state experience population inversion from an excited state to a non-excited state with a stimulated emission of photons. This transition leads up to >1 ms. Hence, an ample inversion time leads to create a slow response time for stimulated emission of Er^{3+} ions. Analytical study of transient effect in EDFAs presented by a rate equation model described in [109]. Generally, EDF is treated as a lumped model block that is not dependent on longitudinally propagating transient saturation.

Effect of slow response time in EDFA signal amplification is observed both for WDM and non- WDM type signals, for example, bursts or packet signals [110]. Upstream traffic in PON is bursty in respect to TDMA protocol, as discussed in section 3.1. Reach extension access networks employing EDFA as an in-line amplifier must support amplification of burst signals in combination with non-burst signals for bi-directional transmission [14]. Hence in this section, I will discuss the EDFA transient effect in burst mode signals.

A numerical model of dynamic EDFA based on two-level system analysis is described in [109]. A three-level system consisting of a 980 nm pump is very unstable and has radiative decay of excited ions to metastable level within 1 μs. For Er^{3+} ions populations densities N_1 *and* N_2

demonstrate lower and upper excited state densities. Therefore, rate equation of upper energy level at fibre location z and time t is given as

$$\frac{\partial N_2}{\partial t} = -\frac{N_1}{\tau} - \sum_i \frac{u_k}{h v_k A} \frac{\partial P_k}{\partial z} \quad 3.1$$

Where, $P_k = P(\lambda_i, z, t)$ is the optical power of input channel k at a wavelength $\lambda_k = c/v_k$ and erbium core effective area $A = n b_{eff}{}^2$ at EDF length z and time t. Solving equation 3.1 for signal power for exciting state level N_2 provide

$$\frac{\partial P_k}{\partial z} = u_k \Gamma_k [\sigma_e(\lambda_k) \cdot N_2 - \sigma_a(\lambda_k) \cdot N_1] \cdot P_k \quad 3.2$$

Equation 3.2 denoted a doped fibre propagation equation representing a static erbium-doped amplifier, where Γ_k is overlap factor between erbium ions and input optical power distribution over the length of erbium gain fibre. Any time and wavelength-dependent amplification function $G_k = \frac{P_{out}}{P_{in}}$, where G_k is signal gain for k^{th}number channel , and $P_{in} and\ P_{out}$ is input and output signal power. EDFA signal gain, therefore, is represented as:

$$P_{out} = G \cdot P_{in} \quad 3.3$$
$$where\ G = exp\big(\big[\Gamma_k\big(\sigma_e(\lambda_k) + \sigma_a(\lambda_k)\big) \cdot (\rho(t)/A) - \Gamma_k\, \sigma_a\,(\lambda_k) \cdot\ N_{dop} \cdot L\big]\big)$$

Equation 3.3 shows EDFA gain as a function of emission σ_e and absorption σ_a parameters at signal wavelength λ_k. $\rho(t)$ is Er^{3+} ions reservoir at the metastable state, and A is cross section area, where N_{dop} , L is doping level and fibre length. Including ASE noise power P_{ASE} result in modelling EDFA dynamic gain behaviour:

$$\rho(t) = -\frac{\rho(t)}{\tau} - \sum_i \frac{P_i^{in}(t)}{h v_i}[G_i(t) - 1] - \sum_{ASE}\left(4 n_{sp} \Delta v_{ASE} + \frac{P_{ASE}^{in}(t)}{h v_{ASE}}\right)[G_{ASE}(t) - 1] \quad 3.4$$

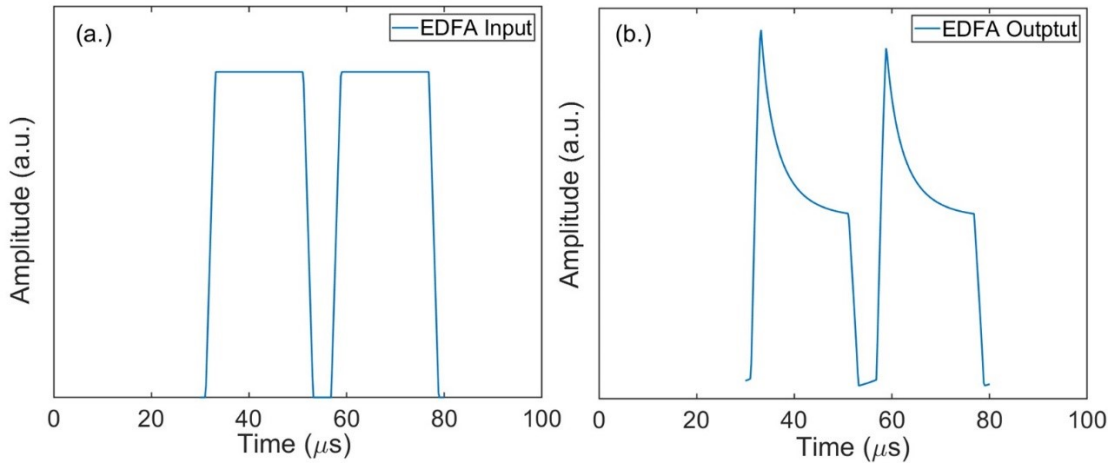

Figure 3.8 VPI modeled EDFA transient effect on 20 μs 10 Gbps OOK burst signal, shows (a) input burst signal before EDFA and (b) output burst signal after EDFA amplification

summation inside the equation 3.4 serves ASE self-saturation, EDFA gain dynamic behaviour is the inclusion of EDFA doped fibre propagation equation, including reservoir of excited ions. Signal power is denoted by P_{in} and gain by $G_i(t)$.

Figure 3.8 shows the transient effect on a burst signal amplified by EDFA simulated through a VPI transmission maker. 10 Gbps OOK input burst signal at 20 μs duration amplified by 20 dB with a dynamic EDFA model. Input burst signal with the 20 μs duration launched to a dynamic EDFA, distorted bursts amplified by EDFA received at the output shown in Figure 3.8(b) amplified by the EDFA model. Bits present at the beginning of the bursts suffer from overshoot, with almost no steady-state achieved within 30 ms. For EDFA dynamic model length of EDF was $L = 10m$, $Er^{3+}\tau = 10ms$ lifetime and pump power $P_p = 100mW$, forward pump wavelength is $\lambda_{P(Fwd)} = 1480\,nm$ and $\lambda_{P(Bck)} = 980\,nm$. Input 10 G burst signal wavelength was at $\lambda_{sig} = 1535\,nm$ with input signal power at $P_s = 0dBm$.

EDFA vulnerability towards burst signal amplification numerically presented in Figure 3.8 (b). Transient effects are severe in saturated EDFAs but observed with low severity at lower signal EDFA gain, especially for burst (packet) type signals [111]. Multiple approaches are employed to suppress transient effects in EDFAs, such as automatic gain control, gain feedback loop, and power shaping [112]. Although the slow response time is inherent, artificially and completely overcoming transient in EDFA is impossible.

Slow response time was also observed within WDM add-drop signal amplification in EDFA's similar to the packet signal amplification [113]. Multi-wavelength optical networks with wavelength routing employ EDFA as optical repeaters to amplify WDM channels. Add and drop of channels occurs in this scenario, which suffers from sudden power excursion observes EDFA transient effects on surviving channels.

3.3.3 Mitigation techniques of EDFA transient

Multiple transient suppression techniques were investigated to mitigate the effect of slow response time in EDFA signal amplification. Well-known techniques are [114]: addition of a dummy signal to maintain the saturation level of EDFA signal gain and reduce gain fluctuations; electronically compensate by a feed-forward scheme known as EFF consisting of a photodiode and electrical amplifier to add proportionally a current to the pump with the input signal: an optical feedback loop consisting of a filter and a variable attenuator equalizes losses and EDFA gain on the lasing wavelength; using spectral hole burning to shape the gain spectrum with optical feedback and a saturable absorber for suppression; dual-cavity optical feedback including dual cavity optical feedback with different wavelengths; gain clamping technique, with electronic feed-forward and optical feedback to clamp power surges.

Above all mentioned techniques, the two most employed techniques were all-optical feedback loop control and automatic gain control [115], [116]. EDFA transient control is done optically by operating an amplifier in a ring laser configuration. Amplified spontaneous emission (ASE) generated at the output of the EDFA is optically feedback to input to the EDFA in a loop configuration. Lasing is controlled by selecting wavelength by filtering and attenuating, and finally reinjecting to the input.

The feedforward and backward electronic gain control method is widely used; signal gain is optimized in a feedback loop controlling power fluctuations by leveling EDFA gain. Feedback is taken before or after the amplifier to equalize the gain requirement. Although the AGC method shows limitations to suppress transient to very short burst durations like in nanosecond scale, it depends on the electronically implemented system. A dummy distributed feedback laser source is used to create a saturated signal to pre-compensate signal overshoots due to transient effects[82]. Power shaping with a combination of electrical and optical control schemes is investigated by which input signal power control could provide transient control [117]. Very fast EDFA for burst mode operations are available commercially for transient free operation but only operate within a few nanometres of C band wavelength currently [106], with suppression limited to low power excursions only.

3.4 Raman Amplifiers

Raman amplification stems from stimulated Raman scattering (SRS), an inelastic process to transfer strong pump energy to signal frequency. In this scattering process, high-energy photon loses their energy to create a lower energy photon, and the energy difference between photons appears in the form of a phonon. This process occurs at a downshifted frequency relative to pump frequency. Material absorption triggers energy transfer from the pump to signal, and optical phonon created due to energy absorption by the material discussed briefly in Chapter 2 section 2.4.1.2. SRS effect is dependent on material property and varies accordingly to provide a different Raman gain spectrum.

In Figure 3.9, an incident pump photon (ω_P) on a medium excites a molecule towards a higher energy state (virtual energy state). Decay in excited molecule energy emits a signal photon (ω_S) in the process. Response of Raman amplification process in very fast ~76 fs [52], in comparison to EDFA response time of ~10ms. The downshift from pump frequency is determined by the vibrational energy of the molecules. This feature makes Raman gain available at any signal wavelength with the required proper selection of pump wavelength. Stokes waves generated through the SRS process propagate both in counter and co-propagating directions with the

incident pump beam [52]. The shift in stokes wave relative to pump is $(\omega_P - \omega_S)$ and shape of Raman gain spectrum is dependent on vibrational energy state of molecules.

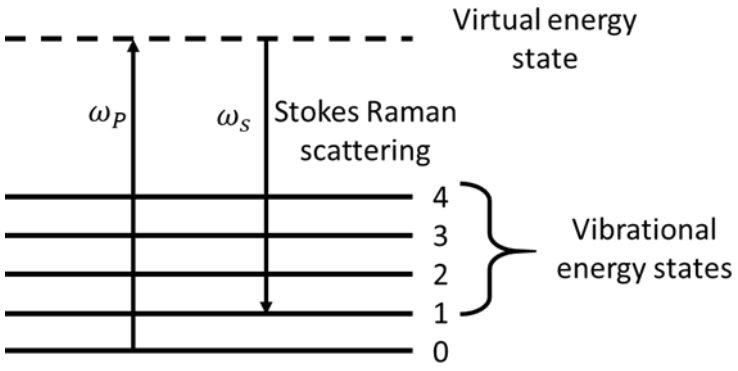

Figure 3.9 Schematic presentation of stimulated Raman scattering process

Polarisation-dependent Raman gain strongly impacts signal gain as Raman gain is polarisation-dependent [118]. Gain fibre employed as Raman gain medium is long in lengths and varies randomly in polarisation. Therefore, depolarized Raman pumps are used to suppress polarisation dependency. Therefore, Raman fibre amplifiers work pretty differently than EDFA. Raman amplifiers are classified into two types: Distributed and Discrete Raman fibre amplifiers. The classification is dependent on their application and choice of fibre types.

In this work, I will primarily discuss discretely or lumped Raman fibre amplifiers. As later, it is employed as an in-line drop-in amplifier for a reach extended access network experimental demonstration.

3.4.1 Discrete Raman amplification

Lumped or discrete Raman fibre amplifier (DRA) provides amplification at a discrete point in a transmission line using a section of gain fibre and high-power pump operating at a wavelength of choice. The type of Raman amplifier could be employed as an in-line amplifier. Similar to the EDFA, amplification is confined to provide net gain within this section of gain fibre medium. A basic schematic of discrete Raman amplifier using a length of Raman gain fibre and backward pump combined via a WDM is shown in Figure 3.10.

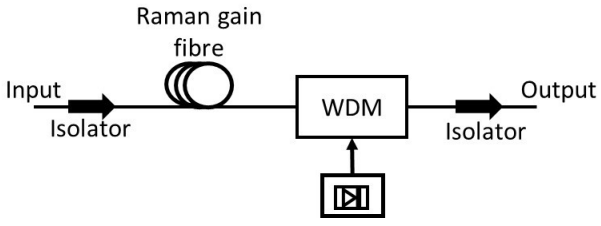

Figure 3.10 A schematic representation of a discrete Raman amplifier

Over EDFA, Raman amplifiers have many benefits, including arbitrary gain bandwidth, flexible gain spectrum control, and many others. Lumped Raman amplifiers are safer as the high pump energy does not propagate in transmission fibre and the signal compared to distributed Raman amplifiers in which pump and signal travel within the transmission fibre line. Choice of fibre gain medium is essential and dependent on gain coefficient and attenuation of gain fibre [119], [120]. In Figure 3.11 gain coefficient (g_r) value against frequency (THz) from [121], demonstrate Raman gain coefficient with respect to 1450 nm pump. Highly non- linear fibre (HNLF) have highest Raman gain coefficient (g_r) of 6.3 with lowest gain coefficient (g_r) of SMF is 0.43 $W^{-1}km^{-1}$, respectively. Although this should be noted that DCF and HNLF have highest attenuation of 0.7 and 0.6 dB/km at 1550 nm. Standard SMF and IDF have lowest attenuation of ~ 0.2 dB/km.

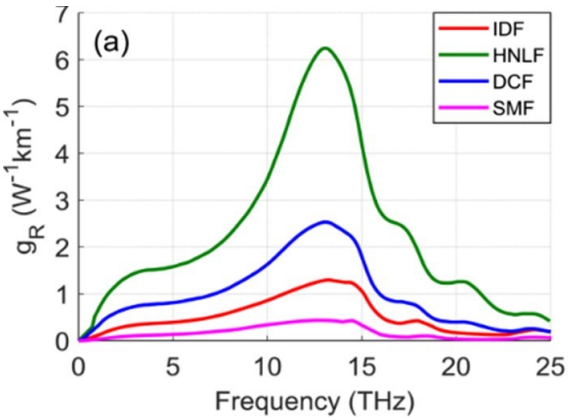

Figure 3.11 Comparison of Raman gain coefficients for IDF, HNLF, DCF, and conventional standard SMF[121] presented by Raman gain spectrum

Discrete Raman amplifiers require higher pump powers to generate high Raman gain. Invoking additional Kerr nonlinearities like inter/Intra channel crosstalk degrading the overall system performance. Nonlinear impairments are compensated by employing proper pump power and by using advanced DSP [122]. (Double) Rayleigh backscattering and lasing (back-reflection) are also limitations when the higher pump power is employed for Raman amplifiers. It is considered one of the limiting factors for high gain in discrete Raman amplifiers [123].

Pumping in Raman amplifiers could employ forward (Signal – Pump co-propagating), backward (Signal -Pump counter-propagating), and bidirectional methods. Each pumping method provides its advantage, for example, a low noise figure in forwarding pumping observed and a lower pump to signal crosstalk in a backward pumping scheme. Another limiting factor observed in both distributed and discrete Raman amplifiers is the transient effect related to amplifier engineering [124]. This topic is discussed in the next section, 3.4.3.

3.4.2 Distributed Raman Amplifiers

Distributed Raman amplifier is another Raman amplification technique where the signal is amplified along with the transmission fibre. Ideally, intrinsic loss of the fibre is counter-balanced at different points by this amplification process. No additional unique gain fibre is required for pumping, making it a more attractive choice than other amplification technologies. Distributed Raman amplifiers were employed in long-haul fibre networks since the 1980s [125], but later, with the development of high power, EDFAs were replaced in the early nineties. With the advances in distributed Raman amplification and availability of high-power Raman lasers, the efficiency of distributed Raman amplification was advanced over the period and demonstrated its presence in high capacity long-haul undersea and terrestrial transmission systems [126], [127].

Distributed Raman amplification provides an improvement in SNR in comparison to discrete amplifiers like EDFAs. Signal SNR does not get degraded over the length of transmission fibre as supported by continuous amplification, whereas; discrete amplification is performed after attenuation.

3.4.3 Transient effects in discrete Raman amplifiers

Raman amplifiers have been proposed and demonstrated in a reach extended access network architecture as an in-line amplifier [128]. Recently ITU-T G.9807.2 has been proposed using a Raman amplifier in an extended-PON [76], an example schematic shown in Figure 3.12. A distributed Raman reach extender is shown as a pre-amplifier located in the central office to amplify bi-directional signals. Both discrete and distributed Raman amplifiers are proposed as an in-line amplifier for reach extender amplifiers [129], [130]. It is also demonstrated in a bi-directional amplification of simultaneous upstream and downstream signals via Raman amplification [129].

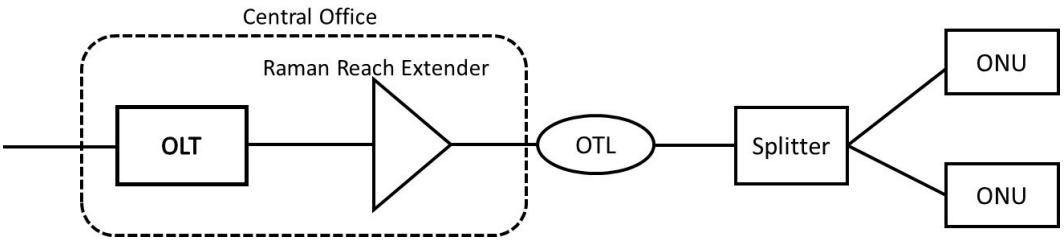

Figure 3.12 Schematic representation of Raman reach extender in PON architecture as per ITU-T G.984.6 [74] with optical line terminal (OLT), optical transmission line (OTL), and optical networking unit (ONU)

However, the ITU-T specification suggests the employment of burst mode (BM) to continuous mode (CW) equipment before Raman amplification in upstream signals. One of the limitations with Raman amplifiers in RE-PON is to amplify upstream burst signal as reach extension

amplifier [131]. In backward pumped discrete and distributed Raman fibre amplifiers, counter-propagation of signal and pump suffers from propagational delay within the long lengths of Raman gain mediums amplifying time-varying signals. Due to longer lengths, the signal's propagation time within the amplifier becomes proportional to the length of the fibre, suffering a longer transition time for a signal after amplification. Additionally, the pump wave also suffers a longer propagation time, similar to the signal. Another critical reason for observing transient effects in Raman amplifier is that at high input signal powers, the leading signal bits achieve maximum gain, therefore draining the pump rapidly. In contrast, the following bits suffer from low pump energy [132]. Therefore, it suffers from a transient effect when propagation time exceeds the burst duration, also explained in detail in [133]. This effect is observed in both forward and backward pumping schemes in Raman amplification [134], including distributed Raman amplifiers [124].

Transient effects in Raman amplifiers have been studied theoretically and experimentally for add/drop channels, including burst mode amplification. I will discuss the transient impact in discrete Raman amplifiers when operated for single-channel amplification as described in [132] when a channel is propagated in burst mode(On-Off mode). For a single-stage backward pumped Raman amplifier, coupled equations for pump and signal propagation for Raman fibre is given as:

$$\frac{\partial P_P}{\partial z} - \tau_g \frac{\partial P_P}{\partial t} = \alpha_P P_P + g_r P_P P_S \tag{3.5}$$

$$\frac{\partial P_s}{\partial z} + \tau_g \frac{\partial P_S}{\partial t} = -\alpha_S P_S + g_r P_P P_S \tag{3.6}$$

Equation 3.5 and 3.6 describes the counter-propagating pump and signal in a single-stage backward pump Raman fibre amplifier. τ_g is total group delay in fibre also attributed as $\tau_g = \frac{1}{V_g}$ and α_P and α_S are fibre attenuation for signal and pump, respectively and g_r is Raman gain coefficient where P_P and P_s are pump and signal power. For backward pump and forward signal configuration $-, +$ are used as a notation for the direction of pump and signal propagation. The equations can be further solved for boundary conditions as shown in equation 3.7

$$\begin{gathered} P_s(L=0,t) = P_s(0,t) \text{ where } P_0, t < 0 \\ = P_1, t \geq 0 \\ P_{P(L=Z)} = P_{Pz} \end{gathered} \tag{3.7}$$

The solution for signal and pump can be derived via iteration method using equations 3.5 and3.6. Initially signal P_S part is neglected in equation 3.5 for finding pump power P_P and substituted in 3.6. After two iterations pump power P_P is derived as equation 3.8 which is exponent of pump attenuation α_P over fibre length $z = 0$, $z = L$

$$P_P = P_{PL} exp\,(\alpha_P(z-L) \tag{3.8}$$

$$P_S = P_{s0}\big(t-\tau_g z\big) exp\,(\Gamma z) \tag{3.9}$$

Equations 3.8 and 3.9 provide a solution for pump and signal propagation in backward pumped Raman amplifiers with

$$\begin{aligned} \Gamma = & -\alpha_s + g_s P_{pL} e^{-\alpha_P L} \frac{e^{\alpha_P z-1}}{\alpha_p z} \\ where, & e^{-\alpha_P L} \frac{e^{\alpha_P z-1}}{\alpha_p z} \approx L_{eff} \end{aligned} \tag{3.10}$$

$$\Gamma = -\alpha_s + g_s P_{pL} L_{eff} \tag{3.11}$$

Equation 3.10 is confinement factor Γ equivalent to signal attenuation in fibre α_s and nonlinear phase shift parameter governed by Raman gain coefficient g_s , pump power P_{pL} over fibre length and effective length L_{eff} is constant and will lie between 1 and 2 for most DRAs. It is rewritten as equation 3.11. Substituting equations from 3.7 to 3.10 into 3.5 provide

$$P_P = P_{pL}\, exp[G_P(z,t)] \tag{3.12}$$

$$\begin{aligned} G_P(z,t) &= \{\alpha_P(z-L) + e^{\Gamma(z-L)} \frac{g_P P_0}{\Gamma}, t \le \tau_g z \\ &= \{\alpha_P(z-L) - \frac{g_p}{\Gamma}\left[P_1\big(e^{\Gamma(Z/2+t/2\tau_g}\big) + P_0\left(e^{\Gamma\left(L-(z/2+t/2\tau_g)\right)}\right)\right], \tau_g z \le t \\ &\le (2L-z)\tau_g \\ &= \{\alpha_P(z-L) + \big(e^{\Gamma(z-L)}\big)\frac{g_P\, P_1}{\Gamma}, t \ge (2L-z)\tau_g \end{aligned} \tag{3.13}$$

Equation 3.12 has total pump power compared to the pump power over fibre length pump gain for length (z) and propagation time (t), where $G_P(z,t)$ shown in equation 3.13 is gain over Raman fibre for the propagation time derived for three boundary conditions of $t \le \tau_g z$, $\tau_g z \le t, \le (2L-z)\tau_g$ and $t \ge (2L-z)\tau_g$ as discussed in equation 3.13.

The above equation substituted to derive for signal power at $z = L$ we get presented in equation 3.14

$$P_{s\,(z=L)} = P_{s0}\big(t-\tau_g L\big) exp[G_s(t)] \tag{3.14}$$

$$
\begin{aligned}
where\ G_s = \{-\alpha_s L + g_s P_{pL} \int_0^L exp\left\{\alpha_P (z-L) + \frac{g_p P_0}{\Gamma} e^{\Gamma(z-L)}\right\} dz, t \le \tau \\
= \{-\alpha_s L + g_s P_{pL} \int_0^u exp\left\{\alpha_P (z-L) - \frac{g_P P_1}{\Gamma}\left(e^{\Gamma(t/2\tau_g - L/2)}\right)\right. \\
\left. + \frac{g_p P_0}{\Gamma}\left(e^{\Gamma(t/2\tau_g - L/2 + z - L)}\right)\right\} dz \\
+ g_s P_{pL} \int_u^L exp\left\{\alpha_p (z-L) + \frac{g_p P_1}{\Gamma}\left(e^{\Gamma(z-L)}\right)\right\} dz\ , \tau \le t \le 3\tau \\
= -\alpha_s L + g_s P_{pL} \int_0^L exp\left\{\alpha_p (z-L) + \frac{g_P P_1}{\Gamma}\left(e^{\Gamma(z-L)}\right)\right\} dz, t \ge 3\tau \\
where\ , u = 3L/2 - t/2\tau_g\ and\ \tau = \tau_g L
\end{aligned}
\tag{3.15}
$$

The set of equations from 3.12 and 3.15 provide analysis of transients in backward pumped Raman fibre amplifiers. Power excursion starts from $t = \tau$ and last up to $t = 3\tau$. For signal gain G_s, no gain fluctuation occurs when $t \le \tau$ for propagation time t is less than delay time τ . Transient in signal start occurring for propagation delay lies between $\tau\ to\ 3\tau$. Fluctuations reach maximum when propagating delay become greater than signal frequency component velocity $t \ge 3\tau$.

Figure 3.13 presents a numerical model of transient effects in a 30 μs burst signal for a discrete backward Raman fibre amplifier. Equations 3.5 and 3.6, used for transient effects analysis within the Raman amplifiers for burst signal amplification. Input square wave at typical 30 μs burst waveform at 10 kHz frequency used as an input signal is shown in Figure 3.13 (a). The parameters used for the model were Raman fibre length L_{eff} =6.5 km, pump power P_p was taken as 2.5 W, Raman gain coefficient value was g_r is 2.5 $W^{-1}km^{-1}$ and signal velocity delay τ_g is taken 0.1 ns for evaluation. The output burst waveform obtained as shown in Figure 3.13(b) have gain overshoot at the beginning of the signal and does not reach a steady state within the duration of burst propagation. The signal gain was fixed at 13 dB to compare results with experimental work. The acceptable result observed shows a narrow overshoot peak in Raman amplified bursty waveform. Numerical analysis was done similar to that in [132].

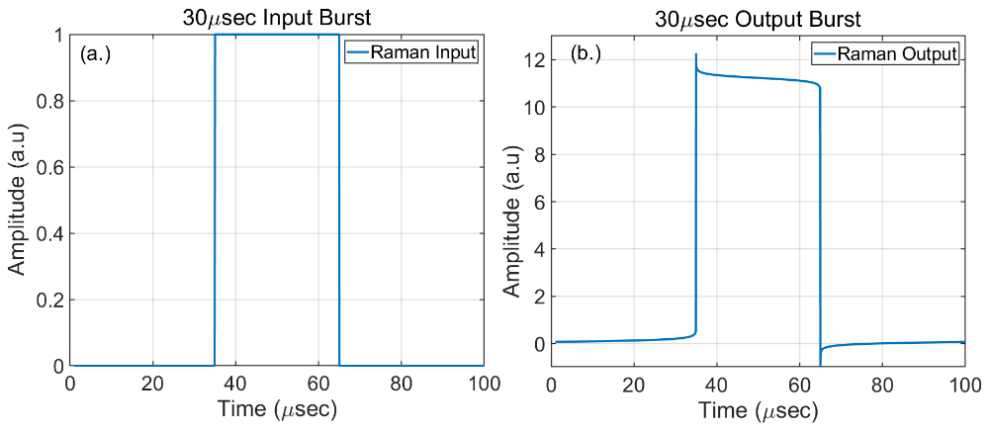

Figure 3.13 Numerical model of the transient in discrete Raman amplifier for 30 μs burst signal amplification at 13 dB net gain

3.4.4 Transient suppression in Raman Amplifiers

In section 3.4.3, I discussed the effects of the transient in lumped or discrete Raman amplifiers. Transient effects are observed in both discrete and distributed Raman configurations in amplification of burst mode and WDM type signals [135], [136]. In burst mode signals, transient effects with discrete Raman amplification were observed for counter-propagating pumps [136] with severe gain excursions.

Similar to the EDFA, different transient suppression techniques were proposed for Raman fibre amplifiers. One mainly discussed method is using an electronic feedback control mechanism using proportional integral derivative (PID) [124]. This method uses ASE generated during the Raman amplification process as a feedback parameter for scaling gain proportionally to level the gain fluctuations. The ratio of input power to output ASE is looped back to the input of the Raman amplifier, providing a reference for gain leveling. An example schematic of transient suppression in Raman amplifiers is shown in Figure 3.14. The feedback scheme uses a WDM splitter with a variable optical splitter (VOA) to reuse the input signal power as a feedback mechanism and hence maintain the gain levels.

Another suggested method is using short lengths of Raman gain fibre in the case of discrete Raman fibre amplifiers and, for example, using highly non-linear fibre with a significant Raman gain coefficient as a Raman gain medium. Short lengths of Raman gain medium reduce the propagation time of a signal and pump through the gain fibre length, therefore making the interaction time of pump and signal faster. It should be noted that the shorter length of the Raman gain medium makes transients faster. A forward pumping scheme could also be helpful for suppressing transient in discrete Raman amplifiers, although co-propagating pump and signal will increase the transfer of noise through the pump.

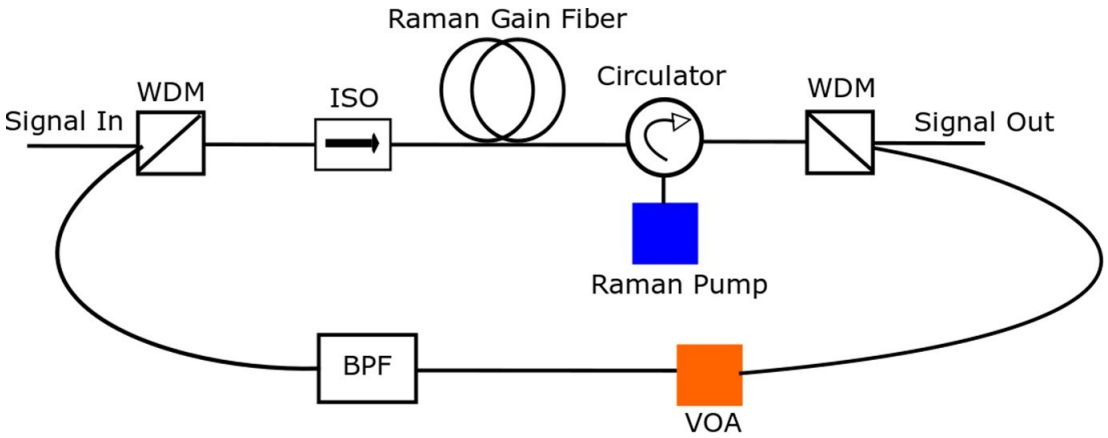

Figure 3.14 Gain clamped discrete Raman amplifier for transient suppression

3.5 Fibre Optic Parametric Amplifier

This section explains in detail the FOPA operating principle, parametric gain generation, and the emergence of the FOPA gain spectrum with its essential features exploiting the effect of third-order nonlinearity. Firstly, the FOPA ultrafast response time due to the underlying process of χ^3 nonlinearity in optical fibres is discussed in section 3.5.1. A generalized FOPA signal gain equation is explained based on the impact of the third-order nonlinear process with the conservation of momentum and energy via an exchange of pump power to signal, and it is conjugate. Also, the effect of SPM, XPM, and FWM is shown in the finally derived FOPA propagation equation in section 3.5.2. Later in the section, the FOPA gain spectrum in a single pump source is discussed with the effects of propagation wavevector $\beta^{(2)}$ & $\beta^{(4)}$ as dispersion in parametric gain fibre medium in sections 3.5.3 and 3.5.4.

3.5.1 Ultra-fast response in FOPAs

Ultrafast response time of FOPAs with sub-femtosecond levels $\ll 10fs$ [137] is the fundamental reason behind negligible transient effects in parametric signal amplification [18]. The non-resonant electron movement is fast in fused silica fibres [137], [138]. The lowest order nonlinearity obtained in optical fibres stimulates ultra-fast response time in parametric amplifiers. Silica-based optical fibres involve χ^3 non-linearity acting as a gain medium for parametric amplifiers. The ultra-fast response time of parametric amplifiers could be understood by discussing the energy transfer process related to the frequency within optical fibres. Optical Kerr effects in solids (glass) are extensively discussed as they are inherently known as the extensive bandgap dielectric material [139]. Band-gap energy E_g is of critical importance in determining response time of dielectric material as shown in equation 3.16:

$$\omega < \omega_g = \frac{E_g}{\hbar} \tag{3.16}$$

The above equation shows the relation between bandgap energy E_g of the dielectric material (i.e., silica in this case), ω_g is bandgap frequency and ω incident frequency, ħ is the universal Plank's constant. Response time in silica analytically can be calculated using equation 3.17 [139] as:

$$\tau_t = \frac{1}{|\omega_g - \omega|} = \frac{1}{E_g/\hbar - 2\pi f}, where\ \omega_g = \frac{E_g}{\hbar}\ and\ \omega = 2\pi f \quad 3.17$$

where $\tau_t$is response time equated as the difference between silica bandgap frequency ω_g and incident frequency as ω . Evaluated response time from equation 3.17 is estimated as 0.08 fs ~0.1 fs for frequencies f<600 THz based on silica bandgap energy E_g of 9 eV [138], [139]. Such a response time can be considered instantaneous for all modern telecom applications and makes FOPA appealing for implementation in bursty networks [18]. Figure 3.15 presents the estimated response time of silica against incident wavelength ranging from deep XUV to U-Band up to 3 μm.

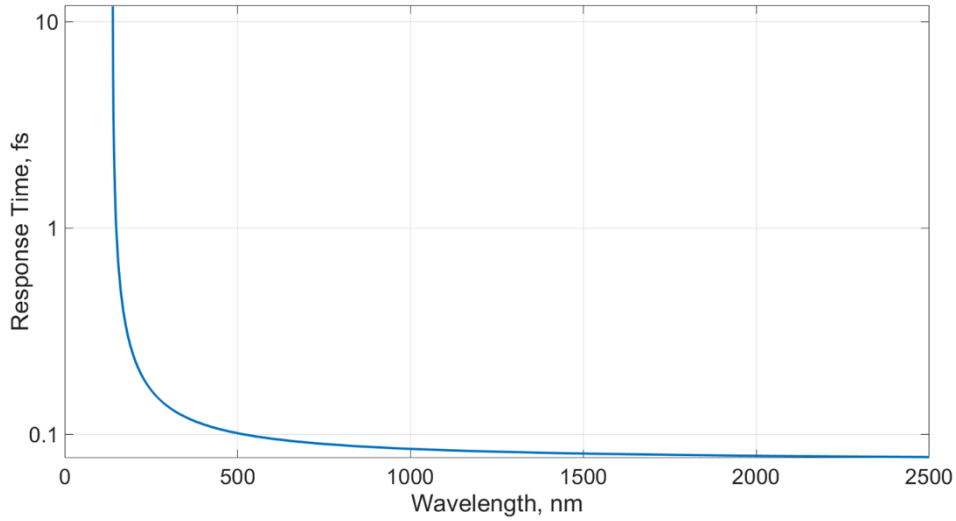

Figure 3.15 Theoretical response time τ of silica based optical fibre showing ~0.1 fs response time for wavelength range 0.5 μm-3 μm. Below <0.5 μm, the response time reaches 12 fs.

3.5.2 Propagation equation in FOPA

In this section, I will discuss the fundamental propagation equation involved in the parametric amplification process. A scalar case where all intermixing waves are linearly propagated through a non-linear medium is considered: the evolution of the non-linear process for the signal electric field through the non-linear medium. A simplified equation is obtained at the end of this discussion. Propagation equations in parametric amplification involve mainly two pumps, a signal wave and an idler wave which pave the foundation of FOPA analysis. I will discuss a simpler scalar case where $\chi^{(3)} \neq 0$ referenced from [140]. Equation 3.18 shows waves intermixing in a nonlinear regime involving additional terms on the right-hand side. Showing a combination of

three electrical envelopes (waves) in all possible combinations when superimposed is shown on the right-hand side of equation 3.18. $\chi^{(3)}$ presents third-order susceptibility of all combined waves considered equal for all participating waves. $K = n_0\omega/c$ is the propagation constant and $n_0 = \sqrt{1+\chi^1}$ is field refractive index at frequency ω.

$$(\nabla + K)^2 E = \frac{\chi^{(3)}}{c^2}\frac{\delta^2 E^3}{\delta t^2} \tag{3.18}$$

Third-order nonlinearity allows mixing up to four frequency components to the equation dependent on the frequency of each wave combined. A coefficient $B(z)$ added to the electric field shows the evolution of electrical field E in the presence of a nonlinear medium shown in 3.19.

$$E = B(z)\,\psi\,(x,y)\,exp\,(i\beta z - i\omega t) \tag{3.19}$$

In the general case, parametric amplification involves four frequency components of pumps, signal and idler. A real electric field E_Σ comprising waves of four single-frequency components, where E_k , where $k = 1 \ldots 4$ E_k is given by 3.20

$$E_\Sigma = \frac{1}{2}\sum_{k=1}^{4}[E_k + E_k^*] \tag{3.20}$$

Substituting equation 3.20 to equation 3.18 generates ${E_\Sigma}^3$ leading to 56 unique terms for evolution of the electrical field within the nonlinear medium. The resulting equation is expressed as unique terms only containing a frequency set of ω_1 of propagation envelope E_1 as equation 3.21

$$(\nabla^2 + K^2)E_{\,1} =$$

$$= \frac{\chi^{(3)}}{4c^2}\frac{\delta^2\left(3{E_1}^2E_1^* + 6E_1E_2E_2^* + 6E_1E_3E_3^* + 6E_1E_4E_4^* + 6E_2^*E_3E_4\right)}{\delta t^2} \tag{3.21}$$

Electrical fields $E_1E_xE_x^*$ have a similar resulting frequency as E_1 and get canceled having a similar exponential part. The term $E_2^*E_3E_4$ equates to $\omega_1 = -\omega_2 + \omega_3 + \omega_4$. The resulting terms on the right-hand side are only related to the frequency E_1 and therefore cause phase shift only to E_1. Therefore, a nonlinear effect of the term $E_1E_xE_x^*$ is called SPM, and a nonlinear effect of the terms $E_1E_xE_x^*$ $(x \neq 1)$ is called XPM. The final term $E_2^*E_3E_4$ describes the evolution of E_1 denoted as FWM. The detailed explanation is covered in [66], not reiterated in this work. Equation 3.21 leads to the sum of propagations involved in FWM, and the propagation constant mismatch $\Delta\beta$ and nonlinear coefficient γ are shown in equation 3.22 and equation 3.23

$$\Delta\beta = \beta_3 + \beta_4 - \beta_1 - \beta_2 \tag{3.22}$$

$$\gamma = \frac{3\mu_0\omega\chi^3}{8\,n_{eff}^2A_{eff}} = \frac{\mu_0\omega n_2}{n_{eff}A_{eff}} = \frac{\omega n_2'}{cA_{eff}} \tag{3.23}$$

where n_2 is the nonlinear refractive index coefficient, A_{eff} is the effective area of the mode and n_2' the nonlinear refractive index. Overall, the FOPA propagation equation describing the evolution of complex amplitude is given by

$$\frac{dA_1}{dz} = i\gamma\left(A_1|A_1|^2 + 2A_1\sum_{k=2}^{4}|A_k|^2 + 2A_2^*A_3A_4exp(i\Delta\beta z)\right) \quad 3.24$$

Equation 3.24 is a fundamental FOPA propagation equation describing third-order nonlinearity in complex amplitude A_1 out of four co-propagating frequency components. The effect of SPM as $A_1|A_1|^2$ on single frequency A_1 , XPM as $2A_1\sum_{k=2}^{4}|A_k|^2$ involving 2 frequencies A_1A_k with twice nonlinear effect and FWM as $2A_2^*A_3A_4exp(i\Delta\beta z)$ involving three frequency component $A_2A_3A_4$.The nonlinear coefficient γ depends on the frequency, but is generally assumed to be a constant for a small frequency range, which greatly simplifies the equations. But nonlinearity coefficient values should be carefully considered when FOPA operates over an extensive range of frequencies. The non-linear coefficient is explained as equation 3.23.

3.5.3 FOPA signal gain

Using propagation equation 3.24, critical features of parametric gain, including the corresponding analytical FOPA gain equation, can be derived. The gain equations are referenced from [140], with specific details. Later, these analytical FOPA gain equations help to model the most common single pump FOPA gain spectrum. Figure 3.16 demonstrates a schematic spectral view of the parametric process in fibre with two pump and single pump configurations. Figure 3.16 (a) shows two pumps at ω_{P1} and ω_{P2}, generating signals at ω_S and its conjugate ω_i known as idler. ω_C shows the zero-dispersion wavelength. Figure 3.16 (b) shows one pump FOPA process, in this configuration pump ω_P is located near to zero dispersion wavelength ω_C , photon transfer from high power pump is equally distributed to signal and idler in single pump FOPA configuration. Signal and idler frequencies ω_S and ω_i are located symmetrically around the pump relevant to the relation $2\omega_P = \omega_S + \omega_i$.

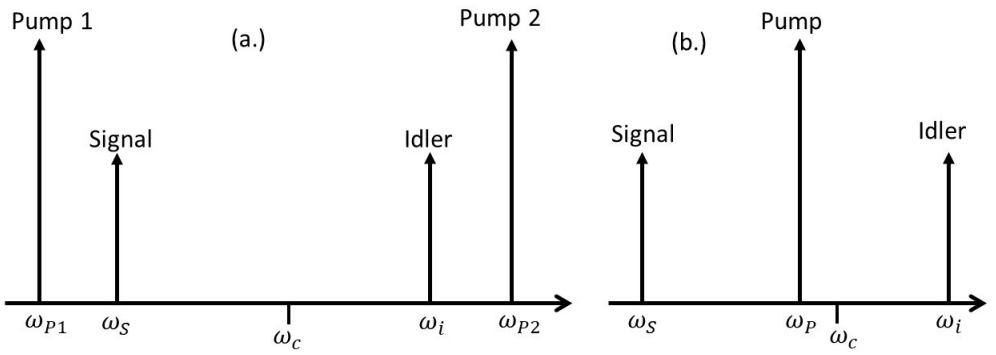

Figure 3.16 Spectral view of FOPA process: (a) dual pump version (b) single pump version[141]

From the above, Figure 3.16 discusses how the parametric signal gain evolves via the FWM process involving pump wave and signal wave to analytically obtain the signal gain equation, which is dependent on wavevector mismatch $\Delta\beta$ and $\Delta\beta_{NL}$ which are interdependent on SPM, XPM, and FWM processes. Frequencies participating are subscripted by $\omega_{P1}, \omega_{P2}, \omega_s \; and \; \omega_i$ where ω_{P1}, ω_{P2} are two pump frequencies and $\omega_s \; and \; \omega_i$ are signal and idler frequencies. The effect of SPM and XPM and nonlinear coefficient γ on input scalar field wave $|A_k|^2$ is rotated in phase but unable to change the amplitude of the input wave vector presented as $\left(\frac{dA_K}{dz}\right)_{SPM.XPM} = i \times A_k \times scalar$ [66].

FWM works differently from SPM and XPM, as the angle between the complex amplitude change due to FWM $(dA_k/dz)_{FWM}$ and the complex amplitude A_k itself depends on the phases of all waves, and a phase mismatch $\Delta\beta z$ accumulates due to dispersion. For example, for a signal in FOPA:

$$\left(\frac{dA_s}{dz}\right)_{FWM} = i \times 2\gamma A_i^* A_{p1} A_{p2} exp\,(-i\Delta\beta z) \tag{3.25}$$

The critical triggering process occurs with the introduction of the FWM and effects on the input wavefield $|A_k|^2$, which is different from the SPM and XPM effects. In the presence of FWM, the amplitude of a phase-matched wave changes. The maximum signal gain is achieved when signal amplitude and its derivative are combined in a phase-matched manner. As the underline principle of the parametric amplification process is FWM, in which energy and momentum are conserved. The process generates a copy of the signal known as an idler. The idler is a phase conjugate of the signal. Equation 3.26 and 3.27 have phase relation between pumps and signal plus idler, which presents that idler phase is always dependent on the phase of the pump(s) and signal with a phase shift of $\frac{\pi}{2}$. Therefore, phase matching is always satisfied at the input of phase insensitive FOPA for any signal frequency, the angle of phase matching changes with propagation length $\theta_s(z)$

$$\varphi_s + \varphi_i = \varphi_{p1} + \varphi_{p2} \tag{3.26}$$

$$\varphi_i = \varphi_{p1} + \varphi_{p2} - \varphi_s + \frac{\pi}{2} \tag{3.27}$$

Therefore, the phase matching is always satisfied at the input of phase insensitive FOPA: $\theta_s(0) = 0$ for any signal frequency. However, the angle $\theta_s(0)$ changes with distance z as follows equation 3.28:

$$\frac{d\theta_s}{dz} = \frac{d\varphi_s}{dz} + \frac{d\varphi_i}{dz} - \frac{d\varphi_{p1}}{dz} - \frac{d\varphi_{p2}}{dz} + \Delta\beta \tag{3.28}$$

Fibre attenuation is necessary as FOPA has fibre as a parametric gain medium. Typically, fibre loss is negligible and often neglected as lengths of fibres used as a gain medium are very short and generally are within a few hundred meters. Therefore, distributed fibre loss is typically below 0.2 dB. Some attempts were made to investigate distributed FOPA where parametric amplification is generated within transmission fibre medium [142], like distributed Raman amplifiers. Within the scenarios, attenuation values >0.2 dB/km should be considered for employed optical fibres.

Derived signal gain equations for FOPA from the above discussion involve propagation wavevector mismatch as equation 3.22.

$$\Delta\beta = \beta_s + \beta_i - 2\beta_P \tag{3.29}$$

Equation 3.29 has wave propagation vector mismatch between signal wave, idler wave, and pump(s). Nonlinear wavevector mismatch $\Delta\beta_{NL}$ describes a total impact of SPM and XPM on phase-matching conditions and is given as 3.30

$$\Delta\beta_{NL} = \gamma(P_{P1} + P_{P2}) = \gamma P_0 \tag{3.30}$$

where the total pump power is $P_0 = P_{p1} + P_{p2}$. Therefore, total wavevector mismatch is a combination of propagation wavevector mismatch and nonlinear wavevector mismatch, which present change of phase-matching angle θ along the fibre length:

$$\Delta\beta_{NL} + \Delta\beta = k \tag{3.31}$$

Parametric gain coefficient g is given by 3.32, where $r = 2\gamma|A_{p1}||A_{p2}| = 2\gamma\sqrt{P_{P1}P_{P2}}$ is amplitude of FWM coupling as described in [140].

$$g^2 = r^2 - \left(\frac{k}{2}\right)^2 \tag{3.32}$$

Signal gain G_s and a signal to idler conversion efficiency G_i is defined as a ratio between output idler and input signal powers are given as:

$$G_i(z) = \left|\frac{r}{g}sinh(gz)\right|^2 \tag{3.33}$$

$$G_s(z) = 1 + \left|\frac{r}{g}sinh(gz)\right|^2 \tag{3.34}$$

Equation 3.33 shows output idler power, and equation 3.34 shows an output signal power as a function of gain coefficient g, where both signal and idler conversion efficiency increase with gain

coefficient g. For equal pump powers where $P_{P1} = P_{P2} = {}^{P_0}/_2$, the maximum gain coefficient is $g_{max} = r = \gamma P_0$ and gain equations are written in simpler forms as:

$$G_{i,max}(z) = [\sinh(\gamma P_0 z)]^2 \; and \; G_{s,max}(z) = [\cosh(\gamma P_0 z)]^2 \qquad 3.35$$

Approximation for large gains ($x > 1 \rightarrow \sinh^2(x) \approx \cosh^2(x) \approx e^{2x}/4$; $10\log_{10} e \approx 4.34$) as follows:

$$G_{s,max}^{dB}(z) \approx G_{i,max}^{dB}(z) \approx (8.69\phi - 6)dB \qquad 3.36$$

Where $\phi = \gamma P_0 z$ is the nonlinear phase shift as shown in equation 3.35. For example, typical phase shift required for standard FOPA gain will have parameters like nonlinear coefficient $\gamma = 10\text{W}^{-1}\text{km}^{-1}$, pump power $P_0 = 3\ W$ and fibre length of $z = 200\ m$, will give a phase shift of $\phi = 6.0$. For example, with the $\phi = 6$ FOPA signal gain can reach ~*46 dB*.

The analytical signal gain in Equation 3.36, demonstrate that for low values of nonlinear phase shift (ϕ <1), signal gain G_s grows very slowly. Whereas, for nonlinear phase shift (ϕ >1), the signal gain G_s grows exponentially. This is because of the impact of the FWM scale with idler amplitude, as shown in 3.34. It is related to the impact of the FWM term on signal and scale by idler amplitude that is increase in idler amplitude will proportionally increase the signal amplitude.

Figure 3.17 shows an example of a single pump FOPA with an input probe signal. The basic configuration involves a high-power continuous-wave pump, a parametric gain medium (example shown as highly non-linear fibre), and a probe signal for amplification. To control the stimulated Brillouin scattering (SBS) effect, as discussed in Chapter 2 section 2.4.1.1, a ditherer is used (shown as a phase modulator with RF frequency tone broadening the input pump signal). Amplified signal monitored via 1% tap coupler through OSA shows residual pump, amplified signal, and the conjugate of signal (also known as idler) separated in frequency as shown in Figure 3.17. The inset of Figure 3.17 shows an example of a simulated spectrum of signal and pump at FOPA input and a spectrum view of amplified signal with idler. Crosstalk products from the FWM process are located at the output spectrum.

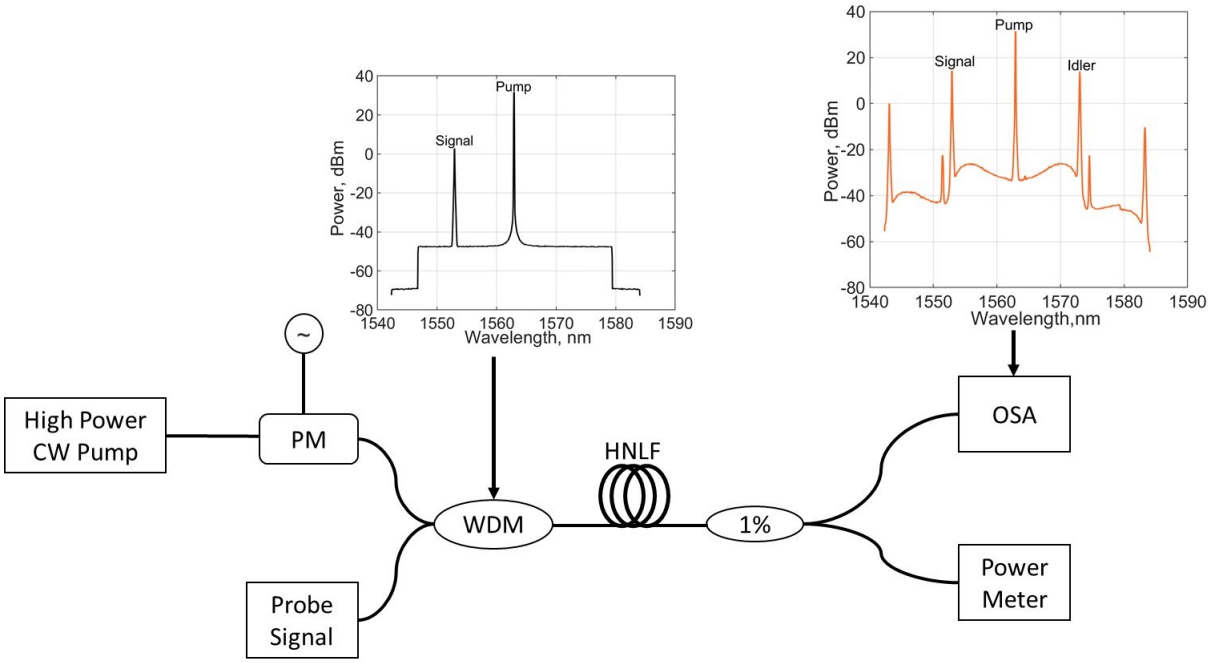

Figure 3.17 Example of a single pump fibre parametric amplifier setup with inset figures showing a spectrum of pump and signal before and after FOPA amplification simulated in VPI transmission maker

3.5.4 Single Pump FOPAs

In this work, single pump FOPAs are employed for parametric amplification of burst signals; this section only details the FOPA gain spectrum for single pump FOPA. Discussion in the subsections is based on [140] with additional discussion on single pump FOPA design requirements. Gain coefficient g for every frequency component is given as

$$g = \sqrt[2]{r^2 - \left(\frac{k}{2}\right)^2} \qquad 3.37$$

Where $k = (\Delta\beta_{NL} + \Delta\beta)$ is the sum of propagation constant mismatch $\Delta\beta$ and constant nonlinearity mismatch $\Delta\beta_{NL}$ is generated between three(four) different frequencies. A real gain in a scalar case of single pump FOPA is obtained via gain coefficient as in Equation 3.37 and explained as previous equations in section 3.5.3. The relation describes an ellipse between gain coefficient and propagation constant mismatch $\Delta\beta$. When gain coefficient is not real in case of wavevector mismatch $k = |\Delta\beta_{NL} + \Delta\beta| > 2$ dispersion causes signal power fluctuations rather than amplification hence no substantial gain. For a scalar case real gain in a single pump, FOPA obtained for the propagation constant mismatch $\Delta\beta$ is within a range of $-4\gamma P_0$ to 0, where state of phase matching is generally described by $K = -\beta/2\gamma P_0$ is the normalized mismatch parameter. Gain coefficient g is real when $2 \geq K \geq 0$, with phase matched gain is observed when $K = 1$ and the perfect phase matching condition is achieved.

Propagation constant mismatch $\Delta\beta$ can be calculated using Taylor series expansion of signal, idler, and pump propagation constant near pump frequency ω_P, as discussed in equation 3.29. All propagation constants, in this case, are defined via derivatives of the constant propagation β at the pump frequency ω_P and odd derivates of the equation are cancelled due to the symmetry of signal and idler. Keeping the first two highest-order terms of propagation constant mismatch $\Delta\beta$ can be presented as:

$$\Delta\beta(\Delta\omega_s) = \beta^{(2)}(\omega_P)\cdot\Delta\omega_s^2 + \frac{\beta^{(4)}}{12}\cdot(\omega_P)\cdot(\omega_s^4) \qquad 3.38$$

where $\Delta\omega_s = \omega_s - \omega_P$ is the signal frequency away from the pump.

Equation (3.38) shows that the FOPA signal gain is symmetric around the pump frequency ω_P and allows one to find the propagation constant mismatch $\Delta\beta$ as a function of signal detuning from the pump. Equation 3.39 expands $\beta^{(2)}$ with respect to pump frequency ω_P as:

$$\beta^{(2)}(\omega_P) \approx \beta^{(3)}(\omega_0)\cdot(\omega_P - \omega_0) \qquad 3.39$$

Frequency dependency of fourth-order propagation constant $\beta^{(4)}$ have a minor effect within the practical tuning range of the pump. Accurate measure of $\beta^{(4)}$ is difficult, therefore generally is characterized by its sign and an order of magnitude provided by the manufacturer.

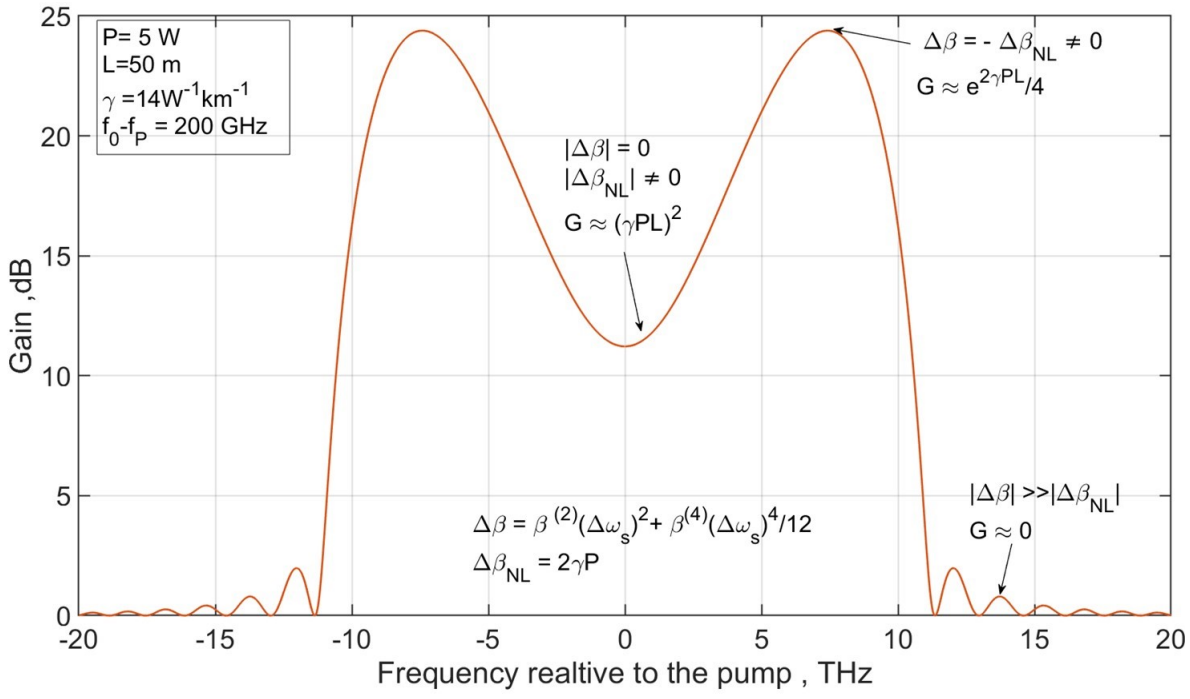

Figure 3.18 Example of a single pump FOPA gain spectrum calculated using analytic equation discussed in section 3.5.3 parameters used listed in the inset

Figure 3.18 present an example of a single pump FOPA gain spectrum showing the most common dual lobe single pump FOPA gain spectrum, analytically calculated using equation 3.37 for signal

gain. The following parameters were used for obtained gain spectrum at pump power $P = 5W$, the nonlinearity coefficient $\gamma = 14\ W^{-1}km^{-1}$, dispersion slope $S = 83\ s^{-1}m^{-3}$ and fibre length of $L = 50\ m$. Pump location was 200 GHz from the zero-dispersion frequency, which introduces significant anomalous dispersion at the pump frequency. Higher-order dispersion $\beta^{(4)}$, in this case, was negligible in comparison to large second-order dispersion $\beta^{(2)}$ and have a strong contribution. In the above gain spectrum $\beta^{(4)}$ was set to zero and the calculated gain spectrum has relevance with cases where $\beta^{(2)} < 0$, $\beta^{(4)} < 0$ and $\beta^{(2)} < 0$, $\beta^{(4)} > 0$.

$\Delta\beta$ is close to zero near the pump and attains moderate quadratic gain $G_{\Delta\beta=0} = (\gamma PL)^2 + 1$. Exponential signal gain for the FOPA is obtained when the pump wavelength is far from the quadratic gain region and ZDW of the parametric gain fibre. When the pump wavelength is further detuned from the ZDW, the FOPA gain spectrum suffers high dispersion and lose its phase-matching condition

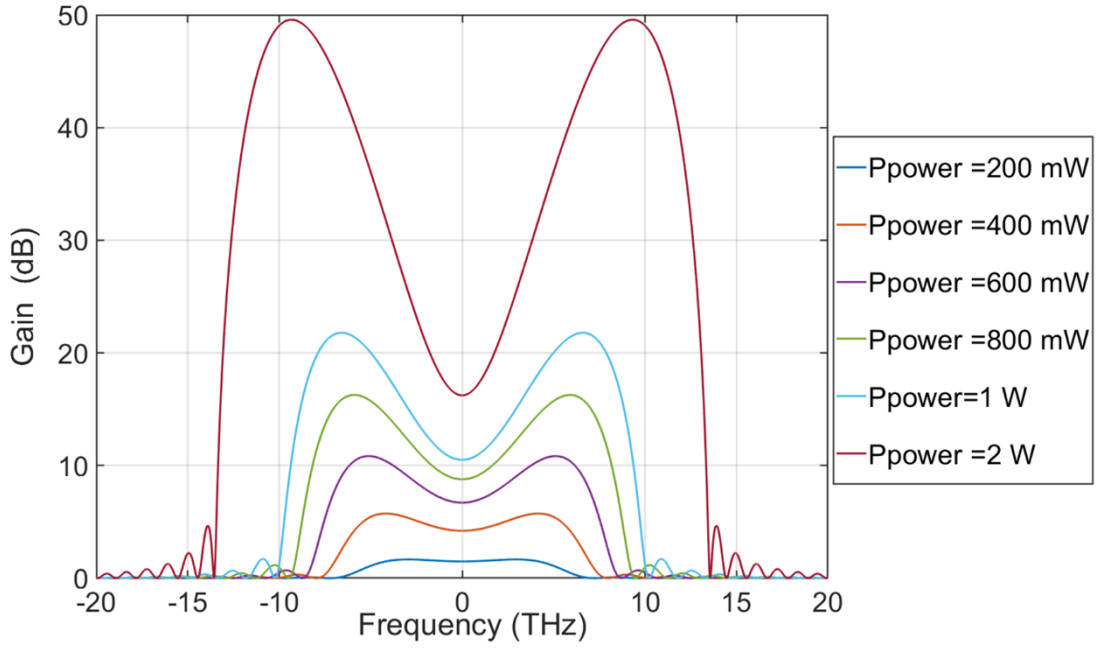

Figure 3.19 Single pump FOPA gain spectrum at various pump powers from 200 mW to 2 W at single pump frequency at 192.04 THz, 200 GHz away from zero- dispersion in the HNLF, length of 200 m with $\gamma = 16\ (W\ km^{-1})$ and dispersion slope S = 0.02 ps/(nm^2km)

Figure 3.19 shows FOPA gain and bandwidth dependency on pump power at a fixed parametric gain; fibre length HNLF is 200m and nonlinear coefficient $\gamma = 16\ (W\ km^{-1})$. Flat FOPA gain spectrum with minimum gain variation is required, along with features like significant gain and bandwidth to amplify WDM combs. Recently >100nm broadband flat gain spectrum was achieved with gain variation <1 dB [143]. Using fibre with correct properties like positive $\beta^{(4)}$ and via tuning pump wavelength in near proximity of ZDW to obtain a small negative value of $\beta^{(2)}$.

3.6 Polarisation impact on FOPA signal gain

Previously in section 3.5.2, all waves were assumed to have the same linear polarisation; therefore, all wave vectors had scalar behaviour. This section considers the arbitrary state of polarisation of an interacting pump and signal waves in a general FOPA case. Interacting waves in a random state of polarisation will impact differently in achieving signal gain in FOPA.

3.6.1 Theory of Vector FOPA

The scalar equation of FOPA propagation is discussed in previous sections and assumed identical frequencies of an electric envelope *E* being close to each other. In this case, the electric field for a relatively simple non-scalar example with a single pump FOPA containing linearly polarized with orthogonal signal pump is given as equation 3.40. As idler has the same polarisation as a signal [144], and therefore it will vanish as the products $\overrightarrow{E_P}\,\overrightarrow{E_s}$ and $\overrightarrow{E_P}\overrightarrow{E_\iota}$, where vector $\overrightarrow{E_P}$, $\overrightarrow{E_s}$ and $\overrightarrow{E_\iota}$ represent the pump, signal and idler fields respectively. Another equation for vector case is written for signal frequency as

$$(\nabla^2 + K^2)\vec{E} = \frac{\chi^{(3)}}{C^2}\frac{\delta^2(\vec{E}\vec{E})\vec{E}}{\delta t^2} \tag{3.40}$$

$$(\nabla^2 + K^2)\vec{E} =$$

$$= \frac{\chi^{(3)}}{4c^2}\frac{\delta^2(3\,\overrightarrow{E_s}(\overrightarrow{E_s}\,\overrightarrow{E_s\,*}) + 2\overrightarrow{E_s}(\overrightarrow{E_P}\vec{E}_p^{*}) + 6\vec{E}_s(\vec{E}_i\vec{E}_i^{*}) + 2\vec{E}_i^{*}(\vec{E}_p\vec{E}_p))}{\delta t^2} \tag{3.41}$$

Equation 3.41 presents 2 and 3 waves involved in a nonlinear process of XPM and FWM affected by polarisation, including a pump that decreased by 1/3 (i.e., reduced from 6 to 2). FWM and XPM will cancel out each other in an orthogonally polarized state and turn to zero. Two significant impacts that are observed in the case of polarized waves are, firstly, coupling gain coefficient, will decrease by a factor of three as compared to scalar (co-polarized) case impacting maximum gain coefficient $g_{max} = r = \frac{2\gamma P}{6} = \frac{\gamma P}{3}$. The second effect is the nonlinear phase shift γPL of signal and idler caused by XPM with pump scaled by 1/3. For the orthogonally polarised pump and signal, the nonlinear phase shift is written as:

$$\Delta\beta_{NL} = -\frac{2\gamma P_0}{3} \tag{3.42}$$

The gain coefficient is real and lies within $0 < \Delta\beta < 4\gamma P_0/3$. Therefore, in contrast to the scalar case, in the case of orthogonal linearly polarised signal, pump and gain will be observed for positive $\beta^{(2)}$ and $\beta^{(4)}$. However, it will affect gain bandwidth, and peak gain is much smaller for orthogonally polarized waves due to the low FWM coupling coefficient. Finally, the following

coefficients have been introduced to calculate the maximum gain coefficient g_{max} and nonlinear wavevector mismatch $\Delta\beta_{NL}$ for arbitrary polarisation states of the pump(s) and signal in FOPA:

$$b = \frac{g_{max}}{\gamma P_0}; u = \frac{\Delta\beta_{NL}}{\gamma P_0} \quad 3.43$$

The above coefficients were used to calculate twelve principle combinations of linear and circular polarisations of pumps and signals for birefringent and non-birefringent cases explained in detail [140].

3.6.2 Polarisation-independent FOPA

The signal gain in FOPA is polarisation-sensitive; therefore, polarisation alignment between parametric pumps and signal becomes necessary to maximize signal gain. Multiple methods were investigated to achieve polarisation-independent gain, such as polarisation multiplexed signals and orthogonally polarized pumps [145]. ~10 dB on-off gain was demonstrated with co- polarised pump and signal in [146] useful for optical phase conjugation application. Large signal gain with orthogonally polarized pumps is complex and depends on polarisation averaging effects [140]. As employing orthogonally polarised pumps reduces achieving high signal gain as in this case, the coefficient $b = \frac{g_{max}}{\gamma P_0}$ is reduced by $1/3\ to\ 4/9$ depending on polarisation averaging. Therefore, gain coefficient is dropped by a factor of 2 to 3 as compared to a co-polarized pump case. Hence other alternatives are to be used to attain large signal gain with FOPA independent of pump polarisation.

In single pump FOPAs, one of the proposed methods is to split a signal orthogonally via a polarisation beam splitter [147]. Using a polarisation beam splitter (PBS), an input signal with arbitrary polarisation splits into two orthogonal polarisations states. A corresponding co-polarised pump independently amplified each state of polarisation. A Mach-Zehnder interferometer arrangement using two HNLF lengths in parallel is one of the methods for polarisation diversity but requires an active optical path alignment for this case [148]. Another method is using a single HNLF length in a loop-like (for example, Sagnac interferometer) architecture. This approach is suitable for small signal gain and for applications like optical phase conjugation but fails to provide large FOPA signal gain due to interaction of counter-propagating high power pumps as explained in chapter 2 section 2.4.1.1, leading to significant signal distortions [149]

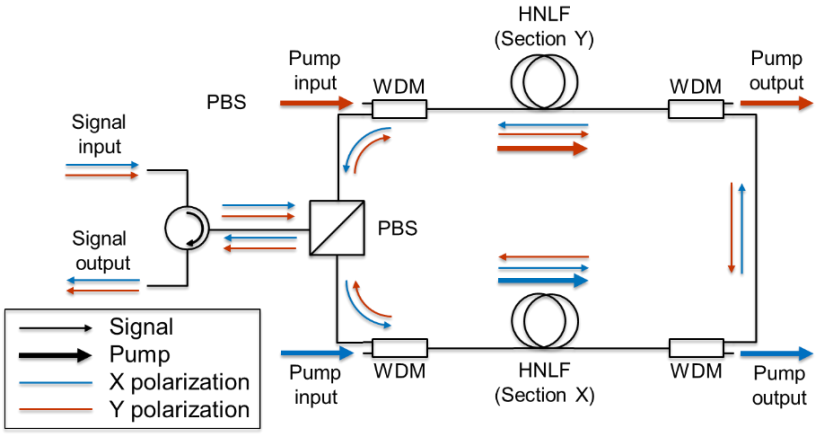

Figure 3.20 Schematic example of two-fibre loop architecture for a polarisation-independent FOPA[66]

A polarisation-independent FOPA loop configuration was recently demonstrated and upgraded by employing two separate sections of HNLFs for two polarisation paths [150] as shown in Figure 3.20, for example. Two similar HNLF lengths are pumped with the single individual pumps through each fibre section. The orthogonally split signal passes an active section of HNLF for signal amplification. It then passes through a passive section for a second orthogonal section arm and, similarly, another SOP amplified with a co-propagating pump. As FOPAs are uni-directional, no counter propagation of pump and signal is possible. The looped FOPA configuration resembles a Mach Zehnder interferometer. Interferometric arrangements have been demonstrated to achieve >20 dB net gain of polarisation multiplexed signals over a range of 2.3 THz bandwidth, showing employability for broadband high gain FOPA [151]. One of the performance limitations in this looped FOPA configuration is the generation of nonlinear crosstalk stemming from the propagation of amplified signals passing an additional HNLF section. Changing of pump direction could tackle this nonlinear crosstalk in two fibre loop arrangements. The direction of the signal passes via the "Loss" section first with low power and lower crosstalk and then gets amplified within the "Gain" section [151]. Another demonstration to suppress nonlinear crosstalk via removing mid-stage idler in a two-loop architecture provides reduction by >4.5 dB with a minor penalty on amplifier performance [152]. Three different polarisation-independent FOPA configurations in diversity loop architectures are recently published, showing Gain-Loss, Loss-Gain, and Gain-Filter-Loss PI-FOPA [153]. Different PI-FOPA configurations can potentially be demonstrated for different telecom applications.

Results from [153], [154] discuss three HPL FOPA architectures such as Gain -Loss: Signal is first amplified in the active (gain) section and then attenuated in power loss through the passive (loss) section. In Loss-Gain architecture, the signal is initially passed through the passive section and is then amplified in the active section of HNLF. And, the third one is Gain-Filter-

Loss (GFL), an amplified signal via gain section propagate through a mid-stage filter where generated idlers are removed, and the passive section incurs a loss. It provides a critical analysis where "Gain-Loss" and "Gain-Filter-Loss" have a noise figure of 6 dB like the EDFA. Although "Loss-Gain" has a higher noise figure >6 dB, the signal is first attenuated and then amplified. An example of low nonlinear crosstalk PI- FOPA architecture is shown in Figure 3.21. "Loss-Gain" HPL-FOPA architecture is helpful for single-span amplifiers links, for example, applications like reach extended PON amplification where high output power signals are required to enhance overall link power budget increasing splitting ratios while being less suspectable towards lower nonlinear crosstalk.

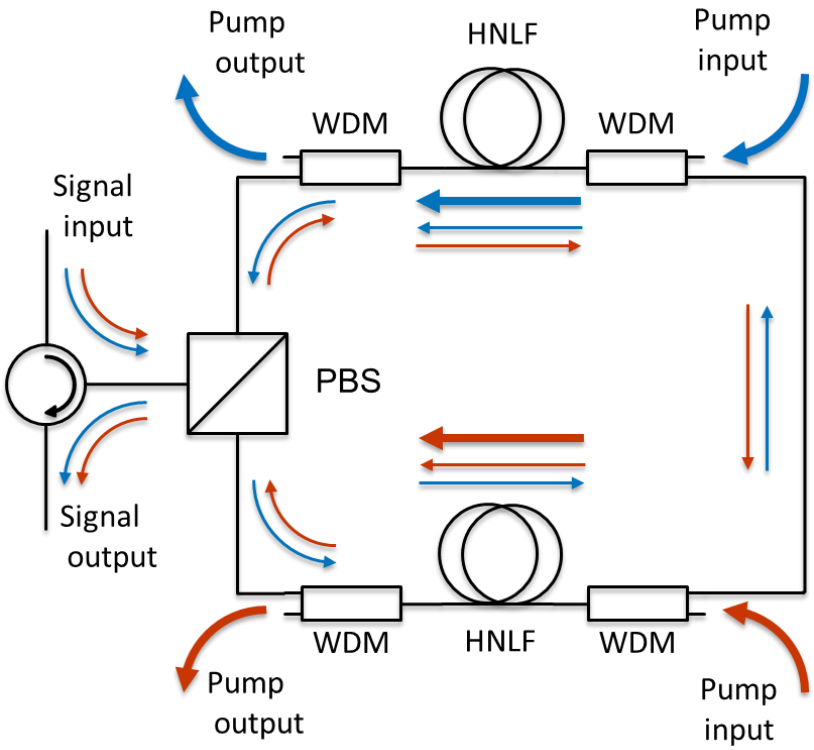

Figure 3.21 Schematic example for HPL-FOPA architecture in Loss-Gain configuration [26]

3.7 Summary

In this chapter, I have discussed a standard access network topology with subsystems included. An optically amplified extended reach access network architecture is potentially possible with in-line optical signal amplification. An optical amplifier should support a few important characteristics for employment within access networks like burst mode amplification, large gain, and high output power without grooming the bi-directional traffic. Conventional optical amplifiers were researched comprehensively for employment in local networks for reach

extension and pre-amplification etc. Although, conventional amplifiers struggle to meet multiple essential parameters required to consolidate a robust access network. The theory responsible for slow response time in conventional fibre amplifiers was discussed in the erbium-doped fibre and Raman amplifier analysis. Mitigation techniques were reported within the discussion for transient suppression. Fibre optic parametric amplifiers demonstrate unique features understood via different research investigations. Few of them provide perfect alignment with future optically amplified access networks like ultra-fast response time, gain on arbitrary wavelengths, and considerable output signal powers. The basic parametric amplification gain theory was discussed with FOPA gain spectrum and signal gain for single pump gain. Recently, a looped polarisation-independent FOPA was presented in [155] to provide up to 20 dB polarisation-independent signal gain, therefore potentially building the path for FOPA in-line signal amplification. In combination with all the potential features, FOPA employment in access networks would enable research work to demonstrate FOPA as a drop-in replacement amplifier.

Chapter Highlights

- **Optical amplifiers in Access networks:** Traditional access networks have a 20 km physical reach limitation. With in-line optical amplification technique reach can be increased by >100 km, although, optical amplifiers in access networks must satisfy requirement like burst mode signal amplification, high output signal power, and gain on arbitrary wavelengths.

- **Transient Effects:** Conventional fibre amplifiers suffer from slow response time for amplification on burst mode signals. EDFA demonstrate ~1 ms of response time when amplifying time varying or burst mode signals. Raman amplifiers due to long lengths of gain medium suffer from transient effects with response time proportional to the fibre length. SOA have fast response time, although suffer from providing high output power and patterning effects when amplifying high speed signals like 10 Gbps.

- **FOPA ultra-fast response time:** FOPA inherently demonstrates ultra-fast response time suitable for burst signal amplification. Silica based optical fibres used as a gain medium in parametric amplification present a response time of ~0.1 fs, much faster than modern optical signals bit rates lying in the picoseconds time scale.

- **FOPA features:** Unique features of FOPA make it a promising candidate for modern optical communication systems. Large gain of 70 dB, ultra-wide flat bandwidth of >100 nm, very low noise figures ~0 dB and arbitrary signal gain outside conventional C band makes it very attractive. Additionally, parametric amplifiers demonstrate ultra-fast response time, hence are suitable for transient free burst signal amplification. FOPA as complying with all requirements of future optical access system can be deployed as in-line amplifier for reach extended access networks.

Chapter 4 FIBRE OPTIC PARAMETRIC AMPLIFIER FOR BURST SIGNAL AMPLIFICATION

TABLE OF CONTENTS

Fibre optic parametric amplifiers (FOPA) are envisaged to be promising amplification technology for optical fibre communication. FOPA offers unique features like very large gain (70 dB) [15], [156], a broadband (~200 nm) and flat gain spectrum >100 nm [157–159], gain on arbitrary wavelengths [16], and phase-sensitive gain potentially allowing for 0 dB noise figure [160]. Another important and attractive feature of FOPA is an ultrafast response time of around ~0.1 fs time owing to the lowest order χ^3 susceptibility in silica-made optical fibres [137] employed as a parametric gain medium. Ultra-fast response time of FOPA can be potentially utilized to mitigate signal penalties when amplifying bursty traffic or time-varying signals shielding signals from transient effects [18]. Compared with the slow response time observed within the conventional state-of-the-art amplifiers like erbium-doped fibre amplifiers and Raman amplifiers [115], [134]. FOPA potentially can redefine reach extended access networks with transient free burst signal amplification. Therefore, the above-listed features, including ultrafast response and providing gain on arbitrary wavelengths, make FOPA very appealing for reach extended optical access networks potentially transmitting traffic in O, E, S, C, and L bands of the low-loss telecom window [161].

Recently, with the introduction of a novel polarisation diverse half pass loop FOPA (PI-FOPA) architecture, in-line signal amplification by FOPA became achievable [162] for arbitrarily polarised signals. The polarisation diversity loop has resolved the dependence of signal gain on pump polarisation [150] via amplifying the signal in the orthogonal state of polarisation. Net gain of 15 dB is demonstrated with 20 WDM channels over 2.3 THz in C-band [12] with PI-FOPA. The operation of FOPA on arbitrary wavelengths bands [13] makes it a promising candidate for several future applications like wide-band signal amplification and especially for multi-band reach extended high capacity future PON [161].

Optically amplified reach extended access networks are demonstrated for consolidating multiple central office locations into a few access nodes while reducing the overall operational expenditure [22]. Consequently, it would increase the overall link power budget via increasing the split ratio and the physical reach of connectivity, extending the generic 20 km trunk fibre length to >100 km [74], although, currently, two main restrictions in extended access networks stem from inherent optical fibre limitations: fibre attenuation and chromatic dispersion [52]. Penalties arising from chromatic dispersion are compensated via advanced digital signal processing (DSP) techniques [6]. However, link power budget enhancement would require in-line signal regeneration without changing the properties of the transmitted signals. Hence, optical amplifiers could provide a potential solution to regenerate and enhance the capacity and reach of the access links.

Although, there are few specific requirements for an optical amplifier deployed within extended reach access networks. Like amplifying upstream bursty data signals without transient [9], high output power allows a high splitting power budget and amplifying signals in different wavelength bands for supporting bi-directional signal transmission within different access network architectures [161] discussed in Chapter 3. SOA, EDFA, and Raman amplifiers have already been considered for deployment in extended reach access links as in-line amplifiers to increase power budget in [83], [84], [110]. SOA can operate in all low loss telecom bands and have a fast response time equivalent to picosecond's signal bit time scale [164], which makes them appealing for access networks and transient free burst signal amplification, although SOAs are limited in providing high output signal powers and suffer from patterning effects for high bit-rate signals, making them less suitable for an optical amplifier in reach extended access links. [89].

On the other hand, EDFAs, are considered mature optical amplification technology with attractive properties like high gain, large output power, and tolerable noise figures, making them perfect amplification technology for especially for WDM-based optical fibre communication [103] links. However, in access networks, EDFA employment suffers from a slow response time of a few hundreds of microseconds [108] to >1 msec for amplifying upstream TDMA (burst mode) traffic. EDFAs, therefore, show vulnerability to amplify burst signals in PON [111]. Transient effects in EDFA are discussed in detail in Chapter 3, section 3.3.2.

Recently, Raman amplifiers have been introduced in reach extended PON [83], [131], but they suffer from transient effects when amplifying signal bursts, too, similar to EDFAs. The response time of Raman amplifiers may significantly exceed that of Raman scattering due to a relative transition time between a pump and signal waves over the long length of Raman gain fibres [132]. Detailed discussion on Raman transient already discussed in chapter 3 section 3.4.3.

Therefore, FOPA can be considered as a potential candidate for a reach extended access network. This work proposes polarisation independent (PI- FOPA) as a drop-in replacement amplifier for a reach extended access network. Interestingly, FOPA supports all specific requirements for optically amplified access networks, such as: can amplify burst signals with ultra-fast response time, providing a high output signal power, and ability to amplify signals across arbitrary wavelengths, as well as supporting bi-directional capable of dual-band signal amplification of bi-directionally transmitted signals.

Experimental results for reach extension in access link with in-line EDFA and discrete Raman amplifiers employed as an in-line amplifiers have been demonstrated for >50 km transmission link, but at a cost of excluded burst traffic and with low signal gain and small output power of signals. This chapter demonstrates and investigates an experimental analysis to compare burst signal amplification by the PI-FOPA as a drop-in amplifier in a reach extended access network

architecture, part of which was also published in [27]. We compare a commercial-grade EDFA and a discrete Raman amplifier with a PI-FOPA for amplification of a burst mode signal at varied burst duration measured by bit error ratio (BER). Polarisation-insensitive FOPA with a net gain of 20 dB was obtained at a signal wavelength of 1535 nm in the C-band. The range of burst duration from 70 μs to 5 μs was amplified by EDFA, DRA, and PI-FOPA at a fixed 13 dB gain to investigate the transient effect. 10 Gbps OOK bursty traffic suffers from significant transient effects with EDFA and Raman amplifier, introducing receiver power penalties up to 3 dB. On the other hand, FOPA amplified burst signal has minor penalties thanks to its practically instantaneous response time. Finally, we demonstrate PI-FOPA to improve receiver sensitivity by 3 dB compared with Raman and EDFA, thus enhancing the extended reach and higher splitter ratios.

In section 4.1, an experimental setup is demonstrated employing a 10 Gbps on-off keying burst mode transmitter with 50 km SSMF access span and drop-in amplifiers to test bursty traffic amplification by EDFA, DRFA, and PI-FOPA, then detected by direct detection receiver. Power spectra and burst waveforms with different experimental setups are discussed for all AUTs in the same section. Section 4.2 performance analysis for detected burst traffic was performed via bit error ratio analysis for all AUTs in non-burst and burst signals at different duration of 50 μs, 30 μs, and 10 μs. BER performance of burst traffic is analysed for EDFA and FOPA, excluding Raman at 20 dB signal gain. Finally, section 4.3 shows receiver sensitivity and sensitivity penalty for a range of burst durations compared between each other against BER at the signal gain of 13 dB, including receiver sensitivity for non-burst mode signals.

4.1 Experimental Setup

In this section, the experimental setup of optically amplified reach extended access network link is demonstrated. The sub-sections demonstrate configurations of a commercial-grade EDFA, a discrete Raman fibre amplifier, and a polarisation-insensitive FOPA in detail, employed as an in-line amplifier. Optical power and gain spectra for all three amplifiers under test shown with 20 dB net gain for EDFA and PI-FOPA excluding Raman and at 13 dB net gain including Raman amplifier. Later, this section compares detected burst waveforms firstly in B2B configuration and after amplification by tested amplifiers. The analysis provides an understanding of transient effects added by tested amplifiers on the amplified burst signal. For PI-FOPA, the amplified burst signals. PI-FOPA gain spectrum obtained by amplifying ASE noise provided an initial understanding of achievable gain bandwidth and net gain. Commercial EDFA employed as a reach extended amplifier was available from the lab and was an off-the-shelf product. An experimental setup of discrete Raman fibre amplifier was developed for this experimental work, employed as an in-line amplifier. A PI-FOPA experimental setup was further modified for the amplification of burst mode

signals. The experimental setup was modified to employ PI-FOPA as an in-line amplifier in a reach extended access link. The setup was changed for burst signal amplification by adjusting such parameters as pump wavelength, pump power, and tuning polarisation controllers. Before amplification, the FOPA gain spectrum was measured using an ASE source to understand the parametric gain peak region for signal wavelength in C-band.

4.1.1 Experimental setup of reach extended optical access link

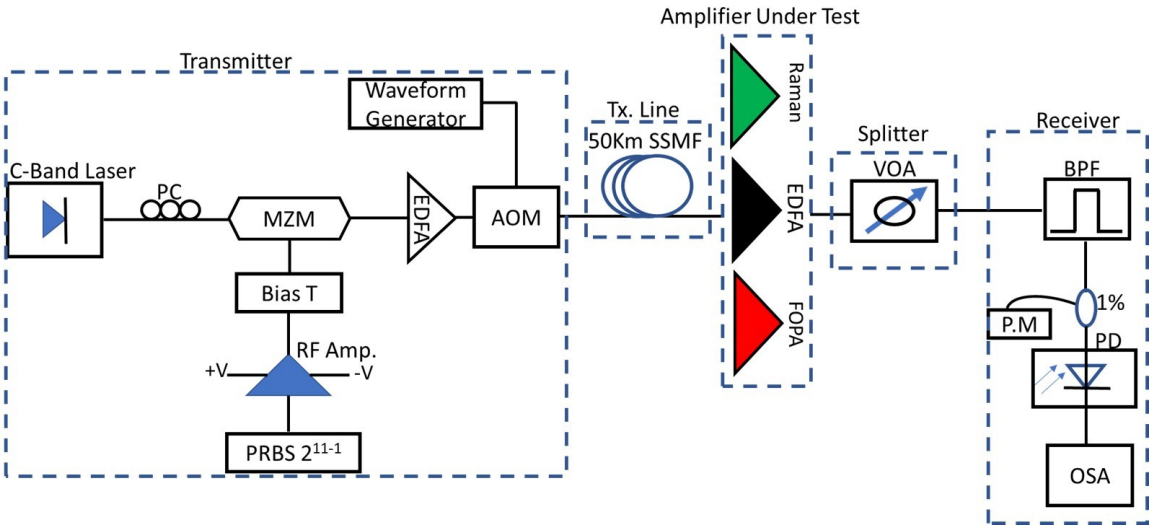

Figure 4.1 Experimental setup to compare the performance of EDFA, Raman amplifier, and PI-FOPA in a 50 km reach extended optical access link transmitting 10 Gbps OOK non-burst and burst signals.

Figure 4.1 presents an experimental setup to compare the performance of a commercial EDFA, a discrete Raman amplifier, and PI-FOPA for an extended reach access network. The experimental setup consisted of the transmitter to generate non-burst and burst mode signals, a 50 km SSMF transmission line, and amplifiers under test (AUT) followed by a VOA emulating an optical power splitter and a receiver.

The signal was sourced from a 100 kHz linewidth tunable laser at the wavelength of 1535 nm and modulated by a Mach-Zehnder modulator (MZM) at 10 Gbps with an OOK modulation scheme. A polarisation controller (PC) was employed after the laser source to maximize input power to the MZM. The MZM includes insertion loss of ~8 dB, and output signal power from the MZM was at -2.3 dBm. The MZM was driven with a pseudo-random bit sequence (PRBS) of 2^{11-1} bit long. Before feeding to the MZM, the RF data signal from the PRBS was amplified by an RF amplifier driven by an external DC supply. A Bias-T was connected between the RF signal, which was connected to the MZM, and allowed the setting to control biasing point of the MZM. The modulated 10 Gbps signal was further controlled via observing the eye diagram with a sampling

oscilloscope and the bias point tuned by DC voltage to maximize eye-opening to provide a reference for setting biasing point of MZM.

The modulated optical signal was launched to a booster EDFA with an output power of 13 dBm. The amplified continuous wave signal was converted to the burst mode signal by employing an acousto optic modulator (AOM). A fibre Q-switched type AOM with a driver was employed to generate fast bursts with rising time ~6 ns and a maximum input power capacity of 1 W.

The schematic of a Fibre Q-switched type AOM is shown in Figure 4.2, demonstrating optical and electrical sections. An electrical driver connected to the fibre Q switch is used to provide an input RF signal connected to a 24V fixed DC power supply. The RF driver is connected to the external arbitrary waveform generator (AWG), providing a square shape carrier wave to the AOM driver. The AWG was fixed at a 10 kHz frequency rate to provide constant burst traffic periods of 100 μs and tuned for burst durations. The insertion loss from AOM was ~5.5 dB, and output signal power was 7.5 dBm at an input optical signal power of 13 dBm. The AOM was fast enough to create bursts with sharp leading edges to investigate the response time of the tested amplifiers.

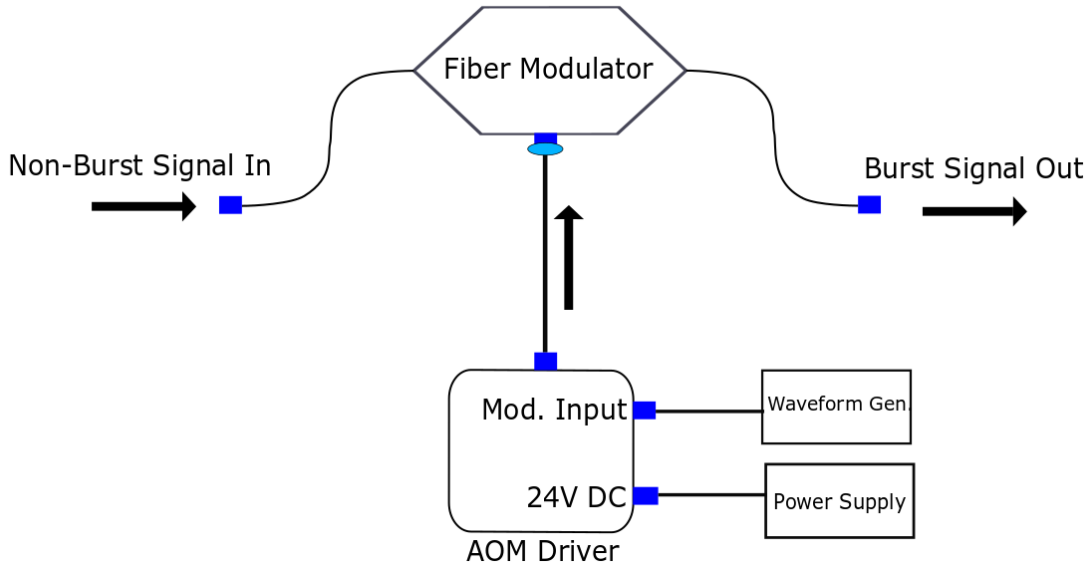

Figure 4.2. Schematic of Fibre-Q switched acoustic optic modulator, showing the process of burst signal generation.

Generated bursts were of 100 μs period and varied in duration from 70 μs to 5 μs. Average burst power levels were calculated by equation 4.1 below. Where average burst power is the ratio of total burst power and duty cycle, and the duty cycle is the ratio of burst duration over burst period given as $Duty\ Cycle\ (\%) = \frac{Burst\ Duration(\mu s)}{Burst\ Period\ (\mu s)}$.

$$Power_{avg.} = \frac{Power_{Burst}}{Duty\ Cylce\%} \quad 4.1$$

Table 4.1 shows average burst powers for the burst durations from 5 μs to 70 μs at a fixed total burst power (non-burst signal) at 7.5 dBm. The non-burst (continuous) signal was obtained at the AOM output via setting the AWG to the pass state. Average burst power decreases with duty cycle as expressed from equation 4.1, at 5% duty cycle average burst power level was - 5.5 dBm.

Duty Cycle (%)	Burst Duration (μs)	Average Power (dBm)
100% (Non-burst)	100% (Non-burst)	7.5
70%	70 μs	6.0
60%	60 μs	5.3
50%	50 μs	4.5
40%	40 μs	3.5
30%	30 μs	2.3
20%	20 μs	0.5
10%	10 μs	-2.5
5%	5 μs	-5.5

Table 4.1 Average burst power for corresponding burst durations

The generated non-burst and burst mode signals were transmitted over a 50 km SSFM transmission link, an optical patch cord connected between two 25 km SMF fibre spools. The total insertion loss of 9.7 dBm was added to the input signal after the propagation of 50 km SMF. Input signal power to the SSMF was at 7.5 dBm. Dispersion and nonlinearity originating from 50 km SSMF are discussed in section 4.2.2 with the performance evaluation of non-burst signal.

Input signal power was fixed at -2.2 dBm for each amplifier under test. Launch power to AUT's was kept constant to maintain a similar power level for the B2B configuration. High input signal power for the tested amplifiers was used due to the limitation of power budget availability with the employed transmitter and receiver. Employed experimental equipment had high insertion loss examples like AOM and VOA add ~10 dB passive loss. Additionally, the discrete Raman amplifier was limited with 13 dB signal gain, and amplification of low input signal power was not possible without saturating the Raman amplifier pump. Amplifiers were optically pumped to obtain two sets of results (a) all AUTs set to 13 dB net gain and (b) all AUTs set to 20 dB net gain except Raman amplifier. 20 dB signal gain was not possible with the employed discrete Raman amplifier at a signal wavelength of 1535 nm. Amplified signals were attenuated with a VOA emulating an optical splitter. The VOA was varied to sweep the received power at the receiver.

The receiver section presented in Figure 4.1 employed a tunable bandpass filter tuned at a signal wavelength of 1535 nm with 1 nm bandwidth. The signal received power was monitored by a power meter connected via a 1% calibrated tap coupler. We employed a direct detection DC-coupled PIN type photodetector with the parameters shown in Table 4.2. The maximum optical power handling of PD was 3 dBm. Therefore, the maximum received burst power was fixed at

0 dBm, making the average burst signal power 3 dB lower from the damage threshold. Hence, the optical detector is protected from unwanted overshoots created by the detected and amplified bursty signals. Detected signals were captured by employing a real-time sampling scope at 23 GHz bandwidth, with a sampling rate of 100 Gs/s. Offline DSP performed signal processing, threshold detection, and bit error counting. In both, the cases of signal analysis, i.e., non-burst and burst signal errors were measured over a set of ten captured traces for swept adjusted power level. BER was measured for attenuated receiver power at the receiver varied VOA attenuation.

Parameters	Spec Values
DC Responsivity	0.7 A/W @ 1550 nm
Rise/Fall Time (10%-90%)	<15 ps
Dark Current	<20nA
Wavelength Range	1000 -1600 nm
DC Bias Voltage	+15 V

Table 4.2 Specific parameters of Direct Detection DC-coupled PIN Receiver

4.1.2 Erbium-Doped Fibre Amplifier

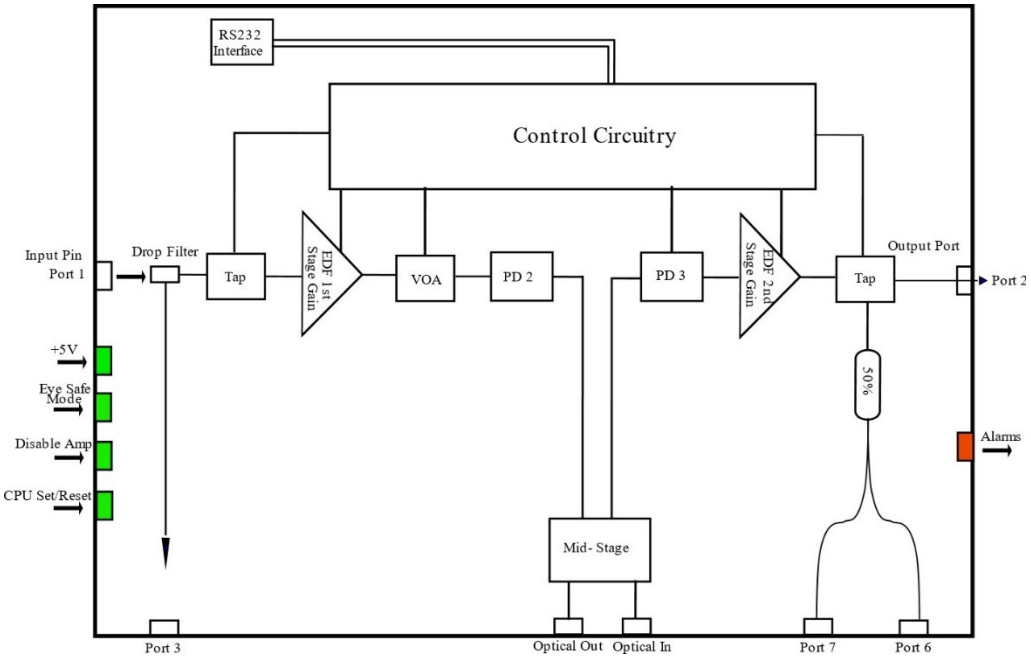

Figure 4.3 Optical block diagram of commercial erbium-doped fibre amplifier

The employed erbium-doped fibre amplifier (EDFA) was a commercial-grade in-line two-stage amplifier, emitting a maximum output power was 23.5 dBm with 20 dB maximum gain provided in two stages. The typical noise figure (NF) of employed EDFA was 5.5 dB, with built-in dynamic gain control and a guaranteed transient settling time of 1 ms. Figure 4.3 explains an optical block diagram for a commercial-grade EDFA, demonstrating two gain stages: EDF 1st and 2nd. The input signal was launched into the Pin port of amplifier module, followed by a drop filter acting as a

supervisor monitory port. The launched signal is transmitted through a tap coupler to monitor input signal power via a control board circuit with the serial communication interface enabling external control. The input signal was amplified via EDFA 1st gain stage, monitored via the control board to set the required gain or output power.

Further, the amplified gain from the 1st stage passes through VOA and gain flattening setup to improve EDFA gain spectrum flatness. Mid-stage ports provide a single-stage EDFA gain and monitoring facility after the single amplifier stage. The 2nd stage EDF gain provides final amplification to the attenuated gain flattened with 1st stage amplification. A 50% tap after the 2nd stage was connected to the ports for monitoring purposes. Finally, the amplified signal was detected by the output port.

Figure 4.4 presents the EDFA amplified signal power spectra and the EDFA signal gain of 20 dB and 13 dB. Power spectra were measured at the input and output of the EDFA. Figure 4.4 (a) presents 13 dB EDFA amplified signal gain, the input signal power at EDFA was at - 29.8 dBm, and amplified output signal power at -17.7 dBm shown at left axis against wavelength. The gain is measured as a difference of input and output signal power scaled on the right axis of the spectrum. The gain spectrum was flattened by removing the additional noise section originating from unwanted ASE on the non-required wavelength region. In Figure 4.4 (b), EDFA signal power spectra for 20 dB input signal gain are shown. Input signal power at the EDFA was -29.8 dBm, and amplified output signal power at –10.6 dBm was measured at 0.1 nm OSA resolution. At 1535 nm achieved signal gain was at 20 dB. As specified in the EDFA operation specification, it is essential to note that when operated in a low gain regime, the noise figure of the EDFA increased from 5.5 dB to ~10 dB.

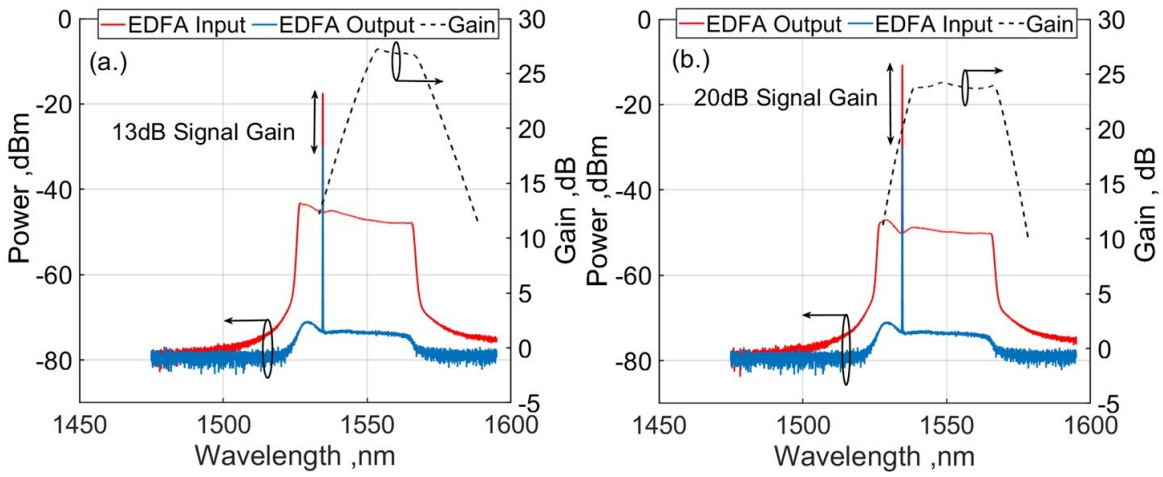

Figure 4.4 Signal power and gain spectra at input and output of EDFA amplified burst signal with (a).20 dB net gain and (b) 13 dB net gain

Figure 4.5 shows amplified output burst waveforms obtained after EDFA amplification was detected at the receiver. Burst waveforms shown in Figure 4.5 were detected at 30 μs burst duration and were captured with a real-time oscilloscope. Input bursts amplified at 20 dB and 13 dB gain with bursts showed evident gain fluctuation at both the gain level stemming from EDFA amplification. Figure 4.5 (a) demonstrates an EDFA amplified burst waveform at 20 dB gain; severe gain fluctuations are observed with a large overshoot at the leading edges of the burst signal. Leading bits of the signal bursts suffer from large gain fluctuations and get destroyed, whereas preceding bits at the latter end do not get amplified equally and suffer from low or no signal gain. The EDFA gain gets completely bleached away by incoming bits due to the observance of transient effects in EDFA. The employed commercial-grade EDFA had inbuilt transient suppression of 1 ms, as explained within the experimental setup. The automatic gain control mechanism provides a feedback mechanism to suppress transient effects within the EDFA.

Similarly, Figure 4.5 (b) shows a burst signal waveform was amplified by EDFA at 13 dB gain. Clear, burst overshoot was observed within the burst waveform, although the overshoot for the burst signal amplified by 13 dB gain is lower than 20 dB amplified signal burst. At 20 dB EDFA signal gain when EDFA was operated in gain saturation, large overshoot due to severe transient effects is observed were observed. Whereas, at 13 dB EDFA signal gain, the transient effects are more pronounced due to short burst duration much smaller than EDFA response time. With longer burst durations greater than the EDFA response time, the effect of transients becomes less effective and even mitigated, while for shorter bursts much lower than EDFA response time, signals suffer from higher transient effects. The EDFA inherently suffers from transient impact due to the slow electronic transition system (response time of >1 ms) discussed in section 3.3 of chapter 3.

It is important to note that burst mode EDFAs with sub-μs response time are commercially available to suppress gain fluctuations due to fast optical packets operational in the channel add-drop system [165]. However, limitations to this EDFA are a working bandwidth to a few nm in C- band, and typically they are not suitable for burst fluctuations with large overshoots >6 dB [165].

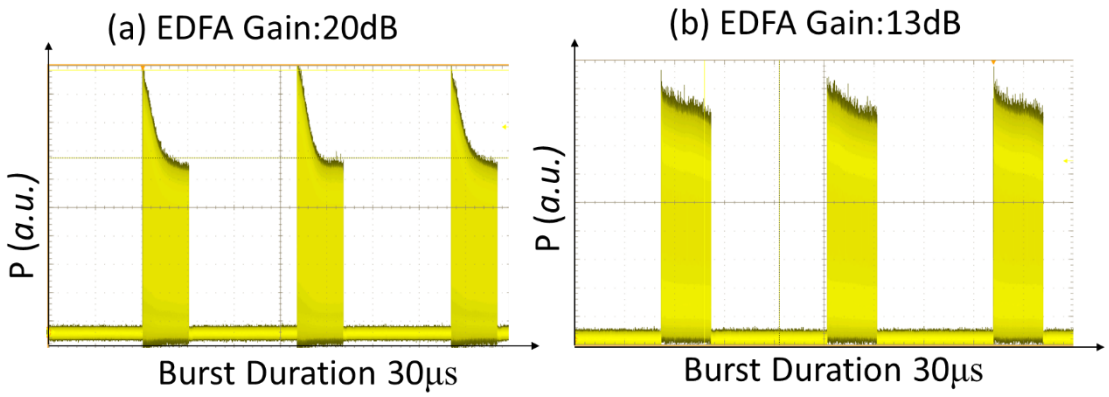

Figure 4.5 30 µs burst waveforms amplified by EDFA at (a) 20 dB and (b)13 dB EDFA net gain showing gain overshoots

4.1.3 Discrete Raman Amplifier

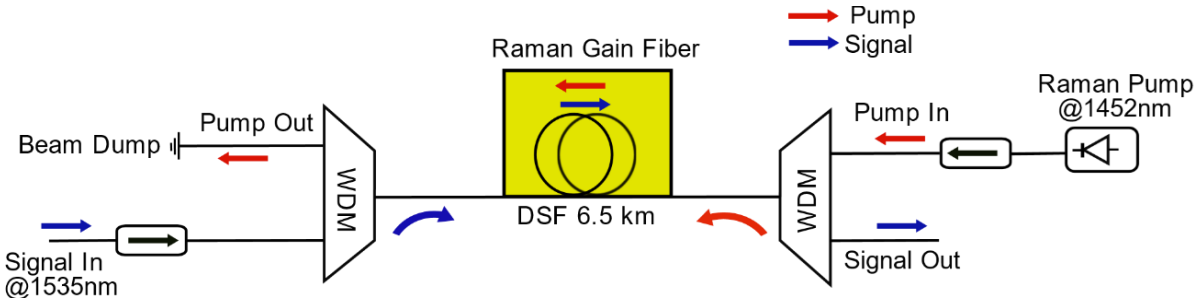

Figure 4.6 Experimental setup of discrete Raman amplifier employed in the experiment for burst signal amplification at 13 dB gain

In Figure 4.6, the experimental setup of a backward pumped discrete Raman amplifier is presented. DRFA was employed as an amplifier under test within this experiment work. A 2.8 W depolarised pump was transmitting at a wavelength of 1452 nm configured in a backward pump direction using a WDM coupler. A 5 W high-power isolator was spliced after the pump to protect from any backscattering towards the pump. The signal at 1535 nm was coupled via WDM in the forward direction to propagate further in a Raman amplifier. After propagating through the Raman gain medium, the backward direction pump was decoupled by the input WDM and transmitted to a beam dump. The Raman gain medium was a long length (6.5 km) of dispersion-shifted fibre (DSF) with zero dispersion wavelength at ~1542 nm. The attenuation of the 6.5 km DSF was ~0.22 dB/km. Another isolator before coupling the signal was employed to protect backward pump leakage towards the signal.

Power spectra with the gain spectrum for the Raman amplified signal are shown in Figure 4.7 for a discrete Raman amplifier. The spectra were measured with an OSA connected to a 1% optical tap coupler at input and output of DRA resolution of 0.1 nm. Input signal power to the amplifier was -2.7 dBm and output power 10.3 dBm. At the OSA, input signal power was at -30.0 dBm, and

amplified output signal power was -17.0 dBm. The total net gain achieved was 13 dB at 1535 nm used as signal transmission wavelength. The Raman amplifier was limited at 13 dB gain at 1535 nm without incurring lasing. It is important to note that peak gain at 1560 nm was around 18 dB by DRFA, which was not suitable for FOPA to provide any gain on that wavelength.

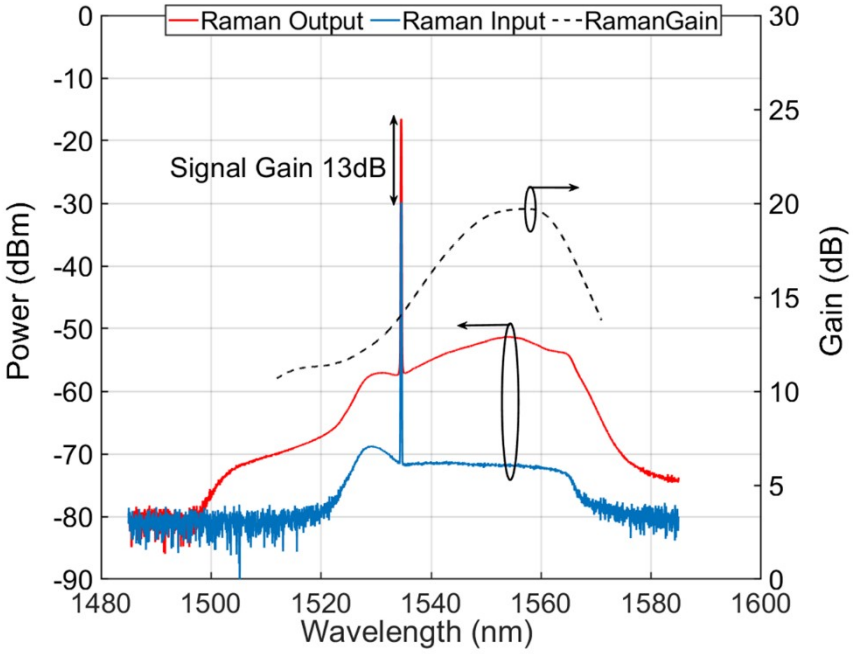

Figure 4.7 Signal power and gain spectra of burst signal at the input and output of discrete Raman amplifier

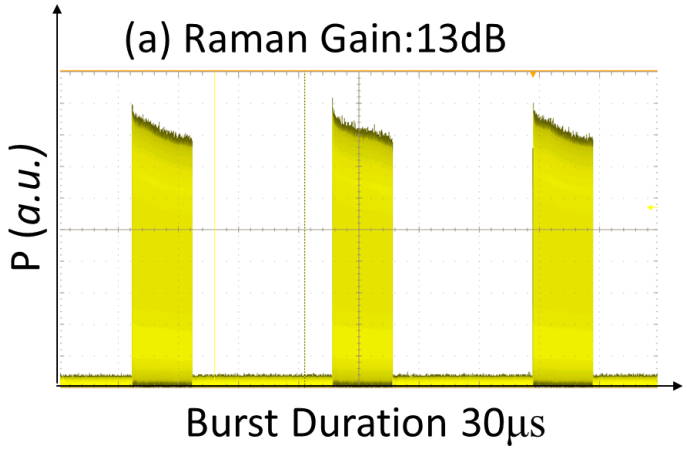

Figure 4.8 Burst signal waveform amplifier by DRA at receiver with 13 dB gain

Raman amplified burst waveform at 30 μs burst duration is shown in Figure 4.8 captured with a real-time oscilloscope. Counter propagating signal and pump within a long 6.5 km Raman gain medium creates a transient effect for amplification of burst signal [166]. Discrete Raman amplification using a counter-propagating pump and signal demonstrate a longer response time due to propagation delay in Raman gain medium. The propagation time of the amplified signal

within 6.5 km of DSF was around 32 µs, for the speed of light inside SSMF is $^{c}/_{n_{silica}}$. 30 µs burst signal suffers from slow response time when amplified by DRFA, as the amplified burst signal duration is less than the overall propagation time within Raman gain fibre length as discussed above. Overshoots at leading edges of the burst is visible due to transient effects in the discrete Raman amplifier. Raman scattering effect is inherently very fast ~76 fs [52], but engineering architectures of Raman amplifiers triggers transient effects.

4.1.4 Polarisation-Insensitive FOPA

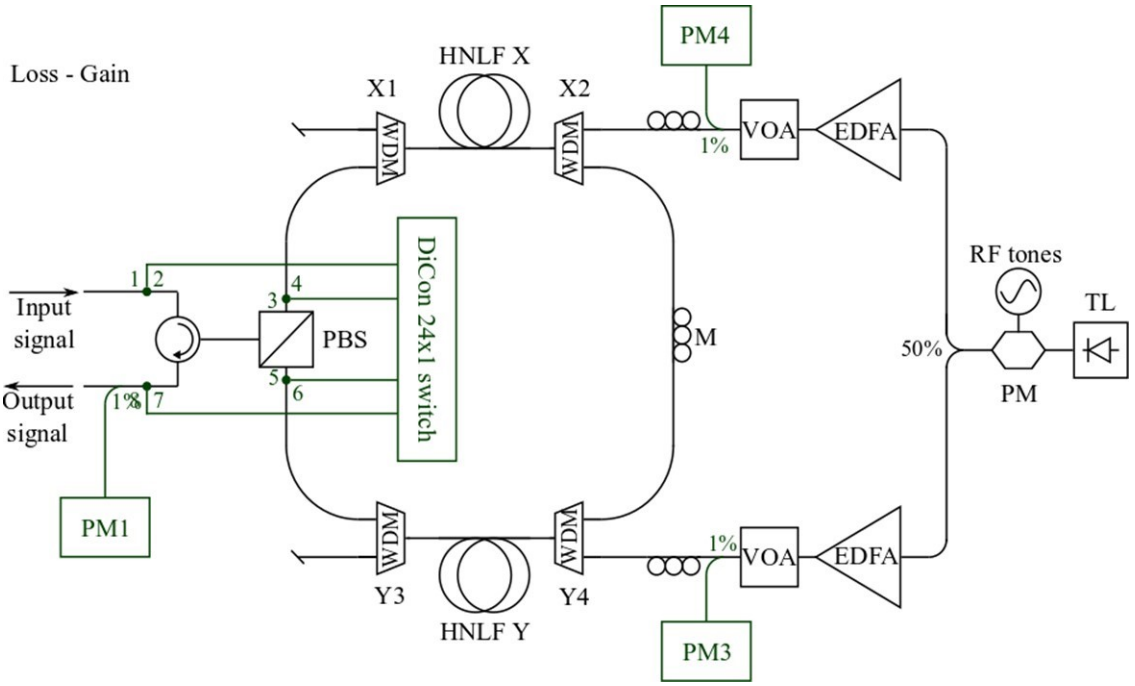

Figure 4.9 Experimental setup of polarisation-independent optical fibre parametric amplifier (PI-FOPA)

A polarisation-insensitive FOPA setup is presented in Figure 4.9, which involves SBS-protected half-pass diversity loop architecture as presented in [162]. The PI-FOPA setup was further controlled and modified within the use of this experimental work. As shown in this setup, an input optical circulator was employed to couple and decouple input and amplified output signals. First, the coupled input signal was orthogonally split by an input polarisation beam splitter (PBS), separating the signal into two orthogonal polarisation states. Further, orthogonally polarised signal components in the X and Y direction propagated in a counter-clockwise direction. Spectral monitoring of PI- FOPA is done via employing an optical switch (Dicon 24x1). Different switch ports were connected in the amplifier sections to monitor the input signal at the input circulator, monitoring signal after splitting and recombining amplified signal at the PBS, etc. Spectral changes were observed using a high-resolution optical spectrum analyser, which enabled real-

time monitoring of any spectral changes, gain, and power spectra measurements, including monitoring insertion loss within the amplifier.

Two high-power pumps were employed coupled with signals propagating in a loop. A tunable laser provided a pump wave fixed at λ_P of 1564.4 nm. The pump signal was split into two using a 50% coupler to get amplified by high power EDFAs and acted as pump sources to pump the two arms of the gain medium shown as HNLF X and HNLF Y. Before splitting the seed after the laser source, the pump dithering is employed to suppress SBS by phase modulating the pump. Three RF tones frequencies at 100, 320, and 980 MHz are used for phase modulating to mitigate SBS via pump broadening, also known as pump dithering [163]. The dithering process broadens the linewidth of the pump wavelength. Amplified pumps were monitored via high power meters using a 1% calibrated tap. After EDFA, each pump section was connected to a manual VOA to control launched pump power into the HNLFs acting as parametric gain media. The pumps were coupled through high power input WDM_{X1} and WDM_{Y4} with an overall insertion loss of ~0.5 dB.

Both pumps were polarisation controlled via individual polarisation controllers placed before coupling with the signal. The combined signal and pumps were sequentially passed through power monitoring stages at the input for input power monitoring and then pumped through the length of HNLF in each X/Y arm, acting as a parametric gain medium. Both paths X/Y were spliced together via a standard loop polarisation controller located in the middle of the HPL to increase input signal power to each arm propagating in the opposite direction. In this PI-FOPA architecture, orthogonally split signals first went through the loss section by propagating in opposites direction and were then amplified in the gain section.

It is essential to discuss that pump SBS was a major limitation when pumps propagated backward to the signals [149], [167]. As FOPA is a unidirectional amplifier counter-propagating, pump-signal interaction creates serious back-reflection, broadens the pump spectrum, and limits signal amplification performance. Therefore, it becomes important to remove pumps from a loop FOPA architecture after signal amplification. As shown in Figure 4.9, high-power pumps were removed via WDM connected after HNLFs in each path.

Each polarisation component was independently and equally amplified in two highly non-linear fibres (HNLFs) through gain arm X and gain arm Y. The HNLFs have a zero-dispersion wavelength of around $ZDW \approx 1564\ nm$. All the parameters described in Table 4.3

Parameters	HNLF $_X$	HNLF $_Y$
Pump Wavelength (λ_P) nm	1564.4	1564.4
Length (m)	250	200
Pump Power @20 dB gain (dBm)	33.8	34.8
Pump Power @13 dB gain (dBm)	33.1	34.5
Nonlinearity (γ)	8.2	8.2
Insertion Loss (dB)	1.4	0.9

Table 4.3 PI-FOPA functional parameters

Overall, the PI-FOPA setup in loss gain arrangement is much more beneficial for single-channel amplification, enabling much larger signal output powers. In access networks, large output powers are desired to enhance higher splitter ratios. Also, unwanted FWM products are controlled by the pump's removal, which improves non-linear crosstalk between signal-pump, pump-pump, and pump-idler. Pump polarisation is controlled by three plate polarisation controllers for X and Y polarisation arms. Another PC is located within the middle of the diversity loop to realign polarisation drifts. The polarisation drifts incur from the parametric gain fibres employed within the PI-FOPA setup. Additionally, unwanted drifts within the signal originate from vibrational and temperature changes affecting FOPA stability. Polarisation controllers within the loop although, the drifts are on a scale of signal bit-level, which are not compensated with employed low bandwidth polarisation controller.

Figure 4.10 shows a gain spectrum of PI-FOPA against wavelength. Using an ASE source acting as a probe to the amplifier, net gain of 20 dB was demonstrated, with an input power of ASE at 10 dBm, and pump powers of parametric amplifiers were 34 dBm and 33 dBm adjusted to achieve 20 dB gain. The gain spectrum shows the peak of FOPA gain at around 1535 nm and is therefore compatible to amplify the signal at 1535 nm with 20 dB FOPA gain. An interesting observation with equal net gain reaching 20 dB was observed at longer wavelengths in the L-Band spectrum. Flat PDG with ~0 dB was obtained for the wavelength range of >80 nm covering FOPA gain bandwidth. PDG was calculated as a difference between the amplified X component and Y component of polarisation independent signal, split orthogonally by an input PBS. The spectrum analyser was used for measuring net gain and also for measuring polarization-dependent gain by offline processing. It confirms that the polarisation diversity loop arrangement is used to obtain independent polarisation gain and minimize polarisation-dependent gain, as discussed in chapter 3, section 3.6.2.

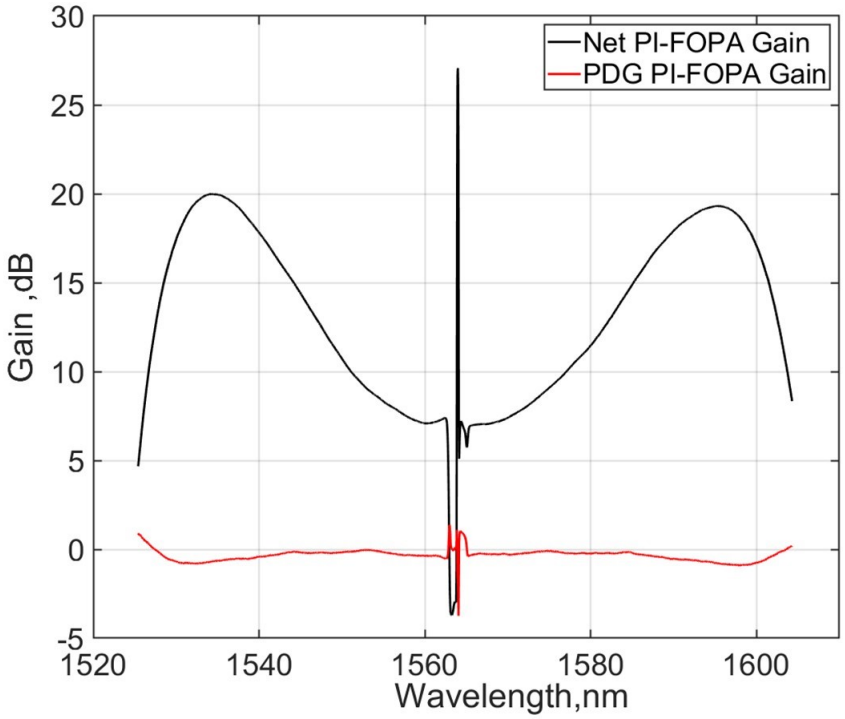

Figure 4.10 Polarisation-independent FOPA 20 dB net gain measured with a C-band ASE source

Figure 4.11 and Figure 4.12 demonstrate power spectra of PI-FOPA amplified 10 Gbps OOK signals at 20 dB and 13 dB net gain. The optical power spectra were measured by OSA at the input and output of PI-FOPA at a resolution of 1 nm. 20 dB polarisation insensitive gain was achieved for an amplified signal at 1535 nm. Residual pump at 1564.4 nm and idler at 1594.4 nm are obtained as a part of parametric amplification as shown in the power spectra. Input signal power was -9.2 dBm, and amplified output signal power was 10.5 dBm.

Figure 4.12 shows input/output signal spectra for PI-FOPA with 13 dB net gain. The spectrum shows the signal at 1535 nm, residual pump at ~1564 nm, and generated idler at 1595 nm. The spectra were measured at 0.1 nm OSA resolution. The spectrum of 20 dB gain and 13 dB differ in visual OSNR due to OSA resolution. The OSNR for 20 dB signal gain spectra was lower than 13 dB signal gain spectra. A small peak at L-band wavelength results from back-reflection occurring from PM fibre spliced to the PBS at an input port. It is not visible for 13 dB gain due to low pump power requirements for achieving 7 dB less net gain. Overall, power spectra confirm PI- FOPA gains at variable gain levels of 20 and 13 dB. The input signal power was measured at - 21.97 dBm and the amplified output signal power was at -8.9 dBm.

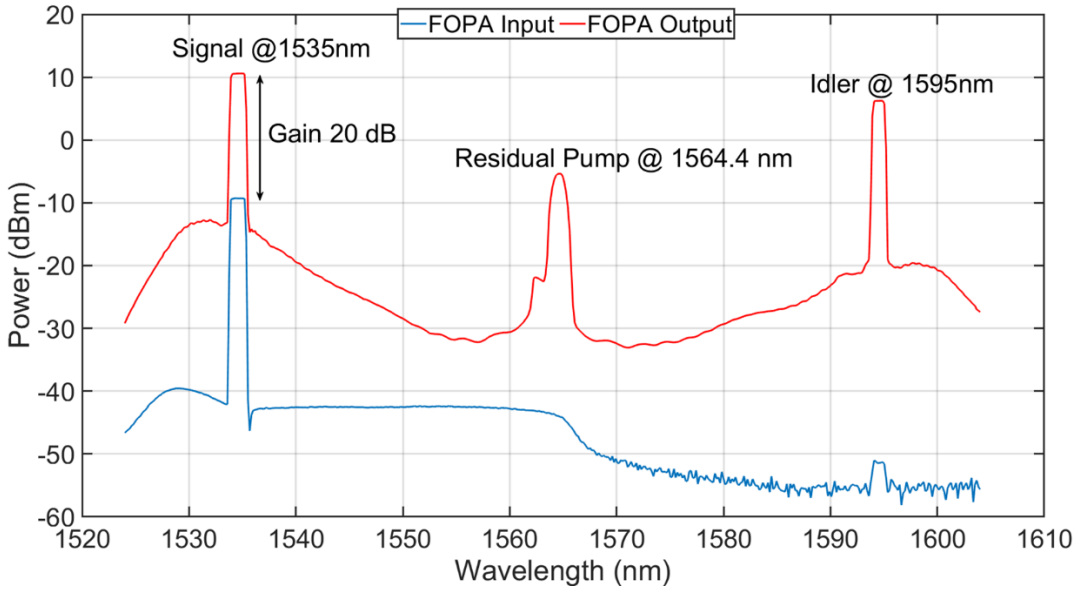

Figure 4.11 Power spectra of PI-FOPA amplified burst signal at 20 dB net gain at input and output of FOPA

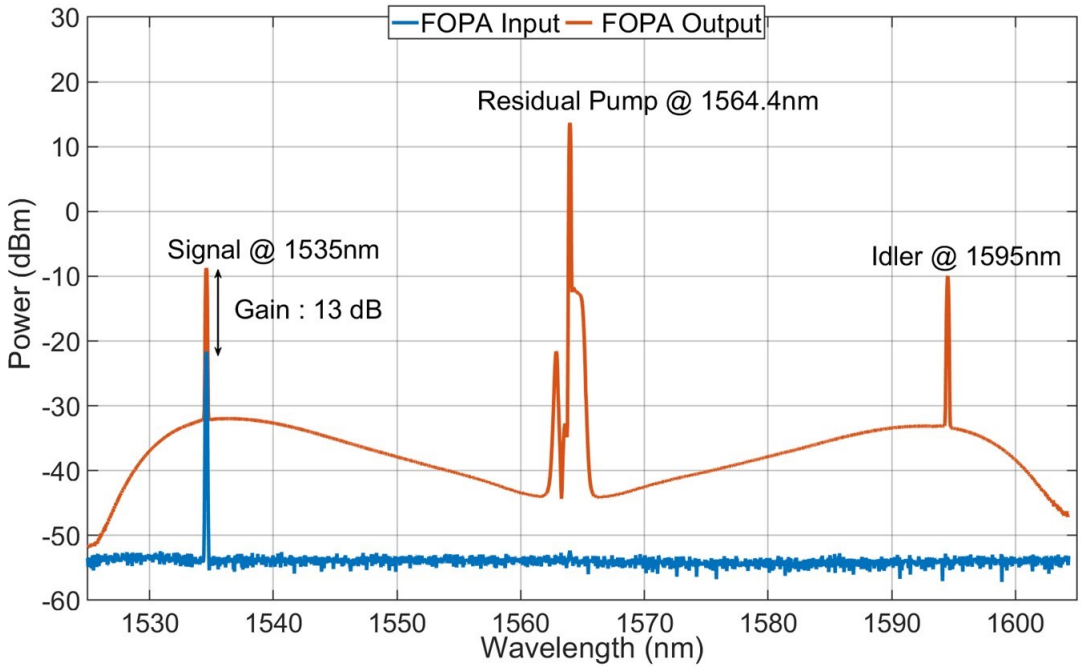

Figure 4.12 Power spectra of PI-FOPA amplified burst signal at 13 dB net gain at input and output of FOPA

Figure 4.13 shows burst waveform at 30 μs burst duration with PI-FOPA amplified net gain at 20 dB and 13 dB. Figure 4.13 (a) shows 20 dB PI-FOPA amplified burst waveforms, no transient effects were observed, and clean amplified bursts were detected. Compared with EDFA amplified burst at 30 μs duration shown in Figure 4.5 (a), FOPA performs much better when amplifying burst signals. In Figure 4.13 (b), a burst waveform at 30 μs amplified by PI- FOPA at 13 dB net gain is shown. Similar to FOPA amplified at 20 dB, no gain fluctuation was obtained, confirming no presence of transient. In comparison with the burst waveforms amplified by EDFA and Raman

amplified shown in Figure 4.5 (b) and Figure 4.8, no burst distortion is noticed for an amplified detected signal, confirming that the ultrafast response time of FOPA prevents any transient or gain fluctuations for sub-microsecond burst durations. The FOPA amplified bursts pattern seen in Figure 4.13 follows those observed in B2B bursts waveforms. This pattern stems from the transmitter and receiver, as discussed in section 4.2.1. The absence of burst distortions in the FOPA case demonstrates the ability of the FOPA to deliver practically instantaneous dynamic gain required for transmission of bursty traffic in reach extended access networks.

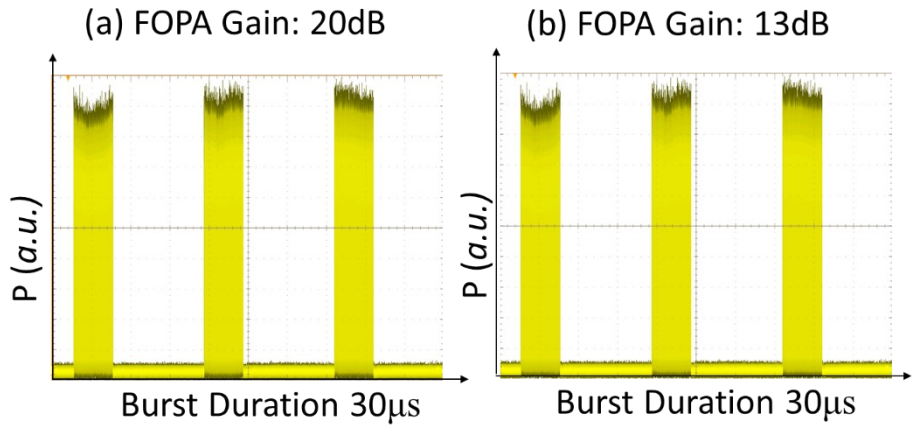

Figure 4.13 Burst waveform amplifier by FOPA detected at receiver with 20 dB and 13 dB EDFA net gain

4.2 Performance Analysis of amplified signals by AUTs

This section presents the performance analysis of each AUT as an in-line amplifier for reach extended access links: a commercial EDFA, a discrete Raman amplifier, and a polarisation-insensitive FOPA. Performance of the signal measured via bit error ratio calculated for amplified non-burst and with burst signal at burst duration of 50 μs, 30 μs, and 10 μ. Firstly, the B2B configuration was analysed by BER vs. received power in both signal scenarios of burst and non-burst to create a reference of performance measurement. A non-burst signal was investigated before the analysis of bursty signals to provide a baseline for studying transient effects in standalone AUT. BER has averaged over ten signal bursts with a total duration of 1 ms was carried out, where analysed bits varied from 10^7 for a non- burst signal to 10^6 for 10 μs signal bursts. Later burst signal performance was compared for 20 dB signal gain with PI-FOPA and EDFA. Further, including Raman amplifier signal performance at 13 dB net gain was analysed for all AUTs. Finally, the evolution of BER along the burst signal duration was measured to understand signal distortion due to transient effects by each tested amplifier.

4.2.1 BER characterization of signals

Before BER measurements for non-burst and burst signals against received power, methodology for signal processing with threshold detection and received power sweep is discussed below. Figure 4.14 shows fluctuations in non-burst signal arising from the transmitter AOM. In Figure 4.14 (a) non-burst signal without AOM is transmitted and detected to compare with B2B signal with AOM. As seen in Figure 4.14 (b), B2B with AOM shows fluctuations arising incurring after employing AOM.

Figure 4.14 (c) shows unstable fluctuating bits in a 30μs burst mode signal, the observed fluctuations were noticed for 100 ns in a B2B detected burst mode signal. The bits between this fluctuating time are discarded before error counting in all the cases, which is equivalent to the total 100 bits:

$$No.of\ Bits = Speed\ of\ Signal\ x\ Duration\ of\ Burst$$

Threshold detection was built in an offline DSP used to measure BER of non-burst and burst mode signals similar to the approach described in [36] with an auto-control function capable of 50 ns settling time.

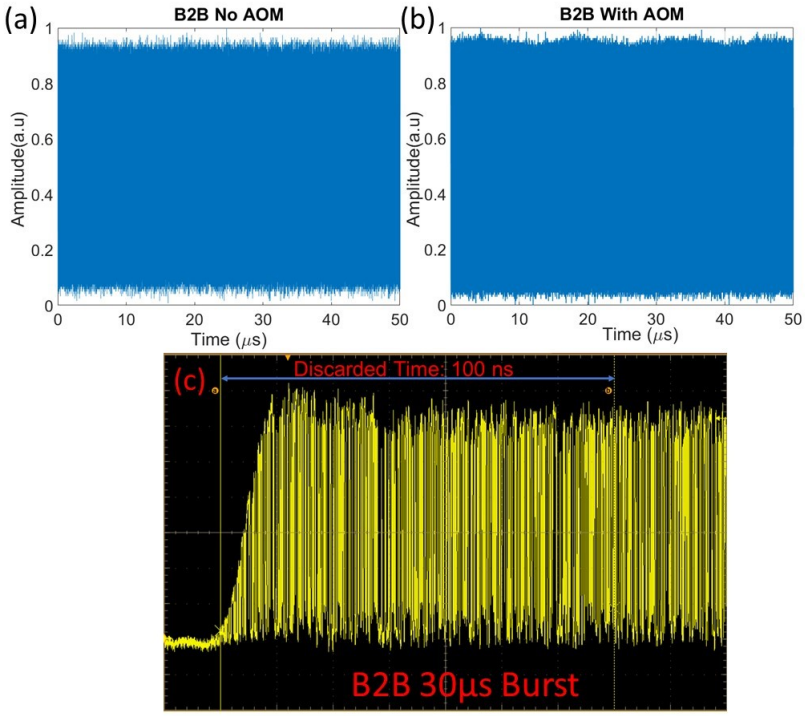

Figure 4.14 Non-burst waveform in B2B configuration with (a). No AOM and (b) With AOM shown with (c) 30 μs burst waveform showing discarding time of 100 ns

A VOA emulating an optical splitter was employed to sweep received burst power. The attenuator had an insertion loss of ~1 dB. Figure 4.15 shows attenuation sweeps for 30 μs B2B burst

waveforms, performed with an attenuation sweep of 13 dB. The burst with the lowest attenuation shows attenuated burst by 0 dB and maximum attenuated burst with 13 dB.

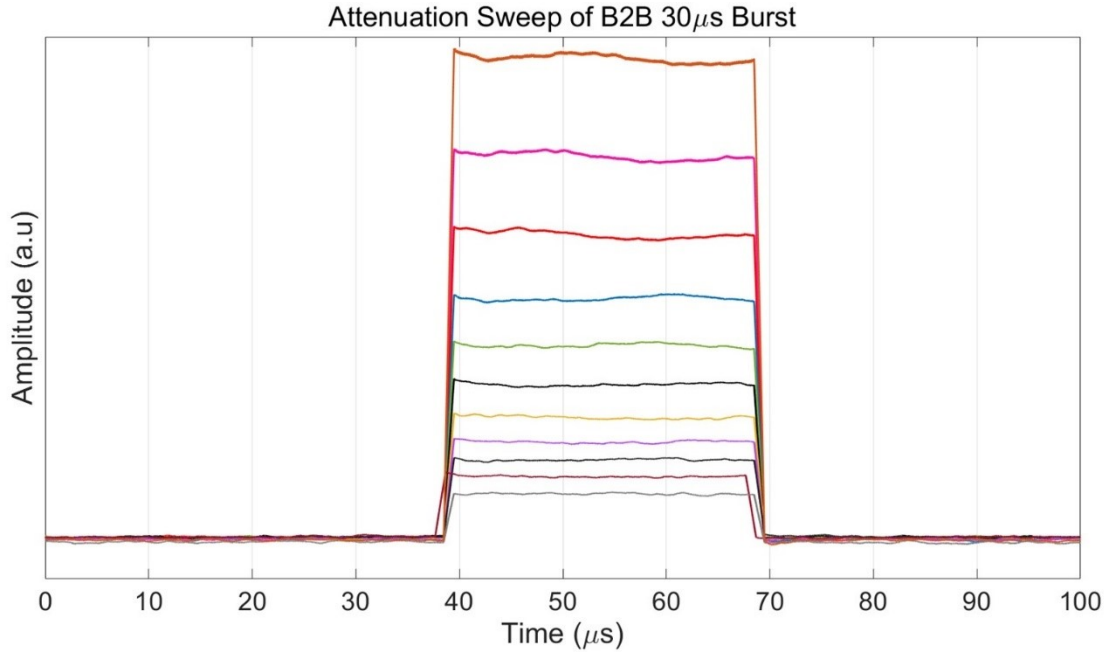

Figure 4.15 Overalapped waveforms of received 30 μs burst signal with 1 dB VOA change for BER calculation against received power

4.2.2 Performance of AUT's for non-burst mode

I first compared BER for non-burst signals in two configurations as B2B and amplified under test with a commercial EDFA, a discrete Raman amplifier, and PI-FOPA in 50 km reach extended PON architecture. Firstly, the B2B configuration for the non-burst signal was measured to set a reference point. Further, to understand penalties incurring from 50 km SMF and AUTs, a non-burst signal was amplified and calculated for BER measurement. BER was measured for two signal gain scenarios for non-burst mode signal amplification (a) 20 dB gain with EDFA and FOPA excluding Raman and (b) 13 dB gain including Raman amplifier.

Figure 4.16 and Figure 4.17 presents BER vs. received power for non-burst signal amplification at 20 dB and 13 dB gain. The analysis provides a standalone performance indication that affects the signal introduced from AUTs: noise figure, dispersion penalty, and nonlinearity stem from transmission fibre and tested amplifiers. Therefore, this analysis provides the study of received power penalty incurred from induvial AUTs in non-burst mode condition. A maximum delay between the signal frequency components due to dispersion was about 85 ps calculated as a product of SSMF dispersion of 17 ps/nm*km^{-1}, a measured signal bandwidth of 0.1 nm, and the transmission fibre length of 50 km using the walk-off equation $\tau = D \times \Delta\lambda \times L$. A bit duration of a 10 Gbps signal is 100 ps, so the delay introduced by dispersion of the transmission fibre is still less than bit duration, but introduce a minor performance penalty [168]. A nonlinear phase shift

of the signal was 0.2 rad calculated as a product of the SSMF nonlinearity coefficient $\gamma = 0.78\ W^{-1}km^{-1}$ [169], the transmission fibre effective length of $L_{eff} = 23\ km$, and the peak input signal power of $P_{in} = 10.5\ dBm$ (11.2 mW). The value of non-linearity in 50 km SMF was not significant to observe signal broadening for a nonlinear phase shift of 0.2 rad.

Figure 4.16 shows BER against received power measurement for B2B, EDFA, and PI-FOPA at 20 dB non-burst signal gain. For non-burst signal amplification, EDFA shows better performance than the PI-FOPA amplified signal. Around 1.5 dB received power penalty is observed between B2B and EDFA. The penalty increased to ~2 dB from B2B to PI-FOPA amplified non-burst signal. A discrete Raman amplifier was excluded from this measurement as it was impossible to obtain 20 dB net gain without incurring lasing [170]. Overall, EDFA as a state-of-the-art amplifier technology validates its performance and amplifies a non-bursty signal better than PI-FOPA by ~1 dB penalty at a BER level of 10^{-6}.

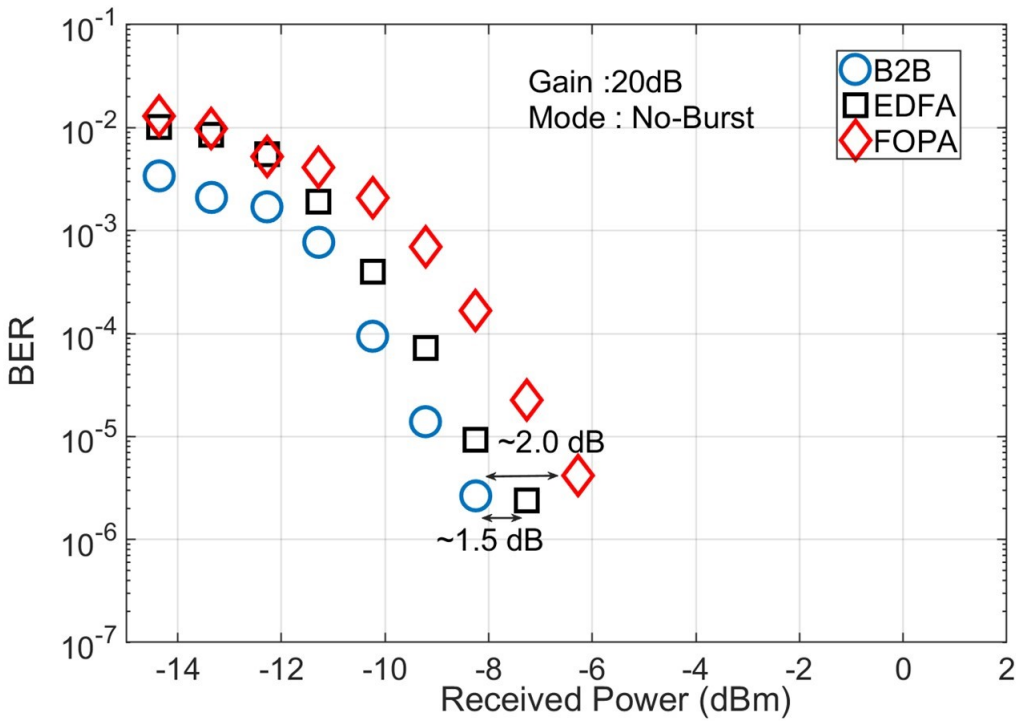

Figure 4.16 BER vs. received power for B2B compared with EDFA and PI-FOPA at 20 dB net gain for non-burst mode signal amplification

Figure 4.17 demonstrates BER vs. received power, including the Raman amplifier measured at 13 dB signal gain. All AUTs were set at fixed signal gain to make a fair comparison as EDFA and PI- FOPA was operational at 20 dB gain. similar to what, 20 dB net gain EDFA still presents better performance than the other two AUTs. ~1 dB received power penalty was noticed between B2B and EDFA at a BER level of 10^{-6}. The received power penalty increased to ~2 dB with FOPA amplification compared to B2B at a similar received power of -8 dBm. The Raman amplifier shows better performance than FOPA, similar to EDFA in non-burst mode with ~1 dB power penalty. In

both the gain scenarios of no-burst mode signal amplification, EDFA demonstrated better performance in received power than DRA and PI-FOPA.

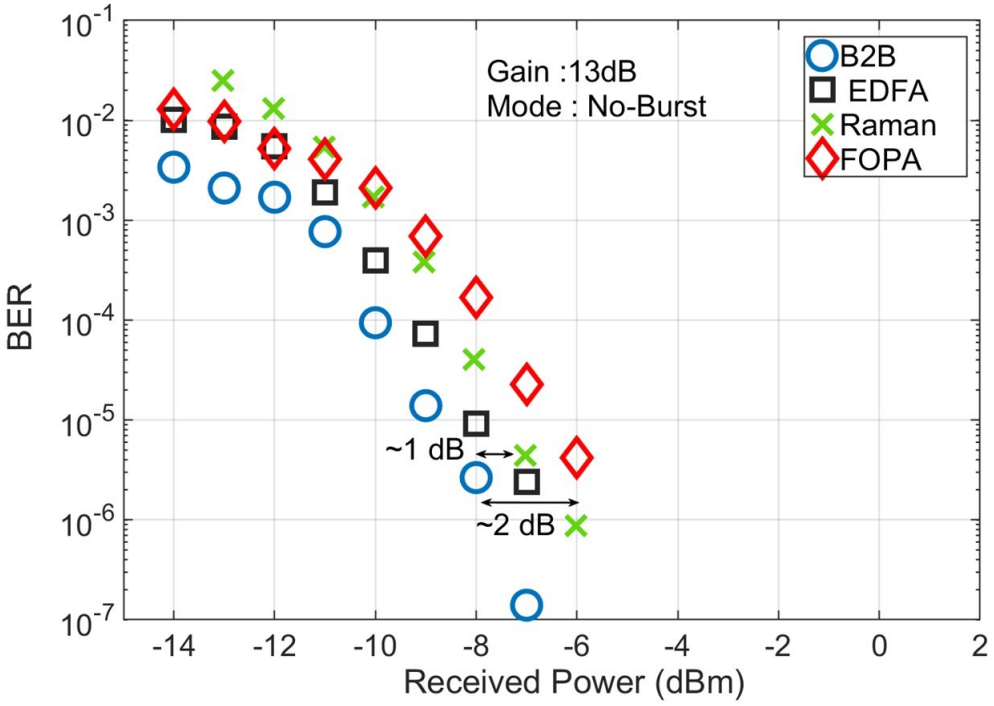

Figure 4.17 BER vs. received power for B2B compared with EDFA, Raman, and PI-FOPA at 13 dB net gain for non-burst mode signal amplification

4.2.3 Burst signal performance at 20 dB net gain

This section analysed BER against received power with 20 dB gain for the burst mode signal amplification with burst duration of 30 μs and 20 μs by EDFA and PI-FOPA. B2B signal in burst mode for similar burst durations was measured for obtaining a reference to compare AUT performance. Figure 4.18 shows BER performance for the amplified burst duration at 30 μs by a commercial-grade EDFA and PI-FOPA. B2B signal performance shifts by ~3 dB in received power when switched from non-burst to burst mode at 30 μs at BER level of 10^{-3}, as shown in Figure 4.18. EDFA performance suffers severe degradation in BER performance, and around 3 dB received power penalty was observed compared to B2B at 20 dB 30 μs burst signal amplification. The inclusion of transient effects incurs large gain fluctuations and destroys leading bits of the burst signal. At higher received signal power from -4 dBm and 0 dBm, a transient floor is visible. It suggests even increasing signal power does not improve the BER level for EDFA amplification of 30 μs burst mode signal.

On the other hand, FOPA amplified burst mode signal at 20 dB net gain demonstrates a minor receiver power penalty compared to the EDFA. FOPA amplified 30 μs bursts compared to B2B demonstrates almost similar B2B performance. FOPA demonstrates ultrafast response time,

therefore amplified 30 μs burst duration occurs without any noticeable penalty in comparison to EDFA with its slow response time.

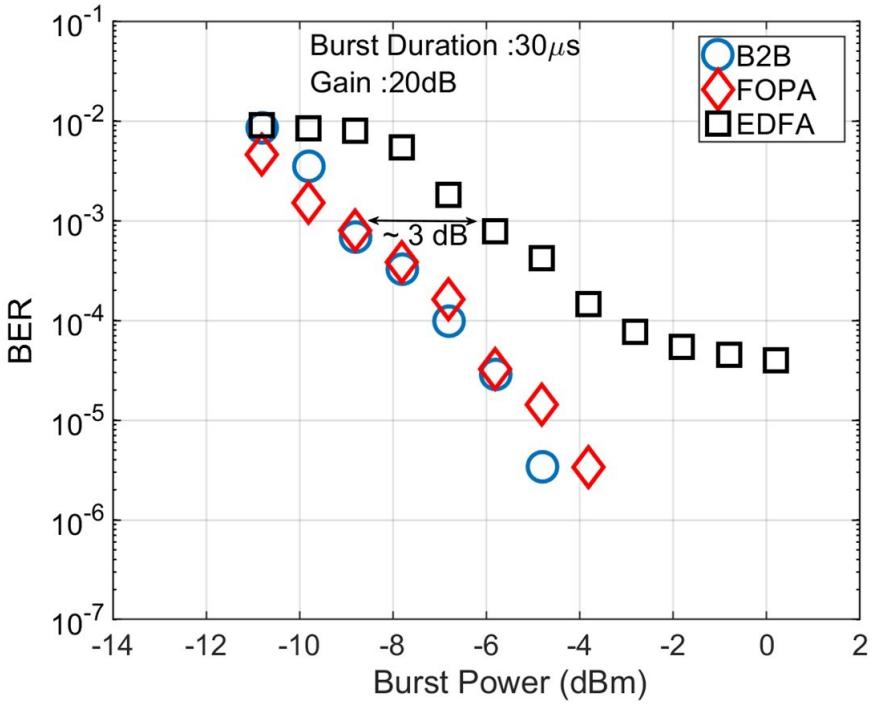

Figure 4.18 BER vs. average burst power for 30 μs burst duration for B2B and EDFA, FOPA amplified signal at 20 dB net gain.

Similar measurements for BER vs. received burst power were done for shorter burst durations of 20 μs amplified by EDFA and FOPA at 20 dB signal gain and are presented in Figure 4.19. As before, B2B in burst mode of 20 μs was measured and added to create a penalty reference for compared AUTs. B2B performance for burst duration of 30 μs and 20 μs was very similar with ~<1 dB penalty. At 20 μs burst duration, EDFA performance degrades to an unrecoverable signal with BER level not even reaching 10^{-3}. BER curve for EDFA does not show any improvement even at higher signal received power levels up to 0 dBm. The visible transient floor in EDFA amplification at 20 dB gain confirms the effect of slow response time for burst mode signals.

FOPA amplified burst signals performance shows virtually no effect of transient on burst signal amplification at 20 μs. A minor received power penalty of <1 dB occurs between B2B and FOPA amplified signal. The penalty in PI-FOPA arises from the looped polarisation diverse architecture that provides bi-directional gain within the loop and becomes susceptible to lasing and multi-path interference. The results show that the PI-FOPA can amplify burst signals at different burst durations with 20 dB net gain. At the same time, the commercial-grade EDFA suffers from the transient effect and degrades the burst signals at both burst duration of 30 μs and 20 μs.

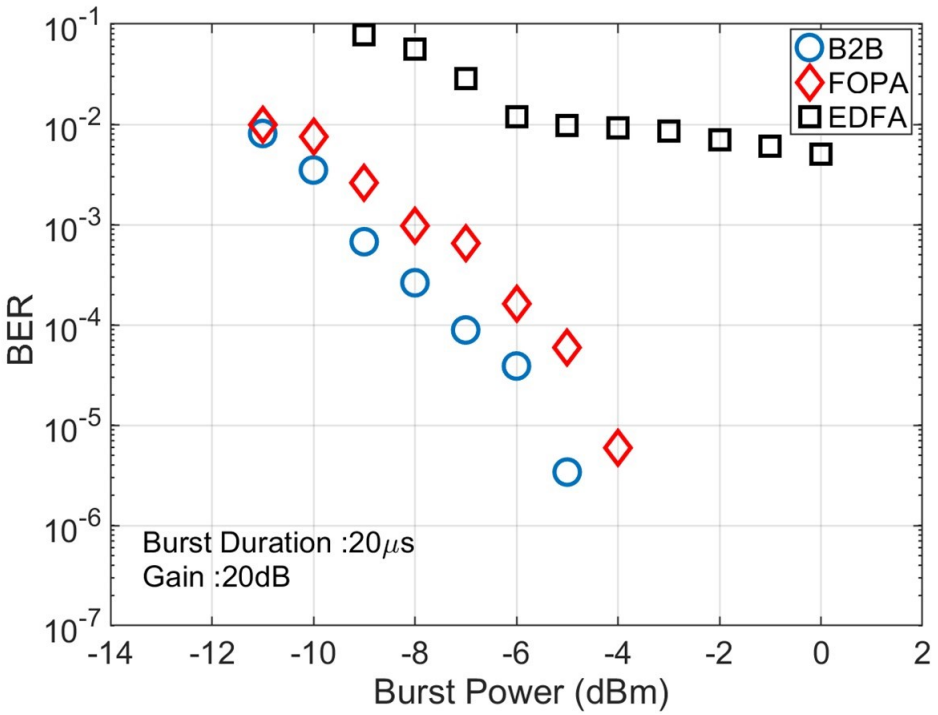

Figure 4.19 BER vs. average burst power for 20 μs burst duration for B2B, EDFA, and FOPA amplified signal at 20 dB net gain.

4.2.4 Burst signal performance at 13 dB net gain

In this section, the performance of bursty signals was analysed, presented in two configurations as B2B and with AUT's including a discrete Raman amplifier for a fixed gain of 13 dB. Similar to the previous section performance of each AUT was analysed via BER measurements at a burst signal duration of 50 μs, 30 μs, and 10 μs amplified by each tested drop-in amplifier to evaluate the impact of transients on the bursty signal. Also, the transmitted burst mode signal in B2B scenario within the same measured burst duration was assessed to provide a benchmark reference point. Observed BER performance individually was compared for B2B+AUT at 13 dB net signal gain.

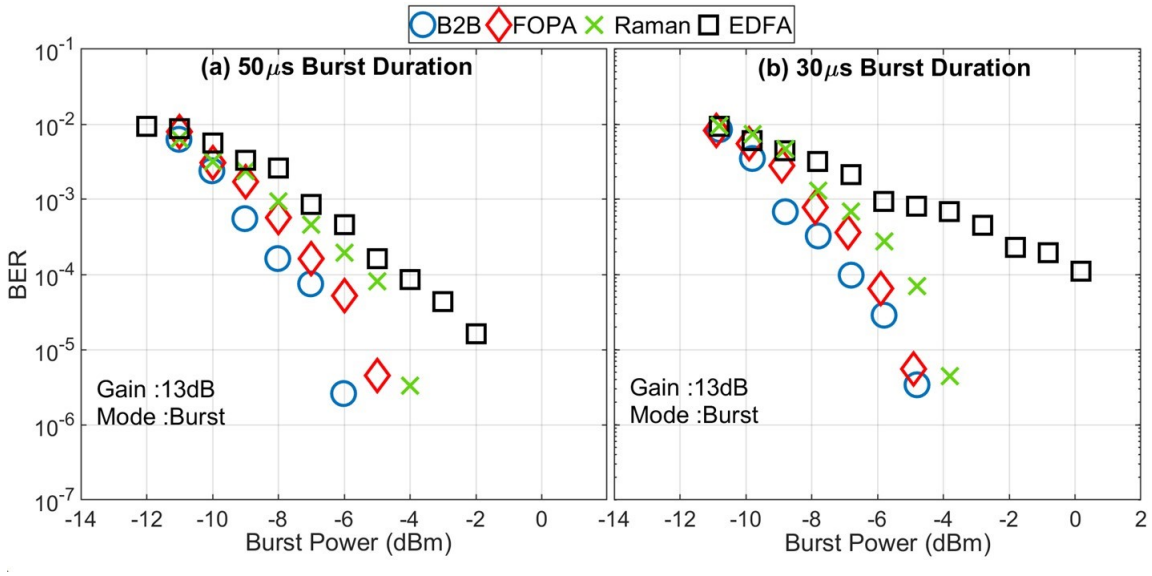

Figure 4.20 BER vs. average burst power measurement with EDFA, DRA, and PI- FOPA for (a) 50 μs and (b) 30 μs

Figure 4.20 shows BER vs. burst power analysis for 50 μs and 30 μs burst durations. Firstly 50 μs burst is amplified, and BER is evaluated as shown in Figure 4.20(a) EDFA amplified burst demonstrate ~2 dB burst power penalty at BER level of 10^{-3} showing degraded performance due to transient effects. Both Raman and FOPA, the amplified signal shows similar BER performance for 50 μs burst. In comparison to B2B, both Raman and FOPA observe a <1 dB power penalty.

Figure 4.20 (b) shows performance analysis for a 30 μs signal amplified at 13 dB signal gain. Similar to 50 μs BER, both tested Raman amplifier and FOPA amplified bursts do not include any major penalties compared to B2B signal, and <1 dB power penalty is observed at BER level of 10^{-3}. Whereas EDFA performance degrades further for a 30 μs amplified burst signal due to incurring transient fluctuations. Compared to B2B at BER level of 10^{-3} ~3 dB signal power penalty is observed from the received power level of -9 dBm at B2B.

Both discrete Raman amplifier and PI-FOPA BER curves show similar dependency as for the B2B scenario. Consequently, the minor power penalty of BER for the 50 μs and 30 μs bursts was mainly due to limitations of the receiver and transmitter rather than due to amplifiers as the effect of burst duration change is observed in B2B also. With the Raman amplifier, the underlying principle is that the SRS effect has a response time with femtosecond time scale (<100 fs), where the propagational delay is not effective concerning burst duration [52]. For large gain and transmission capacity, backward pumped discrete Raman fibre amplifiers are specifically employed in metro and access applications [83]. However, employing Raman amplifiers with a large gain medium has a longer propagation time and therefore incurs transient effects, especially for TDMA based signal protocols.

Amplified bursts with polarisation-insensitive FOPA, as in Figure 4.20, show similar performance as B2B for both the cases of 13 dB amplification for 50 μs and 30 μs burst durations. Received power required to achieve the same BER for both burst signal durations were under 2 dB in all the cases discussed. The penalty occurring in FOPA is mainly attributed to performance limitations of the non-burst mode receiver and non-optimized burst mode transmitter [171].

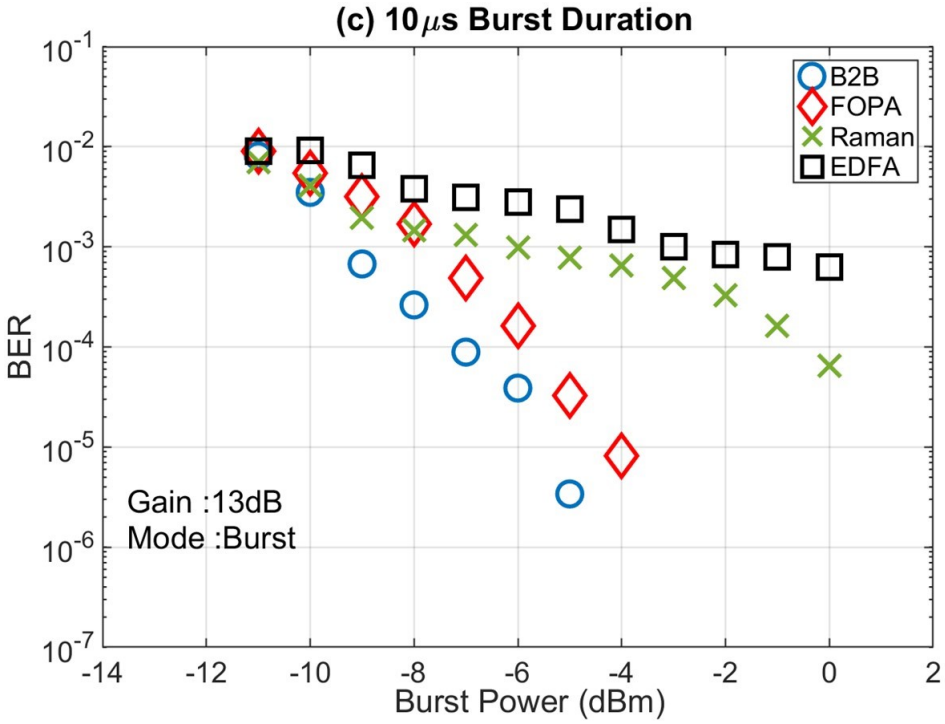

Figure 4.21 BER vs. average burst power for 10 μs burst duration in B2B with EDFA, DRA, and PI-FOPA amplified signal at 13 dB net gain

Figure 4.21 shows BER against burst power comparison between B2B and tested amplifiers at burst duration of 10 μs with 13 dB net gain. B2B at BER level of 10^{-3} shifts by ~1 dB in received power compared to B2B burst signal at 30 μs, showing the non-burst mode receiver suffers from detecting shorter burst duration signals. For EDFA amplified 10 μs burst signal, power penalty increases up to 8 dB compared to B2B at BER level of 10^{-3}. Besides, the power penalties on 10 μs bursty signal were much higher at the lower BER level and could not even reach BER level of 10^{-4} at burst power of 0 dBm. Overall, when amplifying short-duration bursty signals, EDFA further significantly degraded BER at a lower net gain of 13 dB.

In the case of a discrete Raman amplifier, amplifying 10 μs with 13 dB net gain shows significant degradation of BER with increased signal power compared to 30 μs burs signal. A received power penalty of around 4 dB was observed in comparison with B2B. This can be attributed to transients arising in backward pumped Raman amplifiers due to the time required for the pump and the signal to propagate along with a long gain fibre medium[133]. With the

tested Raman amplifier, the propagation time through the 6.5 km long gain fibre is ~32 μs at the signal frequency of 195.4 THz. Therefore, although the Raman amplifier's response time is faster than that of the EDFA's, it depends on the scale of the traffic burst duration. Therefore, the Raman amplifier for burst duration shorter than signal propagation time suffers from transient effects. Transient effects in the Raman amplifiers can be suppressed by using either a forward pumping scheme or a shorter gain fibre [166]. Figure 4.21 with 10 μs burst signal amplification with FOPA performs identically to 50 μs and 30 μs. No noticeable power penalty was observed for 10 μs burst signal amplification, and power penalty was limited within <1 dB from B2B at BER level of 10^{-3}. Lower power penalty within 0- 2 dB confirms the lack of transient effects in FOPA when amplifying burst signals. Overall, FOPAs ultrafast response time makes it very appealing for the amplification of bursty signals.

4.2.5 Burst BER overlap and Eye Diagrams

Figure 4.22 shows BER evolution across burst waveforms amplified as an example for EDFA and FOPA at 20 dB net gain at 30 μs burst duration with received signal power of -5 dBm. EDFA BER evolution shows a continuous error with an overall BER of around 10^{-4}. Leading bits of the burst suffer transient overshoot and demonstrate the highest BER value, as burst transition towards steady-state BER values gets averaged around 10^{-4}. On the other hand, FOPA demonstrates occasional errors with an overall BER of 10^{-5}. This indicates that FOPA, in comparison with EDFA, is not vulnerable to slow response time and instantaneously amplifies bursty traffic. Figure 4.22(b) showing FOPA amplified burst waveform agrees with Figure 4.13 and Figure with 20 dB net gain.

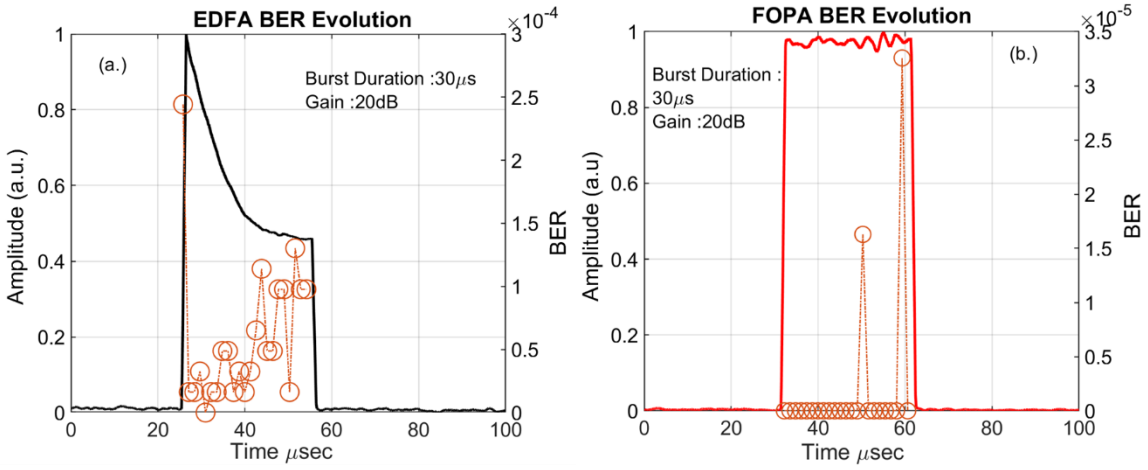

Figure 4.22 shows BER evolution for 30 μs burst for (a) EDFA with multiple errors occurred in bits and in (b) FOPA with occasional number of errors

Figure 4.23 demonstrates BER evolution across burst waveform amplified as an example for discrete Raman fibre amplifier at 10 μs burst duration averaged over 10 signal bursts at 13 dB

signal gain. Received signal burst power was at -2 dBm at a BER level of 10^{-4}. Continuous errors across the bursts present the accumulated effect of the transient in 10 μs burst duration.

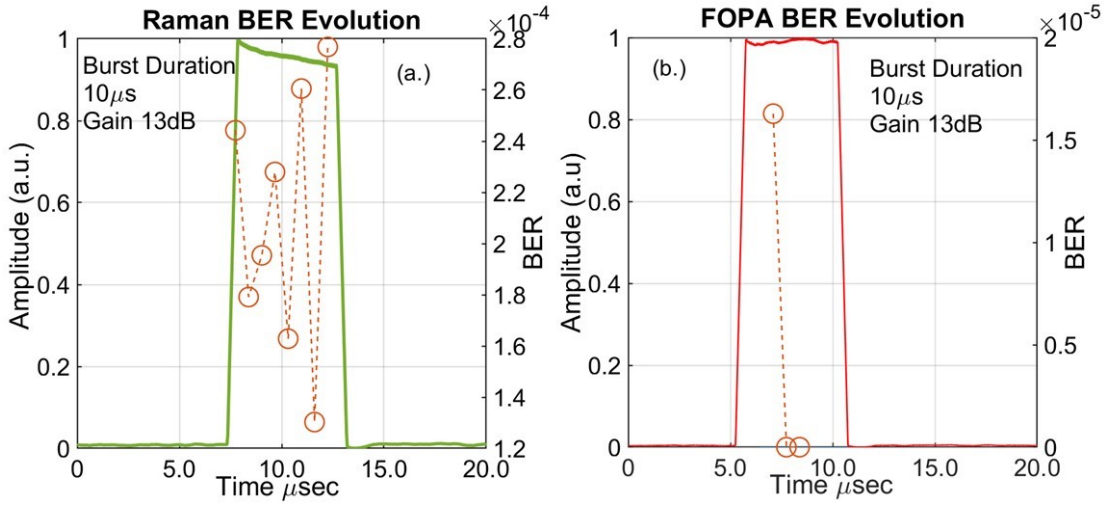

Figure 4.23 Raman and FOPA BER evolution for 10 μs burst signal at 13 dB signal gain averaged over ten signal bursts.

Figure 4.24 shows an eye diagram for all tested AUTs in non-burst and at 10 μs burst duration amplified at 13 dB net gain. For non-burst signals, eye diagrams were measured at received power of -3 dBm. The eye diagrams were measured at the receiver after BPF for all amplifiers. In all the cases, i.e., EDFA, Raman, and FOPA, a clear open eye corresponding to a BER level of 10^{-6} are observed for a non-burst signal. Similar eye diagrams for all AUTs suggest that a non-burst signal does not suffer from any major penalty in a 50 km reach extended access network architecture.

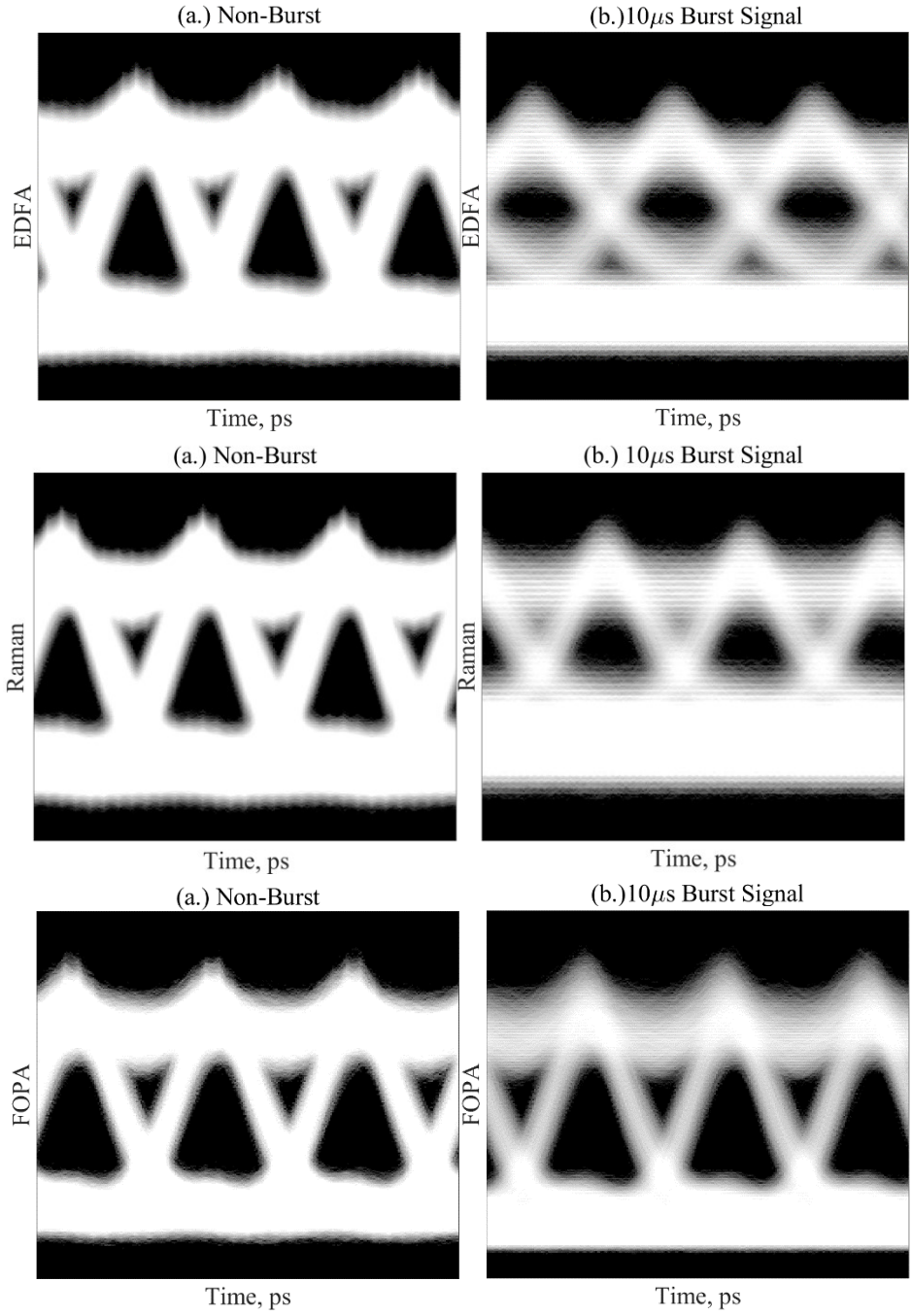

Figure 4.24 Eye diagram for (a) Non-burst (b) Burst of 10 μs amplified with 13 dB net gain by EDFA, Raman, and PI-FOPA at received power of -3 dBm

On the other hand, corresponding eye diagrams for 10 μs received burst signal shows penalty in signal occurring from transient effect for both EDFA and Raman amplifiers. Almost closed eye diagrams were detected for both EDFA and Raman amplifiers at a received power level of -3 dBm, whereas FOPA amplified burst signal at 10 μs at a received power level of -3 dBm shows an open eye confirming FOPA ultra-fast response time. Both the EDFA and Raman amplified burst signal at 10 μs corresponds to BER level of 10^{-3}, while the FOPA eye diagram at the same power level corresponds to BER of the level of 10^{-5}.

4.3 Effect of transient on receiver sensitivity by AUTs

Receiver sensitivity is one of the most critical parameters in access networks defining the available power budget and consequently the reach with maximum achievable split ratio [172]. In this experiment, receiver sensitivity is defined as the required average signal power to reach a BER level of 10^{-3}. The analysis was done with B2B providing a baseline for the performance of all AUTs at 13 dB gain. In this section, receiver sensitivity for burst duration from 70 μs to 5 μs, and the receiver sensitivity for the non-burst signal was also measured. Burst duration was varied according to the typical access network upstream bursts durations between 125 μs to 0.5 μs for measuring the receiver sensitivity with each tested optical amplifier [173].

In section 4.3.2, the sensitivity penalty for standalone AUTs is measured taking B2B as a reference receiver sensitivity at a BER level of 10^{-3}. Further, a penalty in receiver sensitivity was obtained for EDFA and Raman amplifier compared to FOPA.

4.3.1 Burst duration and receiver sensitivity

Figure 4.25 shows receiver sensitivity as a function of burst duration at BER level of 10^{-3} measured for B2B, PI-FOPA, Raman, and EDFA. As shown, burst duration was varied from 70 μs to 5 μs for a fixed burst period of 100 μs. The gain for all AUTs was set at 13 dB. As shown in 4.1.3, the above gain for discrete Raman fibre amplifier was limited by lasing and unable to provide 20 dB net gain at 1535 nm, and for a fair comparison, the gain was fixed at 13 dB.

The non-burst signal in B2B has a sensitivity of -12 dBm, but when switched to burst mode, receiver sensitivity of B2B shifts to 2 dB, reaching -10 dBm at 50 μs reasonably due to limitations in photodetector for burst mode signal detection. From 50 μs- 5 μs burst duration, B2B sensitivity was stable at -10 dBm without any further penalty being observed.

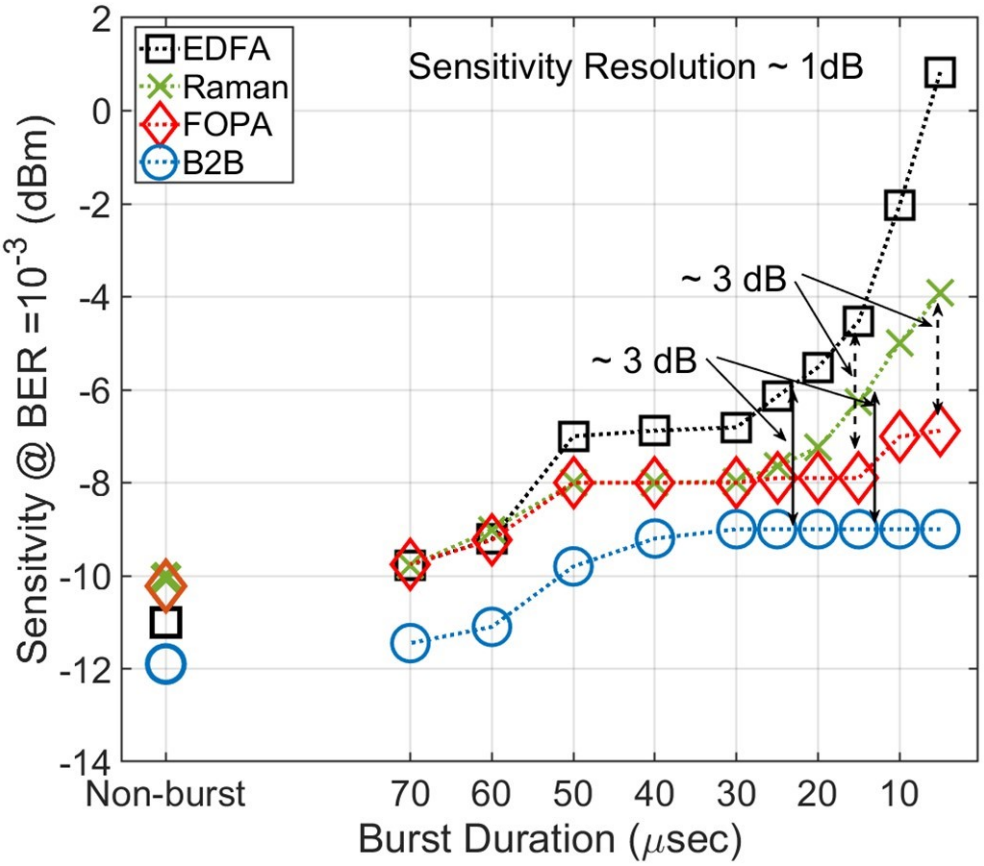

Figure 4.25 Receiver sensitivity vs. burst duration from 100% (non-burst) to 5 μs measured at BER level of 10^{-3} for B2B and AUT at 13 dB gain

The EDFA with non-burst signal displayed receiver sensitivity level at -11 dBm, with better performance than Raman and FOPA amplifiers by ~1 dB. When switched to burst mode due to the occurrence of transient effects, EDFA suffers from 1 dB at 70 μs up to 3 dB at 20 μs compared to the B2B case for receiver sensitivity. This penalty increases and reaches up to ~8 dB for the shortest burst duration of 5 μs from B2B, demonstrating non-recoverable burst signals distorted due to severe transient occurring in a tested commercial grade EDFA.

The discrete Raman fibre amplifier demonstrates very similar receiver sensitivity performance as PI- FOPA for the receiver sensitivity of a non- burst signal at -10 dBm. When switched to burst signal amplification, the Raman amplifier demonstrates the sensitivity of - 8 dBm with ~1 dB penalty from B2B up to 30 μs burst duration similar to the FOPA measured sensitivity. Amplification of bursts with <30 μs degrades receiver sensitivity performance and shoots the penalty up to 3 dB at 15 μs, this increased to ~5 dB penalty at 5 μs in comparison to B2B. This confirms the theory, as the duration of propagation increased for backward pumped discrete Raman amplifier when amplifying short-duration bursts and makes the effect of transients severe. The PI-FOPA amplified non-burst signal achieves an almost equivalent receiver sensitivity to the Raman amplifier at - 10 dBm. The FOPA demonstrates stable performance when

switched to burst mode signal amplification with receiver sensitivity within 1 dB variation in comparison to B2B. FOPA presents >3 dB sensitivity improvement in contrast with tested EDFA and Raman amplifier when amplifying short burst signals of 5 μs.

4.3.2 Receiver Sensitivity Penalty in AUTs

Figure 4.26 shows the receiver sensitivity penalty for the tested AUTs measured from B2B at a BER level of 10^{-3}. The penalty was calculated, keeping B2B as a reference for measuring receiver sensitivity. The receiver sensitivity penalty demonstrates a critical result to demonstrate the performance of PI-FOPA in comparison to EDFA and Raman amplifier in addition to the previous results discussed in section 4.3.1. For the commercial. In EDFA, the worst sensitivity penalty rises to 3 dB for a burst duration of 20 μs is observed. The from FOPA. A penalty from FOPA to EDFA soars up to 8 dB for the burst signal duration of 5 μs.

The discrete Raman amplifier shows a lower sensitivity penalty for the burst durations up to 30 μs with overlapping performance with FOPA. When amplified burst duration becomes shorter than Raman gain fibre length and the signal propagation time becomes shorter than amplified burst duration, the signal suffers from transient effects activate and destroys burst signals with severe gain fluctuation. In comparison to PI-FOPA, a 3 dB sensitivity penalty is observed with Raman amplifier at a 5 μs burst duration. This shows the discrete Raman amplifier is prone to transient effects related to the amplified architecture of the counter-propagating signal and pump with long gain fibre length, as shown in the experimental architecture section 4.1.3.

The PI-FOPA has shown stable performance in comparison with other tested amplifiers and decreases overall receiver penalty below <1 dB. From B2B, FOPA has around 1±0.5 dB sensitivity penalty occurring from non-burst mode receiver and transmitter fluctuations [171]. FOPA and EDFA performance become non-comparable at 5 μs burst signal amplification, while Raman amplifier in comparison with FOPA has around 3 dB penalty but performs similarly for longer burst duration >= 30 μs. Overall, this section and section 4.3.1 have demonstrated FOPA ultrafast response time and its performance with burst signal amplification with minor receiver sensitivity penalty. A minor change of <1 dB is noticed when amplifying bursts of duration <10 μs. This change may be due to the diverse polarisation architecture when amplifying a shorter number of bits with back reflection coming into effect.

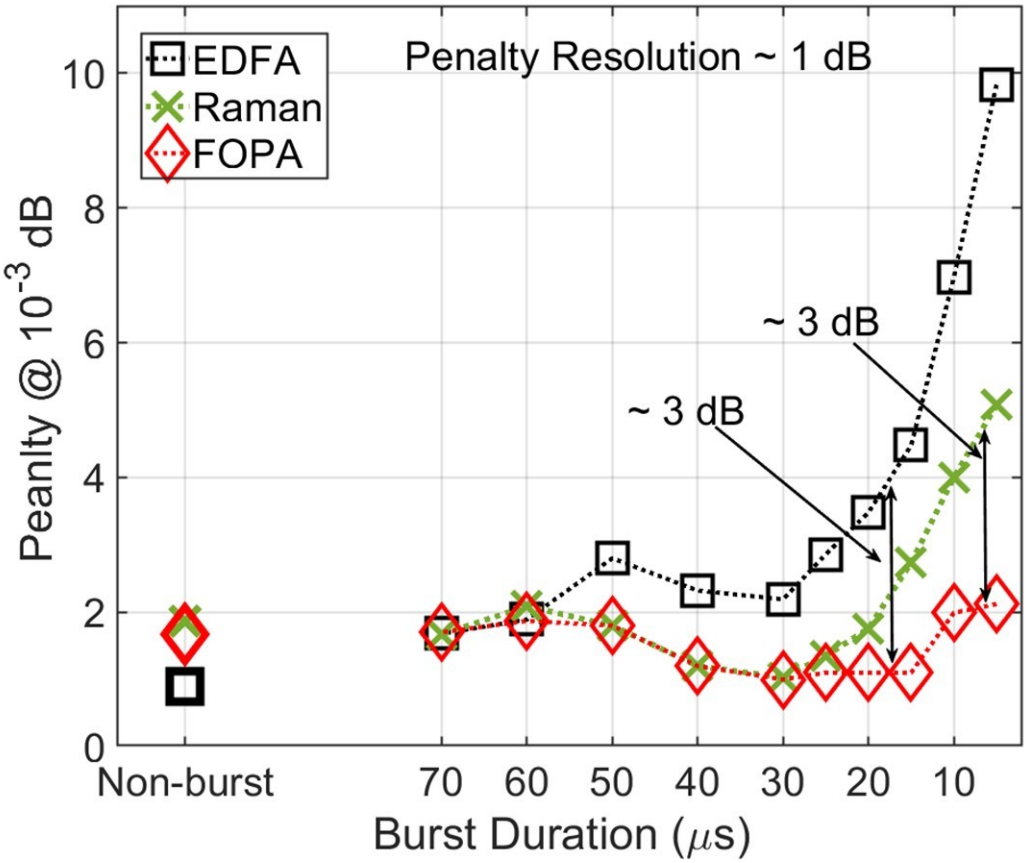

Figure 4.26 Sensitivity penalty for varied burst duration from 100%(non-burst) traffic to 5 μs burst duration for EDFA, Raman, and FOPA measured from B2B as a reference point

4.4 Burst Signal Amplification by SOA

Semiconductor optical amplifier (SOA) presents a fast response time equivalent to the signal bits of around picoseconds [174] timescales and is, therefore, suitable to amplify burst signals [84]. SOAs are demonstrated as pre-amplifiers too in traditional gigabit PON as pre-amplifier [85]. Therefore, a commercially available off-the-shelf SOA available in the lab was also tested for burst signal amplification and compared with parametric amplification. The employed SOA had high fibre to fibre with 20 dB gain, wavelength range from 1510 nm to 1590 nm, with a limited output power of 14 dBm. The 14-pin butterfly package was mounted on the controller with electrical and temperature control features.. Figure 4.27 shows SOA amplified burst waveform at 13 dB gain. A clear burst waveform with no gain fluctuations was observed in a 30 μs amplified burst.

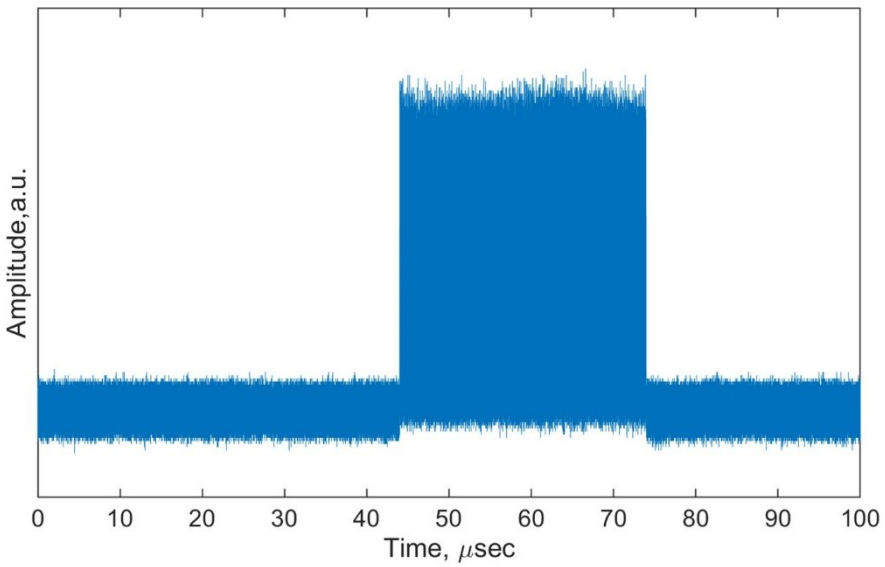

Figure 4.27 30 μs burst signal amplified by SOA at 13 dB gain and detected at received burst signal power of -3 dBm

Further, the performance analysis of SOA amplified 30 μs burst signal at 13 dB was measured against BER and received burst power with FOPA, as shown in Figure 4.28. In comparison with PI-FOPA, around 4 dB received penalty was observed at a BER level of 10^{-3}. At the same time, FOPA shows similar performance as B2B with <1 dB power penalty.

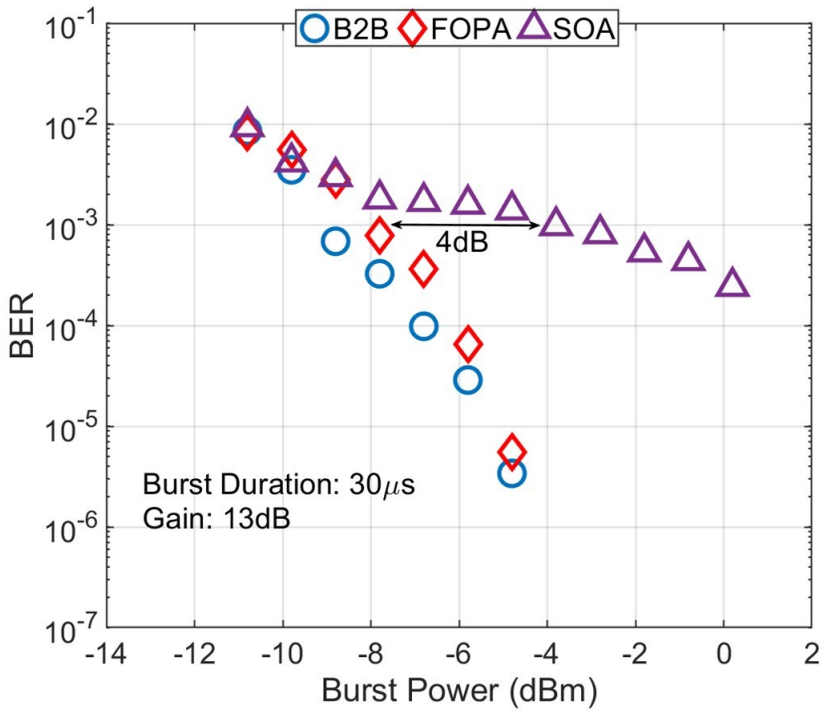

Figure 4.28 BER vs. burst power analysis of B2B, FOPA, and SOA for 30 μs burst duration and 13 dB gain

After investigating, the receiver power penalty in SOA amplified burst signal was incurred due to the patterning effects when amplifying high-speed 10 Gbps signal [89], as shown in Figure 4.29.

Patterning effect or inter-symbol interference is explained in Chapter 3, section 3.2. The bit pattern obtained from a sampling scope at input and output of SOA was observed at -3dBm received signal power. Input bit patterns have no distortion observed, on the other hand, amplified bit patterns after SOA distort multiple bits. It was demonstrated that the received power penalty of 4 dB in comparison with FOPA was due to distorted bits by SOA amplified burst signal originating from patterning effect.

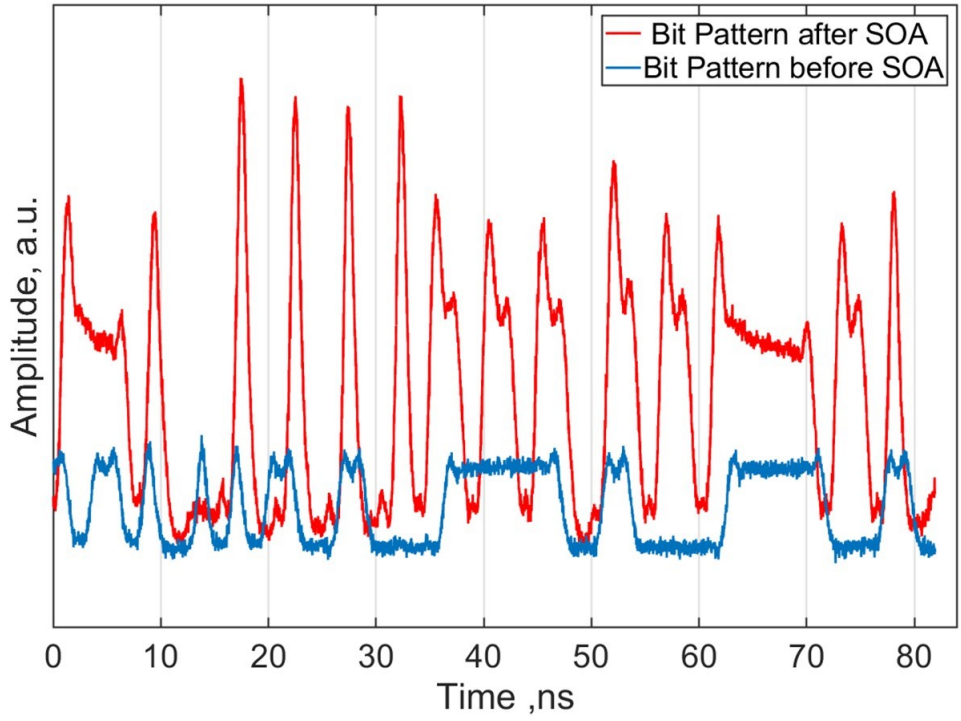

Figure 4.29 Patterning effect in SOA amplified 10 Gbps OOK signal with 13dB gain showing bit pattern before and after SOA amplification

Below, Figure 4.30 shows an eye diagram obtained for an amplified signal from the SOA at two different input signal power levels at -5 dBm and a low input signal power level of -20 dBm. Both eye diagrams show different signal conditions for the energy levels of amplified bits. The signal amplified at high input signal power of - 5 dBm shows an open eye but with distortions of bits at higher energy level as visible, making a horn-like shape. On the other hand, with lower signal power at -20 dBm, no such displacement of bits is observed in the eye diagram. This demonstrates a when SOA amplifies a high input power signal, it suffers from a patterning effect, while at -20dBm input signal power, a clear open eye was obtained. Overall, the SOA in this experimental work was not compatible with the range of signal power analysed. The result with burst amplification with SOA also suggests that for high-speed high-power signals, patterning effects are significant unless mitigated.

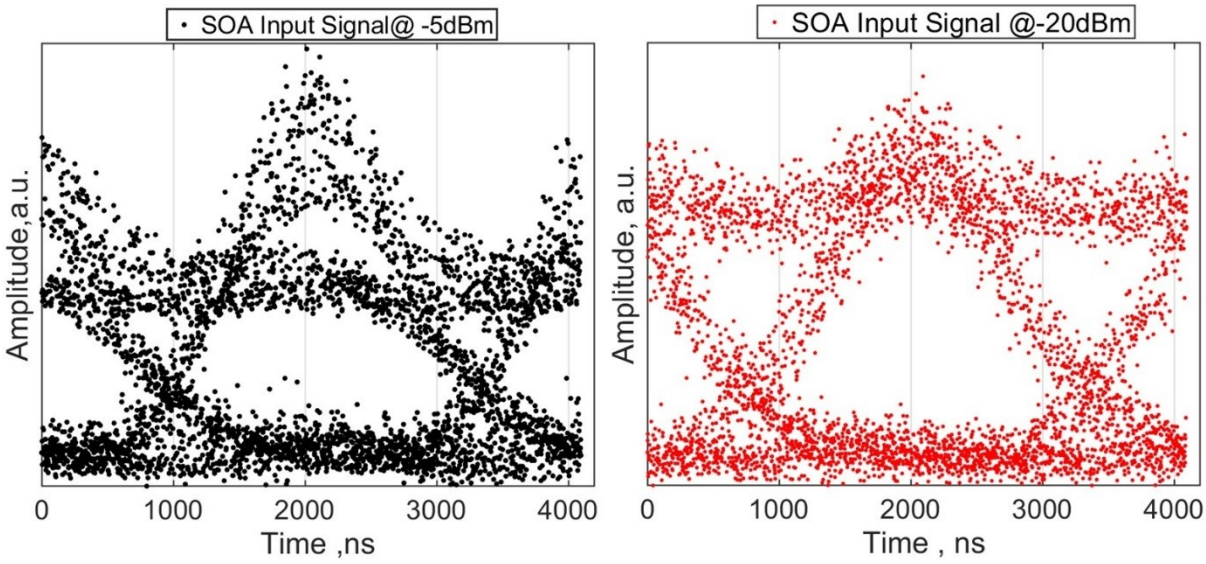

Figure 4.30 Eye diagram of amplified SOA input burst signal at -5 dBm and -20 dBm for 30 μs burst signal

Overall, the tested SOA with the required specification was not suitable for 10 Gbps OOK high-speed burst signal amplification. In comparison to other tested amplifiers, the SOA faces a much higher penalty in amplifying the burst signal although, the burst signal waveform does not present any gain fluctuations.

4.5 Summary

In this chapter, we have demonstrated the experimental demonstration of employment of a polarisation insensitive FOPA with net gain up to 20 dB for amplifying signal bursts of 10 Gbps OOK signal in a 50 km reach extended access network architecture. To investigate the FOPA performance with state-of-the-art fibre amplifiers, I compared PI-FOPA performance with a commercial EDFA and a discrete Raman amplifier for amplification of burst mode signals with various duration from 70 μs to 5 μs and as well as non-burst signal. With BER measurement, it was observed that in a non-burst scenario, PI-FOPA and discrete Raman amplifier introduced <1 dB penalty on the received signal power as compared to a commercial EDFA. On the contrary, Raman amplifier and EDFA suffered from transient effects when amplifying signal bursts leading to BER degradation and eventually observing a significant receiver sensitivity penalty of up to 8 dB in the EDFA case for a short burst duration of 5 μs. On the contrary, the PI-FOPA has not distorted the signal burst waveforms and hence confirms the effect of transient was not noticed for FOPA amplified bursty signals. Overall, FOPA demonstrates a received power and receiver sensitivity penalty of <2 dB for all tested cases. FOPA can allow for a larger power budget for extended reach access networks compared to EDFA and discrete Raman amplifiers. FOPA shows as a promising candidate for the potential of large gain to provide a higher splitting ratio allowing

more customers to be served from the single central office. The work demonstrated in this chapter was the first-ever attempt to employ a fibre-optic parametric amplifier to reach an extended access network. With the achieved 50 km reach extension at 20 dB and 13 dB net gain, the robustness of PI-FOPA was demonstrated to amplify burst with different durations at two gain levels. Figure 4.31 illustrates the ultra-fast response of FOPA provides immunity of burst signal amplification from transient effects in comparison with erbium-doped fibre amplifiers. Large overshoots of bits within the bursts are visible in EDFA, while no such overshoot is seen for FOPA.

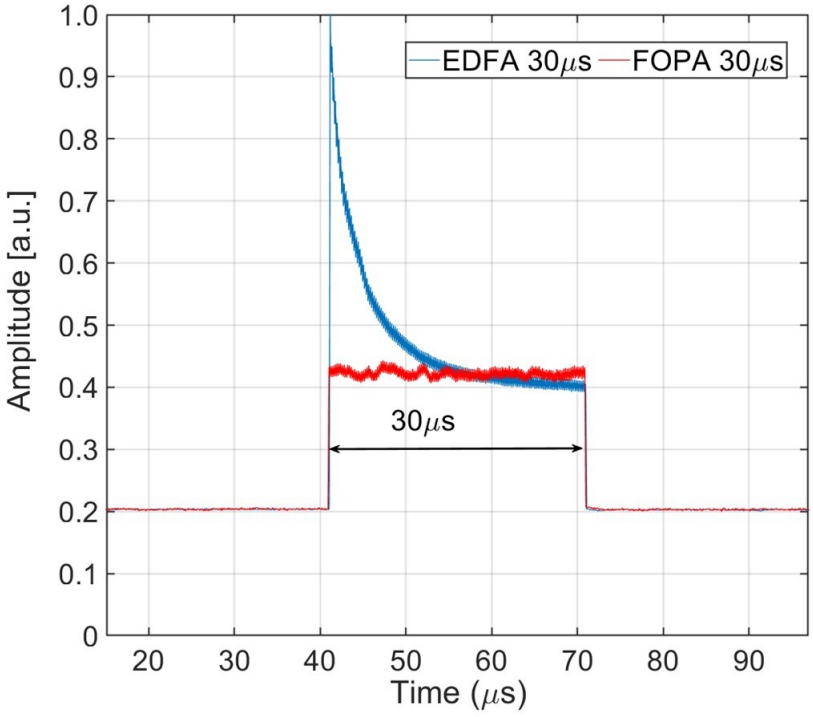

Figure 4.31 Overlap of burst waveforms amplified by FOPA and EDFA at 30 μs burst duration. Visible overshoot has been seen in EDFA while the smooth burst is obtained with FOPA

Chapter Highlights

From the presented experimental reach extended access network link, we found out the following result.

- **Experimental Setups:** The experimental setup was implemented employing a 10Gbps non-burst and burst signal transmitter, a 50 km reach extended optical access link, drop-in amplifiers acting as AUTs with EDFA, DRA and PI-FOPA and a direct detection receiver. Two fibre amplifiers were used: a discrete Raman fibre amplifier and a polarisation insensitive FOPA was developed in-house and employed as in-line amplifier in addition with a commercial EDFA. Amplifiers were set at 20 dB and 13 dB net gain.

- **Large Burst Signal Gain:** PI-FOPA enables burst signal amplification and provides burst mode signal gain of 20 dB. Pump power was set at ~3 W to amplify a signal in a polarisation diverse architecture. Ultra-fast response time of FOPAs amplified burst signals without any observed transient effects at large burst signal gain.

- **Improved signal received power:** We found via BER measurements that FOPA improves received signal power by >5 dB and 3 dB in comparison with tested EDFA and Raman amplifier for burst duration at 10 μs. That is, at the same received signal power, the FOPA observes BER level of 10^{-3}.

- **FOPA enhance receiver sensitivity:** Receiver sensitivity was measured for burst durations from 70 μs-5 μs at BER level of 10^{-3}. The commercial EDFA degrades receiver sensitivity by 3 dB for burst durations below 30 μs and reached to ~8 dB for 5 μs burst duration in a worst-case scenario. The tested Raman amplifier escalated the sensitivity penalty by >3 dB for durations below 20 μs and reaching to worst case of 5 dB at 5 μs burst duration, while FOPA shows constant performance with minimum receiver sensitivity penalty of <1 dB from B2B for the whole tested and varied burst durations.

Chapter 5 HIGH CAPACITY BURST TRAFFIC AMPLIFICATION BY FOPA

TABLE OF CONTENTS

Unique FOPA features such as high gain, ultrawide bandwidth, and near 0 dB noise figures are potentially crucial for future optical communication systems [15], [158], [160]. The FOPA ability of ultrafast response time is useful to amplify bursty upstream transmission in access network with negligible gain transient was demonstrated in [18]. Optical amplification as a drop-in amplifier can potentially improve the overall link power budget and increase physical reach. Optical access networks aim to provide low-cost optical data transmission; over a wide range of customers, FOPA as a reach extended amplifier in access networks could significantly reduce deployment cost via centralizing multiple feeder nodes to a single central office, as shown in [22].

In chapter 4, the FOPA's ability to amplify burst signals for a range of burst durations without incurring transient penalties was compared to conventional EDFA, and a discrete Raman amplifier was experimentally demonstrated, and results were published in [27]. A PI-FOPA was employed as a drop-in burst mode amplifier in a 50 km reach extended architecture for the first time. The PI-FOPA improves receiver sensitivity penalty >3 dB at shortest burst duration of 5 μs in comparison with EDFA and Raman amplifier. Further, PI-FOPA was employed to demonstrate the amplification of a burst signal at a net gain of 20 dB. EDFA and discrete Raman amplifiers suffer from transient effects and distort received signals. Power penalty increases by >5 dB and >3 dB when the transmitted signal is switched from non-burst to burst mode. The previous result in Chapter 4 validates FOPA compatibility as a burst mode amplifier potentially replacing the state-of-art amplifiers. The results demonstrate that implementing the PI-FOPA as a drop-in amplified in a reach extended access network improves splitter attenuation, total link power budget and increases the reach as well [25], [26].

However, bursty TDMA traffic varies in burst duration and changes in traffic density with the varying burst periods in optical access networks. Therefore, an in-line burst mode amplifier is required to amplify variable burst traffic density generated from multiple customers connected on the point to multipoint architecture. The FOPA, owing to its ultrafast response time [138], has the potential to enable near errorless high capacity bursty traffic amplification compared to the state-of-art EDFA and Raman amplifiers showing slow response time.

This chapter extends the previous work in Chapter 4 to compare PI-FOPA, a commercial-grade EDFA, and a discrete Raman amplifier to amplify high capacity bursty traffic densities to discover, demonstrate and quantify the differences in performance of all three tested amplifiers in a reach extended optical access link transmitting a burst of different traffic densities. Section 5.2 presents the experimental setup employed, with burst traffic density generation for fixed burst duration with varying duty cycles. Section 5.3 will present results obtained from experimental work showing BER vs. received burst power penalty in EDFA, Raman, and PI-FOPA by amplifying burst traffic from 5% to 97%. Later in this section, receiver sensitivity for similar varied burst traffic

density of 5% to 97% was measured for all AUTs. Finally, we will compare the sensitivity penalty between FOPA and other AUTs calculated from B2B receiver sensitivity as a reference point and finally compare the receiver sensitivity obtained for fixed burst traffic density and varied burst duration.

5.1 Fibre parametric amplification of high capacity bursty traffic

Traffic in access networks, for example, bursty upstream data transmission in a passive optical network, inter-data center connectivity, or optical free-space communication [10], [175], [176], varies randomly in terms of burst on-off time [177]. Dynamic bursty signals can demonstrate random duration and periods between their transmission [178]. For example, PON upstream traffic has sparse or closely packed bursts of traffic transmitted from multiple clients connected to the access network link where traffic density could vary between 0% to 100% [179]. In this case, burst traffic can vary dynamically in its duration and periods in access networks. Therefore, a drop-in amplifier should be able to amplify bursty traffic with dynamic behaviour (duration and period)

The FOPA, given its ultrafast response time of ~0.1 fs, as discussed in chapter 3 section 3.5.1, was demonstrated for packet signal amplification by Gu et al. in [18]. State-of-the-art erbium-doped and Raman fibre amplifiers suffer from slower response time [110], [134] and degrade receiver sensitivity for >5 dB in EDFA and >3 dB in Raman [26] for burst signal amplification. Chapter 4 experimentally demonstrated that a FOPA can improve the link power budget of a non- burst and burst signal in 50 km reach extended link via enhancing receiver sensitivity >3 dB and advancing to 8 dB maximum compared to EDFA and Raman amplifier. The investigation was done for varied burst duration of (70 μs-5 μs) at a fixed burst period of 100 μs. This section extends previous work with burst signal amplification for varied burst traffic density from 5% to 97% with FOPA, EDFA and Raman experimentally investigated at a fixed burst duration of 30 μs.

5.2 Experimental Setup

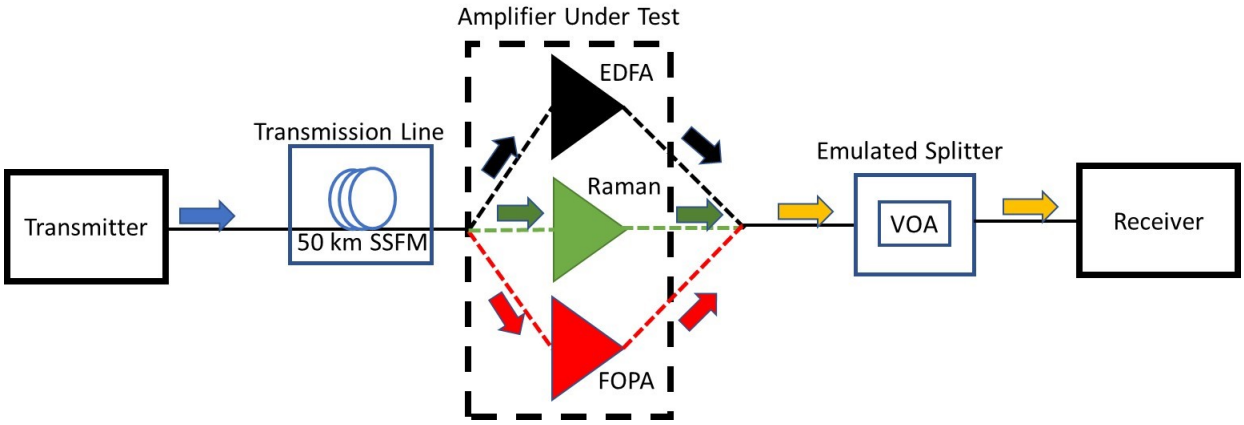

Figure 5.1. Experimental setup of 50 km reach extended access network bursty link optically amplified by AUT as EDFA, Discrete Raman amplifier, and PI- FOPA.

Figure 5.1 shows the experimental setup for a 10 Gbps OOK burst mode 50 km reach extended access network link. A burst mode transmitter is set to transmit burst traffic density from 5% to 97%. The experimental setup is explained in detail in chapter 4, section 4.1.1, including experimental setups of the PI-FOPA, a commercial EDFA, and the discrete Raman amplifier and is therefore not repeated in this chapter. Three Amplifier Under Test (AUT): EDFA DRA, and PI- FOPA were tested within the experimental setup to amplify signals. The signal was sourced from a tunable laser at 1535 nm and was modulated using a Mach- Zehnder modulator (MZM) driven by a pseudo-random bit sequence (PRBS) with the length of 2^{11-1} bits. A tunable laser emitting CW signal was followed by a polarisation controller (PC) to minimize the insertion loss to the MZM. A booster EDFA amplified a 10 Gbps OOK modulated signal to overcome insertion loss of the AOM and 50 km SSMF transmission line. Booster EDFA was set to a fixed output power of 13 dBm. The CW signal is switched to burst mode signal using a fibre Q-switched acousto optic modulator (AOM) connected to an arbitrary waveform generator (AWG).

The experimental setup was modified to generate burst traffic from 5% to 97% density, where burst duration was fixed at 30 μs. Traffic is amplified by three AUTs acting as in-line amplifiers after 50 km SSFM transmission to amplify incoming bursty traffic at the fixed gain of 13 dB. To generate burst traffic density from 5% to 97%, a square waveform generator driving the AOM is varied in frequency rate from 1.7 kHz to 32.2 kHz as discussed in section 5.2.1. The duty cycle of the burst signal was varied in its periods and was changed from 600 μs to 31 μs at a fixed burst duration. A variable optical attenuator (VOA) emulated an optical splitter or array wavelength grating optical demultiplexer. Input power to AUTs was -2.3 dBm for 100% (non- burst) traffic. An amplified bursty signal was detected via a DC-coupled direct detection PIN receiver. Detected

burst signals were processed digitally for measuring BER over ten signals bursts, using offline DSP enabled with threshold detection.

5.2.1 AOM Driver Frequency and Burst Periods

In Figure 5.2, AOM driver frequency was varied to obtain desired burst periods at a fixed burst duration of 30 µs. Generated burst period from 600 µs to 31 µs was specified as $Burst\ Period(\mu s) = \frac{1}{Driver\ Frequency\ (kHz)}$, which is inverse of driver frequency. As shown in Figure 5.2, by increasing driver frequency, short burst periods were obtained. As discussed in previous Chapter 4, the duty cycle is a ratio of burst duration to burst period given as $Duty\ Cycle\ (\%) = \frac{Burst\ Duration(\mu s)}{Burst\ Period\ (\mu s)}$. In this experiment we vary burst period from 600 µs to 31 µs as a function of driver frequency for a fixed burst duration of 30 µs. Hence, the duty cycle is adjusted via changing burst periods.

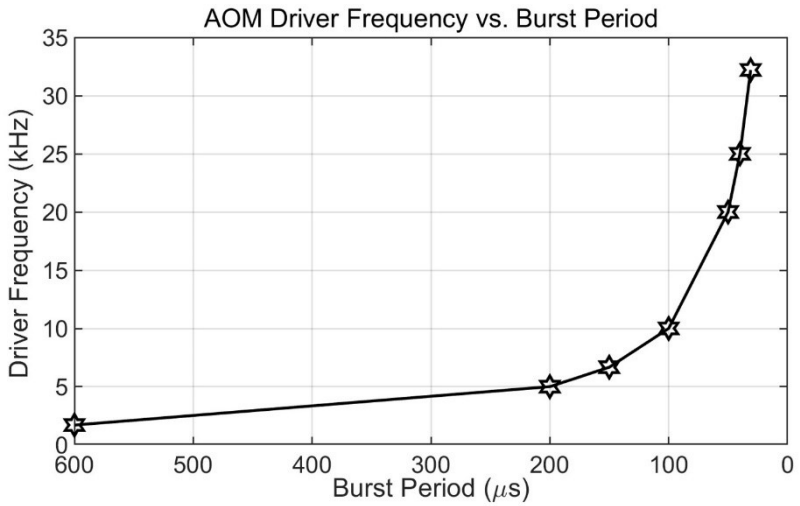

Figure 5.2. A plot of AOM Driver Frequency(kHz) vs. Burst Period(µs)

Table 5.1 shows the resulting average burst powers obtained at different traffic densities for corresponding burst periods and AOM driver frequency. Average burst power is the power ratio during the burst to the duty cycle of the burst transmitted. In this case, burst, power fixed at 2.3 dBm, given as the ratio as shown in 5.1

$$Power_{avg.} = \frac{Power_{Burst}}{Duty\ Cylce\%} \qquad 5.1$$

Burst traffic density generated from 5% to 97% correspondingly varies in three parameters: AOM driver frequency, burst period, and average burst power. The average burst power was fixed at 2.3 dBm at 30 µs burst duration. Average burst power increases with traffic density to 2.2 dBm at 97% traffic (31 µs burst period), whereas for the lowest burst traffic of 5%, average burst power

is -10.7 dBm (600 μs burst period). AOM driver frequency increased with a decrease in the burst period due to the inverse relationship between frequency and burst period shown above.

Table 5.1. Traffic Density for corresponding burst periods and average burst power.

Frequency Rate (kHz)	Burst Period(μs)	Traffic Density (%)	Average Burst Power (dBm)
1.7	600	5	-10.7
5.0	200	15	-5.9
6.7	150	20	-4.6
10.0	100	30	-2.9
20.0	50	60	0.1
25.0	40	75	1.0
32.2	31	97	2.2

Figure 5.3 shows a schematic representation of emulated signal burst with traffic density from 5% to 97%. A burst duration of 30 μs and varying burst periods from 600 μs to 31 μs is shown. Burst power is fixed at 2.3 dBm for 30 μs for the duration. The average burst power at different burst traffic densities is calculated for each varied burst traffic density.

Figure 5.3. Schematic view of varying burst traffic on fixed burst duration from 5% to 97%.

5.2.2 Burst Signal Power Spectra and Waveforms

Figure 5.4 shows a zoomed view of the optical power spectra for the amplified 10 Gbps 30 µs burst signal measured at the input and output of the PI-FOPA. Net signal gain at 1535 nm was 13 dB measured with a 1% optical coupler at 0.1 nm OSA resolution. For a fair comparison, the gain for all amplifiers under test was fixed at 13 dB. Complete PI-FOPA amplified burst signal power spectra at 20 dB and 13 dB are shown in chapter 4, section 4.1.4, showing idlers and residual pump. The measured input signal to OSA was at -22.0 dBm, and the amplified output measured signal was at -9.0 dBm, considering the OSA was connected to a 1% tap coupler.

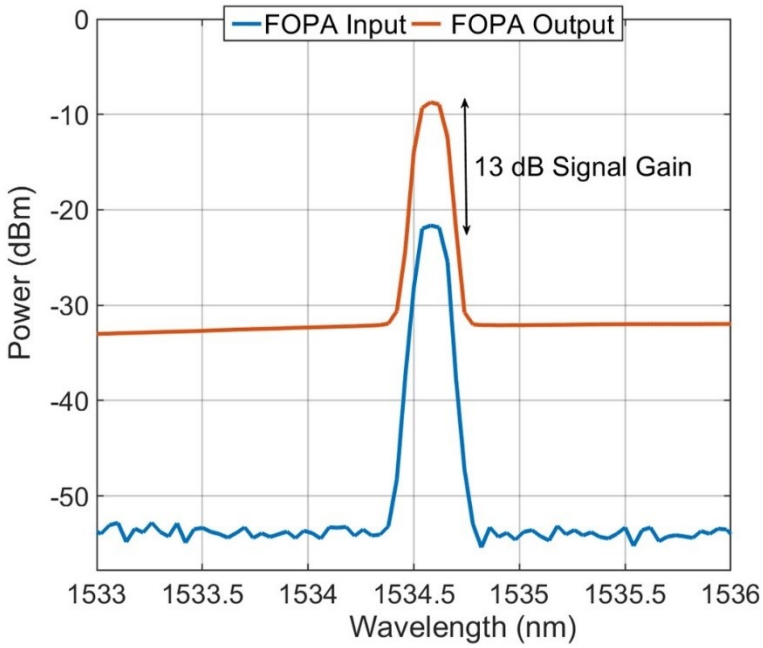

Figure 5.4 Power spectra of PI-FOPA amplified burst signal at 1535 nm measured at input and output showing a net signal gain of 13 dB

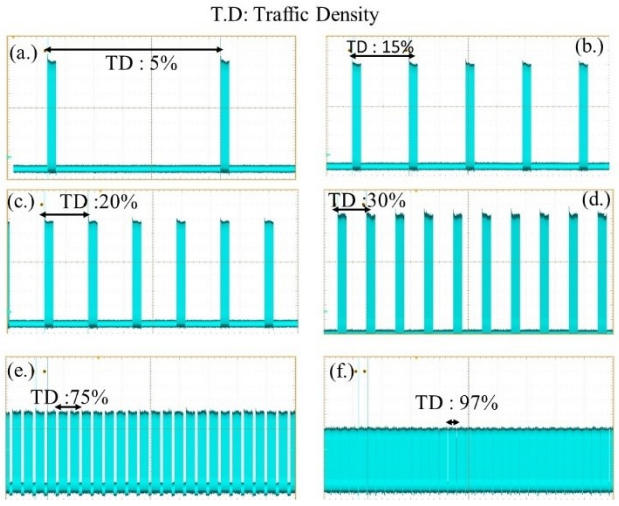

Figure 5.5 Burst Waveform at burst traffic density of 5%,15%,20%,30%,75% and 97% in B2B configuration at fixed burst duration of 30 µs

Figure 5.5. shows pictures of burst waveforms captured via a real-time signal oscilloscope in B2B configuration (where transmission fibre and AUTs were bypassed) for the varied traffic density from 5% to 97%. Figure 5.5 (a) to (f) show burst waveforms at sparse traffic for very low traffic density of 5% and high traffic density for closely packed burst packets at 97%. Burst packets shown in Figure 5.5 (b), (c), (d) and (e) present varied traffic density from 15%, for15%,20%, 30% and 75% duty cycle, demonstrating closed bursts at high traffic density.

Figure 5.6 shows burst waveforms of amplified burst traffic from a commercial EDFA, discrete Raman amplifier, and a PI-FOPA at 5% and 75% traffic density. Detected signal bursts shown in Figure 5.6 are amplified at the fixed gain of 13 dB at a fixed burst duration of 30 μs. Figure 5.6(a) shows EDFA amplified burst signals at 5% and 75% traffic density. In both scenarios, amplified bursts show distorted signals due to transient gain fluctuations in the 30 μs burst signal. The EDFA amplified burst signal at 5% burst traffic shows a large overshoot on the signal with a distorted shape. At 75% or higher burst traffic density, the transient effect was accumulated over all the closely packed bursts; hence the overshoot is hidden.

Figure 5.6 (b) shows Raman amplified burst mode signals at 5% and 75% traffic density at the signal gain of 13 dB. Detected burst signals at 5% and high burst traffic of 75% show visible transients within the amplified burst. At 5% burst traffic, leading signal overshoots to present the transient effects in backward pumped Raman amplifier with a long (6.5 km) gain medium. Further, gain fluctuations were observed at 75% traffic density within all closely packed Raman amplified bursts and accumulated over adjacent bursts similar to the EDFA. However, in both EDFA and Raman amplified bursts, degradation in signal performance will also depend on reaching a steady state if achieved before amplification of the next burst signal.

Figure 5.6 (c) presents PI-FOPA amplified burst signal at 13 dB net signal gain for 5% and 75% burst traffic. The presented scenarios with amplified burst signals at two compared traffic densities do not display gain fluctuations or the presence of transients. Compared with EDFA and Raman amplified burst traffic, FOPA at low and high traffic density performs better. Overall, no observed overshoot or undershoot was noticed with PI-FOPA amplification. Average burst signal power at 5% burst traffic density is -10.7 dBm and at 75% traffic 1.0 dBm at fixed burst power of 2.3 dBm.

Burst waveforms presented below suggest both EDFA and Raman amplifiers suffer from the transient effect at different traffic densities, although transient effects get neutralized faster for low traffic density bursts as amplifiers reach steady states before amplifying the next incoming burst. In the case of high traffic density, transient effects get accumulated over closely packed bursty traffic that does not reach a steady state before amplifying the next burst. Interestingly,

this case is not present in FOPA as it inherently provides ultra-fast response time useful for amplifying bursts.

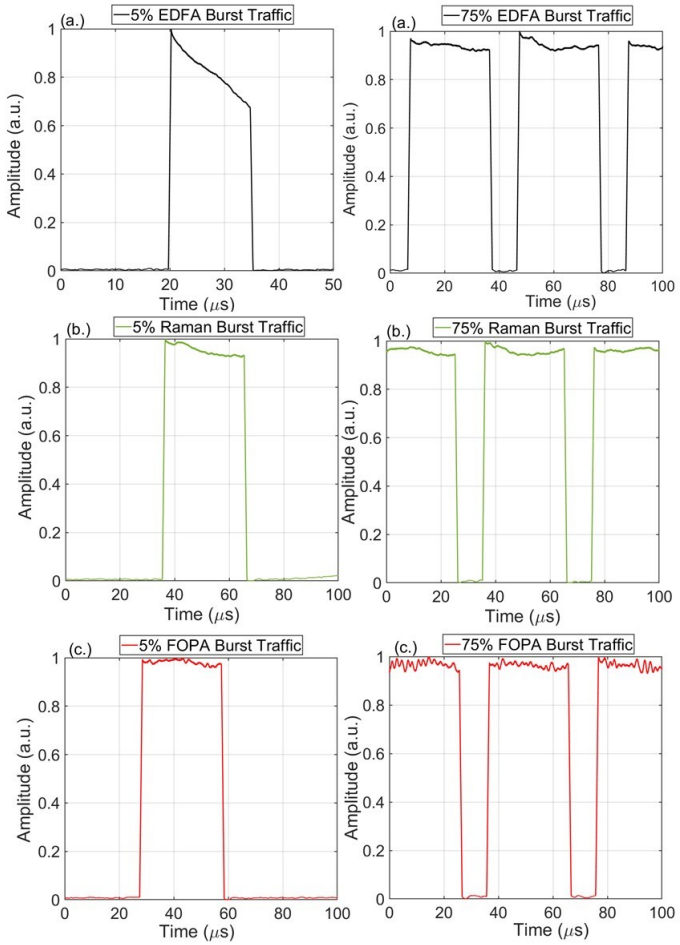

Figure 5.6. Amplified Burst Waveforms for (a) EDFA, (b) discrete Raman amplifier and (c) polarisation-insensitive FOPA at 5% and 75% burst traffic

5.3 Burst Traffic Density Performance Analysis

This section presents burst signal performance analysis by measuring bit error ratio (BER) against received burst power for varied burst traffic density. Additionally, BER measurement provided a comparison between AUTs employed as a burst mode amplifier. Section 5.3.1 presents BER against received burst power for signal amplified by a commercial-grade EDFA, discrete Raman amplifier, and a PI-FOPA. Amplified burst traffic density is compared with the B2B configuration to obtain a reference point. BER was calculated and averaged across ten captured burst signals for all received power values. The VOA was varied to sweep received power across all amplified burst traffic densities between 0 dBm to -14 dBm. Threshold detection is implemented through DSP via discarding the leading 100 ns from the burst signal in all scenarios to compensate for incoming distortion within the signal from the transmitter and receiver, as

explained in chapter 4, section 4.2.1. In section 5.3.2, all three AUTs were compared individually for BER performance against received power at chosen burst traffic density comprising the lowest traffic, 5%, the worst case of 75%, and the highest burst traffic density of 97%. These accumulated results present a broad understanding of AUT performance for burst signal amplification under different traffic densities.

5.3.1 Bit error rate against received burst power

Figure 5.7 demonstrates BER vs. burst received power for the amplified burst traffic from 5% to 97% for (a) B2B, (b) EDFA, (c) discrete Raman amplifier, and (d) PI-FOPA. Signal power launched in 50 km SSMF is 2.3 dBm burst power at 30 μs duration. Input signal power to AUTs was - 7.4 dBm incurring attenuation from 50 km SSMF of ∼9.7 dB. The amplifier gain was fixed at 13 dB for all varied burst traffic densities.

The signal in B2B configuration measured for BER against received burst power is shown in Figure 5.7 (a). Traffic density was varied from 5% to 97% in B2B configuration at fixed burst duration, B2B results were obtained to compare the performance of each standalone AUTs. At maximum burst traffic density of 97% compared to 5% traffic, ∼2 dB received power penalty is observed. At low burst traffic densities for 5% to 30%, a marginal power penalty was obtained of <1 dB at a BER level of 10^{-3}. Received power penalty in B2B is associated with the AOM fluctuations, and a non-burst mode receiver is employed in the extended reach setup. However, DSP provided some compensation to discard the first 100 ns of each burst [27].

Figure 5.7(b) shows burst signal performance comparison of BER and received burst power for traffic amplified by EDFA with 13 dB signal gain from 5% -97%. Almost overlapping BER curves were obtained for sparse burst traffic (low traffic density) from 5% to 20%, with received burst power variation of <1 dB at BER level of 10^{-3}. This penalty increases to 2 dB at 30%, incurring transient effects, reaching the worst case of 5 dB for traffic density at 75%. Small transient gain fluctuations for low traffic density amplification by EDFA are due to longer off-time between two bursts. It provides enough time for EDFA to reach a steady state before amplifying the next incoming burst signal. In the case of higher traffic density, EDFA does not reach a steady-state for closely packed bursts at higher burst traffic density >20% before amplifying the next incoming burst signal. Therefore, EDFA performance degrades at high burst traffic, and ∼ 5 dB extra power is required at 75% traffic to amplify the signal compared to B2B. Further, when the EDFA amplified 97% burst traffic density, a minor improvement in received power penalty by ∼2 dB is obtained at a BER level of 10^{-3}. The improvement was observed when quasi- continuous traffic was approached at 97%, as EDFA displayed no transient penalties for 100% traffic density or non-burst signal, as demonstrated in chapter 4, section 4.2.2. However, even at such high

bursty traffic density as 97%, residual transient penalties were present and did not tend to mitigate receiver power penalty completely [82].

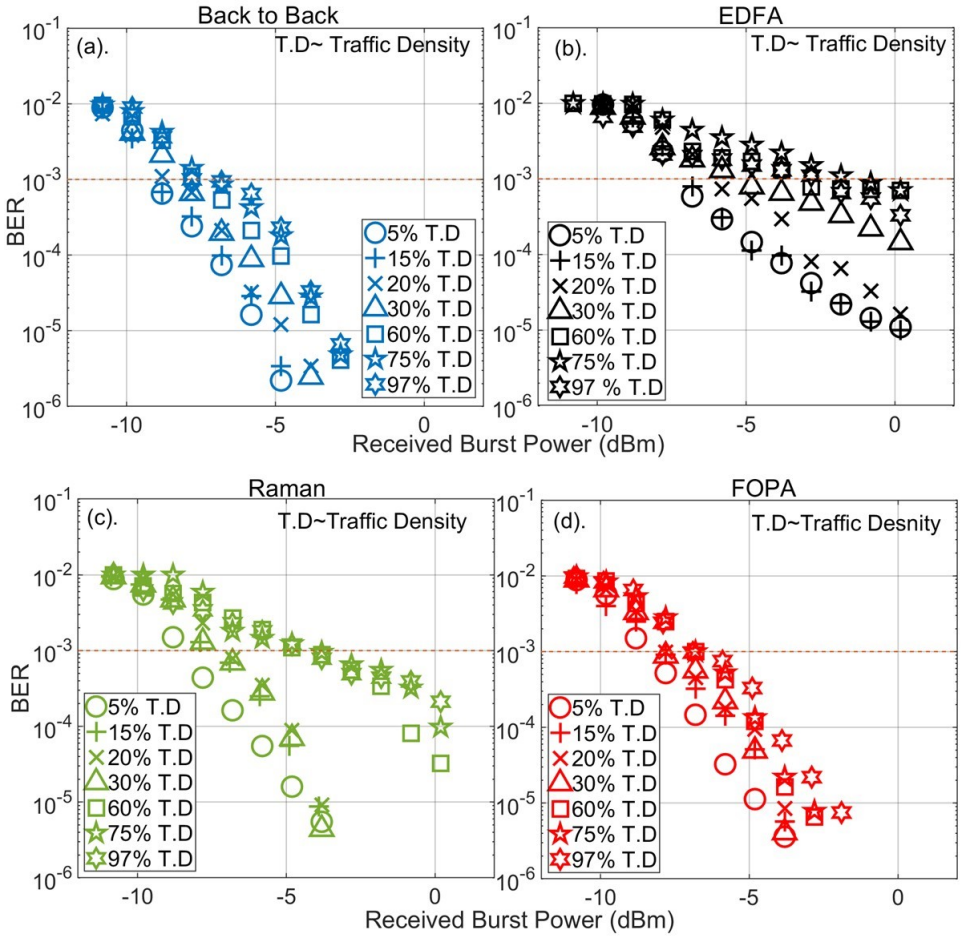

Figure 5.7 BER vs. received burst power comparison for burst traffic density of 5% to 97% in case of (a) B2B, (b) EDFA, (c) Raman, and (d) PI-FOPA. Burst Duration fixed at 30 µs and gain set at 13 dB for all AUT's

Figure 5.7 (c) shows the BER measurement for Raman amplified signal bursts for burst traffic from 5% to 97%. At low traffic density of 5% to mid-range traffic of 30% demonstrate almost overlapping BER measurement with signal power penalty differing by less than 1 dB. On the other hand, when increasing traffic density to 60% and up to 97%, burst power penalty increased by >2 dB. Received power penalty peaked at 75% burst traffic amplified by Raman and required ~3 dB extra power to reach BER level of 10^{-3} in comparison to the B2B for the tested discrete Raman amplifier. The penalty was attributed due to the addition of transient in high burst traffic density. It's known that the Raman scattering effect has a nearly instantaneous response time [52] with femtosecond scale , however backward pumped Raman amplifiers still suffer from transient effects linked to pump propagation time in a long gain fibre as explained in [133], [136]. Transient effects in backward pumped Raman amplification are explained in detail within chapters 3 and chapter 4. In the tested DRA low penalty, burst traffic density amplification is

limited to 30% traffic. Signal performance for both EDFA and Raman amplifiers for low and high traffic density scenarios are different due to:

a. EDFA and Raman amplifiers enter very short repetition periods between two consecutive bursts <10 μs for 75% traffic when amplifying high burst traffic density signals. Therefore, transient effects in both amplifiers are more severe, as observed in the previous chapter for short burst duration amplification by EDFA and Raman. However, large repetition rates or long periods between two successive bursts thus have long off durations between them, causing minor degradation for BER measurement.

b. EDFA and Raman amplifiers recover from transient effects for low traffic density burst signals as repetition periods are large enough to reach a steady state before amplifying another incoming burst signal.

The FOPA amplification of burst traffic density from 5%-97% is shown in Figure 5.7 (d). FOPA shows the best performance in comparison to the other AUTs at all measured traffic densities. At the BER level of 10^{-3} the maximum received a signal penalty in PI-FOPA observed as ~2 dB for reaching the maximum traffic density of 97%. The received power penalty associated with the burst traffic density was incurred from a non-optimised transmitter and receiver for burst mode signal, similar to the case of B2B. The FOPA allows all tested burst traffic amplification with minimum signal power penalty compared to EDFA and Raman amplifiers. The FOPA for amplified traffic density from 5% to 97% shows almost similar BER performance. The analysis demonstrates the validation of an ultrafast response time of FOPA to amplify the range of bursty traffic without any significant distortions.

5.3.2 Performance comparison of EDFA, Raman, and FOPA

Figure 5.8 draws a comparison between all tested amplifiers for amplified burst traffic measuring BER vs. received burst power. The comparison was made for the burst traffic measured at lowest traffic 5%, at the traffic density of 75%, and the maximum traffic density of (97%) is shown in Figure 5.8 (a),(b), and (c). The FOPA performance for all the burst traffic density amplification scenarios at 5%,75%, and 97%was similar to B2B with negligible (<1 dB) received power penalty. The tested FOPA amplified burst signals demonstrate almost error-free performance enabled by its ultrafast response time. The open eye diagrams are shown for the FOPA at BER level of $10^{-5,}$ and 10^{-4} at the received power level of -6 dBm and -5 dBm for 5% and 75% are presented in Figure 5.8 confirms no observable penalty in the amplified detected signal.

On the other hand, discrete Raman amplified burst traffic for 5%,75%, and 97% density presents a different case. At the lowest traffic of 5%, DRA shows a very low received power

penalty (<1 dB) at a BER level of 10^{-3}, demonstrating a minor effect of the transient for sparse transmitted burst signals. However, for 75% BER performance, Raman amplified signal significantly degrades with >3 dB received power penalty at BER level of 10^{-3}. For the maximum traffic density of 97%, the received signal power penalty improved marginally by ~1 dB for Raman amplified burst. The eye diagram of Raman amplified signal at 5% traffic shows open eye at BER of 10^{-6} similar to the FOPA, which gets closed at 75% burst traffic density at BER of 10^{-5}. In contrast, the FOPA demonstrates an open eye for the equivalent burst traffic density.

Similarly, for the EDFA, amplified burst traffic at three different traffic densities is shown in Figure 5.8. The EDFA suffers from a transient penalty and observe received power penalty of 1 dB at a BER level of 10^{-3} in comparison to the FOPA and Raman case. This penalty severely gets increased to ~5 dB as traffic density reaches 75%. Therefore, compared to FOPA and Raman for 5% and 75% burst traffic cases, EDFA shows degraded performance.

At the maximum of 97% traffic density, both EDFA and Raman amplifiers observed ~2 dB power penalty compared to the FOPA amplified burst traffic density at 97%, as shown in Figure 5.8 (c). Both EDFA and Raman still suffer from transients at near-continuous burst traffic density with minor improvement in receiver power compared to the worst case of 75% traffic. Overall, it demonstrates that FOPA was the only amplifier to amplify high traffic density without incurring significant penalties.

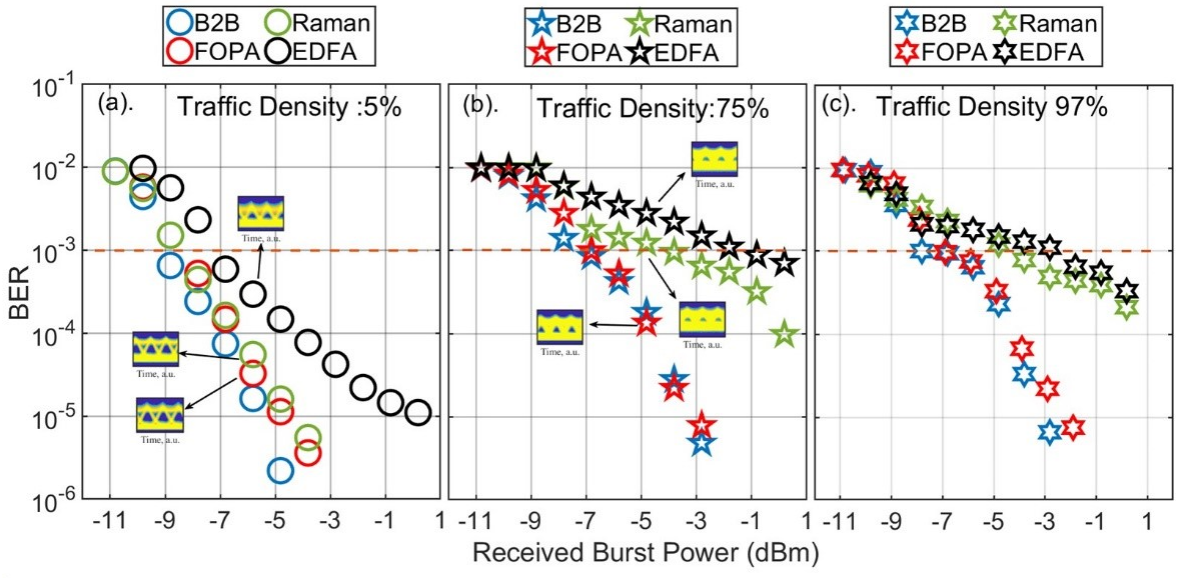

Figure 5.8 BER compares FOPA, Raman amplifier, and EDFA for traffic density of 5%,75%, and 97% with received burst power.

Inset of Figure 5.8 (a) and (b) demonstrate eye diagrams for 5% and 75% burst traffic density amplified by PI- FOPA, Raman, and EDFA. The FOPA and Raman amplified burst at a BER level of 10^{-5} shows open eye at a received power level of -6 dBm. EDFA at BER of 10^{-4} presents a partially open eye diagram at -6 dBm, demonstrating a transient effect on EDFA amplified burst traffic at

5%. At 75% burst traffic density, both Raman and EDFA eye diagrams are shown in the inset at BER level of 10^{-3} at a received power level of -5 dBm showing closed eye diagram due to effects of transient distorting the amplified signals whereas FOPA at a similar received power level of -5 dBm, and BER level of 10^{-4} shows open eye demonstrating no or minor impact of the transient.

5.4 Receiver sensitivity of high capacity bursty link

Section 5.4.1 presents an experimental analysis for receiver sensitivity vs. burst traffic density measured at a range of burst traffic from 5% to 97%. Receiver sensitivity is one of the critical parameters for the performance analysis of optical access links in a reach, extended access network, as receiver sensitivity defines the power budget of the link and consequently the maximum splitting ratio, i.e., a number of customers can be connected over the link. In this work, we define receiver sensitivity as received burst power required to reach the BER level of 10^{-3}. This experiment measured receiver sensitivity for a varied range of burst traffic densities at the fixed burst duration of 30 μs. The measurement was done for B2B and all AUTs (EDFA, DRA, and PI-FOPA) at the fixed gain of 13 dB.

Further, in section 5.4.2, the receiver sensitivity penalty for all standalone amplifiers was measured from B2B as a reference point. It provides insight into the performance of individual amplifiers providing burst mode signal amplification to improve the overall burst mode optical link.

5.4.1 Receiver sensitivity vs. burst traffic density

Figure 5.9 presents receiver sensitivity as a function of varied burst traffic density for 5% to 97% obtained for B2B and all three AUTs. In B2B configuration, the best receiver sensitivity was at -9 dBm for the burst traffic from 5% to 15%. With the increase in traffic >15%, minor fluctuation lowers the receiver sensitivity in the B2B case due to fluctuation occurring from AOM and a non-optimized transmitter and receiver. The receiver sensitivity of B2B reached -7 dBm for a traffic density of 75%. At 97% burst traffic, B2B receiver sensitivity shifts to -8 dBm due to bursty traffic shifting towards near 100% traffic or quasi-continuous state. Further, we evaluate AUTs in terms of receiver sensitivity penalty compared to B2B performance.

For the EDFA case, the best receiver sensitivity was at -7 dBm between burst traffic density from 5% to15%, which corresponds to a sensitivity penalty of ~2 dB introduced by in-line EDFA in comparison to B2B. A further increase of sensitivity penalty with increased burst traffic density imposed by EDFA reached 5 dB when burst traffic density increased to 75%. It indicates that the implementation of EDFA in burst networks can significantly decrease an available link power budget, specifically for traffic amplification of >15% in capacity. At the maximum burst traffic

density measured at 97%, we observed an improvement of ~2 dB in receiver sensitivity penalty. At 97% traffic load, the repetition rate of 1 μs between bursts has improved EDFA receiver sensitivity by 2 dB, although not enough to mitigate transients completely. Also, this suggests that EDFA performance tends to improve when burst traffic shifts towards non-burst or 100% traffic load. As in the non-burst case, receiver sensitivity of EDFA improved by ~3 dB in comparison to the nearest burst traffic amplification case, as shown in chapter 4, section 4.3.2. also published in [26].

Receiver sensitivity in Raman amplification was between -8 dBm and -7 dBm for burst traffic density up to 30%. For Raman amplified burst traffic density of 75% traffic, the received sensitivity was -4 dBm, increasing the sensitivity penalty to 3 dB. It indicates that although the Raman amplifier has introduced a receiver sensitivity penalty of only 1 dB at low traffic density, the penalty has reached >3 dB for traffic density of 60% and above. The worst-case with Raman amplification was noticed at 75% burst traffic. Raman amplifier at a maximum traffic load of 97% also improves the receiver sensitivity by ~1 dB. As for the non-burst case, the performance of Raman improves by ~2 dB in sensitivity as shown previously. Overall, compared to B2B, receiver sensitivity for Raman amplified different burst traffic densities perform better at lower traffic density. With a difference of <1 dB in sensitivity penalty, which occurs due to transient effects when amplifying high burst capacity and degrades the performance, DRA only amplifies burst traffic density up to 30% capacity.

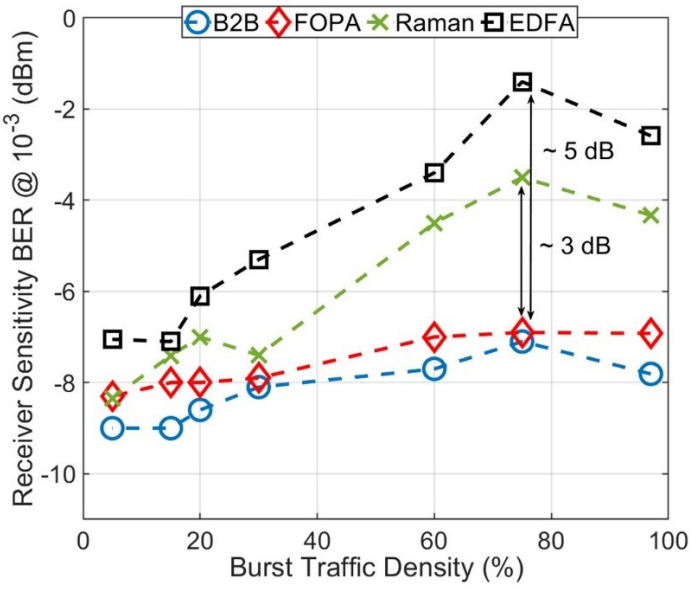

Figure 5.9 Receiver Sensitivity vs. Burst Traffic Density from 5% to 97% at BER level of 10^{-3}.

On the other hand, the FOPA has performed well for all examined traffic densities. Receiver sensitivity in the FOPA case was always within the 1 dB range from the B2B. It was observed that

parametric amplification imposed no significant penalty within the amplified burst signal for different traffic densities. It indicates FOPA performance was stable at75% burst traffic (which was the worst case for EDFA and Raman amplifiers) and at the maximum 97% burst traffic amplification case. Overall, the FOPA improves receiver sensitivity by >3 dB at low and very high burst traffic compared to EDFA and Raman amplifiers, enhancing the overall link power budget five times.

5.4.2 Sensitivity Penalty in AUT's for varied Burst Traffic Density

Figure 5.10 demonstrates the sensitivity penalty for all tested AUTs measured from B2B as a reference. In this analysis, B2B was fixed to measure penalty via deducting the receiver sensitivity of EDFA, Raman, and FOPA from B2B as a function of burst traffic density. The FOPA demonstrated minor penalty and was always within 1 dB of sensitivity penalty for a range of varied burst traffic loads. It indicates that the FOPA, given its ultrafast response time, shows negligible dependency on burst traffic density.

The tested discrete Raman amplifier has almost overlapping sensitivity penalty as FOPA at burst traffic density of 5% and was <2 dB up to burst traffic density of 30%. The penalty increased to >3 dB as burst traffic density increased from 60% to a maximum of 75% compared to FOPA. It shows that at 75% traffic, the Raman amplifier would have 5 dB lower receiver sensitivity than the FOPA incurring due to transient effects.

The performance sensitivity penalty of EDFA for the measured burst traffic was higher than other tested AUTs, i.e., Raman and FOPA. The slow response time of the EDFA incurs heavy transient penalties for very low traffic density of 5% to worst-case sensitivity penalty of 6 dB at 75% burst traffic density. Overall, the EDFA shows the largest penalty when amplifying burst traffic density from 5% to 97% at a burst duration of 30 μs in comparison to the FOPA. Whereas the FOPA showed minimum sensitivity penalty from B2B for a range of bursty traffic and was always stable within 1 dB penalty margin, hence it has the potential to act as an amplifier for high-density burst signal optical networks.

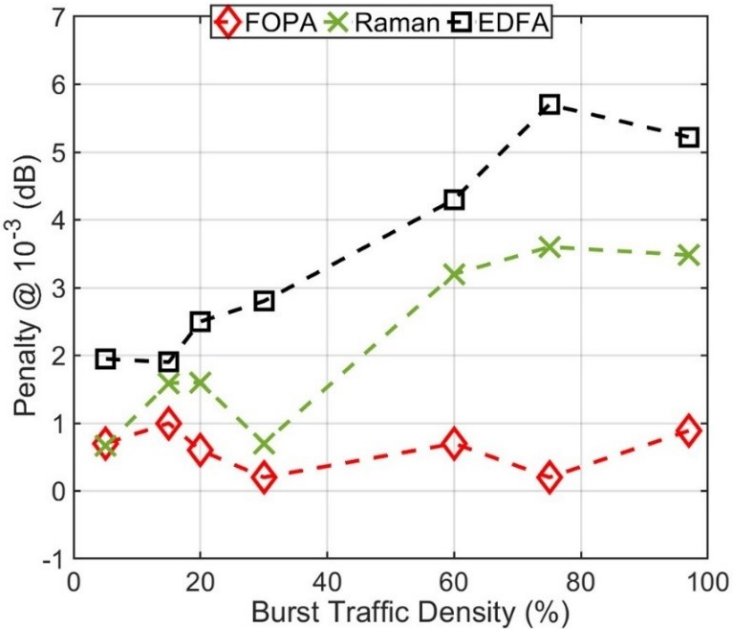

Figure 5.10 Sensitivity penalty measured from B2B for burst traffic density from 5% to 97% for PI-FOPA, Raman, and EDFA amplified burst traffic

5.5 Comparison of receiver sensitivity for varied burst duration and traffic density

This section compares receiver sensitivity for all tested AUTs for varied burst durations from 70 μs to 5 μs and varied burst traffic density of 5% to 97%. The chapter 4, section 4.3.1 results for receiver sensitivity obtained for various burst duration for all tested amplifiers are used to develop this comparison. It is essential to note that, in this comparison, when burst duration was kept constant at 30 μs, traffic was varied from 5% to 97%. On the other hand, burst traffic density was kept constant at 30% for various burst duration of 70 μs to 5 μs. It was not possible to vary both duration and traffic simultaneously with the employed burst traffic generator. The analysis provides a trend of receiver sensitivity for EDFA, Raman, and FOPA for varied burst traffic and burst duration when amplified at 13 dB net gain. It provides an important observation to help understand amplifier functioning when amplifying burst signals.

5.5.1 EDFA Case

Figure 5.11 compares the tested commercial erbium-doped fibre amplifier's receiver sensitivity for varied burst traffic density and burst durations. The EDFA was employed as an in-line burst mode amplifier in a 50 km reach extended access network link. The tested EDFA was fixed to 13 dB net gain for all burst mode signal amplification. In Figure 5.1, red squares present measured receiver sensitivity for varied burst duration from non-burst to 5 μs burst signal. As discussed, the EDFA sensitivity penalty increased for a shorter burst duration and reaching to ~8 dB.

Similarly, black squares are shown with a dashed black line representing receiver sensitivity trend for EDFA when burst traffic density was varied from 5% to 97% at a fixed burst duration of 30 μs. It is observed that bursts get distorted when traffic load increases to >15%.

However, measured receiver sensitivity in both the cases crosses at ~20 μs burst duration and 20% traffic density at receiver sensitivity of -6 dBm. It suggests that for a particular case of EDFA examined with specific burst parameters absolute operating point to operate EDFA is 20 μs at 20% burst traffic.

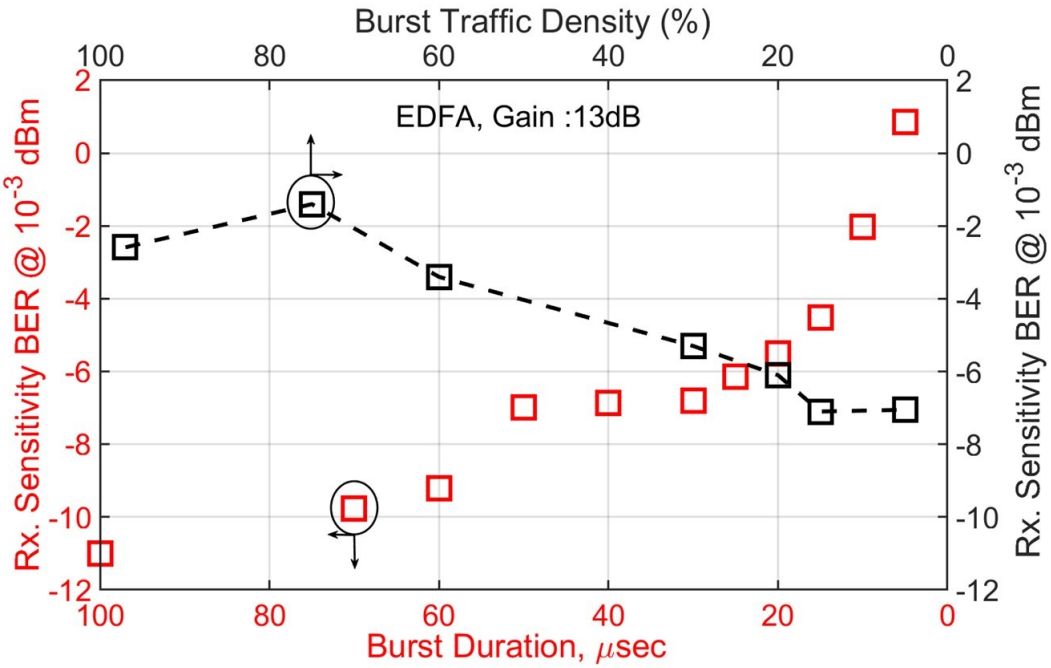

Figure 5.11 Comparison of receiver sensitivity for varied burst duration from non- burst to 5 μs and traffic density from 5% to 97% for EDFA amplified bursty traffic at 13 dB gain

5.5.2 Raman Case

In Figure 5.12 shows a tested discrete Raman amplifier is compared for receiver sensitivity against burst traffic density and burst duration. Like the EDFA case, the analysis provides the trend of the Raman amplifier to obtain receiver sensitivity penalty to understand the operating point of the tested amplifier in the case of amplification for dynamic burst signal scenarios. Receiver sensitivity was affected with transient effects for the Raman amplifier when short burst durations were amplified. In the case of varied burst duration amplification by DRA, the receiver sensitivity penalty increased by >3 dB for the burst duration <30 μs, as shown in Figure 5.12.

In the case of varied burst traffic density, the tested Raman amplifier receiver sensitivity improves at low burst traffic density for <30%, where the sensitivity penalty increases with the increase in burst traffic density >30%. Raman amplifier increases penalty with an increase in

burst traffic load where the transient effect is accumulated and distributed for closely packed bursts. Hence, the next incoming burst gets destroyed before reaching a steady state of the amplifier. Compared results shown as red crosses and black crosses with black dashed lines presenting burst duration and burst traffic density. From 30% to 20% burst traffic and for the same range of burst duration, the Raman amplifier shows stable receiver sensitivity at ~-8 dBm to -7 dBm. This analysis provides an understanding of an operating point for the tested Raman amplifier at specific parameters used for this experimental measurement.

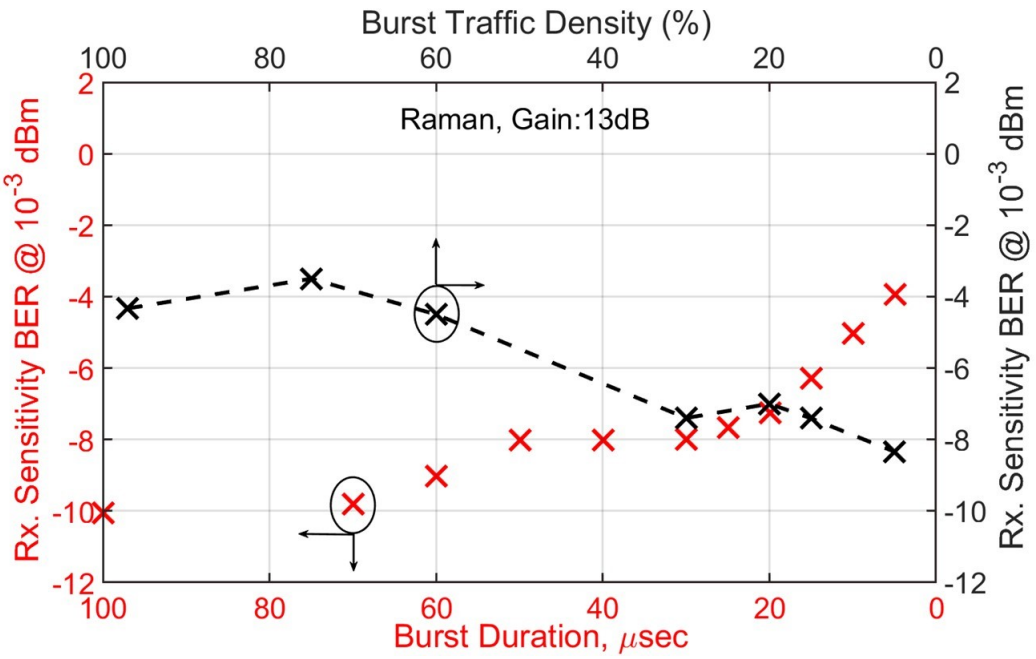

Figure 5.12 Comparison of receiver sensitivity for varied burst duration from non- burst to 5 μs and traffic density from 5% to 97% for Raman amplified bursty traffic at 13 dB gain

5.5.3 FOPA Case

Figure 5.13 demonstrates a similar analysis for PI-FOPA amplified burst signal as done for EDFA and Raman amplifier. In both the scenarios with varied burst duration and traffic, FOPA shows stable performance for the measured receiver sensitivity with less than <2 dB change from burst duration of 70 μs to 5 μs and traffic range of 70% to 5%. For both cases, FOPA receiver sensitivity improves at a non-burst case; this indicates that with the employability of burst-mode receiver, FOPA can further improve and might replicate the performance of non- burst mode for receiver sensitivity. Overall, this result verifies the performance of FOPA amplification of various bursty traffic. The ultra-fast response time of FOPA provides almost transient free burst traffic amplification, invariant towards dynamic bursty nature. This comparison suggests the potential of employing FOPA in a random bursty traffic transmission link with the potential to be used as a burst mode amplifier.

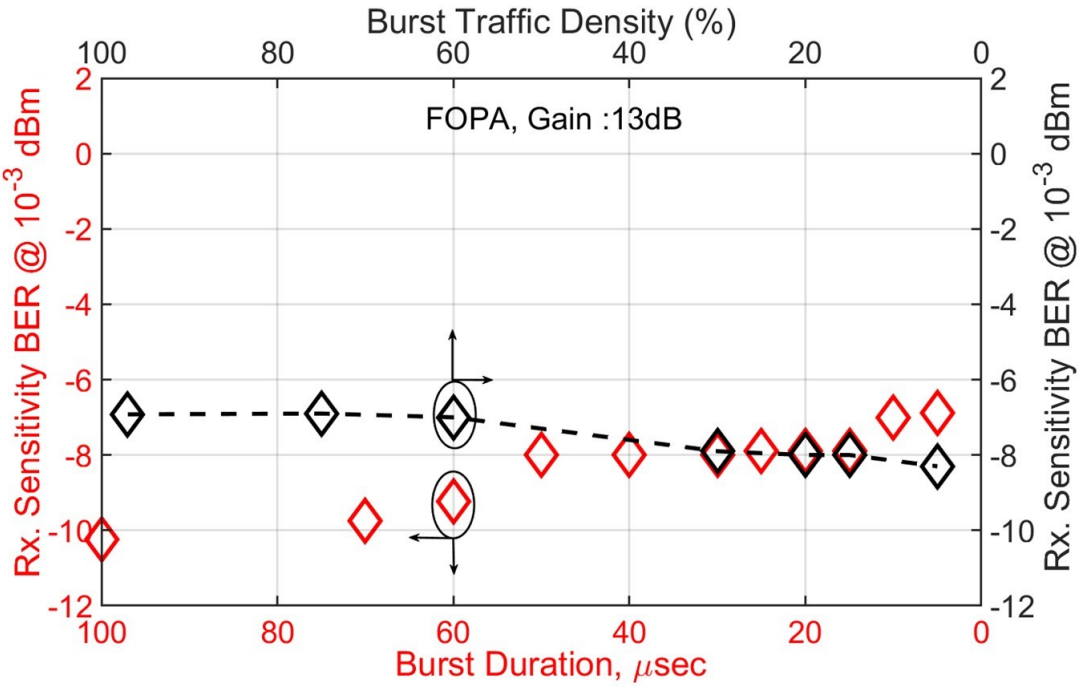

Figure 5.13 Comparison of receiver sensitivity for varied burst duration from non- burst to 5 μs and traffic density from 5% to 97% for PI-FOPA amplified bursty traffic at 13 dB gain

5.6 Summary

This chapter experimentally demonstrated that the PI-FOPA enables high capacity bursty traffic amplification reaching up to 97% traffic density and can be employed as a potential drop-in for amplifier for future reach extended access networks. A comprehensive study is performed by experimentally comparing high capacity burst traffic amplification by a commercial-grade EDFA, a discrete Raman amplifier, and a polarisation-insensitive FOPA when burst traffic load was varied from 5% to 97% at the net amplifier gain of 13 dB.

EDFA and Raman amplifiers observe significant penalties in received signal power and distort the BER at traffic density >15% and 30%, whereas the PI-FOPA provides ~2 dB received power to change for all the amplified burst traffic densities. FOPA BER performance was stable, reaching a level of $10^{-6,}$ while BER of EDFA and Raman amplified burst traffic reached BER of 10^{-4} at a higher traffic density above 30%.

The PI-FOPA receiver sensitivity penalty of <1 dB was obtained compared to the B2B. Alternatively, commercial EDFA and discrete Raman amplifiers suffer from signal degradation when burst traffic density increases over 15% and 30%, respectively. The penalty from EDFA and Raman amplifiers reaches >5 dB and >3 dB in receiver sensitivity from the PI-FOPA at the worst case of 75% traffic load. For a 50 km extended reach burst mode optical access link, FOPA allows amplification for five times higher traffic density than EDFA for the same power budget. We

conclude that FOPA can improve the burst network power budget by >5 dB or its traffic capacity by the factor of 6 compared to a commercial EDFA. The tested Raman amplifier shows stable performance similar to FOPA at low traffic but suffers at high burst traffic and degrades receiver sensitivity by >3 dB. Also, it was observed that when burst traffic reached a near quasi- continuous traffic density of 97%, both EDFA and Raman amplifiers tend to show minor improvement in receiver sensitivity although still not reaching unreachable to reach similar sensitivity as non-burst traffic. Overall, FOPA potential as a burst mode amplifier motivates robust bi-directional fibre parametric amplifiers for future work.

Chapter Highlights

From the high capacity burst traffic amplification, we found out the following results.

- **High capacity burst traffic amplification:** We demonstrated for the first-time high capacity burst traffic amplification by a PI-FOPA. Burst traffic density from 5% to 97% is generated and amplified at fixed 13 dB net gain for all in-line amplifiers.

- **Performance of AUTs:** Bit error rate was measured for detected burst traffic from 5% to 97% amplified by AUTs. EDFA and Raman amplifier degrade BER for high burst capacity >15% and 30% and therefore require much higher received signal power. Penalties for EDFA and Raman reach >3 dB at 75% burst traffic density. The FOPA, shows best performance in BER and improves received burst power by >3 dB at worst case scenario of 75% traffic density in comparison with the other amplifiers.

- **Receiver sensitivity for varied Burst Traffic Density%:** An important result with impact on receiver sensitivity by amplification of burst traffic density 5% to 97% was measured at BER level of 10^{-3}. Both EDFA and Raman amplifiers degrade receiver sensitivity higher than 15% and 30% traffic density and peaks in penalty at 75%. From B2B sensitivity the penalty for EDFA and Raman at 75% was measured as 5 dB and 3 dB. The FOPA, on the other hand allows traffic amplification up to 97% with minimum sensitivity fluctuations of ~1 dB. At 97% EDFA and Raman amplifier tend to improve sensitivity by ~2 dB when reaching near continuous traffic.

- **Comparison of burst duration and traffic:** We compared receiver sensitivity for varied burst duration and traffic to estimate optimum performance for all tested amplifiers. Overall, FOPA presents stable performance in both dynamic conditions with much lower sensitivity degradation than the other two amplifiers. EDFA and Raman amplifiers tend to show better performance at low traffic density with longer burst durations, when amplified for higher burst traffic this trend degrades as the effect of transients increases.

Chapter 6 DUAL-BAND BI-DIRECTIONAL SIGNAL AMPLIFICATION BY FOPA

TABLE OF CONTENTS

With the increase in demand for bandwidth and envisaged capacity crunch in optical networks, signal transmission is employed outside the conventional C Band. Modern long-haul networks are already transmitting C+L bands of low-loss telecom windows [180]. Therefore, wideband optical networks expand from C-band to L and S bands covering >100 nm wavelength of transmission bandwidths[181]. Wide-band signal transmission also extends with the up grading of optical subsystems, including optical amplifiers. Therefore, wideband optical amplifiers are the focal point of research for future wideband optical signal amplification [95]. Recently, bi-directional signals propagated in the C+L band were demonstrated for modern optical communication links [182].

However, optical links in an access network are traditionally bi-directional, transmitting signals downstream and upstream, as discussed in chapter 3, section 3.1. Generic gigabit optical fibre access links transmit downstream non-burst signal in C or S-band and upstream bursty traffic transmitted in O- band wavelengths as defined by ITU-T standards [10]. Therefore, extended reach access network links employing optical amplifiers should be capable of amplification of bi-directional downstream and upstream traffic. Additionally, the optical amplifier should support the random nature of burst mode signal amplification for upstream signal transmission. Additionally, future access networks are envisaged employing all possible wavelengths within low loss telecom windows in O, E, S, C, and L bands [161] for signal transmission. A TWDM-PON architecture with high capacity data rates up to 100 Gbps consisting of in- line optical amplifiers for reach extension is demonstrated to amplify WDM, and bursty signals simultaneously were recently in [84].
The FOPA provides all aforementioned requirements in comparison with the conventional amplifiers employed in optical networks. Some interesting FOPA features are:

- Broadband gain
- Transient free operation
- Amplification on arbitrary wavelengths
- Wide dynamic range
- High output power
- Large gain

All the above-listed features meet the specification required for an optical amplifier in extended reach access networks. The FOPA's ability to provide broadband gain ~200 nm [157] outside conventional C- band, transient free signal amplification, a large-signal gain of 20 dB [25], and high signal output powers are important requirements. Looped polarisation-independent FOPA with WDM signal amplification was demonstrated in [163] with ~15 dB net gain for the first time. Transient free amplification by the PI- FOPA in "Loss-Gain" configuration for a range of burst traffic was experimentally demonstrated in previous chapters 4 & 5. Additionally, it was

demonstrated that FOPA as a drop-in amplifier enhances receiver sensitivity by >3 dB compared to a commercial EDFA and a discrete Raman amplifier. All the above-listed features validate FOPAs ability to enhance the overall link power budget of access networks via improving the critical parameter that is receiver sensitivity [26].

As access networks are bi-directional and signals travel in more than one telecom band, it is important to demonstrate optical amplifier capability to perform dual-band signal amplification. Interestingly, the FOPAs could potentially be employed as a dual-band bi-directional in-line amplifier, as the FOPA is a unidirectional amplifier, that is, the pump and signal should be co-propagated for efficient parametric amplification. Amplification of counter-propagating signals and pumps in the presence of large parametric pump powers is a limitation. Counter-propagating pumps and signals generate SBS and produce unwanted four-wave mixing products, distorting the signals. However, Bi-directional signal amplification by a FOPA with a low gain was demonstrated in [183], [184]. Later, it was confirmed by experimental demonstrations that counter-propagating signal amplification is not feasible due to the limitation of SBS and unwanted FWM generation [149]. Parametric signal gain is limited in counter-propagating pump FOPA architectures, as high-power pump waves interact with each other, quickly reach the SBS threshold, and reflect all excess pump powers as described in [149]. Additionally, it increases nonlinear crosstalk due to unwanted FWM products limiting detartrating the signal performance.

Therefore, this chapter investigates simultaneous amplification of a downstream (non- burst) signal in L-Band and upstream (burst) signal in C-band by a PI-FOPA in a 50 km SSMF bi- directional extended reach access link setup. To the best of my knowledge, for the first time, bi-directional dual-band amplification for >50 nm apart signals transmitted in C and L bands by a dual-band PI-FOPA amplifier was experimentally demonstrated. Section 2 discusses the complex experimental setup of a dual-band bidirectional reach extended access network. Novel experimental setup of bi-directional dual-band FOPA employed as an in-line amplifier and C+L band transmitter is discussed separately. Below crucial findings are presented in this chapter for the first time.

- Parametric amplification of >50 nm apart signals
- A novel scheme for bi-directional signal amplification
- Simultaneous amplification of bursty and non-burst traffic
- >16 dB polarisation independent net gain

Section 3 discusses the bit error rate calculation results against received power for the amplified signals for uni-directional and bi-directional DS and US signals. Finally, in section 4,

improvement splitter attenuation and overall link power budget enhancement for non-burst and burst mode obtained by dual-band PI-FOPA amplification is presented.

6.1 Simulation of Dual-band FOPA

To help verify parametric amplification of dual-band bi-directional signals by FOPA, a simulation model of a C+L dual-band FOPA amplifier in a 50 km reach extension access link architecture was developed using VPItranmission maker V9.9. Dual-band C and L transmitter simulated the US, and DS data streams of 10 Gbps OOK modulated signals using individual continuous-wave transmitter blocks. C-band OOK transmitter was emitting at 1533 nm and was propagated as upstream non- burst traffic. L-band transmitter was emitting at 1586 nm non-burst 10 Gbps modulated signal and was propagated as the downstream signal. The bi-directional signal transmission was done by employing optical circulators. 50 km SSMF acting as reach extended link used with 0.2 dB/km attenuation parameter within the model simulated. A variable optical attenuator (VOA) acted as an optical splitter was placed after the C- band US signal transmitter.

A fibre-optic parametric amplifier model (FOPA) was simulated using a non-linear fibre block (NLF) of 200 m acting as a parametric gain medium. 3 W optical pump power at 1564.2 nm propagated within the NLF block. To suppress SBS in the nonlinear fibre the pump was phase modulated by four radio frequency (RF) tones at 100 MHz, 310 MHz,920 MHz, and 2.7 GHz. Further, the phase-modulated pump coupled with bi-directional C+L band signals through a WDM multiplexer. The input signal at the FOPA input was -7.9 dBm of C-band signal and -17.9 dB of L- band signal.

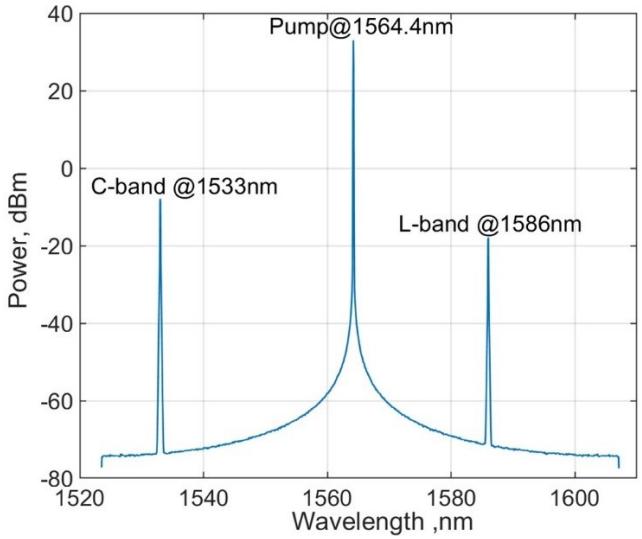

Figure 6.1 Spectrum of multiplexed C band 1533 nm, L band 1586 nm, and pump at 1564.3 nm before parametric amplification.

Figure 6.1 shows the simulated spectrum of multiplexed dual-band signals transmitted in the C and L band with the parametric pump located at 1564.2 nm. Pump power of 3 W was used to obtain parametric amplification. C-band signal transmitted at 1533 nm was propagated bi-directionally after passing through a VOA initially set to 0 dB attenuation. The L - band signal at 1586 nm was propagated through 50 km SMF before coupling to the pump and C - band signal. Therefore, the spectrum shows that L- band signal power was ~10 dB lower than the C-band signal. Input signal power at FOPA was -7.9 dBm for the US and -17.9 dBm for DS signals.

Bi-directional dual-band signals were amplified by a nonlinear fibre acting as a parametric gain medium. Figure 6.2 demonstrates power spectra measured at the input and output of FOPA. Input signals in C and L bands were amplified simultaneously at >50 nm apart wavelength locations at 1533 nm and 1586 nm. The FOPA gain bandwidth of ~10THz was obtained with the listed parameters used for this simulation.

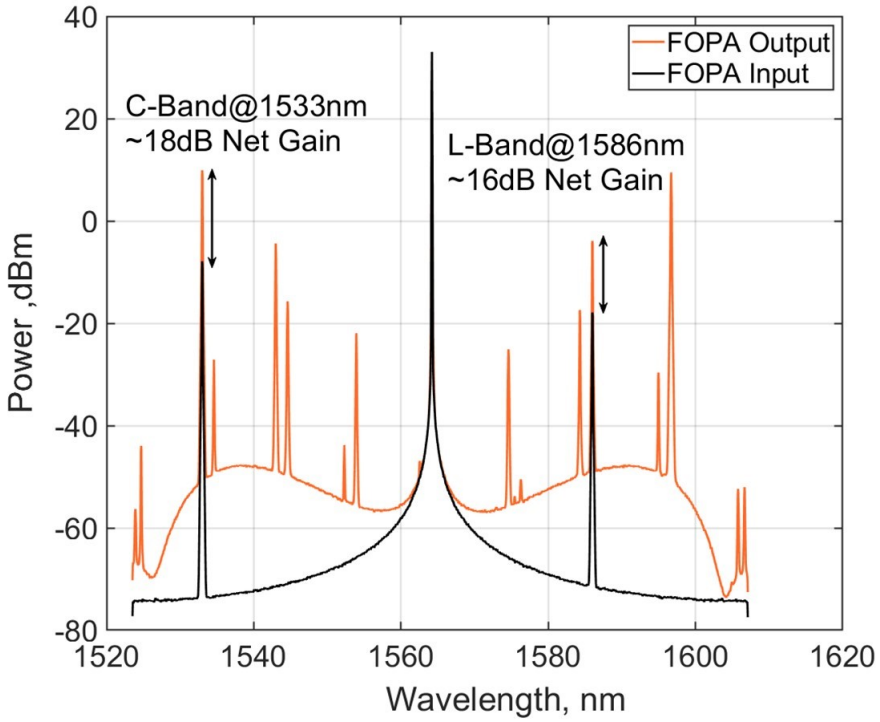

Figure 6.2 Input and output power spectra of FOPA amplified dual-band signals bi-directionally transmitted in DS and US direction simulated by VPI transmission maker

The net gain obtained for the L-band signal was ~16 dB and was ~18 dB for C-band. Idlers generated with the parametric amplification process for C and L-band were located at 1596 nm and 1543 nm of the simulated spectrum. In Figure 6.2, multiple residual non-linear products are visible in the spectrum. Based on the above model, an experimental setup was conducted in the lab to demonstrate dual-band amplification by a FOPA.

6.1.1 BER measurement for simulated bi-directional setup

DS and US signal performance was performed by measuring bit error ratio against the received signal power. In this model, US traffic was a non-burst signal; therefore, both DS and US traffic was transmitted in non-burst mode to simplify the analysis. Two individual direct detection receivers were employed to detect L and C-band signals and calculated for bit-by-bit error detection using a stochastic evaluation model block.

At first, B2B signal performance was analysed by connecting individual C and L band transmitters to their respective receivers, excluding extended reach link and in-line amplifier. Figure 6.3 demonstrates BER vs. received power measured for the C-band signal at 1533 nm. BER values at B2B were calculated first and then amplified via FOPA with a net gain of ~18 dB. Almost the overlapping performance was obtained between B2B and the amplified signal, with a minor penalty of <1 dB by FOPA amplification for the C-band signal. BER with no penalty and an overlapping curve was measured at the BER level of 10^{-3}, although the <1 dB power penalty at higher received signal power simulated was observed at -8 dBm.

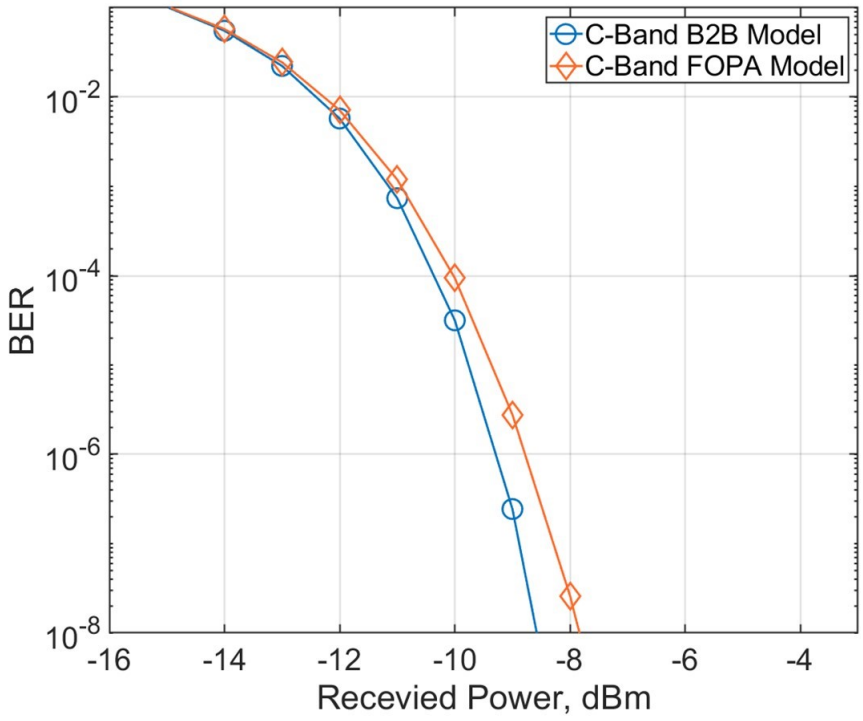

Figure 6.3 BER vs. received power for C band signal@1533 nm measured via VPI model in B2B and FOPA amplified signal with ~18 dB net gain

Figure 6.4 shows measured BER against received signal power for a simulated L-band signal amplified with a FOPA. B2B was measured initially to set a reference point and to compare it with the FOPA amplified signal. The simulation result shows ~1 dB power penalty between B2B and FOPA amplified signal at 10^{-3}. L-band signal was emulated as DS non-burst mode 10 G traffic at

1586 nm, amplified via single pump FOPA with ~16 dB gain. ~1 dB power penalty could occur due to noise addition after FOPA amplification at a longer wavelength.

In the L band, the signal power penalty at the BER level of 10^{-3} was 1 dB from B2B, whereas the C band suffered a minimal penalty compared to B2B <1 dB and ~0.5 dB, respectively. Amplified C and L band signals by dual-band bi-directional FOPA amplifier received a power penalty of ~1 dB. Increased power penalty in L band signal was probably due to FOPA amplification of simultaneous signals >50 nm apart in wavelength.

Overall, this simulation model provides a feasibly check for further experimental work. Results obtained provide an understanding of simultaneous amplification by a FOPA of dual-band signals. Also, the net gain was >15 dB for the transmitted signal with received power penalty <1 dB from B2B.

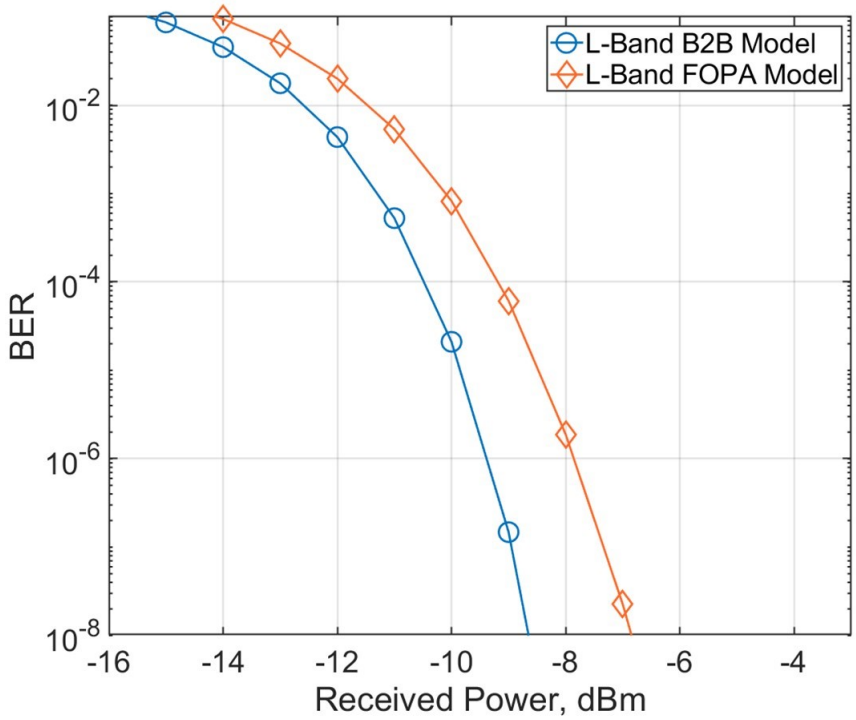

Figure 6.4 BER vs. received power for L band signal@1586 nm measured via VPI model in B2B and FOPA amplified signal ~16 dB net gain

6.2 Dual-Band FOPA amplifier for bi-directional signal amplification

This section presents the experimental setup of the C+L dual-band bi-directional reach extended access network link. The setup consisted of a C and L-band transmitter, a 50 km SSMF link, a dual-band PI-FOPA amplifier, and individual receivers to detect C-band (bursty, non-burst) and L- band (non-burst) signals. The FOPA's features to provide transient free, wide-band, and large gain properties are investigated within this experiment. C+L band transmitter setup is discussed

in section 6.2.2 with details. Finally, a bi-directional dual-band parametric amplifier's experimental setup is discussed in section 6.2.3. Details of the PI-FOPA employed in this experiment in the "Loss-Gain" configuration are not repeated, and they were already is discussed in chapter 4, section 4.1.4.

6.2.1 Experimental setup

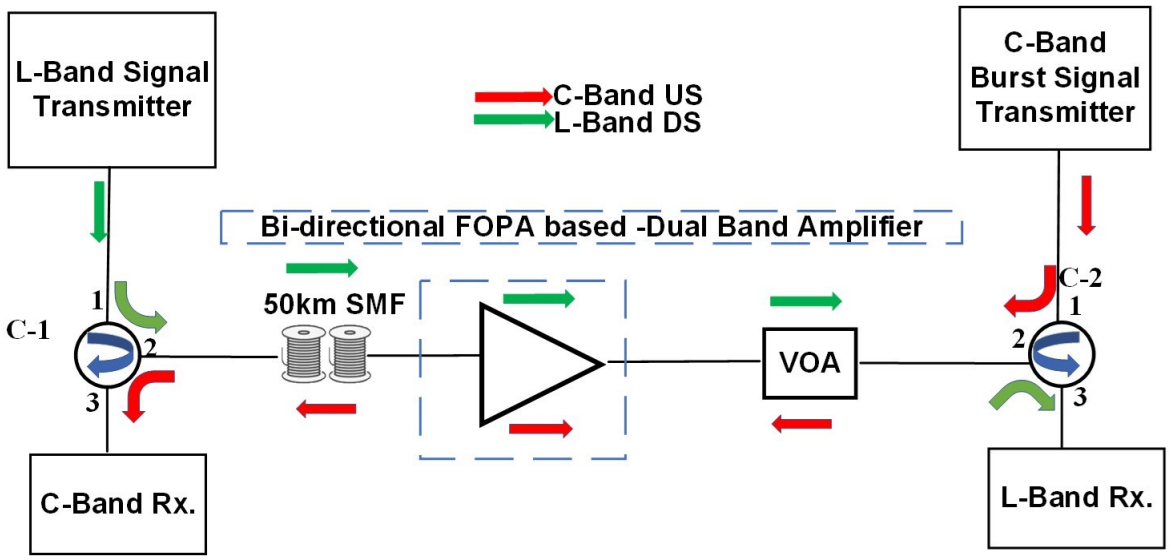

Figure 6.5 Experimental setup of bi-directional dual-band reach extended access network employed with PI-FOPA as a dual-band in-line amplifier

The experimental setup shown in Figure 6.5 demonstrated a scheme for dual-band bi- directional amplification of C+L band signals by PI-FOPA. The experimental setup was divided into a 10 Gbps C+L band transmitter with the receiver, a transmission link of 50km, and a bi-directional dual-band PI- FOPA acting as an in-line amplifier. A bi-directional access network link setup was employed with a 50 km SSMF (using 25-25 km SMF spools) connected by optical patch cords. Attenuation in 50 km SSMF was ~9.8 dB and ~ 9.7 dB in the C and L band signal wavelengths. A variable optical attenuator (VOA) emulating an optical lump loss was considered as an optical splitter. For ease of discussion, we will consider passive lump loss as an optical splitter.

The bi-directional signals from C and L-band transmitters were launched into the setup from opposite ends of the access network link to act as upstream and downstream signals, respectively, and represented with red and green colour arrows in Figure 6.5. The DS and US signals were launched by three-port optical circulators marked as C-1 and C-2. Consequently, the optical circulators guided the DS transmitted signal to the DS receiver. Similarly, the US transmitted a signal to the US receiver towards the opposite ends of the link using circulator C-2. For in-line FOPA amplification, bi-directionally transmitted signals were multiplexed together and launched as an input signal to the amplifier. Parametrically amplified signals were then filtered to remove

idler, noise, and unwanted FWM products accumulated via the amplification process. Further, filtered signals were detected via corresponding receivers. The performance of detected signals was analysed by bit error rate (BER) calculation using offline DSP [26].

6.2.2 C+L Band Transmitter

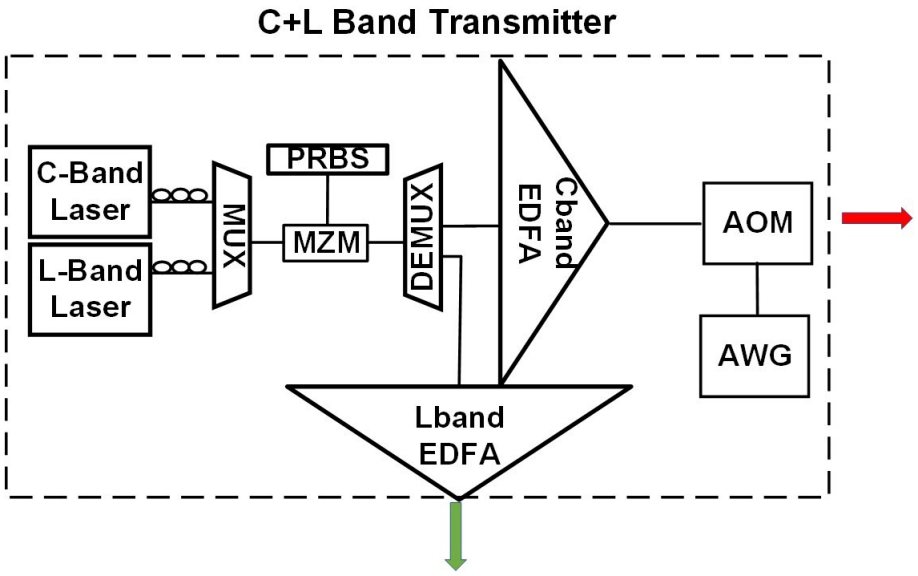

Figure 6.6 Experimental setup for C+L dual-band transmitter employed in a bi- directional 50 km access network link. Transmitting DS and US signal at 1586 nm and 1533 nm.

Figure 6.6 shows a dual-band signal transmitter generating signals in C and L-band wavelengths. L band DS signal in non-burst mode is emitted at 1586 nm, and the C-band US signal in burst mode is emitted at 1533 nm. The dual-band transmitter employed two tunable lasers source generating continuous wave signals. The CW were multiplexed by a C+L band multiplexer and modulated by a Mach-Zehnder modulator (MZM) to generate 10 Gbps OOK signals at a PRBS length of 2^{11-1} bits. Before the C+L band multiplexer, two separate polarisation controllers (PC) were employed to minimize the insertion loss into the MZM. Modulated signals then were demultiplexed using a WDM C+L band splitter to be transmitted as US and DS. Both US and DS signals were amplified by their respective EDFAs acting as a booster amplifier. Input signal power of C+L signals to the booster EDFA was - 2.5 dBm and -2.0 dBm, respectively. C and L band EDFA were set in gain mode and corresponding output power of 13 dBm and 6 dBm for US and DS signals. The EDFAs were employed for maintaining power levels due to various insertion losses within the setup.

An upstream signal in access networks is typically transmitted in burst mode [9], similarly in this experiment, the US non-burst signal after MZM was switched into a burst mode signal of 10 Gbps. The burst signal was generated employing an acoustic optic modulator (AOM) driven by a 10 kHz square wave generator to produce signal bursts of 50 μs at a burst period of 100 μs.

The power during the burst was 5.5 dBm, and the average output power with a 50% duty cycle was 2.5 dBm. The employed AOM has ~7 dB insertion loss.

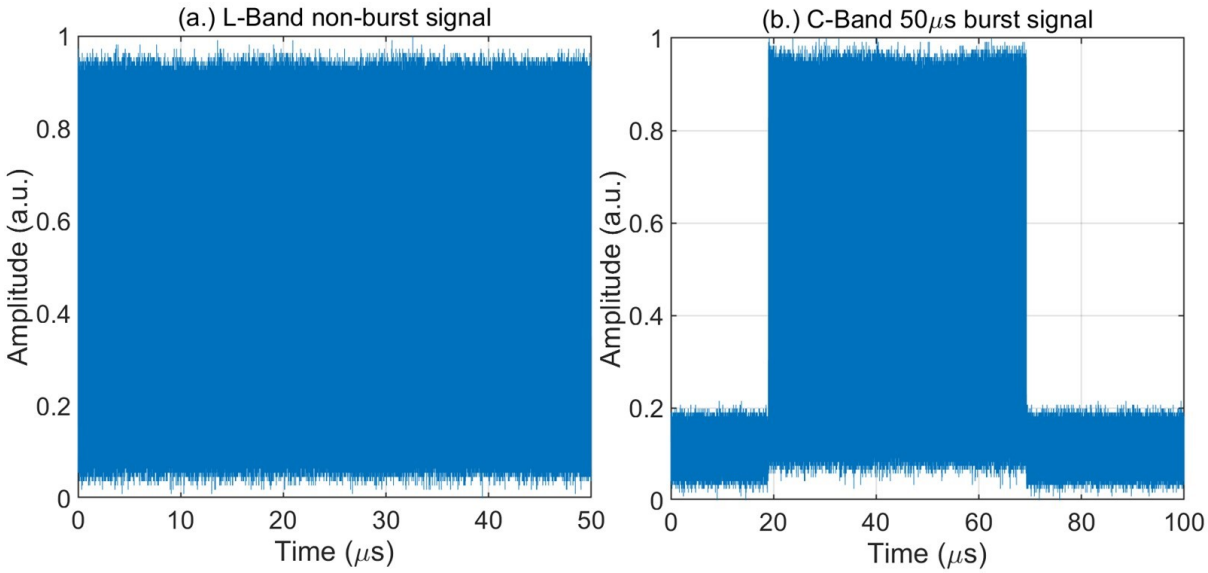

Figure 6.7 Downstream and Upstream signals in bi-directional extended reach transmission showing non-burst L-band signal and 50 μs C-band burst signal measured in B2B configuration

Figure 6.7 shows C and L-band signals in the back-to-back (B2B) configuration, where a 50 km SMF link dual-band amplifier was bypassed. The VOA was set to minimum attenuation (no attenuation) state with an insertion loss of 0.56 dB. Figure 6.7 (a) shows an L-band non-burst signal at 1586 nm, detected via an L-band direct detection PIN receiver with a responsivity of 0.7 AW^{-1}. Figure 6.7 (b) was a C-band 50 μs burst signal transmitted at 1533 nm and was detected via a DC-coupled PIN receiver with a responsivity of 0.7 AW^{-1}. Both DS and US signals were transmitted via a VOA emulating an optical splitter, fixed at 0 dB attenuation.

6.2.3 Dual-Band Bi-directional FOPA Setup

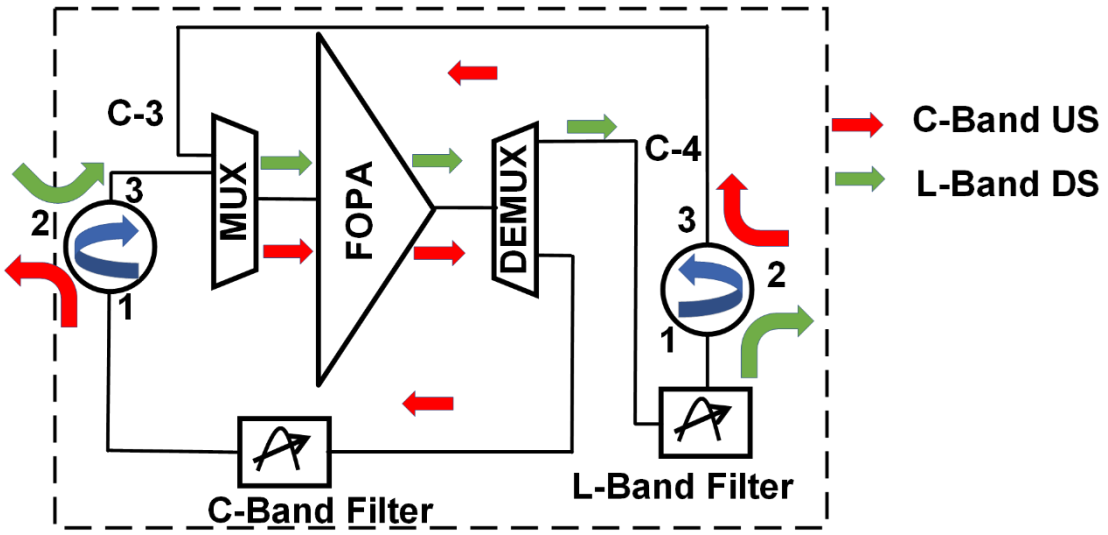

Figure 6.8 Experimental setup of bi-directional dual-band FOPA based C+L band in-line amplifier for reach extended access network link

The experimental setup of diverse polarisation FOPA employed as an in-line dual-band amplifier for bi-directional amplification is shown in Figure 6.8. Counter-propagating C+L band signals were launched in the FOPA for parametric amplification. It is important to note that the FOPA is a unidirectional amplifier [185], and due to high pump power, the amplification of counter-propagating signals is limited by SBS. Therefore, a bi-directional arrangement shown in Figure 6.8 was employed to amplify bi-directional signals simultaneously. Before amplification, the DS signal propagates over a 50 km SMF link, whereas the US signal passes by a VOA before amplification. The DS non-burst signal in the L-band was decoupled from the 50 km SSMF span via optical circulator C-3. Similarly, the US 50 μs burst signal coming from circulator C-4 is decoupled from the VOA. Decoupled C+L band signals were then multiplexed again by a C+L band multiplexer. Coupled signals were parametrically amplified by the dual-band PI-FOPA in a "Loss-Gain" configuration in a half pass loop architecture [155], also described in chapter 4, section 4.1.4. The pump powers in each arm of the PI-FOPA were 33.4 dBm and 32.7 dBm for achieving a net gain of >16 dB. A high power EDFA acting as an optical pump was tuned to the required pump powers to obtain equal signal gain for >50 nm apart signals operating at different wavelengths in the C and L-bands.

As the DS signal has an insertion loss of ~10 dB before amplification by the dual-band, the PI-FOPA C- band burst signal has a higher input power than the L-band DS signal launched into the dual-band FOPA amplifier. After amplification, signals demultiplexed by output C/L band splitter placed after the FOPA. C and L band signals and corresponding idlers with accumulated broadband noise were removed via C and L band tuneable filters. Around 1 nm wide C and L-band

tunable bandpass filters (BPF) had ~2 dB insertion loss to filter signals tuned at 1586 nm and 1533 nm. Amplified and filtered downstream and upstream signals were coupled again with the VOA and the SSMF span, respectively, using optical circulators C-3 and C-4. Signals were received via port 3 of circulator C-1 and C-2 and further transmitted to their individual detectors. The employed receivers were the same PIN photodetector discussed above—the photodetector connected to a real-time oscilloscope for signal analysis. Off-line digital signal processing (DSP) was employed with threshold detection used for DS and US bit error ratio (BER) measurement, which is described in detail in [26].

Figure 6.9 demonstrates the DS and US signal received after amplification by the in-line parametric amplifier at received signal power of -3 dBm. Transient free burst signal amplification was obtained by the FOPA, validating instantaneous response time [25]. Compared with the B2B non-burst and 50 μs burst signal shown in Figures (a) and (b), no difference was observed within the signals after in-line FOPA amplification. Minor fluctuations on the amplified received signal due to back reflections arising from one of the optical circulators in the setup were incurred within both the signals.

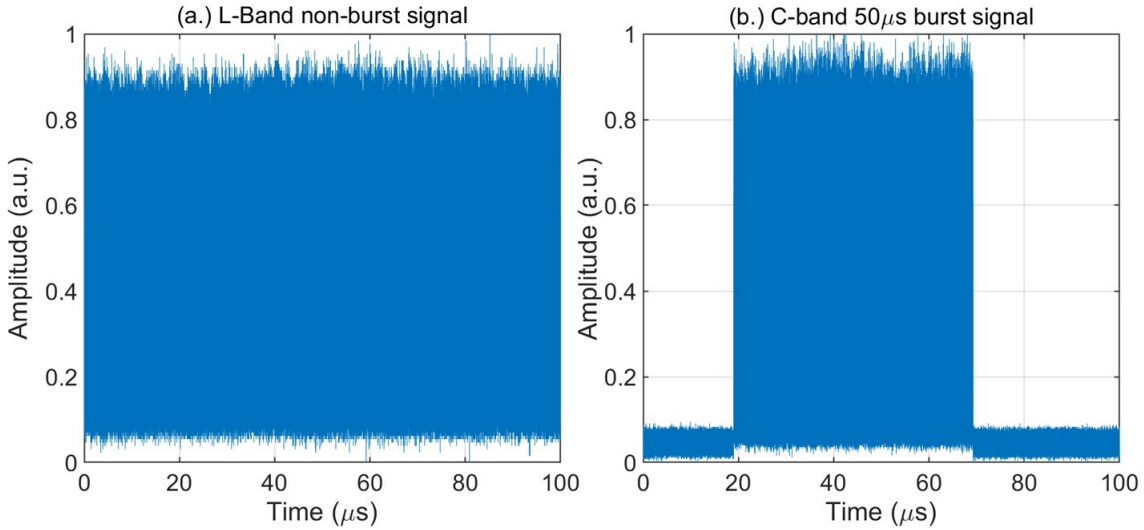

Figure 6.9 Bi-directional FOPA amplified 10 Gbps signals with >16 dB net gain in (a) L-band non-burst signal and (b) C-band 50 μs burst signal shown

6.3 Dual-Band FOPA Spectrum

Figure 6.10 presents an important result of this experimental work. Optical power spectra were measured at an OSA resolution of 0.1 nm at the input and output of PI-FOPA. The power spectra demonstrate an amplified C- band US signal at 1533 nm and L-band DS signal at 1586 nm. Input signal power for the C and L bands were - 1.6 dBm and -7.5 dBm, respectively. The L-band signal faced an additional ~9.7 dB power loss due to propagation through 50 km SMF and, hence, has

lower input signal power. The C-band input signal power to the FOPA is lower by 3 dB because of a 50 μs burst average signal power. Output powers of the amplified C and L band signals were 14.2 dBm and 9.9 dBm, respectively. Overall, input signal power loss from passive components was ~2 dB from WDM couplers, circulators, and optical connectors.

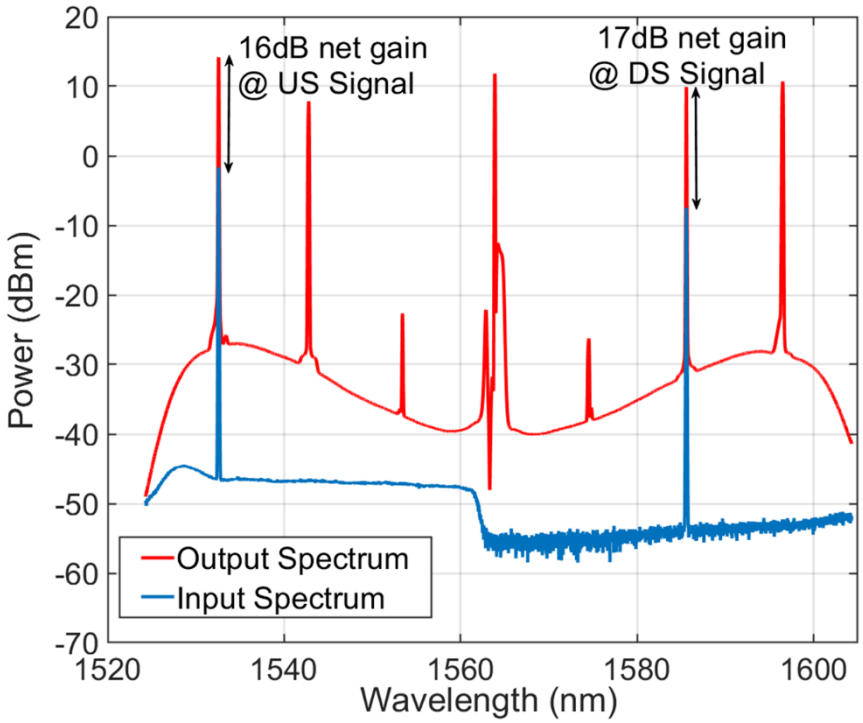

Figure 6.10 Optical power spectra of dual-band FOPA measured at input and output, for amplifying US C-Band and DS L-Band signals achieving a net gain of 16 dB in C-band and 17 dB in L-band signals for >50 nm apart signals

Polarisation insensitive FOPA net gain for DS and US was 17.2 dB for L-band and 15.8 dB for C-band located at >50 nm in wavelength. Wavelength selection for C and L bands channels was based on two main factors: obtaining equal net gain on both the channels and maximum signal-idler separation to avoid signal-idler crosstalk. The C-band wavelength was located at the peak of the FOPA gain spectrum to obtain a higher gain for the bursty channel and to overcome power loss in a 50 μs burst mode signal, whereas the L-band signal was located outside the FOPA gain peak to avoid the effect of additional Raman gain on longer wavelengths. Hence engineering the wavelengths of US and DS signals enables equal net gain for dual-band channels with minimal signal idler interaction. Signal and idler separation for DS and US signals was ~10 nm. Net gain with signal and idler wavelengths is shown in Table 6.1.

Dual-Band Signals	Wavelength (nm)		Output Power (dBm)	Signal Gain (dB)
	Signal	Idler		
Downstream (L-band)	1586	1543	9.7	17.0
Upstream (C-band)	1533	1596	14.2	16.0

Table 6.1 Corresponding signal and idler wavelength and gain values of FOPA amplified C+L band signals

Amplified signals were transmitted bi-directionally towards corresponding detectors. L- band signal power at the input of VOA after BPF was 7.9 dBm, and C-band signal power at the 50 km SMF input after BPF was 13.5 dBm. Correspondingly, C and L band signals' received signal power was 3.8 dBm and 7.1 dBm, respectively. ~3 dB difference between received power at the receiver was observed at the detector between DS and US signals due to opposite transmission paths. The amplified US signal was propagated through 50 km SMF facing ~10 dB attenuation before the US signal detection

6.3.1 Wavelength selection for Dual Band FOPA amplification

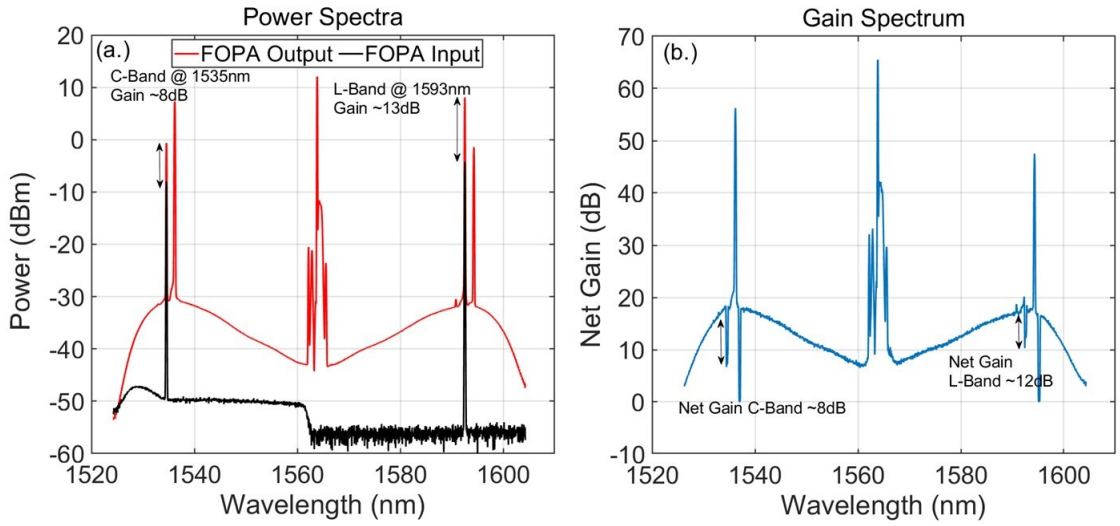

Figure 6.11 Wavelength selection for dual-band FOPA amplifier showing (a) power spectra at FOPA input and output with C band @ 1535 nm and L band @ 1593 nm (b) FOPA net gain spectrum at similar C and L band wavelengths

Wavelength selection for downstream L-band and upstream C-band signals was dependent upon the FOPA gain spectrum. Initially, signals were located at PI-FOPA gain peaks as shown in Figure 6.11 at 1535 nm in the C band and 1596 nm in L-band. Signal gain at FOPA peak was ~8 dB for US signal and ~13 dB for DS signal. Optical power spectra measured at FOPA input and output are shown in Figure 6.11(a) demonstrate that L-band signal gain is ~5 dB higher than the C band signal at the selected signal wavelengths. When measuring the spectra, polarisation controllers were tuned perfectly to align X and Y polarisation states of PI-FOPA to maximize output power at

both wavelengths. Further, in Figure 6.11 (b), polarisation independent net FOPA gain for both C and L band signals is shown. Net gain of ~8 dB in C-band and ~13 dB in L-band is observed. The main factor which might contribute to higher L band signal gain was additional Raman gain at longer wavelengths

Therefore, to obtain equal PI-FOPA gain, the wavelengths of both signals were adjusted. The L band signal wavelength was adjusted towards the lower gain wavelengths of the FOPA gain peak to reduce extra gain and was placed at 1586 nm shifted by ~7 nm. Whereas, C band signal only shifted by ~2 nm and was located at 1533 nm at the peak of the FOPA gain spectrum to obtain high gain for burst signals. In the case of wideband bi-directional dual-band FOPA signal amplification, a flat FOPA gain spectrum will be a target for obtaining equal signal gain. Wideband WDM signals will require a wide flat gain rather than a high parametric gain peak with narrow gain bandwidth. >100nm FOPA flat gain bandwidth was demonstrated in [186], and hence a similar approach can be employed for wideband signal amplification. Another requirement is low polarisation-dependent gain (PDG) for obtaining equal gain for wideband signals, which could be provided by automatic polarisation controllers or by employing polarisation maintaining parametric gain fibres.

6.3.2 Polarisation Dependent Gain of dual-band signals

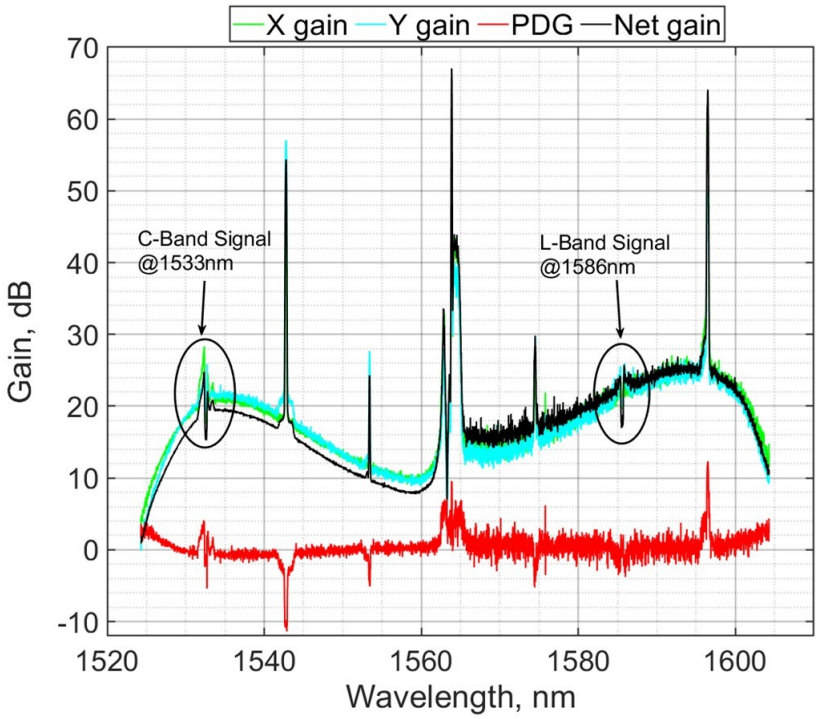

Figure 6.12 PI-FOPA gain spectra demonstrating polarisation-independent X-Y gain, Net gain, and polarisation-dependent gain (PDG)

Figure 6.12 demonstrates individual orthogonal signal gain in each polarisation state as X and Y are measured in each PI-FOPA arm. The net gain is shown as a black curve presenting the total average gain removing the insertion loss of the amplifier. The circular marking indicate C-band signal net gain plus X-Y gain at both US signal 1533 nm and DS signal 1586 nm wavelength. A total net gain of 17 dB and 16 dB is obtained for DS and US amplified signals. The red curve at the bottom of Figure 6.12 demonstrates the polarisation-dependent gain (PDG), showing a gain of ~0 dB for >80 nm PI-FOPA gain bandwidth. The PDG was calculated as a difference of X-Y gain, which means when X-Y signal gain is equal, minimum PDG can be obtained. An increase in the PDG gain tilt within the gain spectrum at the longer wavelength was due to the addition of Raman gain. The idler of C and L band signals is located around 10 nm away from the signal frequency. The residual pump at the center of the spectrum is at 1564.3 nm.

The as PBS employed in the PI-FOPA setup, as explained in chapter 4 section, 4.1.4 was to orthogonally split the signal was bandwidth limited. Hence, recombination of the broadband gain spectrum with the amplified dual-band polarisation-independent signals was the limitation of the low bandwidth of PBS. Therefore, it was difficult to maintain equal gain on both signals with >50 nm separation without continuous polarisation tuning while parallelly operating the amplifier and taking the measurements due to polarisation drifts arising within long lengths of gain fibres.

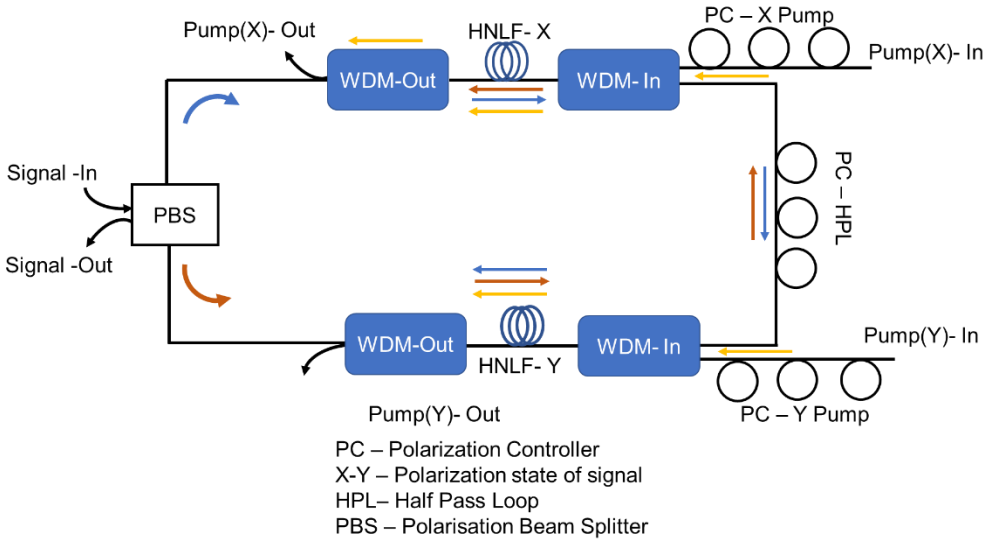

Figure 6.13 Schematic view of polarisation diversity in PI-FOPA via employing three polarisation controllers for pumps and signal recombination

Figure 6.13 demonstrates a schematic of the polarisation diverse half-pass loop FOPA architecture, showing the employment of PCs [152] and two high-power pumps amplifying X-Y polarisation state connected with HNLF for the parametric gain. Two individual polarisation

controllers located before pumps (PC-X/Y) are tuned regularly to control polarisation. Pump PC are tuned to maximize input pump power for orthogonally split signal amplification. The third PC located at the middle of the setup (PC-HPL) is utilized for recombination of propagated signals and mitigating polarisation drifts through long HNLF lengths after amplification. Pumps were filtered out by output WDM (WDM- out) after parametric gain medium.

In a polarisation diverse loop architecture, two separate pumps were coupled to amplify orthogonally splitting signals. Pumps were combined through WDM_{in} and taken out via another WDM_{out} after the first half of the loop. Importantly pump filtering through WDM from each half of the loop section was employed to avoid the SBS generation through counter-propagating pumps and residual FWM interactions. The detailed architecture is discussed in[148].

6.4 Result and Discussion

Performance analysis of received bi-directional signals was undertaken via BER measurement against the received signal power. The BER of DS (L-band) and US (C-band) signals were calculated first in the B2B scenario and further after in-line FOPA amplification with a 50 km transmission link. BER measurement for DS non-burst 10 Gbps signal was compared with B2B, and PI-FOPA amplified non-burst signal. B2B BER was measured as a reference for observing any penalty addition within the detected signal after parametric amplification and reach extended link. Similarly, for the US, the signal was analysed in B2B first and then amplified by PI- FOPA. Additionally, US signal BER measurement was performed for both burst and non- burst signals to analyze penalty in received power for burst signal after FOPA amplification in a bi-directional link.

6.4.1 BER vs. received signal power

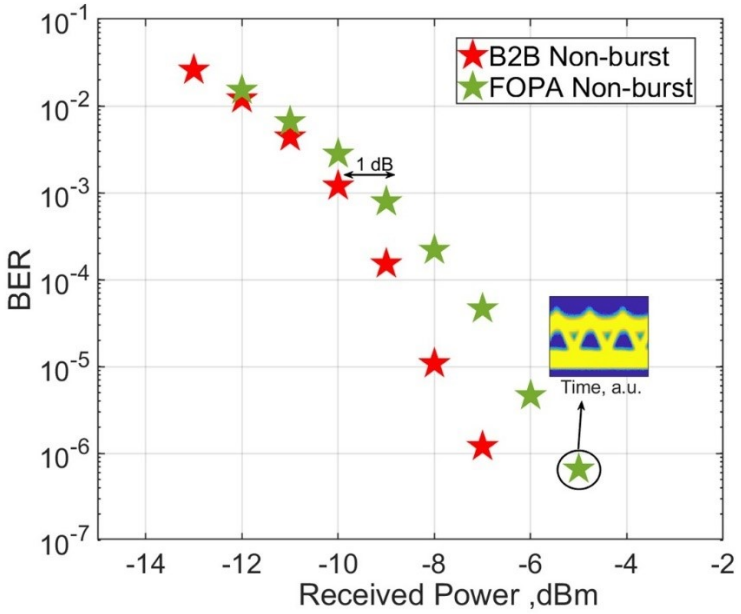

Figure 6.14 BER vs. received power plot for L-band downstream signal at 1586 nm

In this section, DS and US signals were transmitted uni-directionally and individually in the experimental setup. Figure 6.14 shows BER against received power for DS L-band received signal. Net FOPA signal gain for the L-band signal at 1586 nm was 17 dB. BER was first measured in B2B configuration for L-band signal, including transmission span and a dual-band PI-FOPA amplifier. A received power penalty of ~1 dB was observed for FOPA amplified signal at BER level of 10^{-3}. Received signal power swept from -3 dBm to - 14 dBm. The 1 dB difference was due to noise addition within the signal due to PI-FOPA in the "Loss-Gain" configuration and dispersion penalty from the 50 km SMF link. The open eye diagram is shown as an inset of Figure 6.14 for the received power level of - 5 dBm at a BER level of 10^{-7}. The clear open eye shows almost error-free amplification by PI-FOPA achieved for L- band signal amplification.

Figure 6.15 demonstrates BER measurement for US signal in four scenarios: B2B non- burst signal, B2B with 50 μs burst, FOPA amplified C-band for non-burst and 50 μs burst signal. It was observed that bursty signals in B2B configurations have ~1 dB received power penalty compared to the non-burst B2B signal. Degradation in bursty signals is incurred due to fluctuations arising from the transmitter and non-burst mode receiver [26], as explained in chapter 4, section 4.2.1.

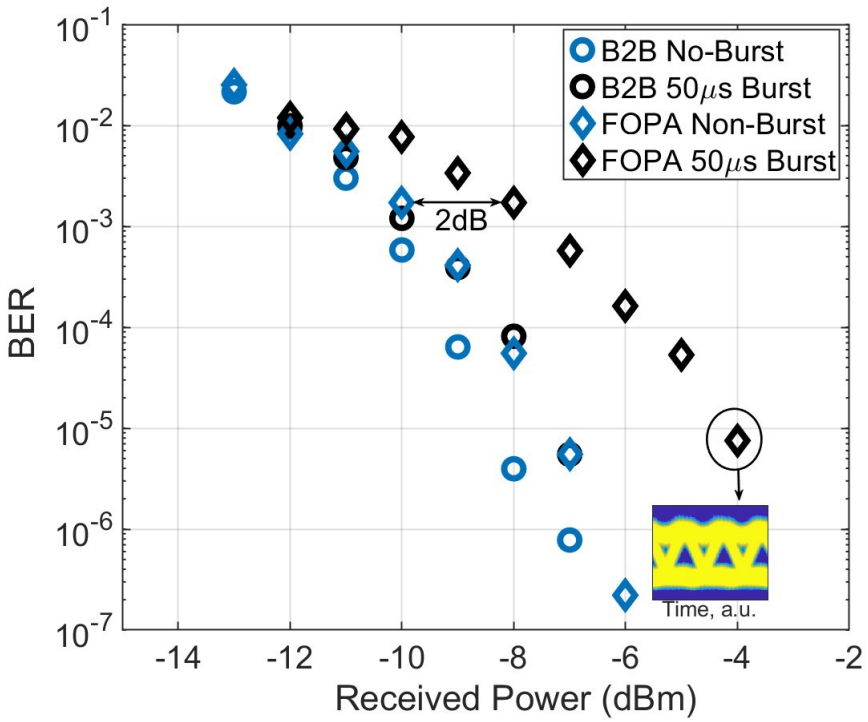

Figure 6.15 BER vs. received power plot for C-band upstream signal at 1533 nm

B2B configuration was further switched to FOPA amplification of the US C-band signal transmitted in non- burst and burst mode. The net gain in the C-band signal was 16 dB. FOPA amplified non-burst signal introduces a minor received power penalty of ~1 dB compared to B2B non-burst scenario due to incurring noise and dispersion within the US signal as discussed above. Around 2 dB received power penalty for 50 μs burst signal amplified by PI-FOPA was observed at BER level of 10^{-3} from B2B. Additional penalty within bursty FOPA amplified signal was due to non-optimized transmitter and receiver, with addition on dispersion and noise arising from a bi-directional link.

Overall, FOPA amplification introduces a minor ~1 dB penalty for non-burst signals and ~2 dB received power penalty for C-band compared to B2B signal. Eye diagram of amplified burst signal by the PI-FOPA is shown in Figure 6.15 at a received power level of -4 dBm at BER level of 10^{-6}. The open eye pattern shows that the PI-FOPA amplifies the burst mode signal without severe penalty. The performance analysis of counter-propagating signals in the C+L band amplified by PI- FOPA demonstrates the ability of FOPA to amplify burst and non-burst signals with minimum power penalty simultaneously.

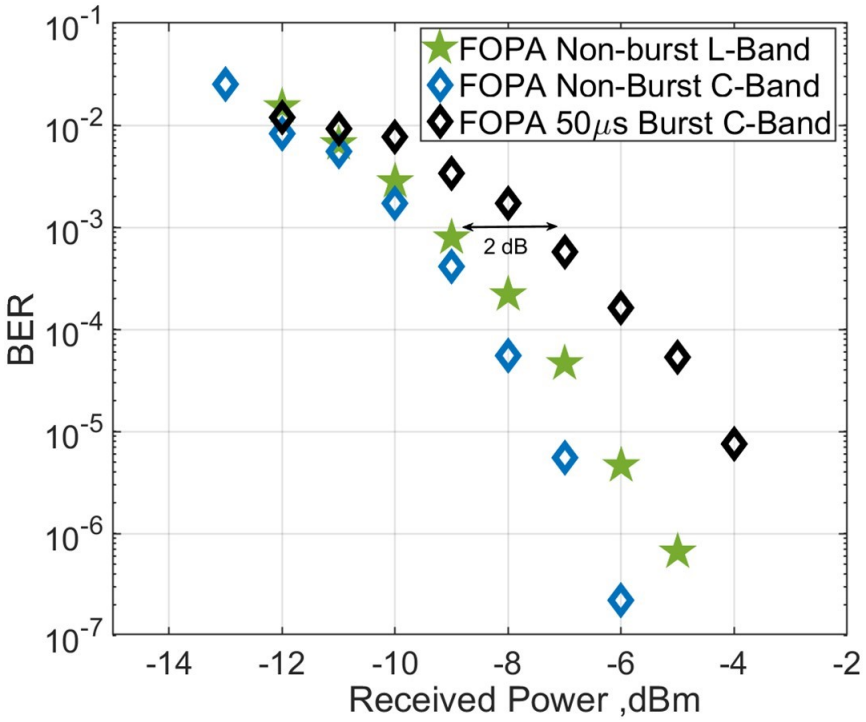

Figure 6.16 BER vs. received power comparison of non-burst L band and bursty C band signal

Further, both DS and US signals were transmitted bi-directionally within the complete setup, and B2B measurement was not performed for this analysis. Figure 6.16 compares BER measurement for FOPA amplified downstream L-band and upstream C- band signals against received power. For non-burst C and L band signals, almost an overlap of BER values is noticed at the BER level of 10^{-3}. At higher received signal power performance, the C band signal is ~1 dB better than the L-band signal at a received power level of -6 dBm. C-band signal in non-burst mode performs better than L-band signal, although, in burst mode, the C-band signal suffers a received power difference of ~2 dB. The received power penalty was added in detected signals due to similar reasons discussed in the previous sections. The L-band signal was unable to be transmitted in burst mode due to the limitation of the AOM to function at the required L-band signal wavelength although, it's predicted to have similar results of FOPA amplification for L-band burst mode signal as the FOPA ultra-fast response is not wavelength restrictive.

6.4.2 Spectra of received C+L band signals

Figure 6.17 shows DS and US signal spectrums measured after individual tunable filters. The spectra for both the channels were measured at a resolution of 0.1 nm with an OSA. Tunable bandpass filters are employed to remove two primary signal degrading sources as idlers, generated through parametric amplification, and ASE noise accumulated through transmission link via booster amplifiers (EDFA) as both idlers and additional noise are the primary sources of BER degradation in the detected signals.

Figure 6.17(a) shows the power spectrum against wavelength for the C-band upstream signal at 1533 nm. The spectrum shows that the L-band idler at ~1543 nm was suppressed by ~40 dB compared to the C-band signal. The attenuated L-Band signal at 1586 nm was observed after the BPF due to the leakage of circulator C-1 before the receiver. The pump at 1564.4 nm was removed almost entirely as the pump is removed initially within the FOPA setup and later by signal BPF.

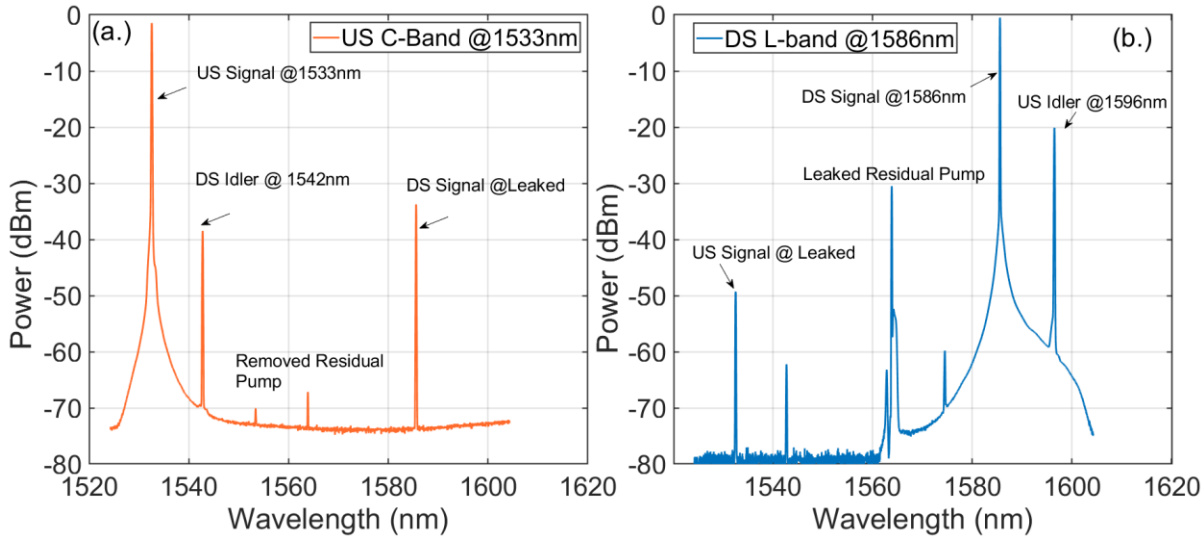

Figure 6.17 Signal power vs. wavelength spectra for (a) Upstream C- band burst signal and (b) Downstream L-band non-burst signal at the corresponding receiver.

Figure 6.17 (b) shows the filter response of the L-band signal at 1586 nm. The plot demonstrates the L- band signal spectrum at the OSA after passing through L-band BPF before reaching the corresponding receiver. The BPF is tuned to filter the L band signal at 1586 nm. Multiple additional waves within the spectrum were due to leakage of circulator C-2 and waves passing the BPF. It was observed that the L-band filter was less efficient than the C-band filter employed within the experiment. The extinction ratio of the L-band signal to C- band idler was ~20 dB, with the residual pump being more prominently visible at 1564.4 nm with an extinction ratio of ~30 dB. It shows the penalty observed in the BER of the L-band signal was due to a large pump and idler with the filtered signal.

6.5 Comparison of Simulation vs. Experimental Results

This section compares experimental BER measurement demonstrated in section 6.4 with simulated BER values obtained in section 6.1. Downstream and upstream signals are compared, respectively.

6.5.1 Downstream L-band simulation vs. experiment

Figure 6.18 compared L-band downstream signal simulated BER curve against received power and experimental curve for B2B, and FOPA amplified non-burst signal. Around 1 dB received power difference was observed between simulation and measured L- band signal values in the B2B scenario.

The <1 dB difference observed a good agreement obtained for FOPA amplified L-band signal between simulated and experimental values. The signal gain in the L-band obtained was ~16 dB, and in experimental demonstration, net FOPA gain for the L band signal was ~17 dB. As a polarisation, insensitive FOPA model was not possible to simulate in the VPI transmission maker, and the obtained result encourages us that signal amplification in the L band by the PI-FOPA with a net gain, ~16 dB is achievable with a signal performance like the simulated work.

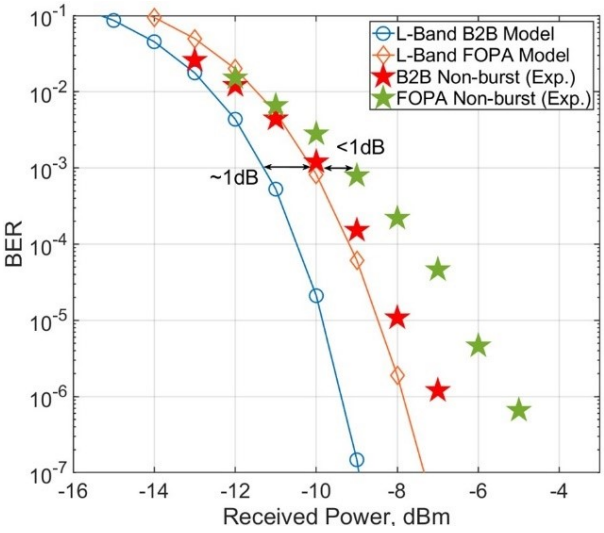

Figure 6.18 Comparison of BER vs. Rx.Power for L band signal in simulated and experimental results

6.5.2 Upstream C-band simulation vs. experiment

Figure 6.19 shows the BER comparison of upstream C band signal for simulated and experimentally measured value in non-burst mode. To investigate dual-band signal amplification by PI-FOPA, DS, and US signals were simultaneously amplified in a dual-band FOPA amplifier. ~1 dB difference was observed in the C band FOPA amplified signal between simulated and experimental results. Good agreement between simulated and observed values for BER level ~10^{-3} were observed, although this difference increases to ~2 dB at the received signal power of -6dBm compared to B2B, due to the addition of nonlinearity in the signal stemming from FOPA and 50km reach span at higher signal power in the experimental work. Another possible reason is the addition of noise in the signal from a large residual parametric pump and downstream idler

within the upstream signal. Within the simulation model, the US signal was transmitted in the non-burst mode.

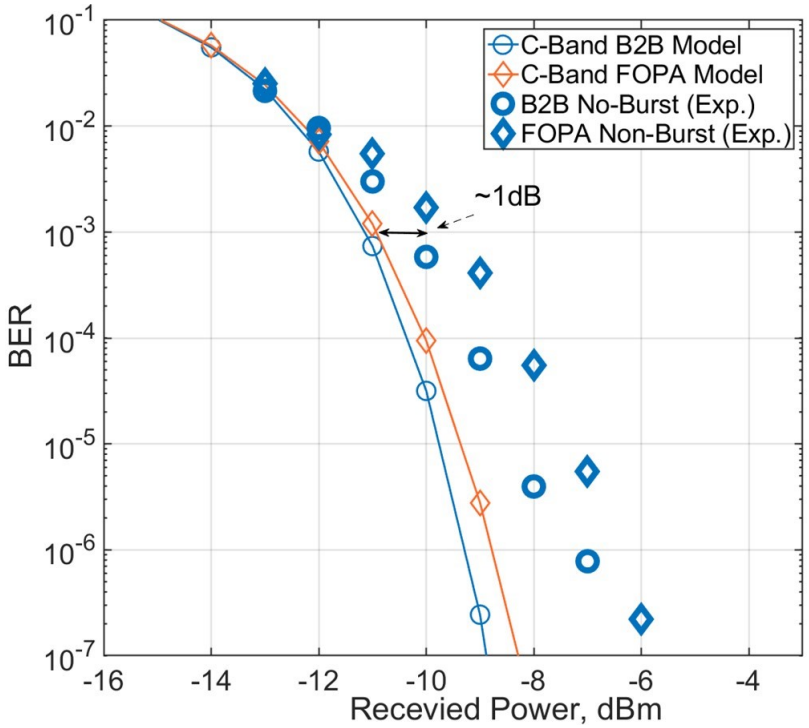

Figure 6.19 Comparison of BER vs. Rx.power for C band non-burst signal in simulated and experimental results

6.6 BER vs. Splitter Attenuation

This section analyses overall link power budget improvement by measuring BER as a function of VOA attenuation emulating an optical splitter. Total attenuation achieved by DS and US signal indicates an increase in splitter power budget via employing an in-line optical amplifier. Measurement for US signal is performed in non-burst and burst mode, for DS similar is measured for non-burst as L-band signal was continuous. The total attenuation was measured at a BER level of 10^{-3} before the signal was completely attenuated in power and not detectable due to electrical noise added by the receiver. The measured attenuation at the BER level of 10^{-3} provides an analysis of splitter power budget improvement.

Figure 6.20 below shows a BER vs. attenuation plot for DS and US signals. Figure 6.20 (a) presents an attenuation of 16 dB achieved at the BER level of 10^{-3} for the DS signal. The attenuation value for the L-band signal indicates splitter attenuation of 16 dB. The DS splitter power budget increase provides an additional splitter power of ~1:64 for the downstream signal in non-burst mode.

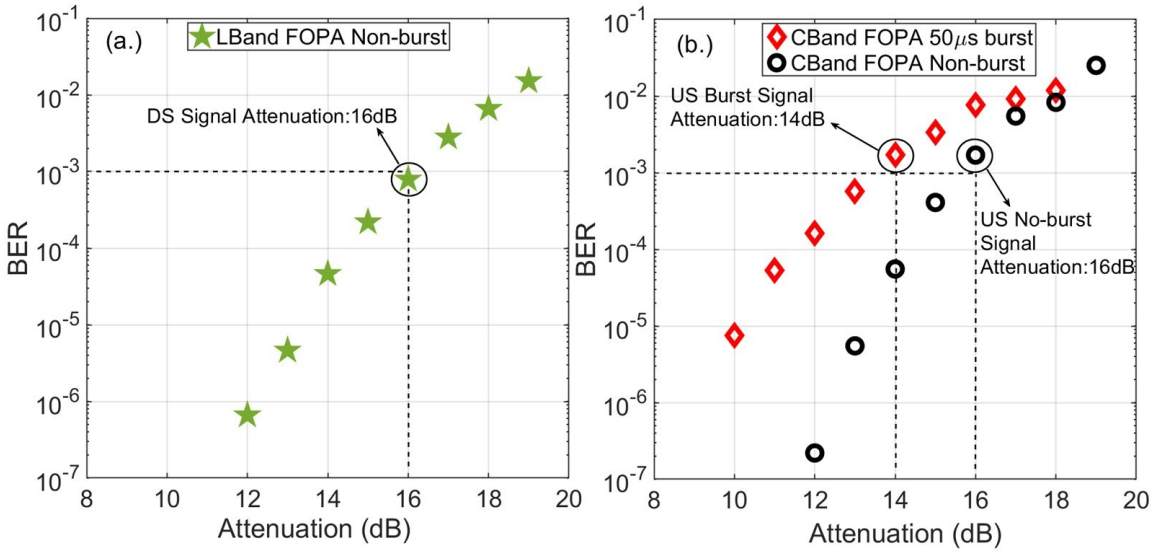

Figure 6.20 BER vs. splitter attenuation for counter-propagating (a) L-band downstream non-burst signal and (b) C-band upstream 50 μs burst signal

Figure 6.20 (b) shows the attenuation vs. BER plot for US (C-band) bursty and non-burst signals at a BER level of 10^{-3}. For the non-burst signal in the C-band, an attenuation level of 16 dB was achieved, which is similar to the L-band non-burst signal at 1586 nm. It demonstrates that the PI-FOPA operates similarly to amplify non-burst type signals in case of >50 nm apart signals. For a 50 μs bursty US signal in C-band, an attenuation factor of 14 dB was achieved at BER of 10^{-3}. Therefore, the requirement to operate the upstream signal in burst mode introduces ~2 dB of an extra penalty compared to the non-burst signal and decreases the available splitter power budget to 14 dB. An enhanced splitter power budget provides an additional splitter ratio of 1:32 for US direction although, this result importantly demonstrates the FOPA's capability to amplify wideband signals with almost equal gain.

6.6.1 FOPA enhanced link power budget

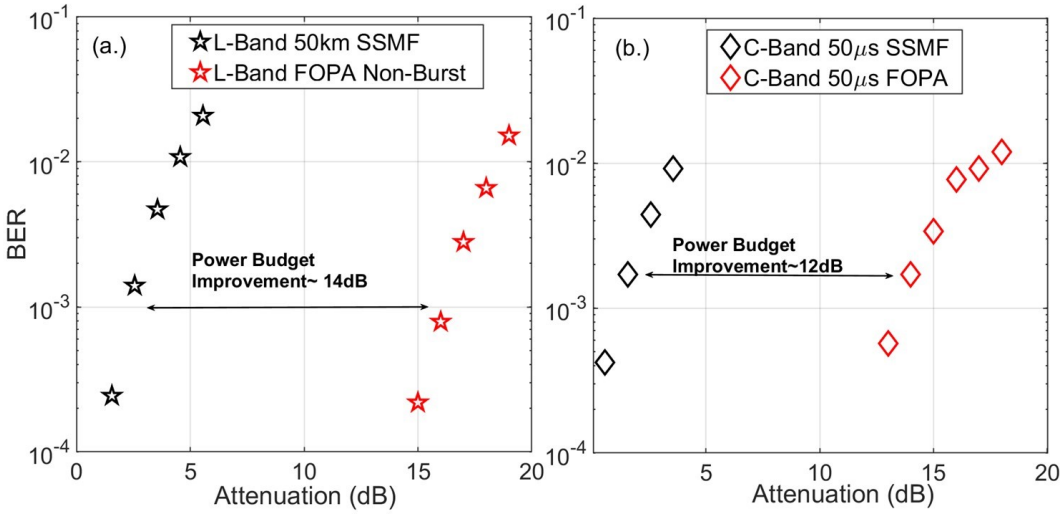

Figure 6.21 BER vs. splitter power budget improvement in C+L band signal after 50 km SSMF propagation enhanced by the dual-band FOPA amplifier

Figure 6.21 shows improvement in splitter attenuation provided by dual-band FOPA for the downstream non-burst and the C-band upstream burst mode signals over 50 km SSMF transmission link. Splitter power budget improvement was measured at a BER level of 10^{-3}. BER was measured for two scenarios as received signal after 50 km transmission excluding in-line amplifier and received signal after 50 km propagation with in-line PI-FOPA amplification. The PI- FOPA was employed as a dual-band amplifier to amplify the signals, enhancing the splitter power budget. The VOA was emulating an optical splitter adjusted for sweeping received power was initially fixed at 0 dB attenuation.

Figure 6.21 (a) shows the BER against attenuation increase for the DS signal at 1586 nm. At the BER level of 10^{-3} the attenuation after 50 km SMF transmission was at 2.6 dB without the amplifier. At splitter attenuation of 1.5 dB, no optical splitter could be employed after 50 km transmission with an available splitter power budget. Whereas after employing a PI-FOPA as an amplifier, the split power budget was increased by ~14 dB for the DS signal. Consequently, an additional optical splitter with ~1:32 split for the downstream signal can be employed.

Similarly, in Figure 6.21 (b), a US C-band 50 μs burst mode signal was propagated first without amplification through the 50 km reach extended transmission line. The burst signal was detected at the received burst power of -8 dBm. At the BER level of $10^{-3,}$ splitter attenuation was at ~1.5 dB after SMF transmission bypassing in-line FOPA amplifier. Similar to the DS signal, no splitter power budget is available to split the US signal. With FOPA amplification, overall splitter attenuation was improved by ~12 dB for the US signal. Therefore, the available total splitter power budget was increased by 12 dB for the upstream burst signal. An optical splitter with 1:16 splits could be employed after 50 km reach extension.

In relation with the above, overall, link power budget improvement can be fragmented into total optical distributed power as splitter power budget, power enhancement via 50 km reach extension, and lost power by passive components. The below relation shows distributed power for an overall link power budget.

$$Total\ Power\ budget, dB = Splitter\ Budget\ (dB) + Reach\ Extension\ (dB) + Passive\ Component\ Loss\ (dB)$$

Enhancement of splitter power budget in the L-band downstream signal was equivalent to 16 dB enabled by FOPA amplification. 50 km SSMF transmission adds a 10 dB increase within the power budget, and the total passive component loss of ~6 dB can be defined as the overall link power budget. Therefore, a total of 32 dB overall link power budget is available for the DS signal. Similarly, in the case of the US bursty C-band signal, increased splitter power from the FOPA was 14 dB, and the total link power budget obtained for the US signal was 30 dB, with 10 dB from 50 km SMF and 6 dB from the passive components.

Overall, by implementing FOPA as an in-line amplifier total, link power budget is enhanced by 32 dB (equivalent to 160 km) for L band DS and C-band US traffic by 24 dB (equal to 150 km). Alternatively, an enhanced splitter power budget of 22 dB and 20 dB with a 20 km standard access link. The result presents the FOPA's ability to improve the overall link power budget by increasing splitter attenuation by 16 dB and 14 dB and consequently overall link power budget by 32 dB and 30 dB for DS and US signals transmitted bi-directionally in a 50 km reach extended access network link.

6.7 Summary

In this chapter, for the first of my knowledge, a bi-directional signal was amplified by dual-band PI-FOPA in a 50 km reach extended access network. The bi-directional signals were transmitted in L-band at 1586 nm and C-band at 1533 nm in non-burst and 50 μs bursty signals of 10 Gbps OOK. In a novel, experimental demonstration, a bi-directional dual-band FOPA amplifier enables amplification of >50 nm apart counter-propagating signals with >16 dB net polarisation insensitive gain. Additionally, for the first time, simultaneous amplification of non-burst and burst signals was amplified by FOPA. Amplify. Consequently, allowing parametric amplification of counter-propagating channels in a 50 km reach extended architecture for the first time.

Results obtained through this experimental work demonstrate that the overall splitter power budget increases for an access network link. A splitter power budget of 16 dB was obtained for non-burst DS and 14 dB for burst mode US signals. Overall link power budget was improved by

32 dB and 30 dB for the first time, counter-propagating signal amplification by FOPA was shown in a polarization-insensitive configuration. With a single parametric pump, ~10THz gain bandwidth was achieved with polarization-insensitive amplification of >50 nm apart signals. In a novel, dual-band directional PI-FOPA configuration, simultaneous amplification of bi-directional signals performed without SBS limitation occurs with high power pumps. Overall, this experimental work demonstrated great potential for FOPA implementation in extended reach access network links and other bi-directional and multi-band transmission links.

Chapter Highlights

From the high capacity burst traffic amplification, we found out the following results.

- **Bi-directional link design:** We introduce a bi-directional 50 km access link to amplify C and L band signals transmitted at 1533 nm and 1586 nm. C-band signal was in burst mode and L-band signal was transmitted as a non-burst signal propagated in upstream and downstream directions.

- **Novel dual-band FOPA:** We demonstrate dual-band FOPA setup for amplification of counter propagating signals. Downstream L-band and upstream C-band signals were coupled together before PI-FOPA amplification and amplified signals are decoupled to propagate bi-directionally.

- **Polarisation independent Gain:** We achieve for the first-time polarisation independent gain for >50 nm apart signals in C and L band simultaneously. We also demonstrate amplification of dual-band signals with >16 dB net gain using a broadband gain spectrum of ~10THz spanning the C and L band.

- **Increasing splitter power budget:** An in-line dual-band FOPA enhanced overall splitter power budget by 16 dB for DS signal and 14 dB for upstream signal. 50 μs bursty signal observed 2 dB less power budget due to penalties induced by receiver and transmitter.

- **FOPA enhanced overall link power:** Link power budget improvement by FOPA was measured via attenuation vs BER. Improved performance provided by FOPA was measured from 50 km SSMF transmission. Overall, link power budget after 50 km was 14 dB for downstream L-band signal and 12 dB for C-band upstream signal. Increasing overall link power by 32 dB and 30 dB distributed over 10 dB of 50 km SMF transmission and 6 dB passive insertion loss.

Chapter 7 CONCLUSION AND FUTURE WORK

7.1 Conclusion

In this thesis, a range of innovative experimental techniques is presented and investigated to make a fibre optic parametric amplifier (FOPA) a drop-in burst mode amplifier technology in a tested reach extended access network architecture. The main focus of this thesis work has been an improvement of burst mode signal amplification provided by the ultrafast response time of the FOPA acting as a burst mode amplifier. The PI-FOPA provides high net gain and improves receiver sensitivity, increasing the overall link power budget of an optically amplified reach extended access network propagating signals in more than one telecom band.

For the first time, I have presented an experimental demonstration of FOPA ultrafast signal amplification for a range of time-varying bursty signals in an optical access network architecture. The ultrafast amplification was validated via extensive practical demonstrations.

A laboratory-based experimental setup of an access network included: a 10 Gbps burst mode transmitter, a 50 km SSMF trunk, optical amplifiers under test connected to a VOA, and an optical receiver including a photodetector connected to a signal analyser. A PI-FOPA was employed to demonstrate amplification of burst signals in scenarios as :(a) Range of burst signal duration from non- burst and switched to burst from 70 μs to 5 μs short burst duration at fixed burst period of 100 μs and (b) Range of burst traffic density from 5% to 97% at fixed burst duration of 30 μs in the first and second experimental work.

The obtained results have shown that employing a FOPA as a drop-in amplifier in an optically amplified access link can significantly improve receiver sensitivity besides increasing the overall link power budget for burst mode signals. The FOPA's ability to achieve transient free amplification for burst mode signals improves signal received power penalty by >3 dB compared with a tested conventional commercial EDFA and a discrete Raman amplifier. For the varied range of burst signal duration from 70 μs to 5 μs, at 13 dB net gain, the FOPA shows stable performance where receiver sensitivity fluctuations were <1 dB compared to the back-to-back signal. While the commercial-grade EDFA and discrete Raman amplifier degrade receiver sensitivity by >3 dB, on the other hand, the FOPA's ultrafast response for bursty signals improves it by >3 dB. Polarisation insensitive FOPA was also demonstrated with 20 dB net gain for burst signal amplification. Compared to the EDFA's bursty signal amplification at 20 dB signal gain, the FOPA improves burst amplification without destroying the signal due to the transient effect. Although

when amplified for a non-burst mode signal, EDFA performance was improved by ~2 dB more than FOPA in received power.

Further, results obtained for experimental investigation showed varied burst traffic density amplified by PI-FOPA, EDFA, and Raman amplifier for low traffic density at 5% to the highest of 97%. EDFA performance was worst with a receiver sensitivity penalty of ~5 dB at 75% traffic. Discrete Raman amplifier performance was stable at low traffic density up to 30%, which got degraded with a further increase in traffic density up to 75%, with a receiver sensitivity penalty reaching ~3 dB. Minor improvement was obtained at maximum allowed burst traffic density of 97% in EDFA and Raman amplifier receiver sensitivity by ~2 dB and 1 dB. It shows that EDFA and Raman amplified tend to perform better with quasi-continuous bursty traffic, although still suffering from residual transient penalties. In comparison, the PI-FOPA performed within 1 dB receiver sensitivity penalty for a fully tested range of 5% to 97% burst traffic density. The FOPA allows for 5- times higher traffic density than EDFA for the same power budget. It was observed and concluded that FOPA could improve a high capacity burst traffic of >5 dB power budget or its traffic capacity by a factor of 6 compared to a commercial EDFA.

For the first time, in another experimental work, bi-directional dual-band signal amplification with a novel dual-band FOPA amplifier was experimentally presented amplifying signals in the C&L band. A novel experimental setup constructed a dual-band transmitter, a 50 km SSMF link, a bi-directional-based dual-band FOPA, VOA, and a dual-band optical signal detector. Bi-directional signals in the L-band at 1586 nm and in the C-band at 1533 nm in non-burst downstream and burst mode in upstream directions were transmitted in counter-propagation. A novel bi-directional dual-band FOPA arrangement consisting of a PI-FOPA amplifier with a C+L band multiplexer/demultiplexer was employed for simultaneous amplification of downstream and upstream signals. >50 nm apart signals were amplified by dual-band PI-FOPA with net gain >16 dB being obtained. A single in-line amplifier achieved a C-band net gain of ~16 dB, and an L-band signal net gain of ~17 dB. Parametric amplification over ~10THz gain bandwidth demonstrated with bi-directional amplification of non-burst and bursty signals.

Overall, the FOPA provides multiple unique features with excellent potential for ultrafast response time amplification, large bandwidth, and high gain, although amplifying signals outside conventional C-band wavelengths is still to be demonstrated in practice. This thesis has significantly developed this potential and advanced state-of-the-art performance by experimentally demonstrating a range of techniques leading to a FOPA based burst mode amplifier showing performance over state-of-the-art EDFA and Raman amplifiers. Further, ~10THz FOPA ultrawide gain bandwidth enabled amplification of C and L signals situated at >50 nm apart wavelengths were demonstrated with an individual single bi-directional dual-band

amplifier. These achievements are viewed as a step towards a significant extension of reach and link power of signal transmission in optical access networks via burst mode FOPA.

7.2 Future Work

The FOPA is the potential choice of future amplification techniques for optical fibre communication systems. The work presented in this thesis made FOPA an obvious promising candidate as an optical amplifier for reach-extended access networks due to the multiple verified qualities. However, significant progress has been made to enable FOPA use outside a research lab. Two main directions of future FOPA development for robust, scalable, and future proof optically amplified access networks can be as:

First, extending previous investigation for parametric amplification of bursty signals by PI-FOPA. A range of new experiments focusing on bursty traffic amplification by FOPA could be conducted as:

(a.) Experimentally investigate upstream burst mode signal amplification by FOPA, EDFA, and Raman amplifier. The results will employ FOPA as a pre-amplifier and measure the dynamic range of parametric amplifier amplifying a range of varied signal power bursts.

(b.) Using an arbitrary traffic generator, amplify the dynamic bursty signal with random burst duration and traffic density by PI- FOPA. Experimental work will provide evidence of real-time burst-type traffic amplification.

(c.) Increasing the reach to 100 km of bi-directional link with advanced modulation format. For example, 100 G QPSK burst signals access link and transmit bursts of high cardinality modern optical signals, amplified via drop-in PI-FOPA.

Secondly, a broadband high gain FOPA demonstrated for wideband spectral regime covering E, S, and O band and focusing on O-band wavelength ~1310 nm employed in typical access networks. To amplify both WDM and bursty signals in future access networks, FOPA gain around O band wavelengths at 1310 nm can be achieved using two main techniques. Achieving parametric gain in the O-band could be obtained via employing a highly non-linear fibre with zero dispersion wavelength located in the O-band. Broadband FOPA gain spectrum in O-band potentially can be obtained by using high-power Raman pumps to achieve parametric amplification.

Another approach to obtain O-band FOPA amplification is by detuning the pump away from the zero-dispersion wavelength in the C-band. Investigating dispersion properties of the highly non-linear fibre can provide gain at arbitrary wavelengths. In this work, simultaneous, dual-band signals are amplified via a single pump source, for example, a signal near the pump in the C-band and a faraway signal~200 nm in the O-band.

REFERENCES

[1] T. Cisco and A. Internet, 'Cisco: 2020 CISO Benchmark Report', 2020.

[2] G. S. Ford, 'Is faster better ? Quantifying the relationship between broadband speed and economic growth', *Elsevier*, vol. 42, no. 9, pp. 766–777, 2018.

[3] A. D. Ellis, N. Mac Suibhne, D. Saad, and D. N. Payne, 'Communication networks beyond the capacity crunch', *Philos. Trans. R. Soc. A Math. Phys. Eng. Sci.*, vol. 374, no. 2062, 2016.

[4] I. Cisco Systems, 'Cisco Visual Networking Index: Forecast and Trends, 2017–2022 White Paper', *Cisco Forecast Methodol.*, pp. 2017–2022, 2019.

[5] M. Ruffini *et al.*, 'DISCUS: End-to-end network design for ubiquitous high speed broadband services', *Int. Conf. Transparent Opt. Networks*, pp. 2–6, 2013.

[6] D. Lavery, S. Erkilinc, P. Bayvel, and R. I. Killey, 'Recent progress and outlook for coherent PON', *2018 Opt. Fiber Commun. Conf. Expo. OFC 2018 - Proc.*, pp. 1–3, 2018.

[7] Emmanuel Desurvire, *Erbium-Doped Fiber Amplifiers : Principles and Applications*. John Wiley & Sons, 1955.

[8] F. Saliou *et al.*, 'Reach extension strategies for passive optical networks', *J. Opt. Commun. Netw.*, vol. 1, no. 4, pp. 51–60, 2009.

[9] ITU-T, 'Gigabit-capable passive optical networks (GPON): Long reach', *Recomm. ITU-T G.984.7*, p. 14, 2010.

[10] ITU-T, 'G.9807.1:10-Gigabit-capable symmetrical passive optical network (XGS-PON)', *Itu-T G-Series Recomm.*, vol. E 41042, pp. 1–286, 2016.

[11] ITU-T, 'ITU-T Recommendation G.989.1 40-Gigabit-capable passive optical networks (NG-PON2): General requirements', *Itu-T G-Series Recomm.*, pp. 1–26, 2013.

[12] T. Horvath, J. Radil, P. Munster, and N. H. Bao, 'Optical amplifiers for access and passive optical networks: A tutorial', *Appl. Sci.*, vol. 10, no. 17, 2020.

[13] P. Ossieur *et al.*, 'A symmetric 320Gb/s capable, 100km extended reach hybrid DWDM-TDMA PON', *Opt. InfoBase Conf. Pap.*, no. 512, pp. 20–22, 2010.

[14] D. P. Shea and J. E. Mitchell, 'Long-reach optical access technologies', *IEEE Netw.*, vol. 21, no. 5, pp. 5–11, 2007.

[15] T. Torounidis, P. A. Andrekson, and B. E. Olsson, 'Fiber-optical parametric amplifier with 70-dB gain', *IEEE Photonics Technol. Lett.*, vol. 18, no. 10, pp. 1194–1196, 2006.

[16] M. E. Marhic, K. K. Y. Wong, and L. G. Kazovsky, 'Wide-band tuning of the gain spectra of one-pump fiber optical parametric amplifiers', *IEEE J. Sel. Top. Quantum Electron.*, vol. 10, no. 5, pp. 1133–1141, 2004.

[17] S. Oda, H. Sunnerud, and P. A. Andrekson, 'High efficiency and high output power fiber optic parametric amplifier', *2007 33rd Eur. Conf. Exhib. Opt. Commun. ECOC 2007*, vol. 32, no. 13, pp. 1776–1778, 2007.

[18] G. W. Lu, M. E. Marhic, and T. Miyazaki, 'Burst-mode amplification of dynamic optical packets using fibre optical parametric amplifier in optical packet networks', *Electron. Lett.*, vol. 46, no. 11, pp. 778–780, 2010.

[19] R. P. Davey *et al.*, 'Long-reach access and future broadband network economics', in *2007 33rd European Conference and Exhibition of Optical Communication, ECOC 2007*, 2007.

[20] G. Talli and P. D. Townsend, 'Hybrid DWDM - TDM long-reach PON for next-generation optical access', *J. Light. Technol.*, vol. 24, no. 7, pp. 2827–2834, 2006.

[21] E. Summary, 'Cisco Visual Networking Index – Forecast and', *Europe*, pp. 2007–2012, 2012.

[22] M. Ruffini *et al.*, 'Access and metro network convergence for flexible end-to-end network design [invited]', *J. Opt. Commun. Netw.*, vol. 9, no. 6, pp. 524–535, 2017.

[23] G. M. T. Teixeira. Antonio, Costa . L,Wada. N, Chanclou P. ,Forin D.M. , Prat. J., Tosi Beleffi, 'All-Optical Processing Toward Next Generation Wavelength Agnostic Passive Optical Networks', *Microw. Opt. Technol. Lett.*, vol. 55, no. 11, pp. 2562–2568, 2009.

[24] V. Bobrovs, S. Olonkins, O. Ozolins, J. Porins, and G. Lauks, 'Hybrid optical amplifiers for flexible development in long reach optical access system', *Int. Congr. Ultra Mod. Telecommun. Control Syst. Work.*, pp. 577–582, 2012.

[25] C. B. Gaur, F. Ferreira, V. Gordienko, V. Ribeiro, and N. J. Doran, 'Demonstration of improved performance provided by FOPA for extended PON in burst-mode operation', *IET Conf. Publ.*, vol. 2019, no. CP765, pp. 1–3, 2019.

[26] C. B. Gaur, F. Ferreira, V. Gordeinko, A. Iqbal, W. Forysiak, and N. Doran, 'Comparison of Erbium, Raman and Parametric Optical Fiber Amplifiers for Burst Traffic in Extended PON', *Opt. Fiber Commun. Conf. (OFC 2020)*, vol. W4B.3, pp. 4–6, 2020.

[27] C. B. Gaur, F. Ferreira, V. Gordeinko, A. Iqbal, W. Forysiak, and N. Doran, 'Experimental comparison of fiber optic parametric, Raman and erbium amplifiers for burst traffic for exended reach PONs', *Opt. Express*, vol. Vol.28, no. 13, pp. 19362–19373, 2020.

[28] C. B. Gaur, V. Gordienko, F. F. Ferreira, V. itor Vibeiro, and N. J. Doran, 'Fibre Optic Parametric Amplifier for High Capacity Burst-Mode Access Networks', *Opt. Express*.

[29] C. B. Gaur, V. Gordienko, F. Bessin, and N. J. Doran, 'Dual-Band Amplification of downstream L-band and upstream C-band signals by FOPA in extended reach PON', *Eur. Conf. Opt. Commun. ECOC*, no. 1, pp. 4–7, 2020.

[30] G. P. Agrawal, *Fiber-Optic Communications Systems, Third Edition.*, vol. 6. John Wiley & Sons, 2002.

[31] G. Singh, R. P. Yadav, and V. Janyani, 'Ti indiffused Lithium Niobate (Ti: LiNbO3) Mach-Zehnder interferometer all optical switches: A review', *New Adv. Technol.*, 2010.

[32] I. Hickman, 'Transmitters and receivers', *Pract. RF Handb.*, pp. 156–170, 2006.

[33] J. M. Senior, *Optical Fiber Communications : Principles and Practice*, Third Edit., vol. 1. Peasron Education, 2011.

[34] H. Takahashi, K. Toge, C. Kito, and F. Ito, 'Individual PON monitoring using maintenance band pulsed pump-probe Brillouin analysis', *2013 18th Optoelectron. Commun. Conf. Held Jointly with 2013 Int. Conf. Photonics Switch. OECC/PS 2013*, 2013.

[35] G. P. Agrawal, *Fiber-Optic Communicaiton Systems*, Fourth Edi. John Wiley & Sons.

[36] P. Servati, 'Reduction of dark current in a-Si:H p-i-n photodetectors', in *Proceedings of SPIE*, 2017, no. August 2017, p. 135.

[37] S. Okhonin *et al.*, 'A dynamic operation of a PIN photodiode', *Appl. Phys. Lett.*, vol. 106, no.

3, 2015.

[38] M. Nakamura, S. Nishihara, T. Ito, T. Kurosaki, M. Nogawa, and Y. Ohtomo, 'Burst-mode optical receiver ICs for broadband access networks', *Proc. IEEE Bipolar/BiCMOS Circuits Technol. Meet.*, pp. 21–28, 2010.

[39] S. Takahashi, K. Shiba, E. Mizuki, K. Makita, and A. Tajima, 'Over 25-dB dynamic range 10-/1-Gbps optical burst-mode receiver using high-power-tolerant APD', *Opt. InfoBase Conf. Pap.*, pp. 27–29, 2009.

[40] I. L. Ebringer and S. Francisco, 'Burst Mode Receiver', 2000.

[41] E. Regnier, I. Flammer, S. Girard, F. Gooijer, F. Achten, and G. Kuyt, 'Low-dose radiation-induced attenuation at infrared wavelengths for P-doped, ge-doped and pure silica-core optical fibres', *IEEE Trans. Nucl. Sci.*, vol. 54, no. 4, pp. 1115–1119, 2007.

[42] ITU-T, 'Recommendation ITU-T G.652: Characteristics of a Single-Mode Optical Fibre and Cable', *Itu-T G652*, pp. 1–28, 2016.

[43] ITU-T, 'Recommendation ITU-T G.653 Characteristics of a non-zero dispersion-shifted single-mode optical fibre and cable'. ITU-T Generic, 2010.

[44] ITU-T, 'ITU-T G.652 Charactersitics of a single-mode optical fibre and cable', *http://people.revoledu.com/kardi/tutorial/kMean/.* ITU-T Generic, p. 22, 2007.

[45] K. Tsujikawa, K. Tajima, and J. Zhou, 'Intrinsic loss of optical fibers', *Opt. Fiber Technol.*, vol. 11, no. 4, pp. 319–331, 2005.

[46] C. J. Hsu, N. D. Foltz, and C. W. Cho, 'Stimulated thermal Rayleigh scattering in argon', *Phys. Rev. A*, vol. 9, no. 6, pp. 2365–2370, 1974.

[47] P. S. André and A. N. Pinto, 'Chromatic dispersion fluctuations in optical fibers due to temperature and its effects in high-speed optical communication systems', *Opt. Commun.*, vol. 246, no. 4–6, pp. 303–311, 2005.

[48] A. Singh, A. K. Sharma, and T. S. Kamal, 'Four-wave mixing analysis in WDM optical communication systems with higher-order dispersion', *Optik (Stuttg).*, vol. 119, no. 16, pp. 788–792, 2008.

[49] M. H. Aly, 'Chromatic Dispersion in Graded-index Single-Mode Optical Fibers', *IEEE Pacific Rim Conf. Commun. Comput. Signal Process.*, vol. 4, no. 3, pp. 57–71, 1991.

[50] W. . G. D.N Payne, 'Zero Material Dispersion in Optical Fibres', *Electron. Lett.*, vol. 11, no. 8, 1975.

[51] I. P. Kaminow, 'Polarization in Optical Fibers', *IEEE J. Quantum Electron.*, vol. 17, no. 1, pp. 15–22, 1981.

[52] G. P. Agrawal, *Nonliear Fiber Optics*, Third Edit. Academic Press, 2004.

[53] J. D. Reis *et al.*, 'Terabit+ (192 × 10 Gb/s) nyquist shaped UDWDM coherent PON with upstream and downstream over a 12.8 nm band', *J. Light. Technol.*, vol. 32, no. 4, pp. 729–735, 2014.

[54] C. Xing, C. Ke, K. Zhang, Z. Guo, Y. Zhong, and D. Liu, 'Polarization- and wavelength-independent SBS-based filters for high resolution optical spectrum measurement', *Opt. Express*, vol. 25, no. 18, p. 20969, 2017.

[55] A. Kobyakov, M. Sauer, and D. Chowdhury, 'Stimulated Brillouin scattering in optical fibers', *Adv. Opt. Photonics*, vol. 2, no. 1, p. 1, 2010.

[56] J. Hansryd, F. Dross, M. Westlund, P. A. Andrekson, and S. N. Knudsen, 'Increase of the SBS threshold in a short highly nonlinear fiber by applying a temperature distribution', *J. Light. Technol.*, vol. 19, no. 11, pp. 1691–1697, 2001.

[57] N. Yoshizawa and T. Imai, 'Stimulated Brillouin scattering suppression by means of applying strain distribution to fiber with cabling', *J. Light. Technol.*, vol. 11, no. 10, pp. 1518–1522, 1993.

[58] K. Tsujikawa, K. Nakajima, Y. Miyajima, and M. Ohashi, 'New SBS suppression Fiber with uniform chromatic dispersion to enhance four-wave mixing', *IEEE Photonics Technol. Lett.*, vol. 10, no. 8, pp. 1139–1141, 1998.

[59] K. Shiraki, M. Ohashi, M. Tateda, and S. Member, 'SBS Threshold of a Fiber with a Brillouin Frequency Shift Distribution', *J. Light. Technol.*, vol. 14, no. 1, pp. 50–57, 1996.

[60] J. M. C. Boggio, A. Guimarães, F. A. Callegari, J. D. Marconi, and H. L. Fragnito, 'Q penalties due to pump phase modulation and pump RIN in fiber optic parametric amplifiers with non-uniform dispersion', *Opt. Commun.*, vol. 249, no. 4–6, pp. 451–472, 2005.

[61] R. H. Stolen, W. J. Tomlinson, H. A. Haus, and J. P. Gordon, 'Raman response function of silica-core fibers', *J. Opt. Soc. Am. B*, vol. 6, no. 6, p. 1159, 1989.

[62] Q. Lin and G. P. Agrawal, 'Raman response function for silica fibers', *Opt. Lett.*, vol. 31, no. 21, p. 3086, 2006.

[63] T. J. EIIingham, L. M. GIeeson, and N. J. Doran, 'Enhanced Raman amplifier performance using non-linear pump broadening', *Eur. Conf. Opt. Commun. ECOC*, vol. 2, pp. 13–14, 2002.

[64] M. A. Iqbal *et al.*, 'Impact of pump-signal overlap in S+C+L band discrete Raman amplifiers', *Opt. Express*, vol. 28, no. 12, p. 18440, 2020.

[65] A. S. Y. Hsieh *et al.*, 'Combined effect of Raman and parametric gain on single-pump parametric amplifiers.', *Opt. Express*, vol. 15, no. 13, pp. 8104–8114, 2007.

[66] V. Gordienko, 'Broadband Fibre Parametric Amplifiers', Aston University, 2018.

[67] Z. Tong, C. Lundstrm, P. A. Andrekson, M. Karlsson, and A. Bogris, 'Ultralow noise, broadband phase-sensitive optical amplifiers, and their applications', *IEEE J. Sel. Top. Quantum Electron.*, vol. 18, no. 2, pp. 1016–1032, 2012.

[68] S. L. I. Olsson, H. Eliasson, E. Astra, M. Karlsson, and P. A. Andrekson, 'Long-haul optical transmission link using low-noise phase-sensitive amplifiers', *Nat. Commun.*, vol. 9, no. 1, pp. 1–7, 2018.

[69] J. A. Harrington, *Infrared Fibers and Their Applications*. SPIE PRESS, 2004.

[70] F. Poletti, X. Feng, G. M. Ponzo, M. N. Petrovich, W. H. Loh, and D. J. Richardson, 'All-solid highly nonlinear singlemode fibers with a tailored dispersion profile', *Opt. Express*, vol. 19, no. 1, p. 66, 2011.

[71] X. Orignac, D. Barbier, X. Min, R. M. Almeida, O. Mccarthy, and E. Yeatman, 'Sol-gel silica / titania-on-silicon Er / Yb-doped waveguides for optical amplification at 1.5um', *Opt. Mater. (Amst).*, vol. 12, 1999.

[72] Y. Fujimoto and M. Nakatsuka, 'Optical amplification in bismuth-doped silica glass', *Appl. Phys. Lett.*, vol. 82, no. 19, pp. 3325–3326, 2003.

[73] N. A. Olsson, 'Lightwave Systems With Optical Amplifiers', *J. Light. Technol.*, vol. 7, no. 7, pp. 1071–1082, 1989.

[74] ITU-T, 'G.9807.2 10 Gigabit-capable passive optical networks (XG(S)-PON): Reach extension', 2017.

[75] D. Nesset, 'PON Roadmap [Invited]', *Opt. Commun. Networks*, vol. 9, no. 1, pp. 71–76, 2021.

[76] I.-T. G.984.6, 'ITU-T G.984.6 Gigabit-capable passive optical networks (G-PON): Reach extension Amendment 2 Recommendation', vol. 6, no. 2008. 2012.

[77] N. Suzuki, H. Miura, K. Matsuda, R. Matsumoto, and K. Motoshima, '100 Gb/s to 1 Tb/s Based Coherent Passive Optical Network Technology', *J. Light. Technol.*, vol. 36, no. 8, pp. 1485–1491, 2018.

[78] A. M. Ragheb and H. Fathallah, 'Performance analysis of next generation-PON (NG-PON) architectures', *8th Int. Conf. High-Capacity Opt. Networks Emerg. Technol. HONET 2011*, pp. 339–345, 2011.

[79] ITU-T G.984.2, 'Gigabit-capable passive optical networks (GPON): Physical media dependent (PMD) layer specification'. 2019.

[80] C. H. Lee, W. V. Sorin, and B. Y. Kim, 'Fiber to the home using a PON infrastructure', *J. Light. Technol.*, vol. 24, no. 12, pp. 4568–4583, 2006.

[81] ITU-T, 'Gigabit-capable passive optical networks (GPON): General characteristics', *Networks*. p. 138, 2016.

[82] H. H. Lee, J. H. Lee, and S. S. Lee, 'All-optical gain-clamped EDFA using external saturation signal for burst-mode upstream in TWDM-PONs', *Opt. Express*, vol. 22, no. 15, p. 18186, 2014.

[83] M. Dalla Santa, C. Antony, G. Talli, I. Krestnikov, and P. D. Townsend, 'Burst-mode analysis of XGPON Raman reach extender employing quantum-dot lasers', *Electron. Lett.*, vol. 52, no. 13, pp. 1157–1178, 2016.

[84] M. Fujiwara and R. Koma, 'Long-Reach and High-Splitting-Ratio WDM/TDM-PON Systems Using Burst-Mode Automatic Gain Controlled SOAs', *J. Light. Technol.*, vol. 34, no. 3, pp. 901–909, 2016.

[85] J. Sugawa and H. Ikeda, 'Development of OLT using semiconductor optical amplifiers as booster and preamplifier for loss-budget extension in 10.3-Gb/s PON system', *Opt. InfoBase Conf. Pap.*, pp. 44–46, 2012.

[86] T. Ivaniga and P. Ivaniga, 'Comparison of the optical amplifiers EDFA and SOA based on the BER and Q-factor in C-band', *Adv. Opt. Technol.*, vol. 2017, 2017.

[87] B. Package, '1490 nm Semiconductor Optical Amplifier, Butterfly Package', pp. 1–4, 2018.

[88] M. J. Connelly, 'Wideband semiconductor optical amplifier steady-state numerical model', *IEEE J. Quantum Electron.*, vol. 37, no. 3, pp. 439–447, 2001.

[89] J. Xu, X. Zhang, and J. Mork, 'Investigation of patterning effect in ultrafast SOA-based optical switches', *Opt. InfoBase Conf. Pap.*, vol. 46, no. 1, pp. 87–94, 2009.

[90] S. Aleksic and V. Krajinovic, 'Methods for Compensation of the Pattern Effect in Semiconductor Optical Amplifiers', no. July, pp. 159–166, 2003.

[91] R. Brenot, G. De Valicourt, F. Poingt, F. Lelarge, and F. Pommereau, 'Potential benefits and limitations of SOA in access networks', *Opt. InfoBase Conf. Pap.*, pp. 5–6, 2010.

[92] P. J. Urban, A. M. J. Koonen, G. D. Khoe, and H. de Waardt, 'Interferometric crosstalk

reduction in an RSOA-based WDM passive optical network', *J. Light. Technol.*, vol. 27, no. 22, pp. 4943–4953, 2009.

[93] M. G. Oberg and N. A. Olsson, 'Crosstalk between intensity modulated wavelength-division-multiplexed signals in a semiconductor laser amplifier.', no. I, p. 90, 1988.

[94] L. C. Elrefaie A, 'Performance Degradation of Multigigabit-per-Second NRZ/RZ Lightwave Systems Due to Gain Saturation in Traveling-Wave Seminconductor Optical Amplifiers', *IEEE Photonics Technol. Lett.*, vol. Vol. 1, p. 6, 1989.

[95] J. Renaudier *et al.*, 'Recent Advances in 100+nm Ultra-Wideband Fiber-Optic Transmission Systems Using Semiconductor Optical Amplifiers', *J. Light. Technol.*, vol. 38, no. 5, pp. 1071–1079, 2020.

[96] Y. Sun *et al.*, '80 nm Ultra wide band EDFA with low noise figure and high output power', *IEE Conf. Publ.*, no. 448 /5, pp. 69–72, 1997.

[97] R. J. Mears, L. Reekie, I. M. Jauncey, D. N. Payne, and R. J. Mears, 'Low-noise erbium-doped fibre amplifier operating at 1.54μm', *Electronics Letters*, vol. 23, no. 19. pp. 1026–1028, 1987.

[98] B. Gain and B. N. Figure, 'Benchtop C + L Band EDFA Benchtop C + L Band EDFA', 2008.

[99] A. Malakzadeh, R. Pashaie, and M. Mansoursamaei, 'Gain and noise figure performance of an EDFA pumped at 980 nm or 1480 nm for DOFSs', *Opt. Quantum Electron.*, vol. 52, no. 2, pp. 1–16, 2020.

[100] J. M. P. Delavaux and J. A. Nagel, 'Multi-Stage Erbium-Doped Fiber Amplifier Designs', *J. Light. Technol.*, vol. 13, no. 5, pp. 703–720, 1995.

[101] P. F. Wysocki, J. B. Judkins, R. P. Espindola, M. Andrejco, and A. M. Vengsarkar, 'Broad-band erbium-doped fiber amplifier flattened beyond 40 nm using long-period grating filter', *IEEE Photonics Technol. Lett.*, vol. 9, no. 10, pp. 1343–1345, 1997.

[102] H. S. Carvalho, I. J. G. Cassimiro, F. H. C. S. Filho, J. R. F. De Oliveira, and A. C. Bordonalli, 'AGC EDFA transient suppression algorithm assisted by cognitive neural network', *2014 Int. Telecommun. Symp. ITS 2014 - Proc.*, 2014.

[103] R. I. Laming, M. N. Zervas, and D. N. Payne, 'Erbium-Doped Fiber Amplifier with 54 dB Gain and 3.1 dB Noise Figure', *IEEE Photonics Technol. Lett.*, vol. 4, no. 12, pp. 1345–1347, 1992.

[104] M. Karásek, 'The design of L-band EDFA for multiwavelength applications', *J. Opt. A Pure Appl. Opt.*, vol. 3, no. 1, pp. 96–102, 2001.

[105] B. J. Ainslie, 'A Review of the Fabrication and Properties of Erbium-Doped Fibers for Optical Amplifiers', *J. Light. Technol.*, vol. 9, no. 2, pp. 220–227, 1991.

[106] D. Systems *et al.*, 'EDFA for Burst Mode Networks', 2015. [Online]. Available: https://www.amonics.com/view?path=/amonics/datasheets/13/datasheet.pdf.

[107] S. Pachnicke, M. Obholz, E. Voges, P. M. Krummrich, and E. Gottwald, 'Electronic EDFA gain control for the suppression of transient gain dynamics in long-haul transmission systems', *Opt. InfoBase Conf. Pap.*, vol. 6, no. 9, pp. 1129–1137, 2007.

[108] C. R. Giles, J. R. Simpson, and E. Desurvire, 'Transient gain and cross talk in erbium-doped fiber amplifiers', *Opt. Lett.*, vol. 14, no. 16, p. 880, 1989.

[109] A. Bononi and L. A. Rusch, 'Doped-fiber amplifier dynamics: A system perspective', *J. Light. Technol.*, vol. 16, no. 5, pp. 945–956, 1998.

[110] N. Brandonisio, D. Carey, S. Porto, G. Talli, and P. D. Townsend, 'Burst-mode FEC performance for PON upstream channels with EDFA optical transients', *22nd Conf. Opt. Netw. Des. Model. ONDM 2018 - Proc.*, pp. 190–193, 2018.

[111] M. Shiraiwa, Y. Awaji, H. Furukawa, S. Shinada, B. J. Puttnam, and N. Wada, 'Performance evaluation of a burst-mode EDFA in an optical packet and circuit integrated network', *Opt. Express*, vol. 21, no. 26, p. 32589, 2013.

[112] Y. A. and N. W. Puttnam, Benjamin J., 'Peformance of an Advanced Transient Suppressed EDFA in Diverse Dynamic Optical Network Scenarios', in *European Conference on Optical Communication, ECOC*, 2009, pp. 6–7.

[113] A. K. Srivastava, Y. Sun, J. L. Zyskind, and J. W. Sulhoff, 'EDFA transient response to channel loss in WDM transmission system', *IEEE Photonics Technol. Lett.*, vol. 9, no. 3, pp. 386–388, 1997.

[114] S. Sergeyev, E. Vanin, and G. Jacobsen, 'Gain-clamped dynamics in EDFA with combined electronic feed-forward - Optical feedback control', *Conf. Opt. Fiber Commun. Tech. Dig. Ser.*, vol. 70, pp. 518–519, 2002.

[115] M.Zirngibl, 'Gain Control In Erbium-Doped Fibre Amplifiers By An All-Optical Feedback Loop', *Electron. Lett.*, vol. 27, no. 7, pp. 560–561, 1991.

[116] K. Motoshima, L. M. Leba, D. N. Chen, M. M. Downs, T. Li, and E. Desurvire, 'Dynamic Compensation of Transient Gain Saturation in Erbium-Doped Fiber Amplifiers by Pump Feedback Control', *IEEE Photonics Technol. Lett.*, vol. 5, no. 12, pp. 1423–1426, 1993.

[117] W. Lin, R. S. Wolff, and B. Mumey, 'Decreasing EDFA transients by power shaping', *Opt. Switch. Netw.*, vol. 5, no. 4, pp. 188–195, 2008.

[118] S. Popov, S. Sergeyev, and A. T. Friberg, 'Polarization dependence of Raman gain due to breaking Of cylindrical symmetry in optical fibers', *Conf. Lasers Electro-Optics Eur. - Tech. Dig.*, p. 650, 2003.

[119] M. Takahashi, R. Sugizaki, J. Hiroishi, M. Tadakuma, Y. Taniguchi, and T. Yagi, 'Low-Loss and Low-Dispersion-Slope Highly Nonlinear Fibers', vol. 23, no. 11, pp. 3615–3624, 2005.

[120] E. G. Turitsyna and S. Webb, 'Simple design of FBG-based VSB filters for ultra-dense WDM transmission 20th January 2005', *Electron. Lett.*, vol. 41, no. 2, pp. 40–41, 2005.

[121] M. A. Iqbal, M. A. Z. Al-Khateeb, L. Krzczanowicz, I. D. Phillips, P. Harper, and W. Forysiak, 'Linear and Nonlinear Noise Characterisation of Dual Stage Broadband Discrete Raman Amplifiers', *J. Light. Technol.*, vol. 37, no. 14, pp. 3679–3688, 2019.

[122] J. Cheng *et al.*, 'Pump RIN-induced impairments in unrepeatered transmission systems using distributed Raman amplifier', *Opt. Express*, vol. 23, no. 9, p. 11838, 2015.

[123] M. Tang, P. Shum, and Y. Gong, 'Design of double-pass discrete Raman amplifier and the impairments induced by Rayleigh backscattering', *Opt. Express*, vol. 11, no. 16, p. 1887, 2003.

[124] C. Chen *et al.*, 'Control of transient effects in distributed and lumped Raman amplifiers', *Electron. Lett.*, vol. 37, no. 21, pp. 1304–1305, 2001.

[125] L. F. Mollenauer, R. H. Stolen, and M. N. Islam, 'Experimental Demonstration of Soliton Propagation in Long Fibers: Loss Compensated By Raman Gain.', *Opt. Lett.*, vol. 10, no. 5, pp. 80–81, 1985.

[126] T. N. Nielsen *et al.*, '3.28-Tb/s transmission over 3 × 100 km of nonzero-dispersion fiber using dual C- and L-band distributed Raman amplification', *IEEE Photonics Technol. Lett.*,

vol. 12, no. 8, pp. 1079–1081, 2000.

[127] R. Espinola, J. Dadap, R. O. Jr, and S. McNab, 'Raman Amplification', *Optics*, no. September, pp. 32–39, 2004.

[128] D. Nesset and P. Wright, 'Raman extended GPON using 1240 nm semiconductor quantum-dot lasers', *Opt. InfoBase Conf. Pap.*, pp. 21–23, 2010.

[129] I. Tafur Monroy, R. Kjær, F. Öhman, K. Yvind, and P. Jeppesen, 'Distributed fiber Raman amplification in long reach PON bidirectional access links', *Opt. Fiber Technol.*, vol. 14, no. 1, pp. 41–44, 2008.

[130] K. C. Reichmann *et al.*, 'A symmetric-rate, extended-reach 40 Gb/s CWDM-TDMA PON with downstream and upstream SOA - Raman amplification', *J. Light. Technol.*, vol. 30, no. 4, pp. 479–485, 2012.

[131] N. Suzuki *et al.*, 'Impairments Due to Burst-Mode Transmission in a Raman-Based Long-Reach PON Link', *Electron. Lett.*, vol. 37, no. 19, pp. 1490–1492, 2001.

[132] L. Zhang, S. Wang, and C. Fan, 'Transient analysis in discrete fiber Raman amplifiers', *Opt. Commun.*, vol. 197, no. 4–6, pp. 459–465, 2001.

[133] A. Bononi, M. Papararo, and M. Fuochi, 'Transient gain dynamics in saturated Raman amplifiers', *Opt. Fiber Technol.*, vol. 10, no. 1, pp. 91–123, 2004.

[134] B. Palsdottir, I. T. Monroy, L. K. Oxenløwe, and P. Jeppesen, 'Impairments Due to Burst-Mode Transmission in a Raman-Based Long-Reach PON Link', *IEEE Photonics Technol. Lett.*, vol. 19, no. 19, pp. 1490–1492, 2007.

[135] S. S. H. Yam, M. E. Marhic, Y. Akasaka, and L. G. Kazovsky, 'Gain-clamped S-band discrete Raman amplifier', *Opt. Lett.*, vol. 96 A, no. 7, pp. 641–642, 2004.

[136] C.-J. Chen, J. Ye, W. S. Wong, and Y.-W. Lu, 'Transient Effects and Their Control in Raman Optical Amplifiers', p. OWA1, 2014.

[137] Robert W Boyd, *Nonlinear Optics*, Third Edit. 2007.

[138] M. Bass, E. Van Stryland, D. R. Williams, and W. L. Wolfe, *Handbook of Optics Vol IV*. 2001.

[139] F. Messina, L. Vaccaro, and E. Vella, 'Optical properties of amorphous SiO 2 near the fundamental absorption edge', pp. 723–724.

[140] M. E. Marhic †, *Fiber Optical Parametric Amplifiers, Oscillators and Related Devices: Theory, Applications, and Related Devices*. Cambrige University Press.

[141] M. E. Marhic and N. J. Doran, 'Prospects for inserting parametric amplifiers in optical communication networks', *Int. Conf. Transparent Opt. Networks*, pp. 1–4, 2011.

[142] A. Bogris and D. Syvridis, 'Distributed optical parametric amplification at 1.3 & mu;: Performance and applications in optical access networks', *IEEE Photonics Technol. Lett.*, vol. 24, no. 8, pp. 694–696, 2012.

[143] V. Gordienko, M. Stephens, and N. Doran, 'Towards Wide-Bandwidth Ultra-Flat FOPAs', in *International Conference on Transparent Optical Networks*, 2017, pp. 31–34.

[144] M. E. Marhic, K. K. Y. Wong, and L. G. Kazovsky, 'Fiber optical parametric amplifiers with linearly or circularly polarized waves', *J. Opt. Soc. Am. B*, vol. 20, no. 12, p. 2425, 2003.

[145] K. K. Y. Wong, M. E. Marhic, K. Uesaka, and L. G. Kazovsky, 'Polarization-independent two-pump fiber optical parametric amplifier', *IEEE Photonics Technol. Lett.*, vol. 14, no. 7, pp. 911–913, 2002.

[146] H. Hu *et al.*, 'Parametric amplification, wavelength conversion, and phase conjugation of a 2.048-Tbit/s WDM PDM 16-QAM signal', *J. Light. Technol.*, vol. 33, no. 7, pp. 1286–1291, 2015.

[147] K. K. Y. Wong, S. Member, M. E. Marhic, S. Member, K. Uesaka, and L. G. Kazovsky, 'Polarization-Independent One-Pump Fiber-Optical Parametric Amplifier', *IEEE Photonics Technol. Lett.*, vol. 14, no. 11, pp. 1506–1508, 2002.

[148] M. F. C. Stephens, V. Gordienko, and N. J. Doran, '20 dB net-gain polarization-insensitive fiber optical parametric amplifier with >2 THz bandwidth', *Opt. Express*, vol. 25, no. 9, p. 10597, 2017.

[149] M. Jazayerifar *et al.*, 'Impact of Brillouin Backscattering on Signal Distortions in Single-Fiber Diversity Loop Based Polarization-Insensitive FOPAs', *J. Light. Technol.*, vol. 35, no. 19, pp. 4137–4144, 2017.

[150] S. Takasaka and R. Sugizaki, 'Polarization insensitive fiber optical parametric amplifier using a SBS suppressed diversity loop', *2016 Opt. Fiber Commun. Conf. Exhib. OFC 2016*, pp. 4–6, 2016.

[151] M. F. C. Stephens, V. Gordienko, and N. J. Doran, '20 dB net-gain polarization-insensitive fiber optical parametric amplifier with >2 THz bandwidth', *Opt. Express*, vol. 25, no. 9, pp. 10597–10609, 2017.

[152] V. Gordienko, F. M. Ferreira, V. Ribeiro, and N. Doran, 'Suppression of Nonlinear Crosstalk in a Polarization Insensitive FOPA by Mid-Stage Idler Removal', *2019 Opt. Fiber Commun. Conf. Exhib. OFC 2019 - Proc.*, pp. 1–3, 2019.

[153] V. Gordienko, F. M. Ferreira, C. B. Gaur, and N. J. Doran, 'Looped Polarization-Insensitive Fiber Optic Parametric Amplifiers for Broadband High Gain Applications'.

[154] V. Gordienko, F. Ferreira, C. Laperle, M. O'Sullivan, K. Roberts, and N. Doran, 'Polarisation-insensitive fibre optic parametric amplifiers for applications in modern communication networks', *Int. Conf. Transparent Opt. Networks*, vol. 2020-July, pp. 4–7, 2020.

[155] M. F. C. Stephens, V. Gordienko, and N. J. Doran, 'Reduced Crosstalk, Polarization Insensitive Fiber Optical Parametric Amplifier (PI FOPA) for WDM Applications', no. c, pp. 7–9, 2018.

[156] A. Peric, S. Moro, N. Alic, A. J. Anderson, C. J. McKinstrie, and S. Radic, 'Two-pump fiber-optic parametric amplifier with 66dB gain and errorless performance', *Opt. InfoBase Conf. Pap.*, pp. 1–2, 2010.

[157] M. C. Ho, K. Uesaka, M. Marhic, Y. Akasaka, and L. G. Kazovsky, '200-nm-bandwidth fiber optical amplifier combining parametric and Raman gain', *J. Light. Technol.*, vol. 19, no. 7, pp. 977–981, 2001.

[158] J. M. C. Boggio, S. Moro, E. Myslivets, J. R. Windmiller, N. Alic, and S. Radic, '155-Nm Continuous-Wave Two-Pump Parametric Amplification', *IEEE Photonics Technol. Lett.*, vol. 21, no. 10, pp. 612–614, 2009.

[159] V. G. Ordienko, M. F. C. S. Tephens, A. E. E. L. Aher, and N. J. D. Oran, 'Ultra-flat wideband single-pump Raman- enhanced parametric amplification', *Opt. Express*, vol. 25, no. 5, pp. 4810–4818, 2017.

[160] Z. Tong *et al.*, 'Towards ultrasensitive optical links enabled by low-noise phase-sensitive amplifiers', *Nat. Photonics*, vol. 5, no. 7, pp. 430–436, 2011.

[161] A. Shahpari *et al.*, 'Coherent Access: A Review', *J. Light. Technol.*, vol. 35, no. 4, pp. 1050–

1058, 2017.

[162] V. Gordienko *et al.*, 'Characterisation of Novel Polarisation-Insensitive Configurations of Fibre Optical Parametric Amplifiers', *Ecoc*, pp. 8–11, 2019.

[163] M. F. C. Stephens, M. Tan, V. Gordienko, P. Harper, and N. J. Doran, 'In-line and cascaded DWDM transmission using a 15dB net-gain polarization-insensitive fiber optical parametric amplifier', *Opt. Express*, vol. 25, no. 20, pp. 24312–24325, 2017.

[164] N. Pleros *et al.*, 'Optical signal processing using integrated multi-element SOA-MZI switch arrays for packet switching', *IET Optoelectron.*, vol. 1, no. 3, pp. 120–126, 2007.

[165] O. Optics, 'Super-Fast Erbium Doped Fiber Amplifier (EDFA)', 2020. [Online]. Available: https://www.ozoptics.com/ALLNEW_PDF/DTS0161.pdf.

[166] G. Bolognini and F. Di Pasquale, 'Transient Effects in Gain-Clamped Discrete Raman Amplifier Cascades', *IEEE Photonics Technol. Lett.*, vol. 16, no. 1, pp. 66–68, 2004.

[167] I. Sackey *et al.*, 'Non-reciprocal gain due to counter-propagating pumps in a polarization-independent FOPA with diversity loop', *Eur. Conf. Opt. Commun. ECOC*, vol. 2015-Novem, no. I, pp. 17–19, 2015.

[168] S. Spolitis and G. Ivanovs, 'Extending the reach of DWDM-PON access network using chromatic dispersion compensation', *2011 IEEE Swedish Commun. Technol. Work. Swe-CTW 2011*, pp. 29–33, 2011.

[169] S. Shakya, A. Supe, I. Lavrinovica, S. Spolitis, and J. Porins, 'Different optical fiber nonlinear coefficient experimental measurements', *2016 Int. Work. Fiber Opt. Access Network, FOAN 2016*, pp. 1–4, 2016.

[170] S. A. E. Lewis, S. V. Chernikov, and J. R. Taylor, 'Characterization of Double Rayleigh Scatter Noise in Raman Amplifiers', *IEEE Photonics Technol. Lett.*, vol. 12, no. 5, pp. 528–530, 2000.

[171] D. Mashimo, J. Sugawa, H. Ikeda, K. Minatozaki, and N. Matsudaira, '10-Gb/s burst-mode receiver for fast settling time', *Opt. InfoBase Conf. Pap.*, vol. 2, pp. 1–2, 2009.

[172] L. G. Kazovsky, S. W. Wong, S. H. Yen, and S. Yamashita, 'Next-generation optical access networks', *Opt. InfoBase Conf. Pap.*, vol. 25, no. 11, pp. 3428–3442, 2009.

[173] H. Debrégeas *et al.*, 'Quasi frequency drift suppression for burst mode operation in low-cost thermally-tuned TWDM-PON', *2017 Opt. Fiber Commun. Conf. Exhib. OFC 2017 - Proc.*, no. Cm, pp. 5–7, 2017.

[174] M. J. Connelly, 'Optical Amplifiers: Semiconductor Optical Amplifiers', *Encycl. Mod. Opt. Five-Volume Set*, vol. 18, no. 9, pp. 308–316, 2004.

[175] X. Lin, W. Sun, X. Wang, S. Yue, M. Veeraraghavan, and W. Hu, 'Time-Space Decoupled SnF Scheduling of Bulk Transfers across Inter-Datacenter Optical Networks', *IEEE Access*, vol. 8, pp. 24829–24846, 2020.

[176] E. Ciaramella *et al.*, 'System for Free Space Optical Communications', vol. 27, no. 9, pp. 1639–1645, 2009.

[177] X. Yu, J. Li, X. Cao, Y. Chen, and C. Qiao, 'Traffic statistics and performance evaluation in optical burst switched networks', *J. Light. Technol.*, vol. 22, no. 12, pp. 2722–2738, 2004.

[178] X. Yu, Y. Chen, and C. Qiao, '<title>Study of traffic statistics of assembled burst traffic in optical burst-switched networks</title>', *Opt. 2002 Opt. Netw. Commun.*, vol. 4874, no. July 2002, pp. 149–159, 2002.

[179] M. Mahloo, J. Chen, and L. Wosinska, 'PON versus AON: Which is the best solution to offload core network by peer-to-peer traffic localization', *Opt. Switch. Netw.*, vol. 15, pp. 1–9, 2015.

[180] A. Napoli *et al.*, 'Towards multiband optical systems', *Opt. InfoBase Conf. Pap.*, vol. Part F106-, pp. 5–6, 2018.

[181] A. Ghazisaeidi *et al.*, 'Advanced C+L-Band Transoceanic Transmission Systems Based on Probabilistically Shaped PDM-64QAM', *J. Light. Technol.*, vol. 35, no. 7, pp. 1291–1299, 2017.

[182] A. Mitra, D. Semrau, N. Gahlawat, A. Srivastava, P. Bayvel, and A. Lord, 'Effect of reduced link margins on C + L band elastic optical networks', *J. Opt. Commun. Netw.*, vol. 11, no. 10, pp. C86–C93, 2019.

[183] G. K. P. Lei and M. E. Marhic, 'Amplification of DWDM channels using a bidirectional fiber optical parametric amplifier', *2014 Optoelectron. Commun. Conf. OECC 2014 Aust. Conf. Opt. Fibre Technol. ACOFT 2014*, vol. 22, no. 7, pp. 548–550, 2014.

[184] K. S. Yeo, F. R. M. Adikan, M. Mokhtar, S. Hitam, and M. A. Mahdi, 'Fiber optical parametric amplifier with double-pass pump configuration', *Opt. Express*, vol. 21, no. 25, p. 31623, 2013.

[185] M. E. Marhic, N. Kagi, T.-K. Chiang, and L. G. Kazovsky, 'Broadband fiber optical parametric amplifiers', *Opt. Lett.*, vol. 21, no. 8, p. 573, 1996.

[186] V. G. Ordienko, M. F. C. S. Tephens, A. E. E. L. Aher, and N. J. D. Oran, 'Ultra-flat wideband single-pump Raman- enhanced parametric amplification', vol. 25, no. 5, pp. 4810–4818, 2017.